AD-A187 136 SUMMARIES OF PAPERS PRESENTED AT THE PICOSECOND ELECTRONICS AND OPTOELECT..(U) OPTICAL SOCIETY OF AMERICA WASHINGTON D C J W QUINN 10 OCT 87 1/3

UNCLASSIFIED N00014-87-G-0050 F/G 9/1 NL

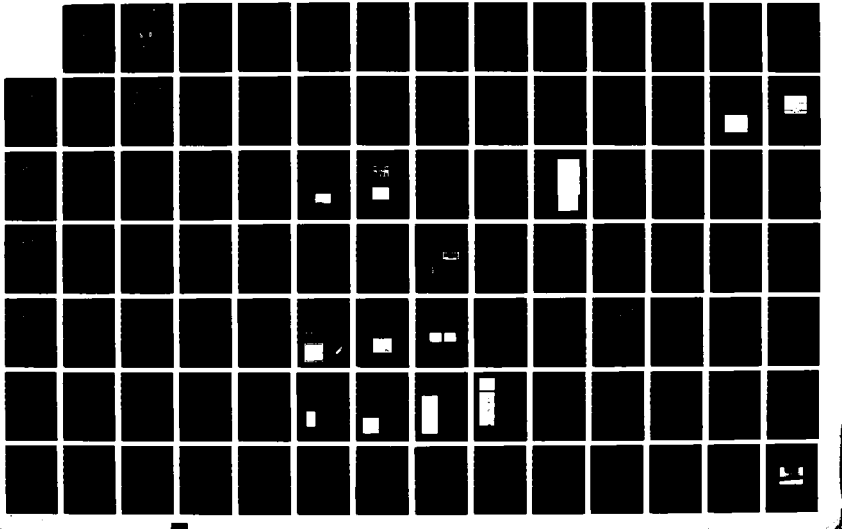

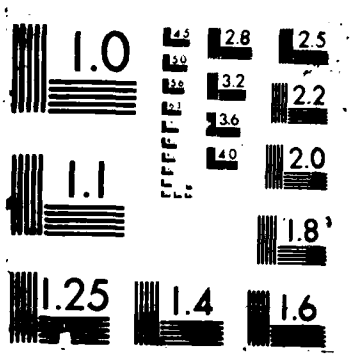
1.0
1.1
1.25
1.4
1.6
1.8
2.0
2.2
2.5
2.8
3.2
3.6
4.0

PICOSECOND ELECTRONICS AND OPTOELECTRONICS

TECHNICAL DIGEST

JANUARY 14-16, 1987
INCLINE VILLAGE, NEVADA

UNCLASSIFIED

SECURITY CLASSIFICATION OF THIS PAGE

ADA187136

REPORT DOCUMENTATION PAGE

Form Approved
OMB No. 0704-0188

1a. REPORT SECURITY CLASSIFICATION Unclassied	1b RESTRICTIVE MARKINGS n/a
2a. SECURITY CLASSIFICATION AUTHORITY	3 DISTRIBUTION / AVAILABILITY OF REPORT Approved for public release - distribution unlimited
2b. DECLASSIFICATION / DOWNGRADING SCHEDULE	
4. PERFORMING ORGANIZATION REPORT NUMBER(S) N-00014-87-G-0050	5 MONITORING ORGANIZATION REPORT NUMBER(S) N-00014-87-G-0050
6a. NAME OF PERFORMING ORGANIZATION Optical Society of America 6b. OFFICE SYMBOL (If applicable)	7a. NAME OF MONITORING ORGANIZATION Department of the Navy- Office of Naval Research
6c. ADDRESS (City, State, and ZIP Code) 1816 Jefferson Place, N.W. Washington, D.C. 20036	7b ADDRESS (City, State, and ZIP Code) Code 1511B:MPB 800 North Quincy Street Arlington, VA 22217-5000
8a. NAME OF FUNDING / SPONSORING ORGANIZATION Optical Society of America 8b OFFICE SYMBOL (If applicable)	9 PROCUREMENT INSTRUMENT IDENTIFICATION NUMBER
8c. ADDRESS (City, State, and ZIP Code) 1816 Jefferson Place, N.W. Washington, D.C. 20036	10 SOURCE OF FUNDING NUMBERS PROGRAM ELEMENT NO / PROJECT NO / TASK NO / WORK UNIT ACCESSION NO

11. TITLE (Include Security Classification)
Organization of a Topical Meeting on Picosecond Electronics and Optoelectronics

12. PERSONAL AUTHOR(S)
J.W. Quinn

13a. TYPE OF REPORT	13b. TIME COVERED	14. DATE OF REPORT (Year, Month, Day)	15. PAGE COUNT
Final	FROM 01/01/87 TO 10/10/87	10/10/87	

16. SUPPLEMENTARY NOTATION

17. COSATI CODES			18. SUBJECT TERMS (Continue on reverse if necessary and identify by block number)
FIELD	GROUP	SUB-GROUP	

19. ABSTRACT (Continue on reverse if necessary and identify by block number)

The purpose of this conference is to bring together workers in the areas of electronics and optoelectronics who share a common interest in the physics and technology of picosecond solid state devices, their multi-gigahertz applications and ultrafast measurement techniques. Subjects covered included: optoelectronic devices; semiconductor device physics; electronic devices; cryo-electronics; device fabrication technology; device characterization; and circuits and signal processing.

20 DISTRIBUTION / AVAILABILITY OF ABSTRACT ☒ UNCLASSIFIED/UNLIMITED ☐ SAME AS RPT ☐ DTIC USERS	21 ABSTRACT SECURITY CLASSIFICATION
22a NAME OF RESPONSIBLE INDIVIDUAL Jarus W. Quinn	22b TELEPHONE (Include Area Code) 202/223-8130 22c OFFICE SYMBOL

DD Form 1473, JUN 86 Previous editions are obsolete

SECURITY CLASSIFICATION OF THIS PAGE

UNCLASSIFIED

TOPICAL MEETING ON PICOSECOND ELECTRONICS AND OPTOELECTRONICS

Summaries of papers presented at the Picosecond Electronics and Optoelectronics Topical Meeting

January 14–16, 1987

Incline Village, Nevada

Conference Edition

Sponsored by the

Air Force Office of Scientific Research

Lasers and Electro-Optics Society of the Institute of Electrical and Electronics Engineers

National Science Foundation

Office of Naval Research

Optical Society of America

In cooperation with

Electron Devices Society and Microwave Theory and Techniques Society of the Institute of Electrical and Electronics Engineers

Optical Society of America
1816 Jefferson Place, N.W.
Washington, DC 20036
(202) 223-8130

Articles in this publication may be cited in other publications. In order to facilitate access to the original publication source, the following form for the citation is suggested:

> Name of Author(s), Title of Paper, Picosecond Electronics and Optoelectronics Technical Digest, 87-1 (Optical Society of America, Washington, D.C. 1987) pp. [xx]-[xx].

ISBN Number
Conference Edition 0-936659-16-5
Postconference Edition 0-936659-36-X

Library of Congress Catalog Card Number
Conference Edition 86-063502
Postconference Edition 86-063501

IEEE Catalog Number 87TH0172-7

This material is based upon work supported by the National Science Foundation under Grant ECS8616911. Any opinions, findings, and conclusions or recommendations expressed in this publication are those of the author(s) and do not necessarily reflect the views of the National Science Foundation.

This work relates to Department of the Navy Task 4143010—01 issued by the Office of Naval Research. The United States Government has a royalty-free license through the work in all copyrightable material contained herein.

TABLE OF CONTENTS

TUESDAY, JANUARY 13, 1987

LOWER LOBBY/SIERRA

6:00 PM-9:00 PM REGISTRATION/REFRESHMENTS

WEDNESDAY, JANUARY 14, 1987

LOWER LOBBY

8:00 AM-5:00 PM REGISTRATION/SPEAKER CHECK-IN

SIERRA ROOM

8:00 AM-8:45 AM CONTINENTAL BREAKFAST

PROSPECTOR/RUBICON ROOM

8:45 AM-9:00 AM
OPENING REMARKS
Chi H. Lee, *U. Maryland* and Frederick J. Leonberger, *United Technologies Research Center, Meeting Cochairs*

PROSPECTOR/RUBICON ROOM

9:00 AM-10:30 AM
WA OPTICAL PROBING OF INTEGRATED CIRCUITS
R. K. Jain, *Amoco Research Center, Presider*

9:00 AM (Invited Paper)
WA1 Noncontact Picosecond Prober for Integrated Circuit Testing, J. A. Valdmanis, S. S. Pei, *AT&T Bell Laboratories.* We describe a noncontact substrate-independent integrated-circuit prober, based on electrooptic sampling, for internal node characterization of picosecond electrical waveforms at the wafer level. (p. 4)

9:30 AM (Invited Paper)
WA2 Picosecond Sampling of Integrated Circuits, M. J. W. Rodwell, K. J. Weingarten, D. M. Bloom, *Stanford U.* Electrooptic sampling provides wide bandwidth measurements of the internal voltages of GaAs ICs. We discuss limitations to bandwidth and sensitivity, and present recent results. (p. 7)

10:00 AM
WA3 Picosecond Electrical Pulses for VLSI Electronics Characterization, J.-M. Halbout, P. G. May, M. B. Ketchen, G. P. Li, C.-C. Chi, M. Scheuermann, M. Smyth, *IBM T. J. Watson Research Center.* Picosecond electrical pulses are photoconductively generated and characterized on structures and materials compatible with silicon VLSI electronics. (p. 10)

WEDNESDAY, JANUARY 14, 1987 — *Continued*

10:15 AM
WA4 Electrooptic Sampling of High-Speed InP-Based Integrated Circuits, J. M. Wiesenfeld, R. S. Tucker, A. Antreasyan, C. A. Burrus, *AT&T Bell Laboratories;* A. J. Taylor, *Los Alamos National Laboratory.* Multigigahertz waveforms in an InGaAs/InP MISFET inverter circuit have been sampled noninvasively using pulses from a gain-switched InGaAsP laser. Propagation delays of 21 ps per MISFET stage have been measured. (p. 12)

SIERRA ROOM

10:30 AM-11:00 AM *COFFEE BREAK*

PROSPECTOR/RUBICON ROOM

11:00 AM-12:30 PM
WB HIGH-SPEED LOGIC
D. A. B. Miller, *AT&T Bell Laboratories, Presider*

11:00 AM (Invited Paper)
WB1 Molecular Beam Epitaxy for High-Speed Devices, A. Y. Cho, *AT&T Bell Laboratories.* Recent development in molecular beam epitaxy pushes the frontier of devices to the ultimate imagination of device physicists and engineers. High-speed devices prepared with epitaxial superlattice structure or multiquantum wells and pseudomorphic strained layers are discussed. (p. 16)

11:30 AM
WB2 Multigigahertz Logic Based on InP MISFETs Exhibiting Extremely High Transconductance, A. Antreasyan, P. A. Garbinski, V. D. Mattera, Jr., H. Temkin, *AT&T Bell Laboratories.* We report high-speed logic at 5.0 GHz based on novel, enhancement mode InP metal-insulator-semiconductor field-effect transistors having a propagation delay of 25 ps/stage and transconductances of 320 mS/mm for a gate length of 1 μm. These measurements are the smallest propagation delay and the highest transconductance measured with a field-effect transistor on an InP substrate. (p. 19)

11:45 AM
WB3 Optically Strobed Sample and Hold Circuit, Chuck McConaghy, *Lawrence Livermore National Laboratory.* A GaAs sample and hold circuit with a 10-ps aperture time and 1-μs hold time has been built and used to sample single shot signals. (p. 22)

12:00 M (Invited Paper)
WB4 High-Speed Optical Logic using GaAs, H. M. Gibbs, N. Peyghambarian, Y. H. Lee, *U. Arizona;* J. L. Jewell, *AT&T Bell Laboratories;* A. Migus, A. Antonetti, *Ecole Polytechnique-ENSTA, France;* D. Hulin, A. Mysyrowicz, *Ecole Normale Superieure, France.* A bulk-GaAs nonlinear etalon can make a decision in $\cong 1$ ps and recover to make another in < 100 ps, making possible high-speed optical logic. (p. 25)

12:30 PM-2:00 PM LUNCH BREAK

PROSPECTOR/RUBICON ROOM

2:00 PM–3:30 PM
WC HIGH-SPEED AND MICROWAVE DEVICES: 1
C. Stolte, *Hewlett-Packard, Presider*

2:00 PM (Invited Paper)
WC1 Millimeter-Wave Integrated Circuits, B. E. Spielman, *U.S. Naval Research Laboratory.* This paper summarizes the technical issues, current research focal points, progress, and trends associated with GaAs and InP based monolithic millimeter-wave integrated circuit technology. (p. 30)

2:30 PM
WC2 Enhanced Performance Ultrabroadband Distributed Amplifiers, G. Zdasiuk, M. Riaziat, R. LaRue, C. Yuen, S. Bandy, *Varian Research Center.* High-gain 2–20-GHz monolithic GaAs distributed amplifiers utilizing novel circuit approaches such as cascade-connected FETs and coplanar waveguide transmission lines are described. Preliminary results on a HEMT-based amplifier are also presented. (p. 33)

2:45 PM (Invited Paper)
WC3 High Performance Quarter-Micron-Gate MODFETs, John J. Berenz, *TRW Electronic Systems Group.* This paper summarizes the latest results obtained with high performance quarter-micron-gate MODFETs used in rf applications. Results for both AlGaAs/GaAs and AlGaAs/InGaAs heterostructures are presented and compared. A projection of future performance achievements is given based on anticipated improvements in materials and fabrication technology. (p. 37)

3:15 PM
WC4 Picosecond Photoconductive Transceivers, Alfred P. DeFonzo, Charles Lutz, Madhuri Jarwala, *U. Massachusetts.* We present the results of a study of picosecond electromagnetic transients generated and detected by photoconductivity in ion bombarded SOS, radiated and received by tapered slot traveling wave antennas. (p. 40)

SIERRA ROOM

3:30–4:00 PM COFFEE BREAK

WEDNESDAY, JANUARY 14, 1987 — *Continued*

PROSPECTOR/RUBICON ROOM

4:00 PM–5:15 PM
WD CRYOELECTRONICS
S. M. Faris, *Hypres, Inc., Presider*

4:00 PM (Invited Paper)
WD1 Photoconductive Generation of Subpicosecond Electrical Pulses and their Measurement, D. R. Grischkowsky, C.-C. Chi, I. N. Duling III, W. J. Gallagher, N. J. Halas, J.-M. Halbout, M. B. Ketchen, *IBM T. J. Watson Research Center.* Experimental and theoretical results exploring the fundamental limits to the generation of ultrashort electrical pulses via photoconductive switching are discussed. Measurement applications demonstrating terahertz spectroscopy and subpicosecond electronics with the subpicosecond electrical pulses are presented. (p. 44)

4:30 PM (Invited Paper)
WD2 Progress and Challenges in HEMT LSI Technology, Masayuki Abe, Takashi Mimura, Kazuo Kondo, Masaaki Kobayashi, *Fujitsu Laboratories, Ltd., Japan.* A high electron mobility transistor is a promising device for ultrahigh speed LSI/VLSI, especially operating at 77 K. Recent progress and technical challenges in HEMT LSI technology are discussed. (p. 46)

5:00 PM
WD3 Picosecond Switching in Josephson Tunnel Junctions, R. Sobolewski, D. R. Dykaar, T. Y. Hsiang, G. A. Mourou, *U. Rochester.* We have developed a superconducting electrooptic sampler and used it to probe the switching of a 30 × 30-μm Josephson tunnel junction. (p. 49)

5:15 PM BREAK

SIERRA ROOM

5:30 PM–7:00 PM
WE POSTER SESSION/REFRESHMENTS

WE1 High-Speed High-Repetition-Rate High-Voltage Photoconductive Switching, William R. Donaldson, *U. Rochester.* We describe robust silicon photoconductive switches which have been operated for several million shots at 1 kHz switching 10 kV in 100 ps without failure. The switches are characterized to maintain the photoconductive state. (p. 54)

WE2 Generation and Forming of Ultrashort High Voltage Pulses, Hrayr A. Sayadian, S. T. Feng, J. Goldhar, Chi H. Lee, *U. Maryland.* Picosecond multikilovolt pulses are generated using coaxial, microstrip, and coplanar pulse forming networks. A longitudinal Pockels effect is used to monitor the ultrashort pulses. (p. 57)

WE3 Graphite as a Picosecond Laser Activated Opening Switch, E. A. Chauchard, Chi H. Lee, *U. Maryland;* C. Y. Huang, *Los Alamos National Laboratory;* A. M. Malvezzi, *Harvard U.* Highly oriented pyrolytic graphite exhibiting a high conductivity in the dark and a high resistivity when illuminated by intense laser light was used as an opening switch. (p. 60)

WE4 Simple Technique to Generate and Gate Microwave Pulses with Picosecond Speeds, Walter Margulis, *KTH, Sweden;* Vytas Grivitskas, *Vilnius State U., U.S.S.R.;* E. Adomaitis, Z. Dobrovolskis, A. Krotkus, *Lithuanian Academy of Sciences, U.S.S.R.* A simple ultrafast optoelectronic arrangement is described, enabling switching a number of cycles from a microwave generator, or shaping a microwave pulse with picosecond speed. (p. 63)

WE5 Proposed Quantum-Well Injection Transit Time Device, Vijay P. Kesan, Dean P. Neikirk, Ben G. Streetman, *U. Texas at Austin.* A new transit time device that uses resonant tunneling through a quantum well is proposed and analyzed. It permits varying injection phase delays, with a wide frequency range of operation and low noise performance. It also promises better output power than quantum-well oscillators. (p. 66)

WE6 Modulation Efficiency Limited High Frequency Performance of the MODFET, M. C. Foisy, J. C. Huang, P. J. Tasker, L. F. Eastman, *Cornell U.* Inefficient charge control is a primary degrading mechanism in high frequency MODFET operation. Numerical simulations illuminate the ramifications of varying each epilayer design parameter. (p. 69)

WE7 Characteristics of Shielded Microstrip Lines on GaAs-Si at Millimeter-Wave Frequencies, M. I. Aksun, H. Morkoc, *U. Illinois at Urbana-Champaign.* GaAs on Si has attracted a great deal of interest. This is in part due to its potential use for microwave monolithic integration. Here we report the first theoretical study of dielectric losses of this composite material. (p. 72)

WE8 Nonequilibrium Phonons and Disorder in $Al_xGa_{1-x}As$, J. A. Kash, J. C. Tsang, S. S. Jha, *IBM T. J. Watson Research Center.* Despite alloy disorder, picosecond Raman measurements show significant nonequilibrium phonon effects in $Al_xGa_{1-x}As$. The virtual crystal approximation is shown to apply. Implications for heterojunction devices are considered. (p. 76)

WE9 Photoconductive Picosecond Microstripline Switches on Self-Implanted Silicon on Sapphire, Penny Polak-Dingels, Geoffrey Burdge, *Laboratory for Physical Sciences;* Chi H. Lee, *U. Maryland;* Alan Seabaugh, Richard Brundage, Michael Bell, John Albers, *U.S. National Bureau of Standards.* Silicon-on-sapphire switches, damaged by Si implantation at fluence levels of 10^{13} to 10^{15} cm^{-2}, were characterized by picosecond cross-correlation, Raman and resistivity measurements. (p. 79)

WE10 Fast GaAs Photoconductive Detectors with High Sensitivity Integrated in Coplanar Systems onto GaAs Substrates, H. Schumacher, U. Salz, H. Beneking, *Aachen U. Technology, F. R. Germany.* An interdigitated photoconductive detector with fingers 1.5 μm wide has been developed for optoelectronic correlation measurements. The very sensitive device fabricated onto s.i. GaAs and integrated in a coplanar line exhibits switching times of ≈ 5 ps. (p. 82)

WEDNESDAY, JANUARY 14, 1987 — *Continued*

WE11 Carrier Lifetime vs Ion-Implantation Dose in Silicon on Sapphire, F. E. Doany, D. R. Grischkowsky, C.-C. Chi, *IBM T. J. Watson Research Center.* We present measurements of the carrier lifetime of a systematic series of silicon-on-sapphire samples over a range of more than 4 orders of magnitude of O^+ ion implantation. (p. 86)

WE12 Picosecond Optoelectronic Switches using Composite Electronic Materials, E. A. Chauchard, Chi H. Lee, *U. Maryland;* V. Diadiuk, G. W. Turner, *MIT Lincoln Laboratory.* Two composite picosecond optoelectronic switches have been investigated. GaAs on silicon-on-sapphire exhibits a 20-ps response while InGaAs on InP shows a strong dependence of its response time on bias voltages. (p. 89)

WE13 Comparison of Sampling Oscilloscopes with < 35-ps Transition Durations, James R. Andrews, *Picosecond Pulse Laboratories, Inc.* A 17-ps tunnel diode pulser was used to measure the transient responses of HP 1430, Tek S4, Tek S6, PSPL S-1430D, and Iwatsu SH-4B sampling oscilloscopes. (p. 92)

WE14 Wing Suppressed IR Sampling: a Technique, John Nees, Steve Williamson, *U. Rochester.* An experiment demonstrating the feasibility of using optical frequency doubling as a tool for wing suppression in infrared sampling experiments is described. (p. 95)

WE15 High-Speed Optical Isolator for Radar Applications, J. P. Anthes, P. Garcia, *Sandia National Laboratories;* K. Y. Lau, I. Ury, *Ortel Corporation.* A high-speed unidirectional electronic coupler/switch that utilizes optoelectronic components is demonstrated. High attenuation of counter propagating radar signals offers improved radar performance. (p. 97)

WE16 Energy Variations in Optical Pulses from Gain-Switched AlGaAs Diode Lasers, R. T. Hawkins, J. H. Goll, N. A. Anheier, *Tektronix, Inc.* Optical pulses from gain-switched AlGaAs diode lasers, measured with a low noise CCD detector, are reported to have energy variation < 1% rms for pulse durations < 60 ps. (p. 100)

THURSDAY, JANUARY 15, 1987

LOWER LOBBY

7:30 AM–12:00 M REGISTRATION/SPEAKER CHECK-IN

SIERRA ROOM

7:30 AM–8:00 AM CONTINENTAL BREAKFAST

PROSPECT/RUBICON ROOM

8:00 AM–9:45 AM
ThA LASERS AND DETECTORS
V. Diadiuk, *MIT Lincoln Laboratory, Presider*

8:00 AM (Invited Paper)
ThA1 Characteristics, Packaging and Physics of Ultra-high-Speed Diode Lasers and Detectors, J. E. Bowers, C. A. Burrus, *AT&T Bell Laboratories.* High-speed semiconductor lasers provide an efficient compact means of generating short tunable high power pulses. InGaAsP waveguide photodetectors have demonstrated high speed and high efficiency at zero bias. (p. 104)

8:30 AM
ThA2 Frequency Chirping in Pulse Modulated Gain and Real-Index Guided Single Quantum-Well Lasers, A. Larsson, P. Andersson, *Chalmers U. Technology, Sweden;* Amnon Yariv, *California Institute of Technology.* We report on a small frequency chirp in pulse modulated real-index guided single quantum-well lasers and a strong influence of the guiding mechanism. (p. 107)

8:45 AM
ThA3 InP/GaInAs/InP PIN Photodiode with FWHM < 18 ps, S. Y. Wang, K. W. Carey, B. H. Kolner, *Hewlett-Packard Laboratories.* High-speed front-side illuminated InP/GaInAs/InP PIN 1–1.6-μm photodetectors have been fabricated from material grown by atmospheric pressure organometallic vapor-phase epitaxy. The devices have external quantum efficiencies of >85% at 1.3 μm and the temporal response has a full width half maximum of < 18 ps. Dark current density is 6×10^{-6} A cm^{-2} at the operating bias of -4 V. The interface is abrupt to two monolayers at the InP (substrate)-GaInAs heterojunction and five monolayers at the GaInAs/InP *p*-layer heterojunction. (p. 110)

9:00 AM
ThA4 Picosecond Measurements of Gain Switching in a Semiconductor Laser Driven by Ultrashort Electrical Pulses, P. M. Downey, J. E. Bowers, R. S. Tucker, J. M. Wiesenfeld, *AT&T Bell Laboratories.* An InGaAsP laser, biased near threshold, is driven by 17-ps wide electrical pulses. Gain-switched pulses as short as 15-ps FWHM have been observed. (p. 113)

THURSDAY, JANUARY 15, 1987 — *Continued*

9:15 AM
ThA5 MESFET Compatible IMSM Detectors, D. L. Rogers, *IBM T. J. Watson Research Center.* A new type of interdigitated metal-semiconductor-metal detector is described using a shallow implant to limit surface trapping making it compatible with refractory gate MESFET processes. (p. 116)

9:30 AM
ThA6 Picosecond Optical Autocorrelation Experiments on Fast Photodetectors, T. F. Carruthers, J. F. Weller, *U.S. Naval Research Laboratory.* The nonlinear component of the output of many picosecond photodetectors can be used to measure their intrinsic response times without resorting to cross-correlation circuits. (p. 121)

SIERRA ROOM

9:45 AM–10:15 AM COFFEE BREAK

PROSPECTOR/RUBICON ROOM

10:15 AM–12:00 M
ThB TRANSIENT TRANSPORT
J. Frey, *Cornell U., Presider*

10:15 AM (Invited Paper)
ThB1 Direct Subpicosecond Measurement of Carrier Mobility of Photoexcited Electrons in GaAs, Martin C. Nuss, David H. Auston, *AT&T Bell Laboratories.* The carrier mobility of photoexcited hot electrons is measured directly for the first time on a subpicosecond time scale using femtosecond electrical pulses. (p. 126)

10:45 AM (Invited Paper)
ThB2 Nonstationary Transport in MODFETs and Heterojunction Devices, K. Hess, *U. Illinois.* New horizons have opened up in semiconductor research with the possibility of band gap engineering and the combination of signal transport by photons as well as electrons in new forms of ultrathin III-V compound layers. We report self-consistent simulations of transient transport processes in single layer and single quantum-well modulation doped structures. Our simulations of picosecond and femtosecond thermalization after optical excitation are also reported and a comparison of our results with the experiments of Knox *et al.* is given. (p. 129)

11:15 AM
ThB3 Monte Carlo Investigation of Hot Photoexcited Electron Relaxation in GaAs, M. A. Osman, M. J. Kann, D. K. Ferry, *Arizona State U.;* P. Lugli, *U. Modena, Italy.* The relaxation of hot photoexcited electrons is investigated in GaAs using an ensemble Monte Carlo approach, taking into account both the electron–hole interaction and the hot photon effect. Immediately after excitation by a 588-nm laser pulse, a considerable fraction of electrons transfers to the upper valleys instead of cascading down the central valley. (p. 130)

11:30 AM
ThB4 Longitudinally Localized Optical Carrier Injection for Femtosecond Transport Studies, M. C. Downer, D. H. Reitze, T. R. Zhang, *U. Texas at Austin.* A novel technique for confining optical carrier excitation within a few hundred angstroms of a semiconductor surface opens new possibilities for observing ballistic, quantum, and other femtosecond transport phenomena. (p. 133)

11:45 AM
ThB5 Femtosecond Nonequilibrium Electronic Heat Transport in Thin Gold Films, S. D. Brorson, J. G. Fujimoto, Erich P. Ippen, *Massachusetts Institute of Technology.* Using a front pump/back probe technique, we have observed ultrafast heat transport through thin gold films. Our results suggest transport occurs via nonequilibrium electrons. (p. 136)

12:00 M BREAK

LAKESIDE ROOM

6:00 PM–7:00 PM DINNER

SIERRA ROOM

7:00 PM–7:30 PM COFFEE/DESSERT

LOWER LOBBY

7:00 PM–9:00 PM SPEAKER CHECK-IN

PROSPECTOR/RUBICON ROOM

7:30 PM–9:00 PM
ThC BALLISTIC TRANSPORT AND RESONANT TUNNELING
S. Luryi, *AT&T Bell Laboratories, Presider*

7:30 PM (Invited Paper)
ThC1 Ballistic Transport in Tunneling Hot Electron Transfer Amplifier Devices, M. Heiblum, *IBM T. J. Watson Research Center.* An unambiguous demonstration of ballistic (collisionless) electron transport was done in GaAs with the aid of a THETA device. Consequently, interesting quantum related phenomena were observed. Ballistic devices are potentially very fast; current gains as high as 10 have already been measured at 77 K. (p. 140)

THURSDAY, JANUARY 15, 1987 — *Continued*

8:00 PM (Invited Paper)
ThC2 Microwave- and Millimeter-Wave Resonant Tunneling Diodes, T. C. L. Gerhard Sollner, Elliott R. Brown, W. D. Goodhue, *MIT Lincoln Laboratory.* Several demonstrated resonant tunneling devices including oscillators, mixers, multipliers, and a variable negative resistance are discussed. Techniques of the millimeter/submillimeter regime are also described. (p. 143)

8:30 PM
ThC3 Quantum Transport Calculation of Resonant-Tunneling Response Time, William R. Frensley, *Texas Instruments, Inc.* The transient response of a resonant-tunneling diode is simulated by calculating the Wigner distribution. Switching times on the order of 100 fs are obtained. (p. 146)

8:45 PM
ThC4 Resonant Tunneling Electron Spectroscopy, F. Capasso, S. Sen, A. Y. Cho, A. L. Hutchinson, *AT&T Bell Laboratories.* We have demonstrated a new electron spectroscopy technique based on resonant tunneling. Direct information on the hot electron distribution function is obtained from the measured resonant tunneling collector current without requiring the use of derivative techniques. (p. 149)

PROSPECTOR/RUBICON ROOM

9:00 PM
ThD POSTDEADLINE PAPERS

FRIDAY, JANUARY 16, 1987

LOWER LOBBY

7:30 AM–2:45 PM REGISTRATION/SPEAKER CHECK-IN

SIERRA ROOM

7:30 AM–8:00 AM CONTINENTAL BREAKFAST

PROSPECTOR/RUBICON ROOM

8:00 AM–9:30 AM
FA QUANTUM-WELL PHYSICS AND DEVICES
C. Weisbuch, *Thomson CSF, Presider*

8:00 AM (Invited Paper)
FA1 High-Speed Phenomena in GaAs Quantum Wells, A. Mysyrowicz, D. Hulin, A. Migus, A. Antonetti, *ENSTA, France;* H. M. Gibbs, N. Peyghambarian, *U. Arizona;* H. Morkoc, *U. Illinois at Urbana.* We discuss different optical phenomena ocurring within a few picoseconds after irradiation of GaAs multiple-quantum-well structures with femtosecond laser pulses. (p. 156)

8:30 AM (Invited Paper)
FA2 Picosecond Carrier Transport in GaAs Quantum Wells, Jagdeep Shah, *AT&T Bell Laboratories.* I discuss recent experiments in which picosecond optical pulses were used to investigate the physics of high field transport in GaAs quantum wells. (p. 159)

9:00 AM
FA3 Quantum-Confined Stark Effect in InGaAs/InP Quantum Wells Grown by Metalorganic Chemical Vapor Deposition, I. Bar-Joseph, C. Klingshirn, D. A. B Miller, Daniel S. Chemla, U. Koren, B. I. Miller, *AT&T Bell Laboratories.* Large shifts of absorption spectrum in InGaAs/InP multiple quantum wells with applied electric fields are reported. Applications for light modulators are discussed. (p. 162)

9:15 AM
FA4 Dynamics of Below-Gap Photoexcitation in GaAs Quantum Wells, J. E. Zucker, Daniel S. Chemla, *AT&T Bell Laboratories;* A. Von Lehmen, J. P. Heritage, *Bell Communications Research, Inc.* Time-resolved transmission experiments in GaAs quantum wells show that photoexcitation in the transparent region of the heterostructure can produce a striking variety of excitonic effects. (p. 166)

SIERRA ROOM

9:30 AM–10:00 AM COFFEE BREAK

FRIDAY, JANUARY 16, 1987 — *Continued*

PROSPECTOR/RUBICON ROOM

10:00 AM–11:45 AM
FB OPTICAL MICROWAVE TECHNIQUES
R. Olshansky, *GTE Laboratories, Presider*

10:00 AM (Invited Paper)
FB1 Radar and EW Applications of Multigigahertz Optical Components and Systems, Henry F. Taylor, *Texas A&M U.* Optical techniques for the generation, control, transmission, and processing of wideband signals in military systems are discussed. (p. 170)

10:30 AM (Invited Paper)
FB2 Characteristics and Applications of Wideband Guided-Wave Devices, C. M. Gee, G. D. Thurmond, H. W. Yen, *Hughes Research Laboratories.* Design and fabrication of wideband and high-speed guided-wave electrooptic and electroabsorption devices are reviewed. Their applications in rf fiber-optic links are presented. (p. 173)

11:00 AM
FB3 Optoelectronic cw Microwave Source, C. J. Clark, E. A. Chauchard, K. Webb, K. Zaki, C. H. Lee, *U. Maryland;* Penny Polak-Dingles, *Laboratory for Physical Sciences;* H.-L. A. Hung, Ho C. Huang, *COMSAT Laboratories.* A new cw microwave source which can be time-synchronized with laser pulses is described. Its phase noise of 3.5-ps is attributed primarily to the laser time jitter. (p. 176)

11:15 AM
FB4 Optical Modulation above 20 GHz using a Waveguide Electrooptic Switch, S. K. Korotky, G. Eisenstein, R. S. Tucker, J. J. Veselka, G. Raybon, *AT&T Bell Laboratories.* We report the intensity modulation of an optical carrier at frequencies above 20 GHz using a Ti:$LiNbO_3$ optical waveguide switch. A self electrooptic sampling technique is used to observe the modulation. (p. 179)

11:30 AM
FB5 Picosecond Response of an Optically Controlled Millimeter Wave Phase Shifter, C.-K. C. Tzuang, D. Miller, T.-H. Wang, T. Itoh, D. P. Neikirk, P. Williams, M. Downer, *U. Texas at Austin.* The dispersion of a picosecond pulse propagating along a coplanar waveguide on a semiconductor substrate is studied. Numerical calculations are used to predict the pulse shape for varying carrier concentrations in a multilayer AlGaAs/GaAs/AlGaAs structure. (p. 182)

11:45 AM–1:30 PM LUNCH BREAK

FRIDAY, JANUARY 16, 1987 — *Continued*

PROSPECTOR/RUBICON ROOM

1:30 PM–2:45 PM
FC HIGH-SPEED AND MICROWAVE DEVICES: 2
G. Burdge, *Laboratory for Physical Sciences, Presider*

1:30 PM (Invited Paper)
FC1 Electron Device Probing in the Femtosecond Time Scale, Gerard A. Mourou, *U. Rochester.* Femtosecond optical techniques have been used to time resolve electrical waveforms with femtosecond resolution or terrahertz bandwidth. They have been used to study the response of ultrafast components such as MESFET, MODFET, permeable base device Josepheson junction, and normal or superconducting transmission lines and more recently transient transport in semiconductors such as velocity overshoot and resonant tunneling. Present and future roles of optical techniques in electronics from a device characterization and physics point of view are discussed. (p. 186)

2:00 PM
FC2 Electrical Pulse Compression by Traveling-Wave Photoconductivity, David H. Auston, Martin C. Nuss, P. R. Smith, *AT&T Bell Laboratories.* A novel technique is described for compressing picosecond electrical pulses by reflecting them from a moving mirror produced by a traveling wave photoconductor having a velocity close to the electrical propagation velocity. (p. 188)

2:15 PM
FC3 Picosecond Optoelectronic Study of a Thin Film Transmission Line Structure, G. Arjavalingam, J.-M. Halbout, G. V. Kopcsay, M. B. Ketchen, *IBM T. J. Watson Research Center.* Using photoconductively generated picosecond electrical pulses the properties of a transmission line structure consisting of coupled microstrip lines separated from a ground plane by a thin insulator layer are studied. In addition to the distortion of the transmitted pulses, the near- and far-end coupled noise are characterized with picosecond resolution. (p. 191)

2:30 PM
FC4 Silicon Pulse Sharpening Diodes: Switching Kilovolts in Tens of Picoseconds, M. D. Pocha, J. D. Wiedwald, C. G. Dease, M. M. Contreras, *Lawrence Livermore National Laboratory.* Silicon diodes, operating in avalanche second breakdown, are used to generate electrically triggered, 2-3-kV pulses with rise times approaching 60 ps. (p. 194)

2:45 PM CLOSING REMARKS
Federico Capasso, *AT&T Bell Laboratories* and
Hadis Morkoc, *U. Illinois at Urbana,*
Meeting Program Cochairs

WEDNESDAY, JANUARY 14, 1987

PROSPECTOR/RUBICON ROOM
8:45 A.M.–9:00 A.M.

OPENING REMARKS

Chi H. Lee, University of Maryland
and
Frederick J. Leonberger, United Technologies Research Center
Meeting Cochairs

NOTES

WEDNESDAY, JANUARY 14, 1987

PROSPECTOR/RUBICON ROOM
9:00 A.M.–10:30 A.M.

WA1–4

OPTICAL PROBING OF INTEGRATED CIRCUITS

R. K. Jain, Amoco Research Center, *Presider*

A Non-Contact Picosecond Prober for Integrated Circuit Testing

J.A. Valdmanis and S.S. Pei
AT&T Bell Laboratories, 600 Mountain Ave., Murray Hill, NJ 07974

Electro-optic sampling has been used extensively for the charaterization of picosecond electronic devices such as photodetectors, transistors, and diodes [1,2]. For the large part, these studies have been with discrete devices coupled to specialized electro-optic modulators in a hybrid electrode geometry. However, there is great interest in being able to probe internal points on integrated circuits. Recently, a specialized embodiment of electro-optic sampling [3] was developed to exploit the electro-optic properties of GaAs and perform sampling directly in the substrate of GaAs integrated circuits. Any internal point of the circuit could be accessed and individual devices could be monitored in their working environment. However, GaAs is the only commonly used electronic material that is also electro-optic. The substrate technique also requires that both surfaces of the integrated circuit be optically polished and that the sampling laser beam has a photon energy below the band gap of the substrate material. One would ideally like a non-perturbative means of probing with high temporal and spatial resolution that is *generally* applicable to circuits fabricated on any type of substrate.

We have developed a new electro-optic prober that satisfies many of the above mentioned requirements. We have demonstrated a temporal resolution of $\sim$30 ps and a spatial resolution of a few microns with sensitivity more than adequate to clearly resolve logic level changes of less than one volt. The system can be used with any high repetition rate mode-locked laser throughout the visible and near infra-red wavelength regimes.

Our system is based on the use of an extremely small electro-otpic probing tip employed as the modulator in a conventional electro-optic sampling system (see Fig.1). The probe tip concept relies on the fact that for two dimensional circuits, not all the electric field lines are contained in the substrate material. Because of the open structure, there exists a fringing field above the surface of the circuit near the metalization lines. By merely "dipping" the electro-optic tip into a region of fringing field, high speed signals can be measured with minimal effect on the circuit performance. The electric field induces a birefringence change in the tip which is then sampled from above by the optical beam. As depicted in Fig. 1, we use a 100 micron thick piece of lithium tantalate bonded to a short (7mm by 3mm diam.) fused silica rod for support. The z-axis of the lithium tantalate is in the plane of the tip face. The tip is polished as a four sided pyramid with a half angle of 30 degrees and tip size of 40 microns square. A high reflectance coating is evaporated onto the tip face so that the sampling beam beam can be reflected back to the optical system. A 10X microscope objective is used to both focus the sampling beam onto the tip face and recollimate the reflected beam. In this geometry we get a spot size of $\sim$5 microns which determines the spatial resolution of the system.

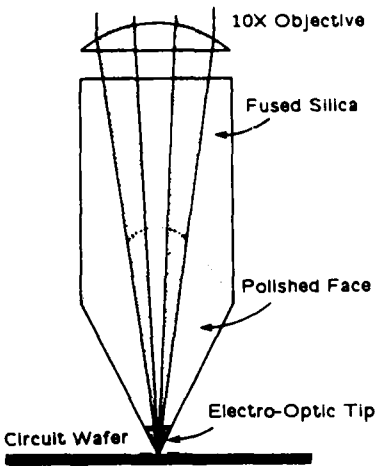

Fig. 1. The electro-optic probe

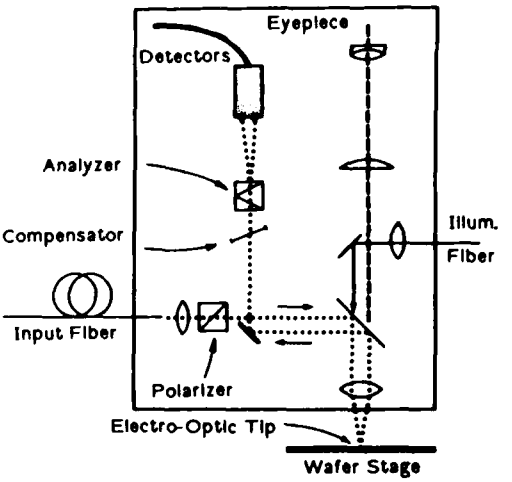

Fig. 2. Schematic of the prober sampling system (not to scale)

The probe tip is situated in the optical sampling system as shown in Fig. 2. Sampling pulses ~100 fs long are generated by a compensated colliding pulse mode-locked ring (CPM) laser and are directed into the system via a polarization preserving single mode optical fiber and 20X microscope objective. The probe tip is mounted optically between crossed polarizers and below a dichroic beamsplitter in such a way as to facilitate viewing of tip face from above via a microscope system. Light of a wavelength different from that of the laser is injected through the beamsplitter, so that both the circuit and the sampling beam spot can be seen together. Quartz compensating plates are included between the polarizers to operate the modulator at one of the "zero-order" quarter wave points. A wollaston analyzer is used to separate orthogonal polarizations and direct the output to dual differential detectors. The detector output is then fed to a lock-in amplifier and signal averager.

The modulator, detector, and viewing arrangement are assembled on a small breadboard which is mounted vertically on a commercial automatic integrated circuit probe station. Such a station is designed to individually test each circuit at the wafer level. For conventional electronic testing, a "probe-card" is used which contains of a ring of fine metal finger probes that contact each circuit's bonding pads. Electrical signals are then applied through the fingers in order to test the basic circuit functions before dicing and bonding. The electro-optic probe system is mounted so the probe tip can be precisely lowered into position above the wafer and between the probe card fingers. In this way it enables the integrated circuit to be tested both by the conventional electronic method and simultaneously at internal points with the electro-optic probe. No special jigs or wafer preparation are required. Synchronization with the laser system can be achieved by driving the circuit testing rig with the RF signal derived from the laser repetition rate.

Our initial test of the system is the measurement of a picosecond electrical pulse traveling along a planar transmission line. The line is a simple waveguide structure having a center electrode 20 microns wide separated from broad ground planes on

either side by 6 micron gaps. Conventional chromium and gold electrodes were evaporated on a standard semi-insulating GaAs integrated circuit wafer. For this preliminary experiment the wafer was mounted between 35 GHz SMMA microwave connectors. The electrical pulse was generated by a 35 GHz GaAs photoconductive detector triggered by the second beam of the CPM laser. The electrical pulse was guided to the GaAs transmission line by a short length of flexible miniature coaxial cable. Relative delay for the sampling system was introduced by a standard motor driven optical delay line.

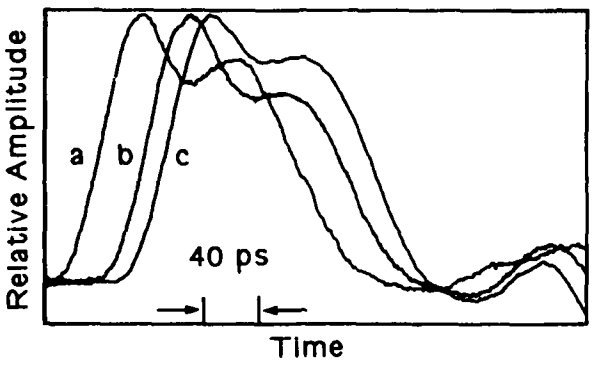

Fig. 3. Transmission line waveforms at a) 0 mm, b) 3.5 mm, and c) 5.0 mm. Propagation delays are 34.8 ps from a to b, and 15.6 ps from b to c.

Figure 3 shows the waveform measured at three successive points along the transmission line, 0 mm, 3.5 mm, and 5.0 mm. For these measurements the probe tip was lowered to within a micron of the surface directly over one of the 6 micron gaps and then translated parallel to the line. A risetime of 30 ps was measured along with a propagation speed of one third the speed of light in vacuum. The peak signal level was approximately one volt. By simply translating the probe tip in the plane of the wafer, it was very easy to characterize the electrical signal at any location. Signals of opposite polarities were clearly observed in each of the 6 micron gaps as well as the effects of dispersion and reflection. Similar test measurements have also been performed on glass and silicon substrates with comparable results.

Current experiments are centered on investigating picosecond signals at internal nodes of complete operational integrated circuits at the wafer level both in silicon and GaAs technologies.

[1] J.A. Valdmanis, *Subpicosecond electro-optic sampling*, Ph.D. dissertation, University of Rochester, Rochester, NY., Oct. 1983.

[2] J.A. Valdmanis and G.A. Mourou, Subpicosecond electrical sampling: principles and applications, *IEEE J. Quan. Elec.*, vol. QE-22-1, pp. 69-78, Jan. 1986.

[3] K.J. Weingarten, M.J.W. Rodwell, H.K. Heinrich, B.H. Kolner and D.M. Bloom, Direct electro-optic sampling of GaAs integrated circuits, *Elect. Lett.*, vol. 21-17, pp. 765-766, Aug. 1985.

Picosecond Sampling of Integrated Circuits

M.J.W. Rodwell, K.J. Weingarten, and D.M. Bloom

E.L. Ginzton Laboratory, Stanford University
Stanford, CA 94305

Introduction

GaAs microwave integrated circuits are now being developed for operation at frequencies as high as 40 GHz, while GaAs digital IC's have been demonstrated with ring-oscillator propagation delays of 5-10 ps, with gate delays of 50-100 ps for larger-scale circuits. Digital IC's are currently tested only by indirect techniques (multistage propagation delay or cycle times), while microwave circuits are tested only by external scattering parameter measurement; if the circuit does not perform to expectations, the cause is not easily identified. Electrooptic sampling, providing picosecond-resolution measurements of the voltages within the IC, permits more detailed circuit evaluation.

Sampling System

GaAs is electrooptic; the electric fields associated with conductor voltages induce optical birefringence, causing a small polarization change to a probe beam passing through these fields. For the longitudinal probing geometry, the change in polarization is proportional to the voltage across the substrate at the test point [1]. Electrooptic sampling is described in detail in the literature [2,3]; our system is shown in figure 1.

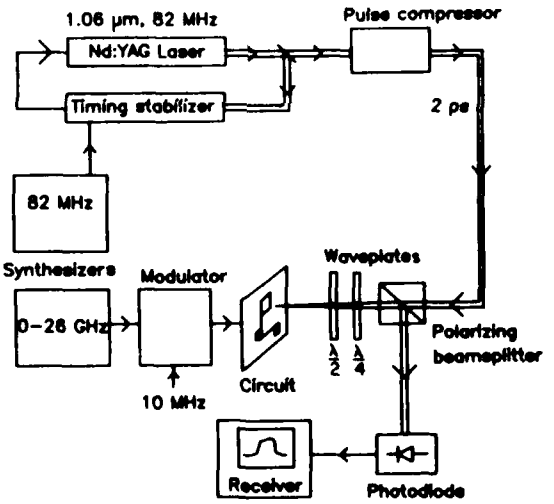

Figure 1: Electrooptic sampling system.

A Nd:YAG laser produces 1.06 μm, 100 ps pulses at an 82 MHz rate. The 3 ps rms timing fluctuations of the laser are reduced to 0.9 ps rms by a feedback system [4], and a fibre-grating pulse compressor shortens the pulses to 2 ps FWHM. The beam passes through a polarizing beamsplitter, two waveplates, and the IC substrate, and is focused to a 3 μm spot on the probed conductor (backside probing), or to a 10 μm spot on the ground plane adjacant to the probed conductor (frontside probing). The light is reflected, recollimated by the focusing lens, and directed through the polarizer onto a photodiode connected to a receiver. The external signal generator is tuned to an exact harmonic of the laser pulse repetition frequency, plus a small offset δf; the sampler then maps out the circuit waveform at this rate δf. The microwave excitation is modulated to allow synchronous detection at a high frequency, enhancing the system sensitivity.

Bandwidth and Noise Considerations

Several components influence the system's bandwidth and sensitivity; among these are the pulse compressor, the timing stabilizer, and the modulator/receiver combination. Timing jitter influences both bandwidth and sensitivity; the impulse response of the sampling system is the convolution of the optical pulse with the probability distribution of its arrival time (neglecting optical transit time), while those fourier components of the jitter lying within the integration bandwidth of the receiver introduce noise proportional to the time derivative of the measured waveform. Stabilization of the laser timing is thus imperative for low-noise measurement of high-frequency signals.

To accurately measure the shape of circuit waveforms, the impulse response of the system must be of short duration and free of "wings" (long-duration substructure). By using 1 km fiber in the compressor, significant group velocity dispersion is introduced, producing a more linear frequency chirp; the resulting compressed pulses are of 2 ps duration (fig 2) and are free of wings [5], and thus the pulse's spectrum is flat to 100 GHz (fig. 3).

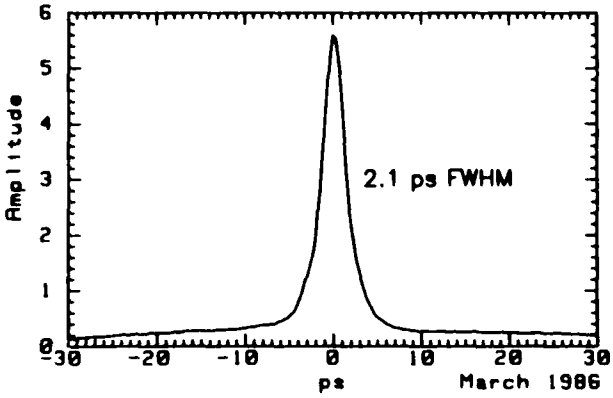

Figure 2: Compressed pulse autocorrelation.

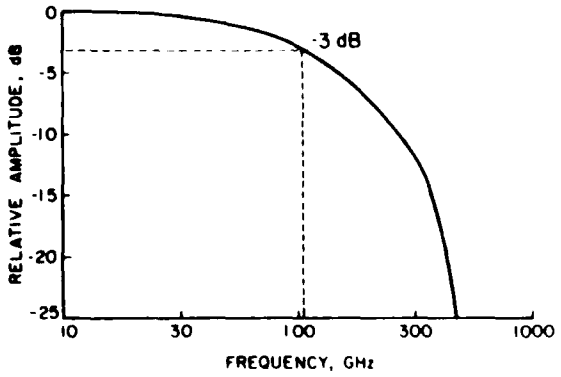

Figure 3: Pulse Fourier spectrum.

The pulse compressor generates excess noise due to Raman scattering. In contrast to shorter fibers, with the 1 km fiber we attain 50X compression at power levels (350 mW from fiber) below the Raman threshold. This occurs because self-phase-modulation occurs over the entire length of the fiber while the interaction length for stimulated Raman scattering is set dispersion-induced walkoff distance between the input and Raman-shifted wavelengths. The Raman threshold is further increased from 400 to 700 mW (1.06 μm power exiting fiber) by trimming the fiber length, avoiding a fiber round-trip transit time equal to a multiple of the Nd:YAG pulse repetition period, as this results in a parasitic fiber-Raman laser [6]. In addition to Raman scattering, the compressor generates broadband polarization noise, possibly arising from guided acoustic wave Brillioun scattering. Given correct adjustment of the compressor, its output intensity varies only to second order in the fiber polarization state; polarization drift in the fiber then results in first-order variations of intensity with polarization, and thus excess noise. An interim solution has been thermal stabilization of the fiber to suppress polarization drift.

Given adequate suppression of phase noise, Raman scattering, and polarization noise, the remaining noise is shot noise and laser low-frequency amplitude noise. To suppress the laser amplitude noise, we chop the input signal to the IC at 10 MHz, translating the measurement to a frequency above the laser 1/f noise corner frequency, where it is detected by a narrowband 10 MHz receiver; the resulting shot-noise-limited sensitivity is sufficient to acquire low-noise measurements at scan rates of 10-100 Hz. For sequential digital circuits, which will not operate correctly with chopped excitation, we use a small-deviation 10 MHz phase modulator; the received signal, proportional to the derivative of the sampled waveform, is integrated in software [7].

Circuit Applications

The sampler can be configured to emulate either a sampling oscilloscope, for waveform measurements, or a network analyzer, for transfer function measurements. Signal timing, risetimes, and propagation delays on a number of digital circuits have been measured [1,7]. On an 8-bit multiplexer, signals on interconnects as narrow as 2 μm were measured, including the serial output of the MUX and the timing of the 8-phase clock. A test structure consisting of a string of 20 buffered-FET-logic inverters was probed, permitting measurement of delays between inverters and between the FET's internal to individual inverters. The system has been applied to the extensive characterization of microwave amplifiers [8], including small-signal internal transfer

functions (fig. 4), and large-signal saturation behavior (fig. 5). In the network analyzer mode, measurements of transmission line standing wave ratio and field distribution have been made at frequencies as high as 40 GHz [9].

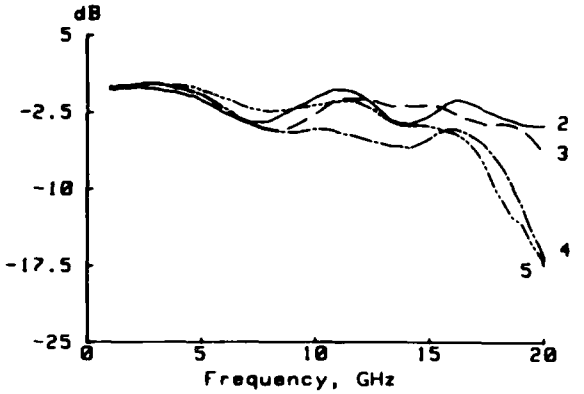

Figure 4: Small-signal gate voltages vs. frequency in a 5-FET 2-18 GHz distributed amplifier.

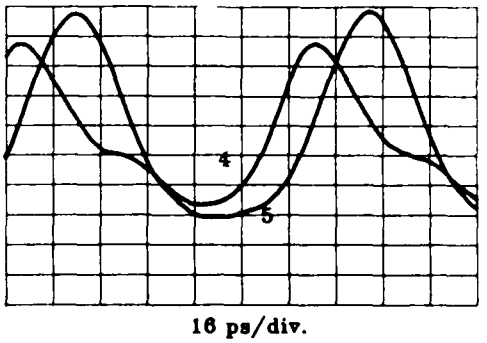

Figure 5: Saturation waveforms at drains 4 and 5 of the distributed amplifier at 10 GHz and 1 dB gain compression

Conclusions

With an 80 GHz bandwidth, a 3 μm spatial resolution, and a noise floor of 300 μV (1 Hz), the electrooptic sampling system is suitable for characterization of ultrafast digital and millimeter-wave analog GaAs IC's. With improvements in the optical pulse generation, the bandwidth can be extended past the millimeter-wave range (30-300 GHz); future use of this system will concentrate on the study of new picosecond/millimeter-wave GaAs structures and devices.

Acknowledgenents

We thank M. Riazait of Varian Associates, S. Swierkowski of Lawrence Livermore National Labs, and K.R. Gleason of TriQuint Semiconductor for their help with the GaAs IC's, and J. Kafka and T. Baer of Spectra-Physics, inc. for their guidance in the modification of the pulse compressor. This work was supported by the Air Force Office of Scientific Research under contract number F49620-85K-0016. M. Rodwell acknowledges an IBM fellowship, and K. Weingarten acknowledges a Newport Research award.

References

1. J.L. Freeman, S.K. Diamond, H. Fong, and D.M. Bloom, Appl. Phys. Lett., 47, 1083 (1985)

2. J.A. Valdmanis, G.A. Mourou, and C.W. Gabel, IEEE J. Quant. Elec., 19, 664 (1983)

3. J.A. Valdmanis and G.A. Mourou, IEEE J. Quant. Elec., 22, 69 (1986), B.H. Kolner and D.M. Bloom, ibid., 22, 79 (1986)

4. M.J.W. Rodwell, K.J. Weingarten, D.M. Bloom, T. Baer, and B.H. Kolner, to be published, Optics Lett., Oct. 1986

5. D. Grischowski and C.A. Balant, Appl. Phys. Lett., 41, 1982, pp. 1-2

6. M.N. Islam and L.F. Mollenauer, in Digest, 1986 Topical Meeting on Ultrafast Phenomena, June 16, Snowmass, Colorado.

7. M.J.W. Rodwell, K.J. Weingarten, J.L. Freeman, and D.M. Bloom, Electron. Lett., 22, 499 (1986)

8. M.J.W. Rodwell, M. Riaziat, K.J.Weingarten, B.A. Auld, and D.M. Bloom, in Digest, 1986 IEEE MTT-S International Microwave Symposium; also, to be published, IEEE J. of MTT, Nov. 1986

9. K.J. Weingarten, M.J.W. Rodwell,J.L. Freeman, S.K. Diamond, and D.M. Bloom, in Digest, 1986 Topical Meeting on Ultrafast Phenomena, June 16, Snowmass, Colorado.

PICOSECOND ELECTRICAL PULSES FOR VLSI ELECTRONICS CHARACTERIZATION.

J-M. Halbout, P.G. May, M.B. Ketchen, G.P. Li, C.C. Chi, M. Scheuermann and M. Smyth.

IBM Watson Research Center, Yorktown Heights, NY 10598.

Opto-electronics techniques allow us to take full advantage of the subpicosecond laser technology to generate and characterize picosecond electrical pulses.(1) These pulses have frequency components extending into the terahertz region and are ideally suited to the characterization of ultrafast transistors. Because of the intrinsic nonlinearities in the response of a fast switching transistor, it is most desirable to study the device directly in the time domain and to characterize it in an electrical environment as close as possible to its working environment. Furthermore, it is most urgent to characterize the very environment where these ultrafast signals are generated and must propagate, i.e. transmission lines with micron design rules fabricated on materials compatible with tomorrow's semiconductor technology.

In this presentation, we describe the technology employed to generate and measure picosecond electrical pulses. The fabrication of photoconductive switches used as pulse generators and samplers is reviewed. Excellent results obtained with polysilicon as the photoconducting material show the possibility of full integration of this technology with either bipolar or MOS silicon devices for in situ characterization.

The laser source in our experiments is a pulse compressed, frequency doubled Nd-YAG laser which gives very reliably pulses of autocorrelated width 2 ps and average power in excess of 350 mW at 532 nm.

With these optical pulses, we generate photoconductively picosecond electrical pulses of 2 psec width, limited by the laser pulse.(2) We study the propagation of these very fast pulses on coplanar transmission lines of dimensions compatible with microelectronics applications. It is experimentally proven that the small dimensions of these transmission lines (1 to 2 μm lines separated by 2 to 4 μm) are essential for preserving the integrity of high speed signals. Measurements on structures fabricated on diverse substrates of different conductivity show dispersion compatible with VLSI applications, even for such very high speed signals.

Moreover, we show that pulses as short as 2 psec and a few hundred millivolts can be generated and propagated through tapers in these transmission lines as well as through short sections of wire bonds, up to 1 mm in length. This is most important for the use of these techniques in device characterization, and it emphasizes that, with a little care, very fast signals can be sent onto or out of a chip, thereby putting stringent requirements on packaging parts.

We also have implemented a measurement technique for high speed true differential sampling of waveforms on coplanar transmission lines.(3) It is an extension to the detection of signals of the "sliding contact" mode of excitation which has the advantage of a very balanced excitation of the line. We have shown experimentally in cross-talk measurements the importance of a true differential sampling, as provided by this "sliding contact" technique. These results are depicted in fig. 1 where the signals recovered by the two sampling techniques are displayed. For both cases, the bottom line is excited and we want to characterize the waveform coupled onto the top line. We see that, whereas the side-gap sampling gives us a measure of the "common-mode" coupled onto the line, the "sliding contact" measurement selects the "differential mode" between the two lines forming the transmission line. These results were confirmed by modelling these situations with a transient circuit analysis program (ASTAP).(4) This simple technique alleviates the need for predesigned sampling gaps along the line and makes the photoconductive measurement technique most attractive.

References:

1. D.H. Auston, in Picosecond Optoelectronics Devices, edt. by C.H. Lee, (Academic Press, London 1984).

2. M.B. Ketchen et al., Appl. Phys. Lett. 48, 751, (1986).

3. P.G. May et al., to be published in Ultrafast Phenomena V, Proceedings of the OSA Topical Meeting, Snowmass, June 1986.

4. ASTAP Program Description/Operation Manual, IBM Documentation SH20-1118-0.

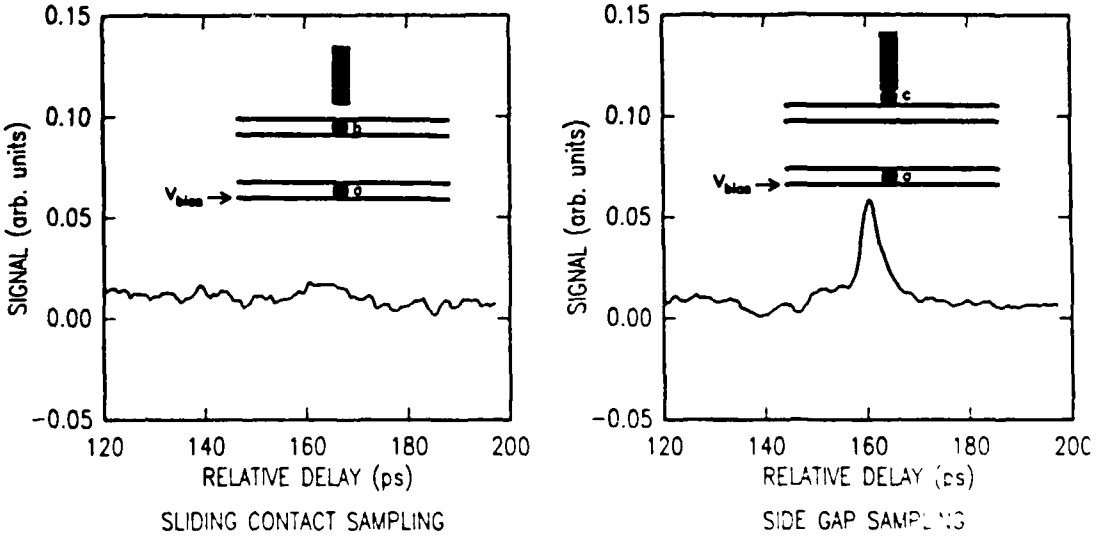

Figure 1: Waveform sampled in a cross talk measurement with the traditional side gap sampling and the sliding contact technique. In both cases a pulse is generated on the bottom transmission line at point "a". Points "b" and "c" are the sampling sites.

Electro-Optic Sampling of High-Speed, InP-Based Integrated Circuits

J. M. Wiesenfeld, R. S. Tucker, A. Antreasyan,*
C. A. Burrus, and A. J. Taylor**

AT&T Bell Laboratories
Crawford Hill Laboratory
Holmdel, N.J. 07733

We report the application of electro-optic sampling[1-3] to measurements of waveforms internal to a high-speed InP integrated circuit. This is possible because InP is an electro-optic material with electro-optic coefficient comparable to that of GaAs. Waveforms and propagation delays through a two stage InGaAs/InP metal-insulator-semiconductor FET (MISFET) inverter circuit[4,5] have been measured. The observed propagation delay through an individual FET is 21±7 ps. The measurement uses an electro-optic sampling system based on a 1.3 μm InGaAsP injection laser[3] that is gain-switched. This work extends to InP-based circuits previously developed techniques for non-invasive sampling using the electro-optic effect in GaAs[2].

The experimental arrangement is shown in Fig. 1. Two microwave frequency synthesizers are phase-locked and offset in frequency by an amount Δf. One synthesizer drives the integrated circuit, and the other is used to gain-switch an InGaAsP double-channel planar buried heterostructure (DCPBH) laser. The 1.3 μm radiation from this laser is below

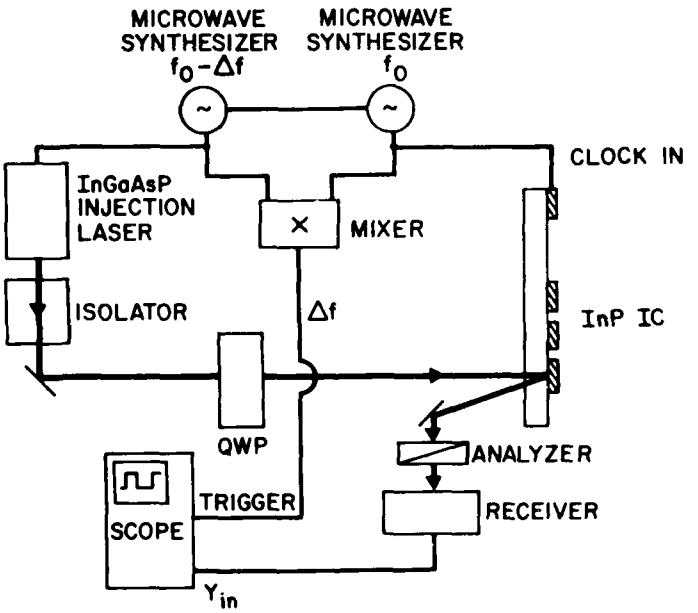

Figure 1: Experimental schematic. QWP is a quarter-wave plate.

* AT&T Bell Laboratories, Murray Hill, N. J. 07974

** Present address: Los Alamos National Laboratory, Los Alamos, N. M. 87545

the bandgap of InP. For these experiments, the test frequency f_0 is varied between 1 and 5 GHz, and the DCPBH laser produces pulses of duration 15 - 20 ps. The beam from the injection laser is made circularly polarized, impinges from the back side of the InP chip, and is reflected from the active side of the chip. The back side of the chip is chemically polished to reduce scattering. The polarization of the optical beam is changed by the longitudinal electro-optic effect in InP, and the change in polarization, which is proportional to the electric field at the sampling point, is measured by a sensitive optical receiver placed after the analyzer. Since the laser and the circuit are driven at frequencies offset by Δf, the laser pulses sample the waveform on the circuit at this rate. The offset frequency was chosen to be 4 kHz. A "real time" reconstruction of the sampled waveform is displayed on an oscilloscope triggered at the offset frequency Δf, using a signal generated by a microwave mixer. This trigger arrangement permits measurement of absolute propogation delays between various points in the circuit. The timing resolution of the sampling system is limited by the 15 - 20 ps optical pulsewidth from the gain-switched laser. However, it is possible to measure peak positions of pulses, and hence pulse propagation delays, to within 10 ps. The ohmic contacts in the present circuit scatter the reflected light, and reduce the voltage sensitivty of the present experiment to 20 $mV/\sqrt{Hz}$.

The circuit used in the present experiments is an InGaAs/InP enhancement mode MISFET two-stage inverter[5], with the drain of the first FET connected to the gate of the second FET. The MISFETs have integrated 500 Ω load resistors. The bias voltage was 1.5 V. We sample at the input (gate) of the first FET, the output (drain) of the first FET, and the output of the second FET.

The first measurements we report used a 5 GHz sinusoidal input waveform of amplitude 1.5 V p-p with a dc offset of 1 V. The input and output waveforms of the first stage are shown in Fig. 2. The waveform at the output is inverted and shows approximately 20 ps delay with respect to the input. The voltage swing at the output (0.8 V) is close to the maximum possible swing for this device with a 1.5 V bias voltage.

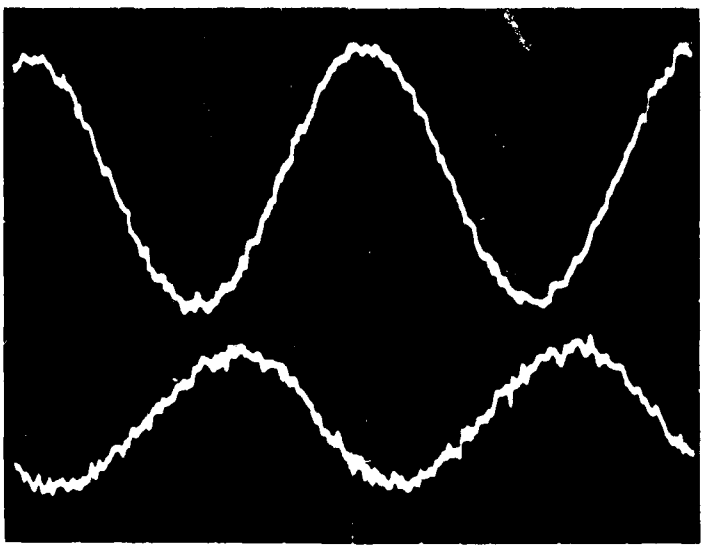

Figure 2: Measured waveforms for a 5 GHz sinusoid. Top is sampled at the input of the first FET, bottom is sampled at the output of the first FET. Vertical scale is 0.4 V/div and horizontal scale is 40 ps/div.

For measurement of pulse propagation delays, a comb generator which produces 2 V, 43 ps FWHM pulses[3] is inserted between the frequency synthesizer and the input of the first stage of the InP circuit. Fig. 3 shows waveforms for the pulse input from the comb generator. The upper curve is the input to the first FET, the middle curve is the output of the first FET, and the lower curve is the output of the second FET. No significant broadening of the pulse occurs in the MISFETs, but there is significant propagation delay in each stage. From this measurement we determine the propagation delay time through each MISFET to be 21±7 ps. The negative voltage swings at the output of the second inverter, just before and after the main pulse, may be due to capacitive coupling.

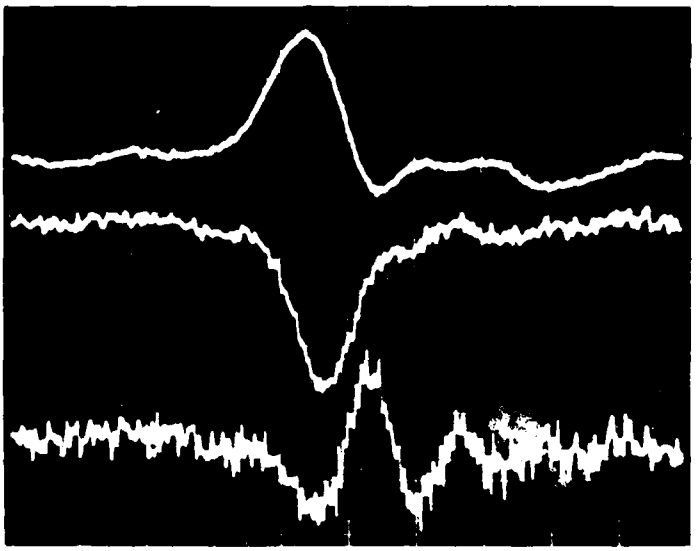

Figure 3: Measured waveforms for the comb generator. Traces are input to the first FET (top), output of the first FET (middle), and ouptut of the second FET (bottom). Horizontal scale is 50 ps/div. Vertical scale is 0.8V/div (top), 0.08 V/div (middle) and 0.04 V/div (bottom).

In summary, we have extended the application of non-invasive characterization of integrated circuits by electro-optic sampling to InP-based circuits. We have measured waveforms internal to an InGaAs/InP MISFET inverter circuit, and have measured propagation delays through individual MISFETs.

References

1. J. A. Valdmanis and G. Mourou, IEEE J. Quant. Electron., *QE-22*, 69 (1986).
2. B. H. Kolner and D. M. Bloom, IEEE J. Quant. Electron., *QE-22*, 79 (1986).
3. A. J. Taylor, J. M. Wiesenfeld, G. Eisenstein, R. S. Tucker, J. R. Talman, and U. Koren, Electron. Lett., *22*, 61 (1986).
4. A. Antreasyan, P. A. Garbinski, V. D. Mattera, and H. Temkin, Appl. Phys. Lett., to be published, Sept. 1, 1986.
5. A. Anteasyan, P. A. Garbinski, V. D. Mattera, N. J. Shah, and H. Temkin, Electron. Lett., to be published.

WEDNESDAY, JANUARY 14, 1987

PROSPECTOR/RUBICON ROOM
11:00 A.M.–12:30 P.M.

WB1–4

HIGH-SPEED LOGIC

David H. Auston, AT&T Bell Laboratories, *Presider*

Molecular Beam Epitaxy (MBE) for High Speed Devices

A. Y. Cho
AT&T Bell Laboratories
Murray Hill, New Jersey 07974

Recent development in molecular beam epitaxy (MBE)[1] is to broaden the scope of the technology to cover a wider range of materials from semiconductors to metals and insulators. For III-V compounds, gas source molecular beam epitaxy (GS MBE, MO MBE or CBE) is used to grow compounds containing phosphorous[2-6]. Precisely controlled electron-gun evaporation is used for Si-MBE[7] and metal-MBE[8]. Fast loading of Hg source is used for II-VI compounds[9]. The impact of MBE does not only contribute to new discoveries in quantum physics[10,11] but also to technology for generating a whole new generation of microwave[12] and optical[13] devices. The capability of MBE to engineer the band structure by superlattices and spatially varying the composition of semiconductors to create a specific gradient at the conduction and valence band edge or to accurately and abruptly control the layer growth to atomic dimensions pushes the frontier of devices to the ultimate imagination of device physicists and engineers.

The main concerns of MBE for production are large-area uniformity, defect levels, and through-put. MBE has made major advances in all three areas in recent years. For uniformity, variation in thickness of less than 1% over a 3-inch GaAs wafer has been achieved[14]. Oval defects as low as 100 cm^{-2} (Ref. 15), and multi-wafer deposition or automated wafer handling up to three 3-inch wafers or seven 2-inch wafers were reported[16].

High purity GaAs with Hall mobility of 163,000 cm^2/vs at 77 K with a peak value as high as 216,000 cm^2/vs at 46 K has been achieved[17]. Interface smoothness to one atomic layer is accomplished by interrupted growth or periodic high substrate temperature pulses between the heterostructures[18,19]. The precision in switching from one compound to another upon the completion of a full atomic layer (phase-locked epitaxy) may be monitored by reflection high energy electron diffraction (RHEED) intensity oscillation[20].

High speed devices require size reduction in lateral and vertical dimensions. The effect of lateral variation, such as the gate-length of an FET on speed of operation, has been investigated[21]. A record propagation delay time of 5.8 ps/gate was measured for a 0.35 μm gate 19-stage ring oscillator at 77 K, with a power of 1.76 mw/gate, and a bias voltage of 0.88 V. The maximum switching speed at room temperature was 10.2 ps/gate with 1.03 mw/gate and 0.8 V bias voltage[21].

Low noise GaAs/AlGaAs modulation doped FET's with 0.25 μm gate length were operated over 40 GHz with 2.1 dB noise figure and 7dB associated gain[22]. More recently, $In_{0.15}Ga_{0.85}As/Al_{0.15}Ga_{0.85}As$ pseudomorphic modulation doped FET's with 0.25 μm length gates were

operated at 62 GHz with a noise figure of 2.4 dB and an associated gain of 4.4 dB[23]. Large lattice mismatched strained $(InAs)_m(GaAs)_m$ superlattice has been grown with MBE[24]. A proposal was made for a high-speed $In_{0.52}Al_{0.48}As/In_{0.53}Ga_{0.47}As$ modulation doped FET with a $(InAs)_m$ $(GaAs)_m$ superlattice channel with $m \leq 4$ where the electrons in the active channel do not suffer any alloy scattering and thus result in an increase in mobility of about an order of magnitude at 77 K[25,26].

Monolithic integration of GaAs/AlGaAs MODFET's and N-metal-oxide-semiconductor (N-MOS) silicon circuits was reported earlier[27]. Fully monolithic integration of interconnected GaAs/AlGaAs double-heterostructure light emitting diodes (LED's) and Si MOSFET's is demonstrated for the first time[28]. The GaAs/AlGaAs layers were grown on a Si substrate with MBE. LED modulation rates up to 27 mb/s have been achieved by applying a stream of voltage pulses to the MOSFET gate. The modulation rate is limited by the speed of the MOSFET for this preliminary demonstration. GaAs on Si substrates opened a new direction of development where Si VLSI circuits can be complemented by III-V optoelectronic components and high-speed electronic circuits.

The most significant development in telecommunications in recent years has been the evolution toward digital transmission and switching. Optical communications promises high capacity and high reliability because of its immunity to the electromagnetic radiation effects. As the capacity increases and the speed of lightwave transmission begins to exceed the processing capability of the fastest electronic circuits, we need a device technology capable of switching and processing lightwave signals in their photonic form. A recent development is to use a superlattice structure or multi-quantum well device. Bistability can be observed with 18 nW of incident power or with 30 ns switching time at 1.6 mW with a reciprocal relation between switching power and speed[29]. Electroabsorption in an InGaAs/GaAs strained-layer multiple quantum well structure has been observed[30]. The novel quantum-confined stark effect modulator with 6.4% transmission modulation was obtained at 0.95 μm with 2 V reverse bias[30].

New avalanche multiplication phenomenon in quantum well superlattices[31], ultra sensitive photodetectors with effective mass filter[32], and novel transistors with resonant tunneling[33-36] have opened new directions in device fabrication.

References

[1] A. Y. Cho, Thin Solid Films *100*, 291 (1983).
[2] M. B. Panish, J. Electrochem. Soc., *127*, 2729 (1980).
[3] A. R. Calawa, Appl. Phys. Lett. *38*, 701 (1981).
[4] M. B. Panish, H. Temkin and S. Sumski, J. Vac. Sci. Technol. *133*, 657 (1985).
[5] N. Vodjdani, A. Lemarchand and H. Paradan, J. de Physique C5, *43*, 339 (1982).
[6] W. T. Tsang, Appl. Phys. Lett., *48*, 511 (1986).
[7] J. C. Bean, J. Crystal Growth *70*, 444 (1984).
[8] E. Ziegler, Y. Lepetre and I. K. Schuller, Appl. Phys. Lett. *48* 1354 (1986).
[9] J. P. Faurie, A. Million, R. Boch and J. L. Tissot, J. Vac. Sci. Technol. *A1* 1593 (1983).

[10] For a review see H. L. Stormer, Surf. Sci., *132*, 519 (1983).
[11] L. Esaki in The Technology and Physics of Molecular Beam Epitaxy, Ed. E.H.C. Parker, Plenum Press 1985, pp. 143-284.
[12] H. Morkoc in The Technology and Physics of Molecular Beam Epitaxy, Ed. E. H. C. Parker, Plenum Press 1985, pp. 195-231.
[13] F. Capasso, K. Mohammed and A. Y. Cho, IEEE J. Quantum Electronics *QE 22* 1853 (1986).
[14] C. Chaix - presented at Riber MBE user meeting, York, September 11, 1986.
[15] H. Fronius, A. Fischer and K. Ploog, Appl. Phys. Lett. *48*, 1392 (1986).
[16] Most MBE manufacturing Co's offer such systems. In particular, Riber and Anelva announced such designs.
[17] E. C. Larkins, E. S. Hellman, D. G. Schlom, J. S. Harris, Jr., M. H. Kim and G. E. Stillman, Appl. Phys. Lett. *49*, 391 (1986).
[18] H. Sakaki, M. Tanaka, and J. Yoshino, Jpn. J. Appl. Phys. *24*, L417 (1985).
[19] J. Singh, S. Dudley and K. K. Bajoj, J. Vac. Sci. Technol. *B4*, 1986.
[20] J. H. Neave, B. A. Joyce, P. J. Dobson and N. Norton, Appl. Phys., *A31*, 1 (1983); ibid *A34*, 1 (1984).
[21] N. J. Shah, S. S. Pei, C. W. Tu and R. C. Tiberio, IEEE Trans. on Dev. *ED-33*, 543 (1986).
[22] P. C. Chao, S. C. Palmateer, P. M. Smith, U. K. Mishra, K. H. G. Duh and J. C. M. Hwang, IEEE Electron. Dev. Lett. EDL-6, 531 (1985).
[23] T. Henderson, M. I. Aksun, C. K. Peng, H. Morkoc, P. C. Chao, P. M. Smith, K. H. G. Duh, and L. F. Lester, to be pubhished in Electron Dev. Lett..
[24] M. C. Tamargo, R. Hull, L. H. Greene, J. R. Hayes and A. Y. Cho, Appl. Phys. Lett. *46*, 569 (1985).
[25] T. Yao, Jpn. J. Appl. Phys. *22*, 680 (1983).
[26] J. Singh, IEEE Elec. Dev. Lett., EDL-7, 436 (1986).
[27] R. Fischer, T. Henderson, J. Klem, W. Kopp, C. K. Peng, and H. Morkoc, Appl. Phys. Lett. *47*, 983 (1985).
[28] K. K. Choi, G. W. Turner, T. H. Windhorn, and B. Y. Tsaur, to be published.
[29] D. A. B. Miller, D. S. Chemla, T. C. Damen, T. H. Wood, C. A. Burrus, Jr., A. C. Gossard, and W. Wiegmann, IEEE J. Quantum Electron, *QE-21* 1462 (1985).
[30] T. E. Van Eck, P. Chu, W. S. C. Chang, and H. H. Wieder, Appl. Phys. Lett., *49*, 135 (1986).
[31] F. Capasso, J. Allam, A. Y. Cho, K. Mohammed, R. J. Malik, A. L. Hutchinson and D. L. Sivco, Apply. Phys. Lett. *48*, 1294 (1986).
[32] F. Capasso, K.Mohammed, A. Y. Cho, R. Hull and A. L. Hutchinson, Appl. Phys. Lett. *47*, 420 (1985).
[33] L. L. Chang, L. Esaki and R. Tsui, Appl. Phys. Lett. *24*, 593 (1974).
[34] F. Capasso and R. A. Kiehl, J. Appl. Phys. *58*, 1366 (1985).
[35] F. Capasso, K. Mohammed and A. Y. Cho, Appl. Phys. Lett. *48*, 478 (1986).
[36] M. A. Reed, J. W. Lee and H. L. Tsai, Appl. Phys. Lett. *49* 158 (1986).

Multigigahertz Logic Based on InP-MISFET's Exhibiting Extremely High Transconductance

A. Antreasyan
P. A. Garbinski
V. D. Mattera, Jr.
H. Temkin

AT&T Bell Laboratories
Murray Hill, NJ 07974
(201) 582-5106

InP metal-insulator-semiconductor field-effect transistors (MISFET) offer significant potential in high-speed digital circuits[1] and high-frequency power devices[2]. This is due to the high saturation velocity and mobility of electrons in InP. In addition, metal-semiconductor field-effect transistors cannot be realized on $Ga_{0.47}In_{0.53}As$ as a result of the low Schottky barrier. The fabrication of InP MISFET's has turned out to be difficult in the past[3] due to the formation of surface defects at the dielectric-semiconductor interface. In this paper we report a novel, high-speed, ultra high transconductance $Ga_{0.47}In_{0.53}As/InP$ MISFET. The devices exhibit a propagation delay of 25 ps/stage and extrinsic dc transconductances as high as 320 mS/mm for a gate length of 1 μm. These are to our knowledge the highest transconductance and the lowest propagation delay measured with an FET on an InP substrate. High-speed digital circuits based on these MISFET's are capable of operating at 5 GHz.

A cross-sectional view of the MISFET structure is shown in Fig. 1(a) (not to scale). The epitaxial layers for this structure consist of an undoped InP buffer layer, an undoped $Ga_{0.47}In_{0.53}As$ layer, an n-type GaInAs layer ($5x10^{17}cm^{-3}$) and an n^+-$GaInAs$ ($10^{18}cm^{-3}$) contact layer grown by chloride vapor phase epitaxy on semi-insulating InP substrate. The undoped layers are characterized by an extremely low impurity level of $n{\sim}5x10^{14}cm^{-3}$. The MISFET's are fabricated by etching mesa structures on the substrate. After the definition of the source-drain metallization through lift-off, grooves are etched between source and drain contacts through a photoresist mask utilizing a selective etchant until the InP buffer layer is exposed. Subsequently, a 500 Å thick layer of SiO_2 and gate metals are deposited in an electron beam evaporator and the gate is defined by lift-off. Figure 2 shows the drain-source I-V characteristic of a MISFET at room temperature having a transconductance of 80 mS for a gate length of 1 μm and a gate width of 250 μm, corresponding to a g_m of 320 mS/mm.

For these MISFET's we have measured saturation drift velocities as high as $3x10^7 cm/s$ and channel mobilities of 2800 cm^2/Vs. Two important features of the MISFET structure need to be emphasized. First, an undoped GaInAs layer is grown between the highly doped n-GaInAs layer and the undoped InP buffer layer to prevent dopant back-diffusion into the undoped InP layer. Gate etching can be then performed utilizing a non-critical selective etchant. Second, the gate dielectric is deposited in an electron beam evaporator with a process that we believe results in a significant reduction of surface defects. In fact, we have obtained extremely low gate-to-source leakage currents of 10^{-7} A for a gate voltage of 1.5 volts. Excellent switching properties of these transistors have allowed us to prepare monolithically integrated inverters, each consisting of three MISFET's and three integrated resistors as illustrated in Fig. 3. Such inverters are basic building blocks of digital circuits. A cross-sectional view of a MISFET and an integrated resistor structure is illustrated in Fig. 1(b). The etching process of load resistors is monitored to obtain load resistances of about 500 ohms. Figure 4 shows a typical characteristic for a two-stage inverter where the inverter output is plotted as a function of gate voltage, the bias voltage being a parameter. It can be deduced from Fig. 4 that the inverters provide sufficiently high noise margins of 200 mV at a bias of 1.6 volts. Measurements by electro-optic sampling[4] reveal the capability of these inverters to operate at frequencies of 5 GHz, and having a propagation delay as small as 25 ps/stage at room temperature.

The achievement of the highest transconductance ever measured with an FET made on InP substrate, demonstration of 5 GHz logic, and a propagation delay of 25 ps/stage as well as excellent inverter characteristics make this InP MISFET suitable for high speed electronics on InP.

1. L. J. Messick, IEEE Trans. Electron Devices, *ED-31*, 763 (1984).
2. T. Itoh, and K. Ohata, IEEE Trans. Electron Devices, *ED-30*, 811 (1983).
3. K. P. Pande, and D. Gutierrez, Appl. Phys. Lett. *46*, 416 (1985).
4. A. J. Taylor, J. M. Wiesenfield, G. Eisenstein, R. S. Tucker, J. R. Talman, and U. Koren, Electron. Lett. *22*, 61 (1986).

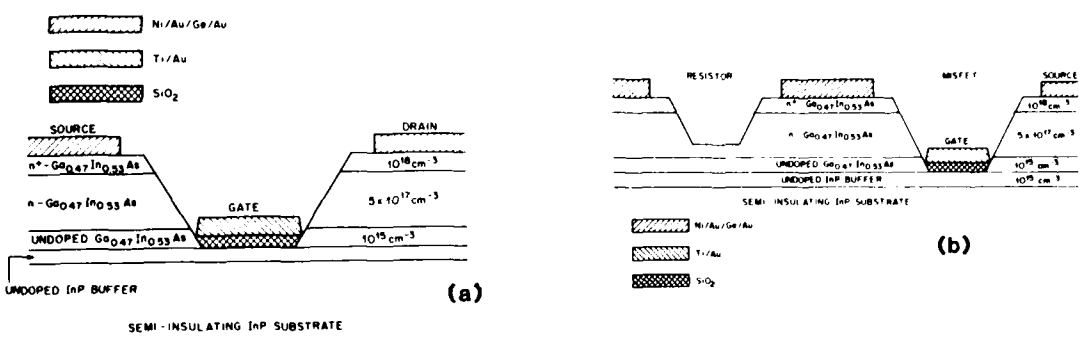

Figure 1 (a) Cross sectional view of the MISFET structure;
(b) Cross sectional view of MISFET and integrated load resistors. Both figures not to scale.

Figure 2 Drain-source I-V characteristic of a MISFET at room temperature having a gate length and gate width of 1 μm and 250 μm, respectively. Vertical scale is 10 mA/div, horizontal scale is 200 mV/div, gate voltage is increased in steps of 200 mV.

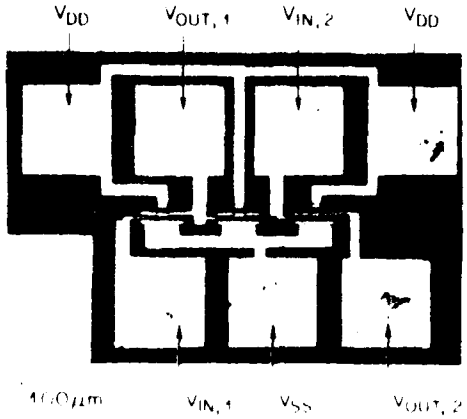

Figure 3 Top view of a monolithically integrated inverter circuit, consisting of 3 MISFET's and 3 resistors.

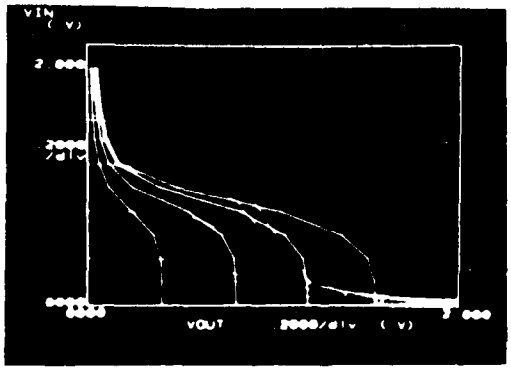

Figure 4 A plot of voltage transfer characteristics for an inverter whose output is linked to the gate of a second MISFET. Two separate traces are obtained by plotting V_{OUT} vs. V_{IN} and repeating the plot after interchanging the axis. Both horizontal and vertical axis extend linearly from 0 volt to 2.0 volts, while V_{DD} is a parameter varying from 0 to 1.6 volts in steps of 0.4 volt. V_{SS} is connected to ground.

An Optically Strobed Sample and Hold Circuit*

Chuck McConaghy
Lawrence Livermore National Laboratory
7000 East Avenue
Livermore, California 94550

Introduction

Radiation damaged photoconductors have been shown to be useful devices for sampling repetitve electrical signals with time resolution to less than a PicoSecond[1,2]. However, the sampling of low repetition rate or single shot events with these photoconductors has not been possible due to the need for lock in detection methods to observe the sampled signal. In this paper, a radiation damaged photoconductor serves as the sampling element in a sample and hold circuit. It has been possible to sample single shot electrical signals with about a 10 picosecond aperture time. Once sampled the signal can be held for about 1 microsecond by an on-chip holding amplifier.

Circuit Description

The circuit shown in Figure 1 was fabricated in Lec GaAs. The circuit consists of a 50 ohm microstrip transmission line which propagates the fast electrical signal onto and back off of the chip. Two sets of 25 micron gap photoconductors border the main microstrip transmission line. Photoconductor 1 is connected to the input of a MesFet Source Follower with an active load. The dimensions of the Mesfets in the amplifier are 1 um gate lengths with 30 um width for the source follower and 10 um width for the active load. The input of the source follower has an additional .3 pf polyimide storage capacitor which can be bonded into use. It turned out that parisitic capacitance was enough to give a hold time of 1 microsecond, so this capacitor was not utilized. Photoconductor 3 and 4 were for electrical autocorrelation testing of the basic photoconductor response times. Photoconductor 2 is not radiation damaged and can be utilized as an optically strobed step generator. The radiation damaging was accomplished with 200 Kev protons at a dose of $10^{15}/cm.^2$ A thick (3 microns) layer of photoresist was utilized to protect the undamaged switch as well as the MesFets during the proton implant. The radiation damaged photoconductors were independently measured by electrical autocorrelation to have a 1/e time of 10 picoseconds including the effect of the finite 5 picosecond wide laser pulse.

Circuit Performance

The experimental setup is shown in Figure 2. The Laser utilized as the strobe generator is a mode locked Nd:Yag laser which has been pulse compressed to provide 5 PicoSecond 1.06 um pulses. One of these pulses is switched out of the continuous train by a Pockel cell at a maximum rate of 10 per second. The pulse is then frequency doubled to 532 nm and focussed onto the 25 um sample gap with a 5X microscope objective. The energy in the laser pulse at the gap is about 1 nanoJoule. The electrical test pulse was generated with an Avtech AVM-C pulse generator that was synchronized to the Laser pulse. The timing between the optical strobe pulse and the electrical test pulse was variable by means of a voltage controlled delay generator. This allowed the single sample and hold circuit to sample through an entire waveform rather than just one point on the waveform.

* This work performed under the auspices of the U.S. Department of Energy by Lawrence Livermore National Laboratory under contract No. W-7405-Eng-48.

Prior to radiation damaging, the circuit had a sensitivity of 270 mv/Volt of input signal. After radiation damaging the circuit had a sensitivity of 2.7 mv/Volt of input signal. Although the output level is quite low for input signals in the volt range , the circuit is quite useable if care is taken in processing the output. For the data presented in Figure 3, the output of the GaAs circuit was resampled with a slower(10 Ns aperture) sampler and held for at least 100 milliseconds which was the interpulse time of the laser set by the Pockel cell.

Figure 3a shows a series of about 50 single shots at a rate of 10/second with about 80 picoseconds time shift of the input waveform per shot (400 ps/division). The data is not averaged and the noise in the waveform is primarily due to laser amplitude fluctuation from shot to shot. In addition to laser amplitude variation there was a significant amount of jitter between the electrical pulse and optical pulse due to the requirement for tens of nanoseconds in the internal delays in the pulse generator and electronic delay. Figure 3b shows an expanded view of the electrical pulse rise time at 160 ps/division. Figure 3b has been slightly averaged by a factor of 5 to enhance the signal to noise. Figure 3c shows the same rise time displayed on a Tektronix S4 sampling head. The electrical pulse was rep rated at about 100 khz for the picture in 3c.

Conclusions

An optically strobed sample and hold has been fabricated and utilized to sample a 200 picosecond risetime electrical signal in a single shot manner. The ultimate response time of the circuit may be as fast as 10 picoseconds. Present testing has been limited by the available electical test signal.

1. P.M. Downey,"Subpicosecond Response Times From Ion Bombarded InP," Picosecond Elect. and Optoelect. Conference,Incline Village,1985

2.R.B. Hammond,N.G. Paulter,R.S. Wagner,Appl. Phys.Lett.45(3),1 Aug 1984

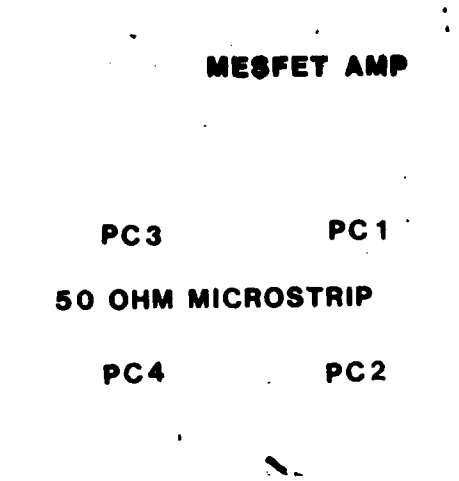

Figure 1: GaAs Optical Strobed Sample and Hold circuit

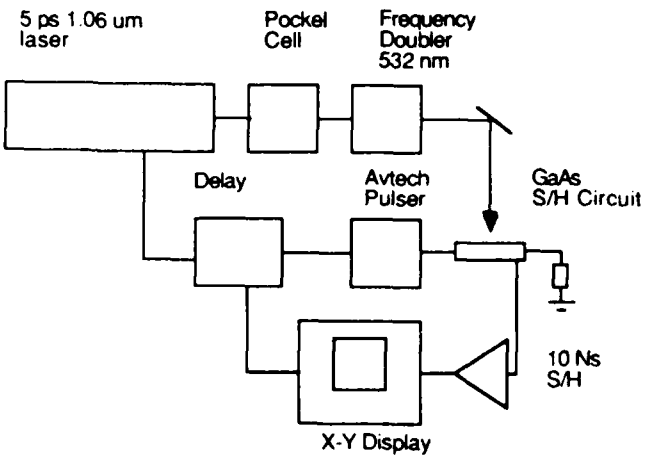

Figure 2: Experimental Setup

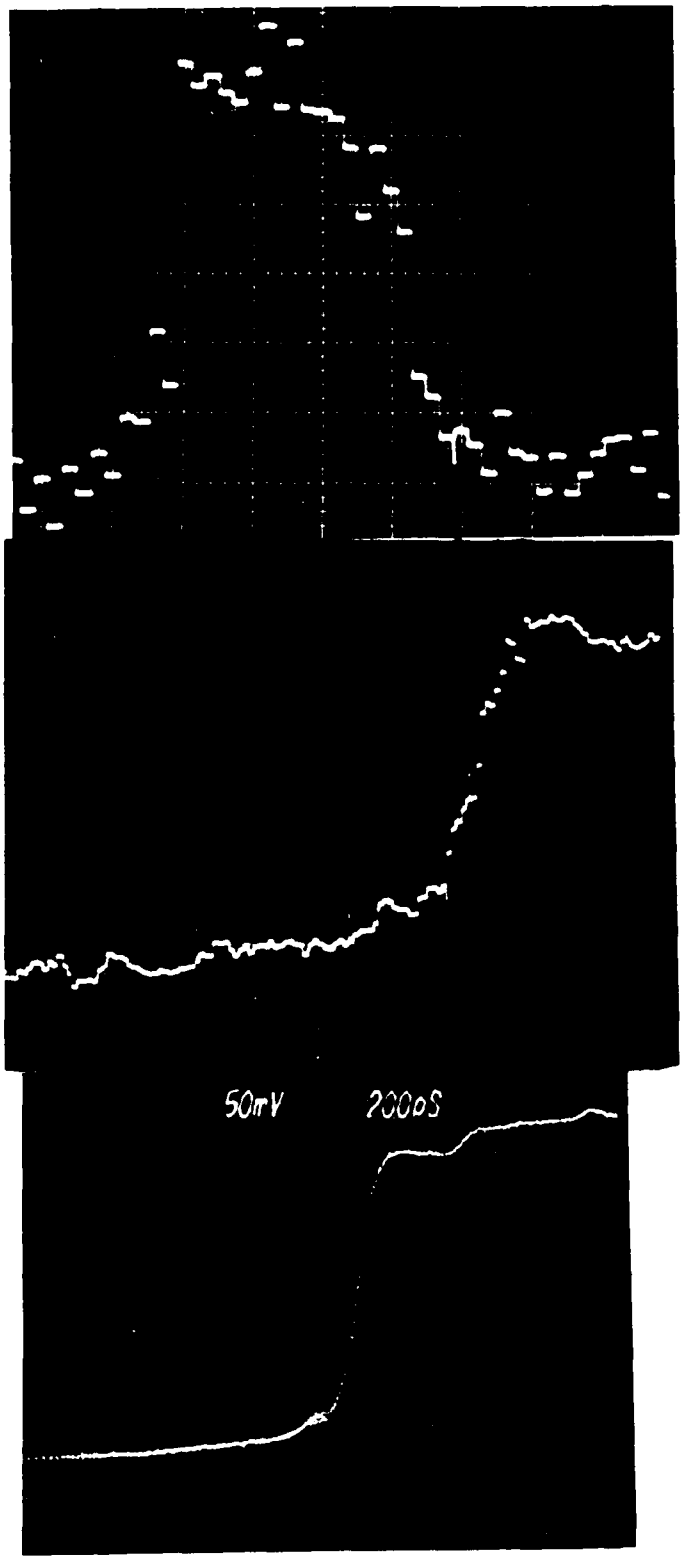

Figure3A: 50 Single shots of an electrical transient with an 80ps time shift of the input transient per shot.
(400ps/div and .5v/div)

Figure 3B: Blow up of rising edge of transient.
(160ps/div and .5v/div)

Figure 3C: Same rising edge as 3B but recorded ata 100kHz rep rat on a Tek S4 sampling head.
(200ps/div and .5v/div)

HIGH-SPEED OPTICAL LOGIC USING GaAs

H. M. Gibbs,[1] N. Peyghambarian,[1] Y. H. Lee,[1] J.L. Jewell,[2]
A. Migus,[3] A. Antonetti,[3] D. Hulin,[4] and A. Mysyrowicz[4]

[1]Optical Sciences Center, University of Arizona, Tucson, Arizona 85721; [2]AT&T Bell Laboratories, Holmdel, NJ 07733; [3]Laboratoire d'Optique Applique, Ecole Polytechnique-ENSTA, F-91120 Palaiseau, France; [4]Groupe de Physique des Solides, Ecole Normale Supérieure, 2 Place Jussieu - Tour 13, F-75005 Paris, France"

The status of bulk-GaAs etalons and their application to high-speed optical logic will be summarized. Several characteristics are of particular importance: time to make a logic decision ("switch-on time"), time required for the device to recover and be ready to make the next decision (recovery time), energy required per logic decision (switching energy), ability to switch the next device (cascadability) or perhaps several devices (fanout), etc.

Recently, research has centered on the use of a nonlinear etalon as a logic gate with the inputs at a wavelength having good absorption leading to index changes at a second probe wavelength.[1] With an appropriate initial detuning between the Fabry-Perot transmission peak and the probe wavelength, each of the logic operations can be performed. Several logic gates have been demonstrated using a high-finesse etalon containing GaAs-AlGaAs multiple quantum wells at room temperature.[2] Input pulses with energies less than 3 pJ focused to 5 to 10 μm on the device produced contrasts greater than 5:1 in the NOR gate. A recovery time of 5 ns permitted 82-MHz continuous operation. Thermal stability was demonstrated in the NOR gate even though the device was poorly heat sunk. And the NOR gate has been operated using diode laser sources.[3]

Because the physical mechanisms leading to refractive index changes are extremely rapid, one expects a very short switch-on time. A Fabry-Perot peak was shifted in $\int_0$ to 3 ps; the etalon consisted of alternating layers of 152-Å GaAs and 104-Å AlGaAs with a total GaAs thickness of $\cong 1.5\mu$m.[4] Less than 100 fJ/μm^2 energy per unit area incident on the device was used for the logic operation.

The recovery times of the first GaAs gates were typically 5 to 10 ns, determined by the lifetime of the carriers in the light beam. The recovery time was greatly reduced by enhancing surface recombination by removing one or both of the AlGaAs windows used to stop chemical etching and reduce surface recombination. A 1.5-μm-thick bulk-GaAs etalon without the top AlGaAs window and

etched to form a 2 D array of 9μm x 9μm pixels with 20 μm center-to-center spacing was shown to have a recovery time of less than 200 ps with resolution limited by the input pulse duration.[5] Then 5- to 10-ps input pulses were used to study etalons with no AlGaAs windows and with no etching of pixels.[6] A thickness of 0.5 μm was found to be optimum for current etalon designs: complete recovery in 150 ps with 16-pJ input-pulse energy. A 0.3-μm-thick sample showed even faster recovery (down to about 40 ps) with 20-pJ input-pulse energy. A 1350-Å-thick sample of inferior quality showed recovery times as fast as 30 ps but required much higher energies. Bombardment by 2-MeV protons was less effective. The most heavily bombarded sample ($2x10^{14}$ protons/cm^2) showed 270-ps complete-recovery time, but the contrast was severely degraded (2:1) even with more input-pulse energy (40-pJ).

These recovery times are probably quite adequate for parallel computations where thermal considerations will limit the product of pixel density and repetition rate. Answers emerging from one etalon can proceed to the next etalon, etc., so that many etalons can be used to avoid using any one too often. Where very high-speed response is needed, for example, in a waveguide directional coupler encrypting or multiplexing data in a pipeline mode, the newly discovered AC Stark shift may be the answer.[7,8] If the pump pulse is tuned far enough below the exciton frequency, in the transparency region of the material, the carrier lifetime is no longer a limitation since carriers are not excited. A complete shift/recovery cycle of the Fabry-Perot transmission peak has been accomplished in 1.5 ps.[9]

The gates described herein utilize different wavelengths for inputs and probe (output), making cascading difficult. Two-wavelength operation utilizing an isolated resonance is one possibility. We are reassessing one-wavelength operation (optical transistor or bistability operation) to see what price one must pay for ease of cascadability.

We gratefully acknowledge support for the Arizona research by the Air Force Office of Scientific Research, the Army Research Office, the National Science Foundation (Grant Nos. 8317410 and 8610170), and the Optical Circuitry Cooperative.

1. J. L. Jewell, M. C. Rushford, and H. M. Gibbs, Appl. Phys. Lett. *44*, 172 (1984).

2. J. L. Jewell, Y. H. Lee, M. Warren, H. M. Gibbs, N. Peyghambarian, A. C. Gossard, and W. Wiegmann, Appl. Phys. Lett. *46*, 918 (1985).

3. M. Ojima, A. Chavez-Pirson, Y. H. Lee, J. F. Morhange, H. M. Gibbs, N. Peyghambarian, F.-Y. Juang, P.K. Bhattacharya, and D. A. Weinberger, Appl. Opt. *25*, 2311 (1986).

4. A. Migus, A. Antonetti, D. Hulin, and A. Mysyrowicz, H. M. Gibbs, N. Peyghambarian, and J. L. Jewell, Appl. Phys. Lett. *46*, 70 (1985).

5. Y. H. Lee, M. Warren, G. R. Olbright, H. M. Gibbs, N. Peyghambarian, T. Venkatesan, J.S. Smith, and A. Yariv, Appl. Phys. Lett *48*, 754 (1986).

6. Y. H. Lee, H. M. Gibbs, J. L. Jewell, J. F. Duffy, T. Venkatesan, A. C. Gossard, W. Wiegmann, and J. H. English, "Speed and Effectiveness of Windowless GaAs Etalons as Optical Logic Gates," talk FK2, p. 364, Technical Digest of Conference on Lasers and Electro-Optics, June 9-13, 1986, and Appl. Phys. Lett. *49*, 486 (1986).

7. A. Mysyrowicz, D. Hulin, A. Antonetti, A. Migus, W. T. Masselink, and H. Morkoc, Phys. Rev. Lett. *56*, 2748 (1986).

8. A. Von Lehmen, J. E. Zucker, J. P. Heritage, and D. S. Chemla, postdeadline talk PD18, International Quantum Electronics Conference, June 9-13, 1986.

9. A. Migus, D. Hulin, A. Mysyrowicz, A. Antonetti, W. T. Masselink, H. Morkoc, H. M. Gibbs, and N. Peyghambarian, postdeadline talk ThU9 Conference on Lasers and Electro-Optics, June 9-13, 1986.

NOTES

WEDNESDAY, JANUARY 14, 1987

PROSPECTOR/RUBICON ROOM
2:00 P.M.–3:30 P.M.

WC1–4

HIGH-SPEED AND MICROWAVE DEVICES: 1

C. Stolte, Hewlett-Packard, *Presider*

WC1-1

Millimeter-Wave Intergrated Circuits

Barry E. Spielman
Naval Research Laboratory, Code 6850
Washington, DC 20375-5000

BACKGROUND

The opportunities offered by monolithic millimeter-wave technology span radar, communications, electronic warfare, and missile seekers. These opportunities relate to size, weight, and cost reduction advantages over standard metal waveguide and hybrid integrated circuit implementations. However, specific technical challenges remain in realizing some important circuit building blocks.

CIRCUIT BUILDING BLOCKS

Circuit building blocks for monolithic millimeter-wave ICs encompass semiconductor devices and transmission line media. Table 1 lists most of the semiconductor device candidates for use in millimeter-wave source, mixer/detector, and modulator circuit functions. Of these, the most well established candidates are: the IMPATT, TED, and MESFET for sources; the Schottky diode, Josephson junction diode, and MESFET for mixers/detectors; and the PIN and MESFET as modulator elements. As is suggested by the multitude of source candidates, current efforts are exploring new concepts to achieve reasonably high output power levels (25 mW or higher) with reasonable gain and efficiency (dc to RF) for above 60 GHz applications, especially in three-terminal device configurations.

The transmission media most commonly considered for monolithic millimeter-wave ICs are standard microstrip, coplanar waveguide, and fin line or slot line. The unloaded Q value at 30 GHz for these (excluding fin line) transmission lines range from about 100 to 200. Similar values for trapped inverted microstrip, inverted microstrip, fin line, and suspended microstrip lie in the range from 400 to 700, while those for image line and metal rectangular waveguide fall in the 2500 to 3000 range. Other characteristics for such media are also important. Table 2 qualitatively summarizes some of the more significant circuit medium properties for monolithic-compatible media, hybrid IC compatible media, and metal waveguide. It is clear that application-dependent tradeoffs must be made.

It is becoming increasingly apparent that for monolithic IC designs new and more refined models are needed for semiconductor device representations and for treatment of device to circuit-medium interfaces (e.g. parasitic effect treatment), especially for these higher frequencies. Once such models are developed and verified, it would be desirable to have such design capability available in a mode which is widely accessible. Possibly CAD workstation equipment could incorporate a software base for such a purpose.

In the area of testing there are at least two important needs. One is to expand the commercial availability of error-correcting, automated network analyzer equipment to at least 100 GHz. Also, a need exists for on-chip wafer prober units to function accurately and reproducibly over the same frequency range.

RECENT/CURRENT MONOLITHIC EFFORTS

Monolithic efforts to date have focused primarily on non-transmitter related functions. This trend is observed in the listing of representative programs provided in Table 3. A notable exception in this list is the 32 GHz transceiver program. This program employs an approach where the output of a microwave source is frequency multiplied to provide a 32 GHz transmit signal. Other activities await efforts either to refine and improve existing source devices in planar format or to innovate devices for signal generation directly at the millimeter wave frequency of interest.

To best illustrate the technology being pursued in the monolithic receiver area, attention is drawn to the second entry in Table 3. This program is to provide a technology base for receivers to operate instantaneously over the full 75 to 110 GHz frequency range. The focus of this development is the receiver front end configuration depicted in Figure 1. This configuration requires: four mixers, four common IF amplifiers, four local oscillators, and an RF multiplexer. One design in GaAs pursued for the mixer is depicted in Figure 2. This mixer has provided 7 to 9 dB conversion loss over the 75 to 110 GHz band for an IF band from 8.5 to 17.5 GHz.

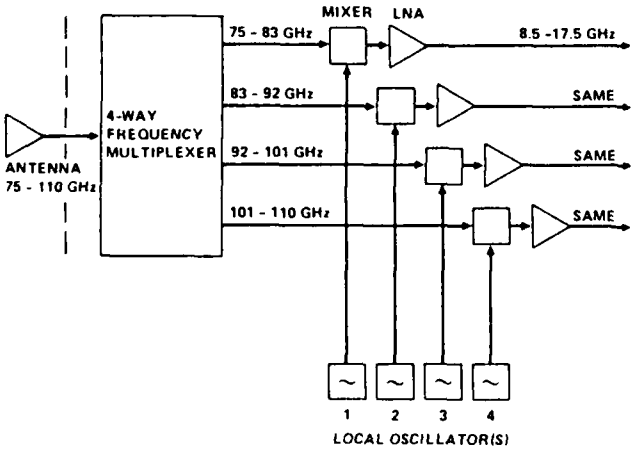

Fig. 1 Four-Channel Receiver Front-End

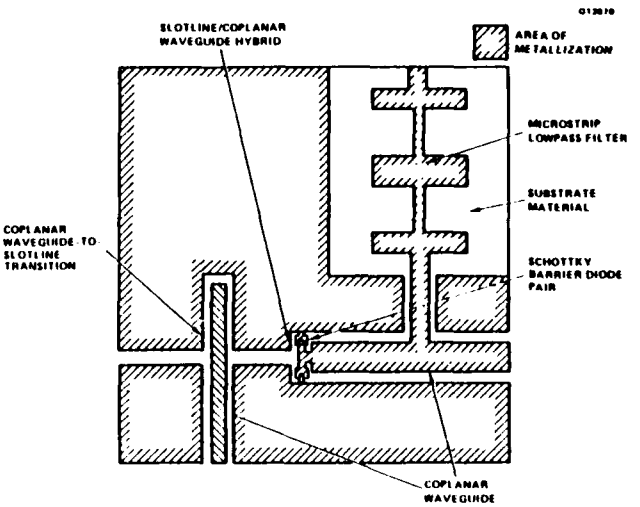

Fig. 2 Planar Balanced Monolithic Mixer Circuit

Table 1 DEVICE CANDIDATES

SOURCES:

- IMPATT
- TED
- MESFET
- MODFET
- HJBT
- CHINT
- NERFET
- OGST
- PBT
- PDBT
- CHIRP(superlattice)
- QUANTUM-WELL (QST)
- DIMPATT
- SSTWA
- SS-OROTRON
- SS-MAGNETRON
- SS-GYROTRON
- SPACE-HARMONIC AMPLIFIER

MIXER/DETECTOR:

- SCHOTTKY DIODE
- JJ/SIS
- MESFET
- MODFET
- CHIRP
- QUANTUM-WELL

MODULATORS:

- PIN
- MESFET

Table 3

MILLIMETER-WAVE MONOLITHIC IC EFFORTS

- 32 GHz TRANSCEIVER
- 75 TO 110 GHz RECEIVER TECHNOLOGY
- 35 TO 38 GHz RECEIVER
- 44 GHz RECEIVER
- 90 TO 100 GHz RECEIVER
- 110 GHZ QUASI-OPTICAL MIXER
- 215 GHz DETECTOR DIODE ARRAY
- 44 GHz PIN PHASE SHIFTER
- K_a-BAND PIN DIODE WINDOW COMPONENTS
- 30 TO 50 GHz AND 75 TO 100 GHz SWITCHES

Table 2 SUMMARY OF CIRCUIT MEDIUM PROPERTIES

PROPERTY	WAVEGUIDE	HYBRID IC's	MONOLITHIC IC's
APPLICABLE FREQUENCY	1 GHz TO 300 GHz	1 GHz TO APPROX 70 GHz	1 GHz TO 100 GHz+
RELATIVE COST	HIGHEST	MODERATE TO HIGH	LOWEST
SIZE	LARGEST	MEDIUM	SMALLEST
RF COMPONENT AVAILABILITY	GREATEST	EXTENSIVE	LIMITED
BANDWIDTH CAPABILITY	LESS THAN OCTAVE	GREATER THAN OCTAVE	GREATEST
CONNECTOR AVAILABILITY	COMPLETE	COMPLETE	NEEDS DEVELOPMENT
SOLID-STATE DEVICE COMPATIBILITY	POOR	FAIR/GOOD	BEST
MODELING DATA BASE	COMPREHENSIVE	MODERATE	INCOMPLETE
POWER HANDLING	BEST	MODEST-ARRAYS NEEDED	MODEST-ARRAYS NEEDED
REPEATABILITY	POOR	FAIR	POTENTIALLY EXCELLENT
LOSSES	LOW	MODERATE	HIGHEST
VOLUME PRODUCTION SUITABILITY	POOR	MODERATE	BEST

Enhanced Performance Ultrabroadband Distributed Amplifiers

G. Zdasiuk, M. Riaziat, R. LaRue, C. Yuen and S. Bandy
Varian Research Center, Palo Alto, CA 94303

Distributed amplifiers have been used in recent years to achieve amplification over multioctave bandwidths extending to millimeter-wave frequencies [1]. The distributed (or traveling wave) amplifier topology has been especially suitable for monolithic integration using GaAs technology due to low sensitivity to component parameter variations and a relatively high active/passive component ratio. A major drawback of the approach has been the relatively low gain per stage (4-7 dB) and high current consumption. This paper describes the application of novel circuit approaches (such as cascode-connected FETs and coplanar waveguide transmission lines) and advanced devices such as high electron mobility transistors (HEMTs) to improve performance, simplify fabrication and achieve over 10 dB of single-stage gain over the 2-20 GHz band. This band is of significance for electronic countermeasures systems and microwave measurement applications

A circuit diagram for the 2-20 GHz distributed amplifier is shown in Fig. 1. Input and output capacitances of the FET devices are incorporated into an artificial transmission line structure, which have a low pass response. A simplified gain expression, $G(\omega)$ [2], for the circuit is given by

$$G(\omega) = \frac{g_m^2 Z_o^2}{4} \left[\frac{e^{-A_g(\omega)n} - e^{-A_d(\omega)n}}{A_g(\omega) - A_d(\omega)} \right]^2 \qquad (1)$$

where g_m is the FET transconductance, Z_o is the input and output artificial line impedance (assumed to be the same here), A_g, A_d are the gate and drain line losses (per section) respectively, and n is the number of sections. The frequency response of the amplifier is determined by the frequency behavior of the input and output line attenuation, $A_g(\omega)$, $A_d(\omega)$. The overall gain is determined by the active device g_m.

The monolithic distributed amplifier circuit fabricated with MESFET active devices on a semi-insulating GaAs substrate is shown in Fig. 2. A novel feature of this circuit is the use of coplanar waveguide (CPW) transmission lines (rather than microstrip) for forming the high impedance inductive sections of the input and output artificial transmission lines. The use of coplanar waveguide eliminates the need for through-the-substrate via holes which are difficult to fabricate. Gain is also improved, since the residual inductance of the via posts can reduce the overall amplifier gain by ~1 dB. CPW is also highly compatible with both high frequency contacting on wafer measurements and contactless electro-optic wafer probing techniques [3].

The active devices are GaAs MESFETs with gate lengths of approximately 0.6 μm, defined with optical lithography. The overall gain periphery is 725 μm. Active layers are epitaxially grown using metalorganic chemical vapor deposition. Figure 3 shows the gain versus frequency of the amplifier. Approximately 9.5 dB of gain is achieved from 2-17 GHz.

If a wafer with slightly lower active layer doping is used, thereby lowering the gate capacitance and increasing the cutoff frequency of the transmission lines, useful gain can be obtained to above 20 GHz. Decreasing the doping also reduces the device g_m, so that the overall gain is lowered to ~7.5 dB.

By Fourier transforming the frequency domain data, the impulse response is obtained. Typically, the circuits of Fig. 2 exhibit 75 psec of pulse delay with ~100 psec of spreading.

An alternate approach to increasing distributed amplifier gain per stage is to utilize 2 cascode-connected FETs in place of single FETs as shown in Fig. 4. The output conductance of the "cascode block" of Fig. 4 is reduced by the factor $(2 + g_m r_{ds})^{-1}$ from a single FET, where r_{ds} is the output resistance of an individual FET. This will reduce the drain line attenuation and hence increase the overall amplifier gain. Other advantages of the cascode configuration include higher output power (due to the second FET being connected as a grounded gate stage), improved isolation, and the ability to use the second gate for automatic gain control (AGC).

Figure 5 is a photomicrograph of a monolithic cascode distributed amplifier. This circuit utilized 5 "cascode sections" consisting of 2 FETs each. In this case, the FET gates were written with E-beam lithography with an average gate length of 0.3 μm. The circuit was fabricated on MOCVD-grown GaAs epitaxial material. Over 11 dB of gain was obtained over the 2-18 GHz band from the amplifier. This is currently the highest reported gain for a single-stage amplifier covering the 2-18 GHz band.

A final approach for increasing the gain and bandwidth of distributed amplifiers is to use high-transconductance (g_m) devices such as high electron mobility transistors (HEMTs). HEMTs are especially suited to distributed amplifiers, since they have lower drain conductance than MESFETs and the gate capacitance is less dependent upon gate voltage. Other advantages include lower noise figures and higher associated gains in a 50-ohm environment and higher noise bandwidths [4].

A monolithic HEMT amplifier has been fabricated using a "conventional" topology (i.e., microstrip transmission lines, no cascode-connected devices, etc.). A photomicrograph of the circuit is shown in Fig. 6. The HEMT active layers are grown by MBE on a semi-insulating GaAs substrate. Preliminary results indicate that approximately 10 dB of gain is achieved from 2-20 GHz. These are the first reported results for a distributed amplifier fabricated with HEMT devices.

In summary, we have demonstrated enhanced performance ultrabroadband distributed amplifiers by the use of: (1) novel circuit techniques such as coplanar waveguide transmission lines and cascode-connected FETs; and (2) high-performance heterostructure active devices such as HEMTs.

References

1. M. N. Yoder, "Distributed Traveling Wave Monolithic Amplifiers", in IEEE GaAs IC Symposium Digest (October 1984).
2. Y. Ayasli, R. L. Mozzi, J. L. Vorhaus, L. D. Reynolds and R. A. Pucel, "A Monolithic GaAs 1-13 GHz Traveling-Wave Amplifier", IEEE Trans. on Microwave Theory and Techniques MTT30(7) (July 1982).
3. M. Rodwell, M. Riaziat, K. Weingarten and D. Bloom, "Internal Microwave Propagation and Distortion Characteristics of Traveling Wave Amplifiers Studied by Electro-Optic Sampling", in 1986 IEEE MTT-S International Microwave Symposium Digest (June 1986).
4. S. Weinreb and M. Pospieszalski, "X-band Noise Parameters of HEMT Devices at 300K and 12.5K", in IEEE MTT-S Symposium Digest (June 1985).

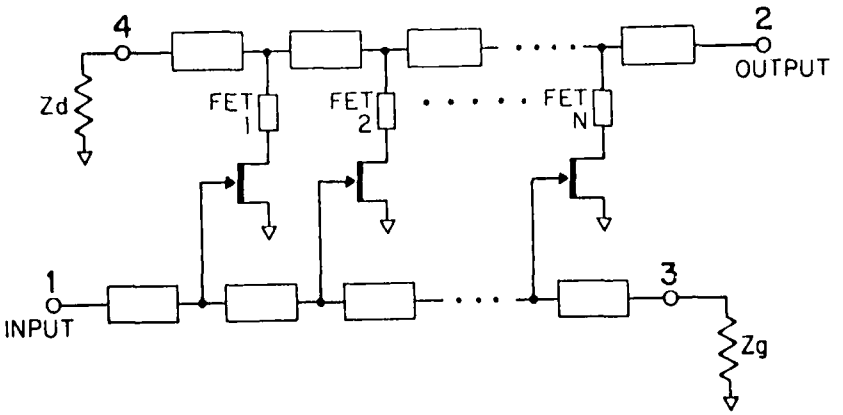

Fig. 1 Distributed amplifier schematic.

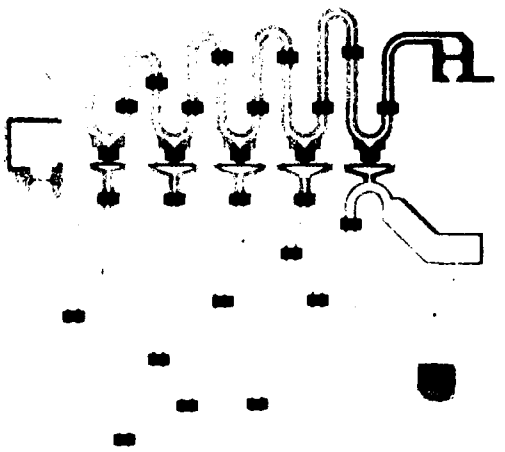

Fig. 2 2-20 GHz coplanar distributed amplifier.

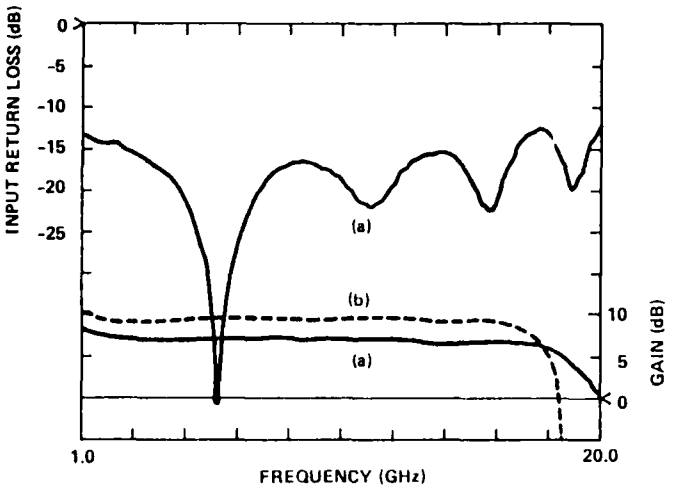

Fig. 3 (a) Distributed amplifier gain and return loss with nominal channel doping of 3-5 x 10^{17} cm^{-3}; (b) amplifier gain with nominal doping of 5 x 10^{17} cm^{-3}.

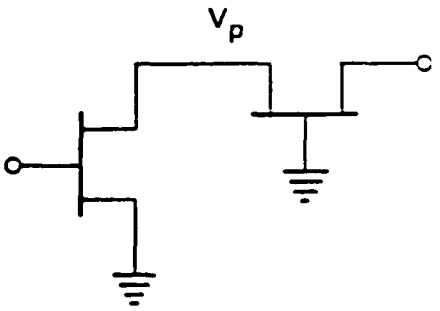

Fig. 4 Cascode connection of of two FETs.

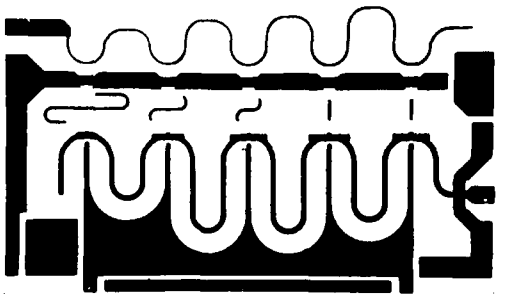

Fig. 5 2-20 GHz cascode distributed amplifier.

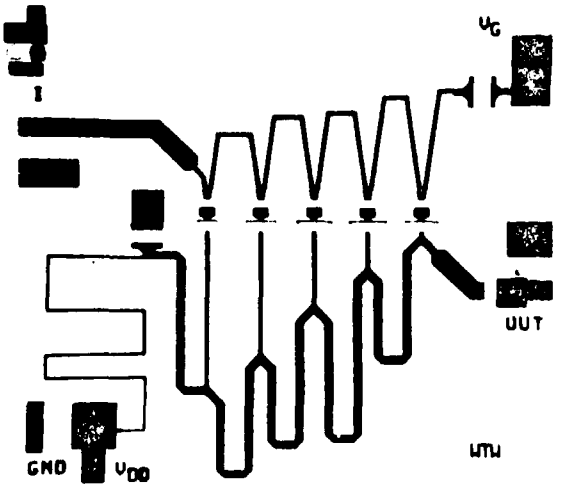

Fig. 6 HEMT distributed amplifier.

High Performance Quarter-Micron-Gate MODFETs*

John J. Berenz

TRW Electronic Systems Group
One Space Park
Redondo Beach, CA 90278

Modulation-doped FETs provide a significant performance advantage over conventional GaAs FETs due to the superior transport properties of the two-dimensional electrons which form the conductive channel in these devices. Table 1 compares the material and device characteristics of different FET devices. At TRW quarter-micron-gate AlGaAs/GaAs MODFETs have been fabricated with cut-off frequencies as high as 80 GHz. These devices exhibit noise figures as low as 2.4 dB at 60 GHz with over 7 dB of associated gain. Power-added efficiencies as high as 42 percent have been achieved at 20 GHz. Figure 1 clearly shows the performance advantage of MODFETs over MESFETs in these RF applications.

Further improvement in performance is expected for InGaAs MODFETs due to their higher electron velocity, higher electron mobility, and lower thermal noise. Pseudo-morphic AlGaAs/InGaAs MODFETs made by the University of Illinois exhibit a noise figure of 0.9 dB at 18 GHz with 10.4 dB associated gain. This is comparable to the state-of-the-art performance achieved with AlGaAs/GaAs MODFETs (Table 1). With further improvement of the fabrication and material technology, performance better than GaAs MODFETs will ultimately be achieved.

---

* Also known as High Electron Mobility Transistors (HEMT)

Table 1. Comparison of Material and Device Characteristics

ACTIVE LAYER	MOBILITY cm^2/Vs	VELOCITY cm/s	F_T GHz	NF (18 GHz) dB
GaAs	3500	1×10^7	35	1.1
AlGaAs/GaAs	8000	2×10^7	80	0.9
AlGaAs/InGaAs	9500	3×10^7	80	0.9

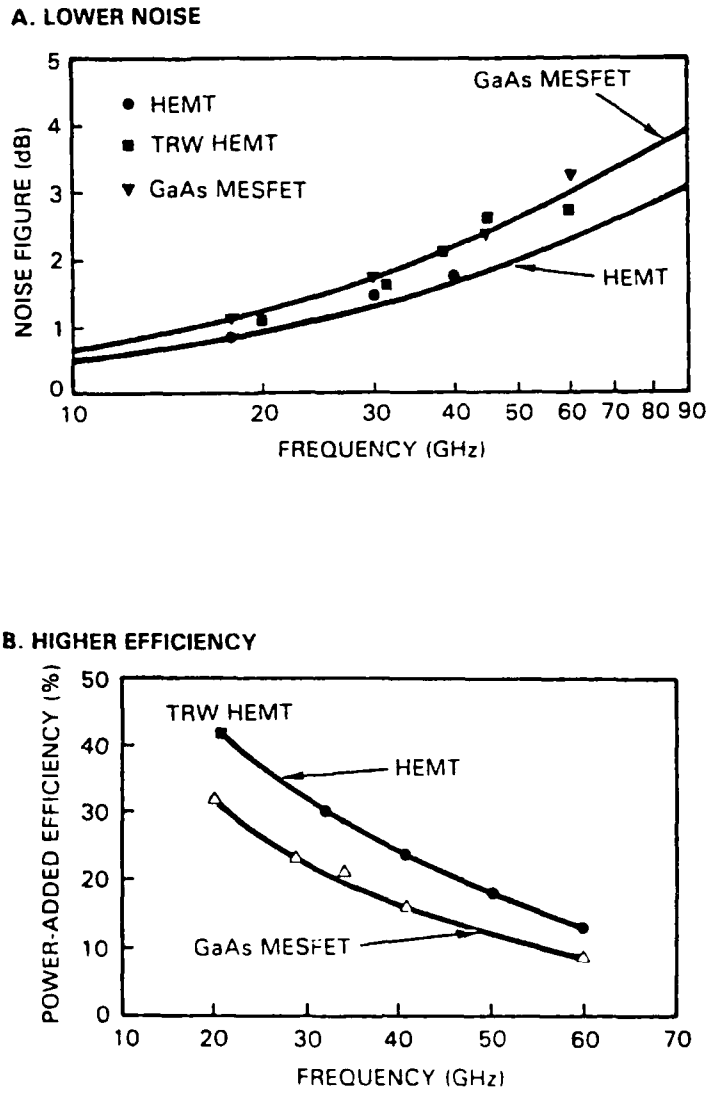

Figure 1. Comparison of MESFET and HEMT Performance

Picosecond Photoconductive Transcievers

Alfred P. DeFonzo, Charles R. Lutz and Madhuri Jarwala

Department of Electrical and Computer Engineering
The University of Massachusetts, Amherst

Recent studies [1,2,3] of electromagnetic transients from gap discontinuities in microstrip structures driven by picosecond and subpicosecond photoconductive currents indicate a potential for using optical means for generating and detecting milllimeter waves. It has been demonstrated [ ]that short coherent burst of radiation with wavelength components in the millimeter and submillimeter range can be used to perform fundamental studies of materials suitable for a variety of uses including: electro-optic samplers, modulators and millimeter wave circuits. It is desirable to have more sophisticated antenna elements than gap discontinuities that can provide a greater degree of control of the space and time distribution of photoconductively generated and detected radiation. To be of general use, it is also desirable that such antennas be of a size comparable to other device elements found in integrated millimeter wave cicuits and be fabricated on standard substrate materials using planar technology.

In this paper we will present the results of a series of measurements that compare the picosecond transient response of two photoconductive antenna elements in matched transmitting and receiving pairs, that have the foregoing desirable features. Each transcieving pair was similar in all respects (size, sustrate etc.) except for the shape of the radiating/receiving surface. They were fabricated on aluminized silicon on saphire substrates (substrate thickness= 425 microns , epilayer thickness .5 microns) using standard photolithographic techniques. The silicon epilayer was prebombarded with 100kev and 200 kev oxygen ions. One transcieving pair was an exponentially tapered slot, "ETSA". A linear tapered slot antenna ,"LTSA", was chosen for the other pair. The lengths,L, and apertures sizes, A1 and A2, were the same for both pairs (L=2.96mm , A1= 25 microns, A2= 1.9mm).

Shown schematically in Figure 1 is the antenna configuration used in our measurements. Unlike previous configurations [1,2], our configuration is completely planar and does not use apertures between the transmitter and reciever in order to avoid unwanted defraction,filtering or spurious radiation. The generation and recieving elements were spaced 9mm apart with the antennas operating in end fire. We used a picosecond pump-probe autocorelation measurement scheme similar to that used by Auston [1] and others [2] to study Hertzian dipoles.

In Figure 2(a) we show a trace of the correlation for the ETSA pair. Superimposed is a direct correlation of the photoconductive transient measured directly on the same material using a conventional microstrip correlator. The data clearly demonstrates that the radiation correlation is the time derivative of the microstrip correllation. Earlier work at much longer time scales[4] indicates that the ETSA takes the derivative of the generator signal on transmission. This leads to the conclusion that the ETSA replicates the transmitted signal on reception and detection. The secondary pulses are reflections and arrive at the detector delayed by the time it takes the radiation, propogating at the speed of light, to travel the roundtrip distance, 18 mm, between the generator and detector.

In Figure 2 (b) we show a trace of the correlation for the LTSA pair again superimposed on the directly correlated photoconductive signal. The data clearly demonstrates that , apart from small moduiation of the tails, the LTSA correlation nearly replicates the overall time dependence of the photoconductive generator signal. These results indicate that the LSAT is very broadband and that the transmitter and reciever response functions have similar .

The reflected pulse is clearly resovled with neglible spurious pulses. Since the pulses are decidedly shorter than the transit time along the antenna length , this indicates that the antennas radiate primarily in a traveling wave mode. The antennas have matched loads only during a small time because they are time gated by the short optical pulses. Thus for a given sampling event most of the radiation is reflected . The relatively slow rate of anttenuation of the reflected signal indicates good confinement of the radiation in the endfire direction.

Experimental and theorectical studies are underway to precisely characterize and model the transient gain of a variety of antenna elements.

We conclude that picosecond photoconductivity can be used in conjunction with appropiate antenna technology to achieve practical generation, control and sensing of millimeter waves. Our results indicate that these antennas can be readily scaled to dimensions suitable for operation with femtosecond transients.

1.D.H. Auston, K.P. Cheung and P.R. Smith, "Picosecond photoconducting HErtzian dipoles",Appl.Phys. Lett.,45,p284-286 (1984)

2.J.R. Karin, P.M. Downey, and R.J. Martin,"Radiation from picosecond photoconductors in microstrip transmission lines", IEEE Journ.of Quantm. Electrns., QE-22,,p 677-681,(1986)

3. D.H. Auston, K.P. Cheung, J.A. Valdmanis, and D.A. Kleinmen, Phys.Rev. Lett.,53,155(1984)

4.R.Heidemann, Th. Pfeiffer,and D.Jager,Electrncs. Lettrs.,19,p316 (1983)

Figure 1. Schematic of experimental configuration using matched picosecond photoconductive planar antenna pairs. Solid lines indicate exponentially tapered slot antennas (ETSA). Dashed lines indicate linearly tapered slot antennas (LTSA). The pump pulse excites the transmitter at time T and the probe pulse samples the receiver at T+ t.

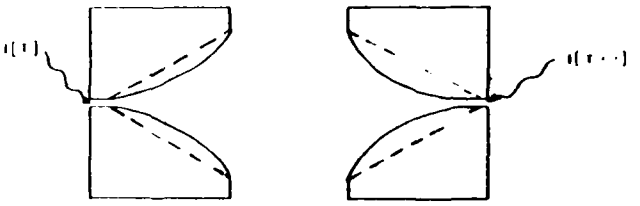

Figure 2. Traces of microstrip and antenna autocorrelations: upper trace measured for ETSA; lower trace measured for LTSA.

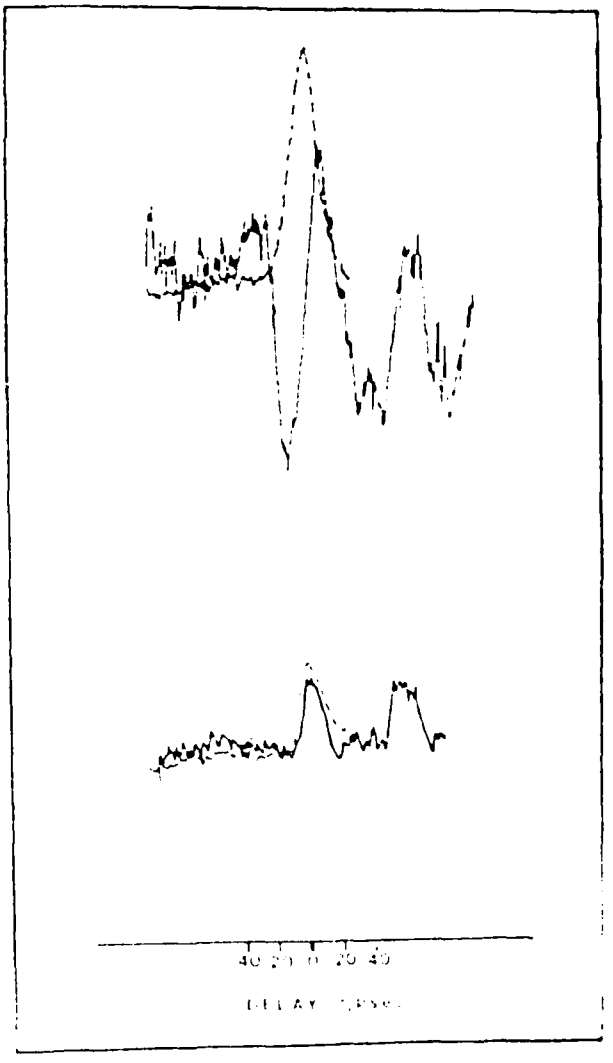

WEDNESDAY, JANUARY 14, 1987

PROSPECTOR/RUBICON ROOM
4:00 P.M.–5:15 P.M.

WD1–3

S. M. Faris, Hypres, Inc., *Presider*

Photoconductive Generation of Sub-Picosecond Electrical Pulses and their Measurement Applications*

D. Grischkowsky, C-C. Chi, I.N. Duling III, W.J. Gallagher, N.J. Halas**
J-M. Halbout, and M.B. Ketchen

IBM Watson Research Center, Yorktown Heights, New York 10598

The generation of short electrical pulses via optical methods has for some time been performed by driving Auston switches (photoconductive gaps) with short laser pulses.(1) The shape of the electrical pulse depends on the laser pulseshape, the material properties of the semiconductor, the nature of the charge source, and the characteristics of the associated electrical transmission line. The same techniques can also measure the generated electrical pulses by sampling methods. An alternative measurement approach has been to use the electro-optic effect in a nonlinear crystal.(2) In this case, the field of the electrical pulse is sampled through the rotation of the polarization of the optical sampling pulse. Because it has demonstrated 460 fsec time resolution,(3) the electro-optic method is presently considered to be the fastest sampling technique. However, recent work utilizing photo-conductive switches has generated and measured subpicosecond electrical pulses.(4) This order of magnitude reduction in the generated pulsewidth demonstrates the ultrafast capability of the Auston switches and calls into question the conventional wisdom that electro-optic methods must be used to obtain ultrafast time resolution.

In the initial demonstration of subpsec electrical pulse generation using photoconductive gaps, the sampling measurements gave a total measured pulsewidth of 1.1 psec.(4) When the response time of the sampling gap was deconvolved from this value, the generated electrical pulse was determined to be of the order of 0.6 psec. The data analysis followed Auston's theory(1) and assigned capacitances of 1 fF to the "sliding contact" generation site and 4 fF to the sampling gap. The carrier lifetime was considered to be 250 fsec. Since this measurement, we have generated and measured the electrical pulses using only sliding contacts.(5) This improved technique reduced the capacitance at the optical sampling site to approximately 1 fF and resulted in a total measured pulsewidth of 0.85 psec. This value was significantly larger than expected in view of the assumed carrier lifetime of 250 fsec. Later direct measurements of the carrier lifetime obtained a limiting value of 600 fsec for ion-implanted silicon-on-sapphire(SOS).(6) Thus, the generated pulsewidths are limited by the carrier lifetime to 600 fsec. These conclusions will be discussed in detail, measurements and supporting numerical analysis will be presented.

The fact that we can now generate and propagate subpsec electrical pulses with frequency bandwidths extending to beyond 1 THz allows us to consider spectroscopic applications in this frequency range. In order to make these measurements, the pulse reshaping must be determined only by the dispersion and absorption properties of the transmission line materials, and not by spatial dispersion or multi-mode effects. We elimi-

nated these complications, as follows: firstly, by reducing the dimensions of our co-planar transmission line to 5 micron lines separated by 10 microns, the spatial dispersion effects were eliminated; secondly, by using the sliding contact method of pulse generation only the differential mode was excited. Ordinary side gap generation equally excites both the differential mode and the common mode. Consequently, our initial propagation studies with an Al coplanar transmission line showed less dispersion than had been previously demonstrated. Via Fourier analysis of the input and propagated pulses we were able to characterize the dielectric response of the transmission line to beyond 1 THz.(7) Our next spectroscopic application was to study superconducting niobium lines. Following the same methods, we were able to demonstrate that reshaping of the propagating pulse was determined by the superconductor. Fourier analysis of the propagated pulses allowed us to obtain the line absorption as a function of frequency which showed an abrupt absorption increase at a frequency corresponding to that of the superconducting gap.(8) Furthermore, we were able to measure the temperature dependence of the gap frequency. These techniques and applications will be discussed in detail and new results will be shown.

* This research was partially supported by the U.S. Office of Naval Research.

**Bryn Mawr College, Bryn Mawr, Pennsylvania.

References

1. D.H. Auston, in "Picosecond Optoelectronic Devices, edited by C.H. Lee (Academic, London, 1984), pp. 73-116.

2. J.A. Valdmanis, G.A. Mourou, and C.W. Gabel, IEEE J. Quantum Electron. QE-19, 664 (1983).

3. G.A. Mourou and R.E. Meyer, Appl. Phys. Lett. 45, 492 (1984).

4. M.B. Ketchen, D. Grischkowsky, T.C. Chen, C-C. Chi, I.N. Duling III, N.J. Halas, J-M Halbout, J.A. Kash, and G.P. Li, Appl. Phys. Lett. 48, 751 (1986).

5. P.G. May, G.P. Li, J-M. Halbout, M.B. Ketchen, C-C. Chi, M. Scheuermann, I.N. Duling III, D. Grischkowsky and M. Smyth, "Proceedings of the 5th International Conference on Ultrafast Phenomena", Snowmass, Colorado, June 16-19, 1986.

6. F.E. Doany, D. Grischkowsky, and C-C. Chi, "Proceedings of the 2nd Topical Meeting on Picosecond Electronics and Optoelectronics" Incline Village, Nevada, January 14-16, 1987.

7. N.J. Halas, I.N. Duling III, M.B. Ketchen, and D. Grischkowsky, Digest of Technical Papers, Conference on Lasers and Electro-Optics, San Francisco, June 9-13, 1986.

8. I.N. Duling III, C-C. Chi, W.J. Gallagher, D. Grischkowsky, N.J. Halas, M.B. Ketchen and A.W. Kleinsasser, "Proceedings of the 5th International Confernce on Ultrafast Phenomena" Snowmass, Colorado, June 16-19, 1986.

WD2-1

Progress and Challenges in HEMT LSI Technology

Masayuki Abe, Takashi Mimura, Kazuo Kondo, and Masaaki Kobayashi

Fujitsu Laboratories Ltd., Fujitsu Limited
10-1 Morinosato-Wakamiya, Atsugi 243-01, Japan

I. Introduction

Six years have now passed since the announcement in 1980 of the High Electron Mobility Transistor (HEMT)[1], and HEMT technology has certainly opened the door to new possibilities for ultra-high-speed LSI/VLSI applications[2]. Due to the supermobility GaAs/AlGaAs heterojunction structure, the HEMT is especially attractive for low-temperature operations at liquid nitrogen temperature. For LSI level complexity, HEMT technology has made it possible to develop a 1.5 kgate gate array with an 8 x 8 bit parallel multiplier[3] for logic circuits, and 4 kbit static RAM for memory circuits.[4]

This paper presents the performance advantages of HEMT approaches, and recent progress and future technical challenges for LSI/VLSI applications.

II. Performance Advantages and Self-Aligned Gate HEMT Structure

HEMT has performance advantages over conventional devices, because of the superior electron dynamics of HEMT channels and unique electrical properties of device structure. During switching, the speed of the device is limited by both low-field mobility and saturated drift velocity. Low field mobility routinely obtained is 8 000 $cm^2/V.s$ at 300K and 40 000 $cm^2/V.s$ at 77K. Saturated drift velocity measured with HEMT structures at room temperature has been reported to be 1.5 to 1.9 x 10^7 cm/s. These superior transport properties in HEMT channels would result in a high average current-gain-cutoff frequency f_T value. In Fig. 1, the current-gain-cutoff frequency f_T versus gate length summarizes for experimental HEMTs and GaAs MESFETs reported so far. At room temperature, the values of f_T were 38 GHz[5] and 80 GHz[6] for HEMTs with gate length of 0.5 μm and 0.25 μm, respectively, and about twice those for GaAs MESFETs. Goine to LSI circuits with low power dissipation per gate, logic voltage swing should be minimized. The smaller level of logic voltage swing requires more precisely controlled threshold voltages with the smaller standard deviation.

Figure 2 is a cross-sectional view of a self-aligned gate structure of enhancement-mode (E) and depletion-mode (D) HEMTs. The basic epilayer structure consists of a 600 nm undoped GaAs layer, a 30 nm $Al_{0.3}Ga_{0.7}As$ layer doped to 2 x 10^{18} cm^{-3} with Si, and a 70 nm GaAs top layer with a thin $Al_{0.3}Ga_{0.7}As$ layer, successively grown on a semi-insulating GaAs substrate by MBE. The key technique to achieve stable fabrication of self-aligned gate HEMTs is the selective dry etching of the GaAs/AlGaAs layer using CCl_2F_2 + He discharges. A high selectivity ratio of more than 260 is achieved, where the etching rate of $Al_{0.3}Ga_{0.7}As$ is as low as 2 nm/min and that of GaAs is about 520 nm/min. State-of-the-art standard deviations are 6 mV for E-HEMTs and 11 mV for D-HEMTs respectively, for 10 mm x 10 mm area.[7] The ratio of 6 mV to the logic voltage swing (0.8 V for DCFL) is 0.7 %, indicating excellent controllability for realizing the ICs with LSI/VLSI-level complexities.

The material problems in HEMT LSI fabrications have been greatly improved to achieve high quality MBE wafer with large size and high throughput.[8] Selectively doped GaAs/n-AlGaAs heterostructures were grown on semi-insulating GaAs substrates mounted on a substrate holder with a diameter 190 mm. The variations of both the thickness and carrier concentration of

Si-doped n-AlGaAs layer were less than ±1% over a diameter of 180 mm. The density of oval defects was also greatly reduced to achieve a density of less than 40 cm^{-2} by optimizing the growth conditions.

III. HEMT LSI Implementations and Future Prospects

The current implementations and future prospects of HEMT logic and memory LSIs are reviewed and discussed.

For logic LSI circuits, a HEMT 1.5 kgate gate array with E/D type DCFL circuits is designed and fabricated.[3] The chip size is 5.5 mm x 5.6 mm, containing 6 656 devices with 1.2 μm gate length and 2 μm line width and spacing minimum. A microphotograph of the chip is shown in Fig. 3. For a test vehicle an 8 x 8 bit parallel multiplier with a carry look ahead circuit was designed. The multiplier consists of 888 basic cells. Multiplication times of 4.9 ns at 300K, and 3.1 ns at 77K, were achieved, where supply voltages and total chip power consumption were 2.2V, 5.8W and 0.95V, 3.2W, respectively, including a 5 stage I/O buffer delay.

Performance of HEMT VLSI for future high-speed computers is projected and discussed.[9] Chip delay time is the sum of intrinsic gate delay, logic layout delay on fan-out capability, and delay in the wiring on the chip. Here we assume that fan-out is 3, logic voltage swing is 0.8 V, wiring capacitance is 100 fF/mm, average line length is 1 mm in the chip, and heat flux for liquid cooling is 20 W/cm^2. Figure 4 shows chip delay as functions of complexity, under 0.5 μm design rule HEMT technology. At 10^4 gates, the chip delays are 70 ps at 300K and 40 ps at 77K, and system delays including external wiring delays for packaging are 100 ps at 300K and 70 ps at 77K, sufficient for future high-speed computer requirements.

For memory LSI circuits, a HEMT 16K x 1 bit fully decoded static RAM[10] has been successfully developed with the E/D-type DCFL circuit configuration. As the result of the RAM layout design, the chip size is 4.3 mm x 5.5 mm, and the RAM cell size is 23 μm x 30 μm with the switching devices having gate length of 1.2 μm. The RAM has a total device count of 107 519. The minimum address access time obtained was 3.4 ns, with a chip dissipation power of 1.34 W at 77K. Figure 5 shows the address access time and power dissipation of the HEMT static RAMs, compared to SiMOS, bipolar, and GaAs MESFET static RAMs. The plots show the performances of the HEMT 1 kbit, 4 kbit and 16 kbit static RAMs at 77K. The shadow area shows the projected performance assuming device technologies between 1 and 0.5 μm. By using 0.5 μm gate device technology, subnanosecond address access time can be projected for the 64 kbit static RAM.

VI. Summary

Recent progress and future technological challenges in HEMT technology for high-performance VLSI were reviewed and discussed.

HEMTs are very promising devices for VLSI, especially operating at liquid nitrogen temperatures, because of their ultra-high speed and low power dissipation. The performance described here will achieve speeds required for future large-scale computers.

Acknowledgment

The authors wish to thank Dr. T. Misugi, Dr. M. Fukuta for their encouragement and support. The present research effort is the National Research and Development Program on the "Scientific Computing System," conducted under a program set by the Agency of Industrial Science and Technology, Ministry of International Trade and Industry, Japan.

References

1) T. Mimura, et al., Japan. J. Appl. Phys., 19 (1980) L225.
2) M. Abe, et al., IEEE Trans. Electron Devices, ED-29 (1982) 1088.

3) Y. Watanabe et al., ISSCC Dig. Tech. papers, XXIX (1986) 80.
4) S. Kuroda et al., IEEE GaAs IC Symp. Tech. Dig. (1984) 125.
5) K. Joshin et al., IEEE MTT-S Dig. (1983) 563.
6) P. C. Chao et al., IEEE Electron Device Letters, EDL-6 (1985) 531.
7) N. Kobayashi et al., IEEE Trans. Electron Devices, ED-33 (1986) 548.
8) J. Saito et al., the 4th Int. conf. on MBE, D-12 (1986).
9) M. Abe et al., IEEE GaAs IC Symp., Tech. Dig. (1983) 158.
10) M. Abe et al., 10th Int. Vacuum Congress, EM-Mo5 (1986).

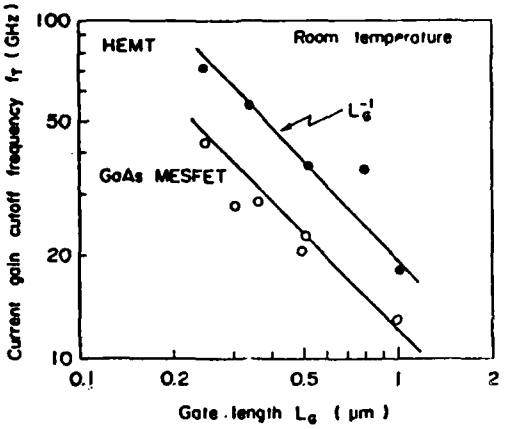

Fig. 1 Current-gain-cutoff frequency versus gate length for HEMTs and GaAs MESFETs.

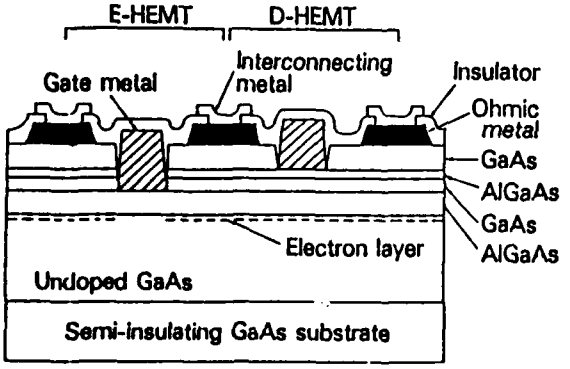

Fig. 2 Cross sectional view of a self-aligned gate E/D-HEMTs.

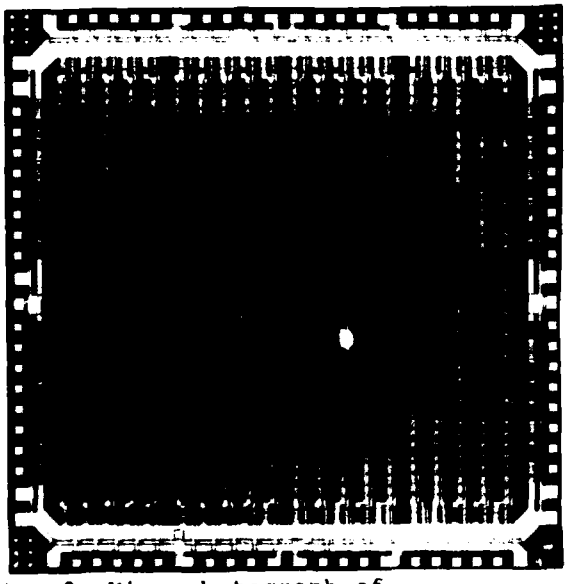

Fig. 3 Microphotograph of HEMT 1.5 kgate gate array.

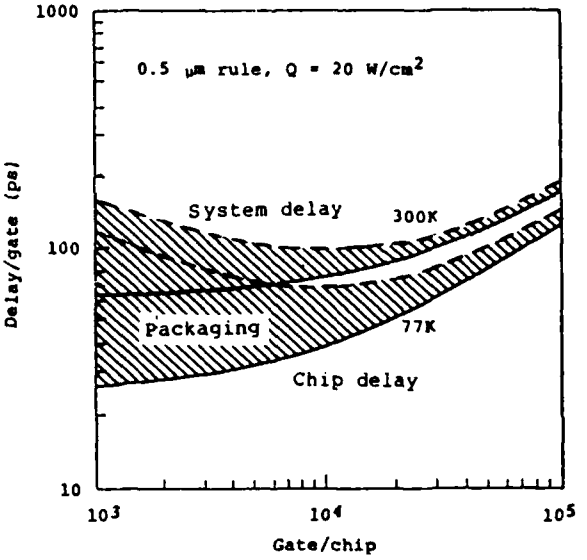

Fig. 4 Chip and system delays calculated as a function of complexity.

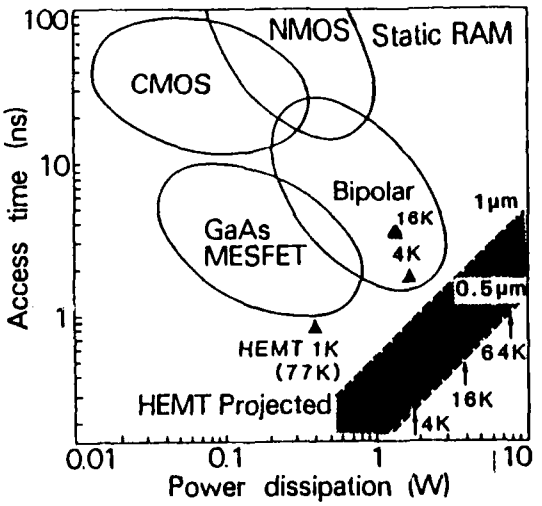

Fig. 5 Address access time and power dissipation of the static RAMs. The plots show the performances of the HEMT static RAMs.

Picosecond switching in Josephson tunnel junctions

R. Sobolewski,[a]* D.R. Dykaar,[ab] T.Y. Hsiang[a] and G.A. Mourou[b]

Department of Electrical Engineering[a]
The University of Rochester
Rochester NY 14627
716-275 4054

Laboratory for Laser Energetics[b]
The University of Rochester
250 East River Road
Rochester NY 14623
716-275 5101

In this work we have followed our earlier attempts to apply the electro-optic sampler to superconducting electronics,[1] and developed a fully cryogenic electro-optic sampler by integrating and immersing in superfluid helium both the photo-conductive switch and the birefringent lithium tantalate sensor. The ultimate temporal response of the system[2] as determined by measuring the transient onset of photoconductivity in a GaAs switch was less than 400 fs. The system was arranged in to two different configurations and used to probe the switching of a 30 x 30 μm^2 Josephson tunnel junction.

(a) A coplanar transmission line configuration was arranged in the same way as a typical transfer function measurement in a two-port microwave network. For a fixed input signal, we measured the signal waveform with a resistor substituted for the junction and compared this with the waveform obtained with the junction included in the transmission line. We attribute the observed (see Fig. 1) difference in the waveforms to the different propagating conditions, caused by the junction switching from the zero-voltage to the finite-voltage state.

(b) The voltmeter or "side sampling" configuration was designed to measure directly the switching voltage across the junction. In this case the input pulse propagates in the main transmission line on GaAs, while the junction signal is transmitted into the $LiTaO_3$ coplanar waveguide.

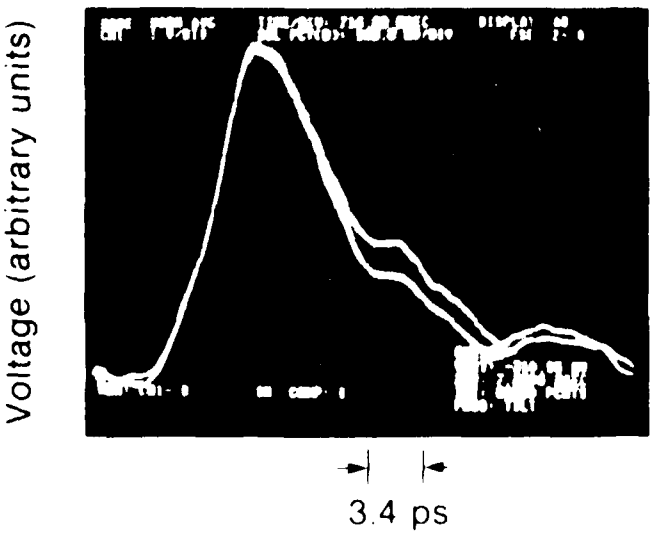

Figure 1. Junction voltage waveforms. Upper curve corresponds to the "no junction" condition in the transmission line, and the lower curve in the unbiased junction response.

The difficulty of these measurements lied in discriminating between the junction response of less than three millivolts, and much larger signals from the photoconductive switch. In order to achieve the desired sensitivity, the lock-in reference frequency (switch bias) was chosen in the 2 - 4 MHz range, above the 1/f region of the CPM noise spectrum. As in the previous low frequency arrangement,[1] a differential measurement was made using the two polarizations from the final polarizer to increase the signal to noise ratio.

The time domain studies were supplemented by systematic measurements of the current-voltage (I–V) characteristics of the junction. The junction I-V characteristics for two different excitation conditions (switch pulse amplitudes) are shown in Fig. 2. As can be seen in Fig. 2a for small input pulses only the positive branch of the I-V curve is affected. The negative branch in practically untouched (we noted only a small decrease in the amplitude of I_C). This corresponds to the case where the switching pulse amplitude was roughly equal to the critical current, and the switching events were completely independent.

A very different situation is shown in Fig. 2b. Based on the estimation made in the former case, the input pulse amplitude is now about $3I_C$. The positive branch displays a smooth curve, typical for quasiparticle tunneling, while on the negative branch we observe very rapid oscillations between the gap voltage state and some voltage around the midgap value. The entire I-V curve shifts slightly along the positive current axis. Finally, we note that the gap voltages for both positive and negative branches remain the same as for the unperturbed junction. Thus, the entire behavior must be associated with the junction response itself, because the DC superconductive properties of junction electrodes are unchanged.

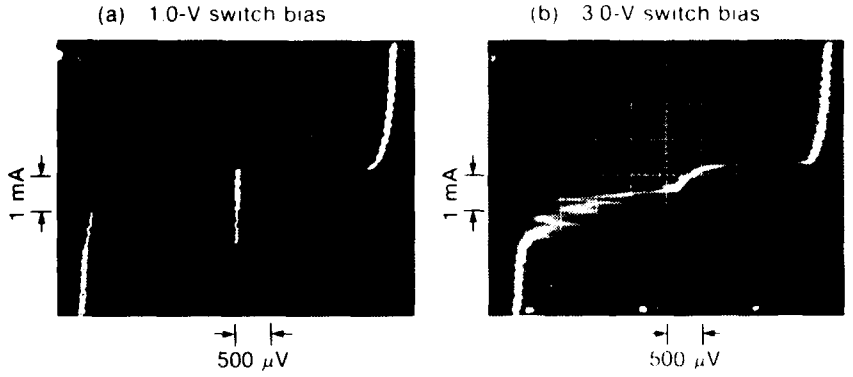

Figure 2. Junction DC I–V curves for two different values of the amplitude of the input pulse. Due to the corrected, two-wire measurements, the gap voltages displayed appear to be slightly reduced.

We also performed extensive numerical simulations, based on the resistively and capacitively shunted junction (RCSJ) model. A typical simulated junction response for a picosecond input pulse with amplitude equal to $1.2I_C$ is presented in Fig. 3. One notices that despite the fact that the input pulse amplitude is larger than I_C, the junction output voltage peak reaches only about half of the value corresponding to the gap voltage. The pulse exhibits a very short rise, followed by a substantial, exponential decay. The turn-on delay time is negligible.

The physical mechanisms can be easily understood in terms of a simple model that approximates the junction response as the charging of the junction capacitance.[3] The only limiting factor in the junction response time is how fast the input pulse charge, Q, is delivered to the junction capacitance. The switching voltage is just $Q(t_p)/C_J$, and the corresponding rise time is roughly the input pulse width itself. On the other hand the junction decay is totally dominated by the properties of the dielectric layer and the associated RC time constant. These features agree very well with the experimental observations shown in Fig. 1.

For very high amplitude input pulses we noticed that when there is no DC bias to maintain the switching conditions, the switching voltage is not the gap voltage itself, but rather the point on the quasiparticle I-V curve characterized by the longest time constant.

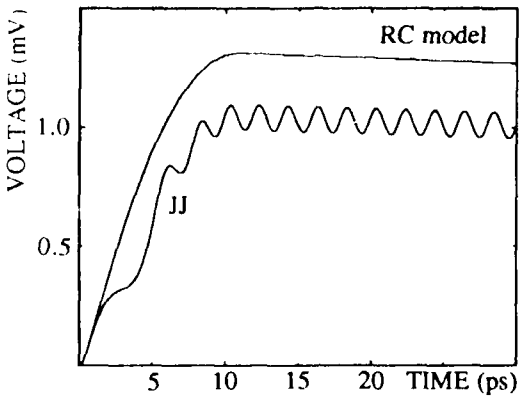

Figure 3. The simulated Josephson junction response (JJ curve) to a stepped input pulse of amplitude $1.2I_C$ and duration $t_p \approx 10$ ps. The full solution of the RCSJ model is compared to the prediction of the charging capacitance model.[3] Junction parameters are the following: $I_C = 2.75$ mA, $R_J = 0.6\ \Omega$, $R_1 = 35\ \Omega$, $C_J = 16$ pF.

This work was supported by the National Science Foundation (DMR-85-06689). In addition, the laser facility was partially supported by the Laser Fusion Feasibility Project at the Laboratory for Laser Energetics. The Josephson junction structures were fabricated at the Cryogenic Division of National Bureau of Standards, Boulder, Colorado. One of us (R. S.) would like to thank C. Hamilton and others members of the Cryogenic Division Group for their hospitality and help during his visit.

References

*Permanent address: Institute of Physics, Polish Academy of Sciences, PL-02668 Warszawa, Poland.

1. D. R. Dykaar, T. Y. Hsiang and G. A. Mourou, "An application of picosecond electro-optic sampling to superconducting electronics," IEEE Trans. Magn., **MAG-21**, 230, 1985.
2. D. R. Dykaar, R. Sobolewski, J. F. Whitaker, T. Y. Hsiang, G. A. Mourou, M. A. Holis, B. J. Clifton, K. B. Nichols, C. O. Bozler and R. A. Murphy, "Picosecond characterization of ultrafast phenomena – new devices and new techniques" in **Ultrafast Phenomena**, Springer & Verlag Series on Chemical Physics -- in print.
3. D. R. Dykaar, R. Sobolewski, T. Y. Hsiang and G. A. Mourou, "Response of a Josephson junction to a stepped voltage pulse," IEEE Trans. Magn. -- in print.

NOTES

WEDNESDAY, JANUARY 14, 1987

SIERRA ROOM
5:30 P.M.–7:00 P.M.

WE1–16

POSTER SESSION

High Speed, High Repetition Rate, High Voltage Photoconductive Switching

William R. Donaldson
Laboratory for Laser Energetics
University of Rochester
250 East River Road
Rochester, NY 14623
716/275-5101

We describe a method of producing robust silicon photconductive switches. These switches are used in high power applications where it is necessary to switch high voltages on the picosecond time scale. They have the advantage that they are activated by the bulk absorption of light in a semiconductor.[1] Thus avalanching and transit time effects normally associated with high voltage switches are absent. As a result the switches have no jitter with respect to the optical pulse and very little heating due to the joule energy deposited in the switch as they turn on.[2] These qualities make these switches desirable in applications which require parallelism or low thermal energy deposited in the switch. However, photoconductive switches cannot be used in practical applications until they can be proven reliable.

The photoconductive switch is inherently a very simple and robust device consisting only of a block if intrinsic silicon. Silicon is the material of choise for these applications because its long recombination time enables the the switch to stay on for long periods of time which increases the amount of energy delivered to the load. It is possible to obtain current densities as high as 13 kA/cm^2.[3] The difficulty of constructing a reliable photoconductive switch comes from the external connections to the silicon. First, it is necessary to produce an appropiate contact pad on the silicon itself. We have found that by laser annealing evaporated gold or aluminium contacts we can produce a contact which is ohmic and reduces the dark current leakage.[4] However, the question still remains on how to achieve a contact to the external circuit. Wirebonding is inadequate because of the high voltages and current densities. Mechanical pressure contacts would be compatible with these high current densities. However, contact must have a geometry which is compatible with the frequency requirements of the external circuit. Typically, a photoconductive switch is mounted in a transmission line to provide the cleanest electrical pulse with a mimium of electrical reflections. Conductive epoxies provide a convenient method of attaching the switch to the circuit, but our experience is that the high electric fields in the off state cause the epoxy to migrate. Eventually, this resulted in the switch shorting out. In high repetition rate systems this was the dominate mode of failure and it limited the switch lifetime to 10^5 shots. We have devised a simple method of soldering the silicon into the circuit with low temperature indium solder which produces mechanically sound contacts that blend smoothly into the transmission line geometry.

These switches were tested using a high repetition rate regenerative amplifier. With the switch mounted in silicone oil, a 10 kV bias pulse was placed across a 2 mm wide silicon switch and triggered at 1 kHz. The results were 10 ns wide pulses with a 100 ps rise time. There was no degradetion in switch performance with over 10^8 shots applied.

In addition to the lifetime time test listed above we studied the persistance of the photoconductivity as function of the time after the trigger pulse. This information is

important for determining the amount of energy the switch can deliver to the load. The photoconductivity decays exponentially with time. The time constant was found to increase approximately linearly as the density of photogenerated carriers increased up to the maximum density we observed of $1x10^{18}$/cc. This behavior is shown in Fig. 1 for a bias of 100 v applied to the switch. The time constant of the decay was also found to to be related to the applied electric field. As the voltage was increased the time constant decreased. This seems to indicate that the charge carriers are being swept out of the silicon by the field. This effect can be at least partially compensated by increasing the initial carrier density.

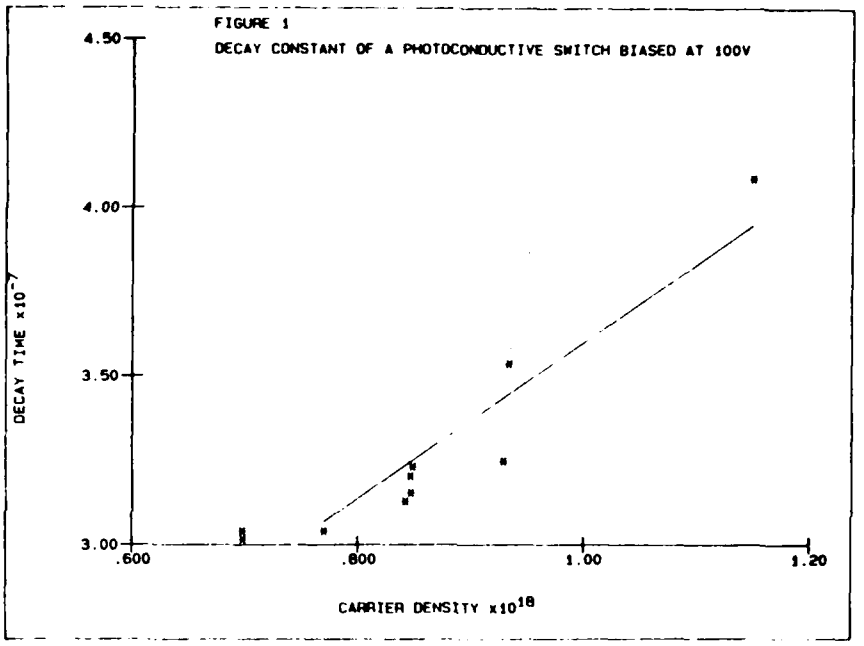

We have demonstrated a method of constructing silicon photoconductive switches which yields robust high voltage switches whose performance has been shown not to degrade in high repetition rate operation. Time dependence of the photconductive signal has been studied and found to be dependent on the initial concentration of carriers and the applied field.

Acknowledgment

This work was supported by the sponsors of the Laser Fusion Feasibility Project at the Laboratory for Laser Energetics and by the Air Force Office of Scientific Research.

References

1. D.H. Auston, "Picosecond Optoelectronic Switching and Gating in Silicon," Appl. Phys. Lett. 26, 101 (1975).

2. A. Antonetti, M.M. Mally, G. Mourou, and A. Orszag, "High Power Switching with Picosecond Precision," Opt. Commun. 23, 453 (1977).

3. W.C. Nunnally and R.B. Hammond, "Optoelectronic Switch for Pulsed Power," Picosecond Optoelectronic Devices, ed. Chi H. Lee (Academic Press, New York, 1984), p. 509.

4. W. Donaldson and G. Mourou, "Improved Contacts on Intrinsic Silicon for High Voltage Photoconductive Switching," Fifth IEEE Pulsed Power Conference, ed. P. Turchi and M. Rose.

Generation and Forming of Ultrashort High Voltage Pulses

Hrayr A. Sayadian, S. T. Feng, J. Goldhar, and Chi H. Lee
Department of Electrical Engineering
University of Maryland
College Park, MD 20742

High voltage pulse forming techniques, utilizing spark gaps, is a mature field. However, problems associated with synchronizing spark gap switching, in the picosecond regime, limit its application. A new approach, developed over the past few years, is to use laser controlled photoconductive switches in generating ultrashort high voltage pulses.[1] The use of photoconductive switches achieves picosecond synchronization and very long lifetimes. Furthermore such switches can be readily incorporated into various types of pulse generating and forming structures. We report here on an investigation of the performance of various types of high voltage generating structures with photoconductive switches. These include Blumleins (with multiple switches), Marx banks, stacked lines and L.C. generators in coaxial, microstrip and coplanar geometries. High voltage pulses with picosecond rise and fall times were generated and monitored using Pockels cells monolithically integrated with the pulse forming structures. Using dc charged voltage multiplication circuits, up to 5 kv was generated in nanosecond pulses. Also, 5 kv of peak to peak RF single cycle pulses were generated using a similar multiplication circuit. This type of RF pulses have important applications in high resolution radar systems.[2]

Representative data is shown in Fig. 1. The pulse generator consisted of 5 mm microstrip structure, with composite GaAs-glass dielectric with GaAs as the switch, whose effective round trip length is 100 picoseconds. The microstrip is biased to 2 kv dc. The observation of the electrical pulse was made using a miniature homemade longitudinal Pockels electro-optic modulator. The electro-optic material used was KD*P. An active-passive mode-locked Nd:YAG laser was used to generate 200 μJ of 0.53 μm radiation with 35 picoseconds pulsewidth. Each optical pulse was split into two pulses, one going through the Pockels cell so as to probe the electrical pulse, the other optical pulse was used to trigger the GaAs photoconductive switch. By varying the optical delay between the probing and switching pulses, we have monitored the generated electrical pulses. In Fig.1 we show the transmission of the 0.53 μm radiation through the Pockels cell as a function of delay between the probe and switch pulses. The maximum transmission is 10%, corresponding to $\sim$ 1 kv pulse. This is consistant with the bias on the microstrip. Note that the full width at half maximum is 100 picoseconds corresponding to the electrical pulse width.

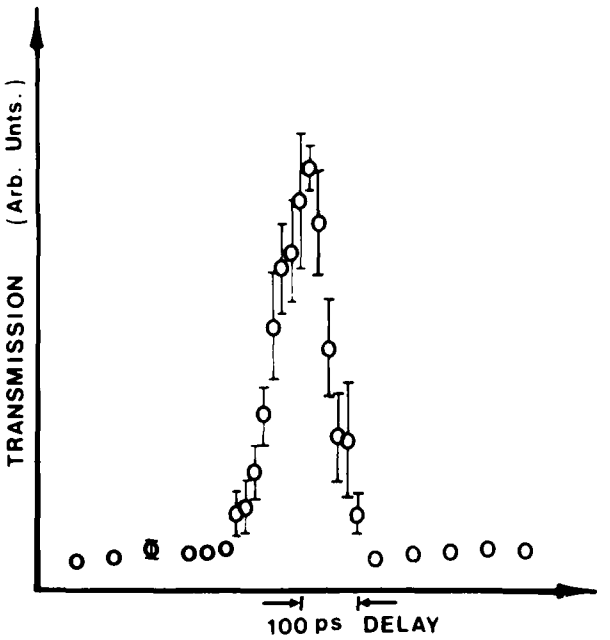

Fig.1 Transmission of 35 ps 0.53μm radiation through KD*P, corresponding to a 1 kv pulse of 100 ps width. Maximum of transmission is $\sim$ 10%.

A problem inherent in dc voltage holding switches is the necessity for gap separation to increase with the magnitude of the voltage held off. Photoconductive switches are prone to the same problem. On the other hand, practical design considerations, e.g. maintaining a matched impedance throughout the switch area and minimizing stray inductance and capacitance effects, become more difficult as the gap length increases. Furthermore, the energy in the optical pulse, required to trigger the photoconductive switch, increases as the gap length squared. Hence, there are practical limitations on the charging voltage, when dc biased. We are examining multistage schemes of HV generation, where a high voltage of relatively short pulse width, $\sim$ 10 nanoseconds, is used to charge the pulse generating and forming structures. Since the bias voltage remains for a short time, overbiasing the photoconductive switches can be maintained without breakdown, thus avoiding the problems mentioned above. A single optical pulse, split into two, can be used to trigger the voltage pulse so as to charge the HV generating structure, which in turn is triggered by the optical pulse generating high voltage picoseconds

pulses. This technique will also allow us to examine breakdown phenomena, as the photoconductive switches are biased to higher voltages.

The voltage multiplication structures use the principle of parallel charging and series discharging of pulse forming lines.[3] Marx banks require a switch per stage, whereas only one switch may be used for the entire stacked line structure. We have constructed 3 stage coaxial stacked line structures capable of generating 5 nanosecond pulses with GaAs as the photoconductive switch. With 2.5 kv dc bias, up to 5 kv pulses were obtained. The efficiency is limited by the laser energy and the short carrier lifetime of the GaAs switch ($\sim$ 1 nanosecond). A modified version of this circuit generates single cycle RF pulse with peak to peak voltage of 5 kv.

In summary, we have discussed the generation, shaping, and monitoring of high voltage picosecond pulses using pulse forming techniques in conjunction with photoconductive switches integrated with electro-optic probes.

We acknowledge the assistance of Messrs. D. Butler, C.S. Chang, and G.S. Krishnan during various stages of the project. This work is supported by AFOSR.

References

1. G. Mourou, W.H. Knox, and S. Williamson, ch. 7 of " Picosecond Optoelectronic Devices ", edited by Chi H. Lee, Academic Press, 1984.
2. E. Brokner, " Radar Technology ", Artech House, 1977.
3. R.A. Fitch, and V.T.S. Howell, Proc. IEE, vol. 111, 849 (1964).

Graphite as a Picosecond Laser Activated Opening Switch

E.A. Chauchard and Chi H. Lee
Department of Electrical Engineering
University of Maryland
College Park, MD 20742

C.Y. Huang
Los Alamos National Laboratory
Los Alamos, NM 87545

A.M. Malvezzi
Gordon McKay Laboratory
Harvard University
Cambridge, MA 02138

In a recent experiment, Malvezzi et al. have observed a large decrease in the reflectivity of a semimetallic sample of highly oriented pyrolytic graphite (HOPG) as it is illuminated by an intense picosecond laser pulse when the fluence is above the melting threshold. They have found that the imaginary part of the refactive index reaches lower than =0.5 at 566 nm [1]. This unexpected result indicates that a phase transformation occurs and that the high temperature phase, which they believe to be liquid, is non-metallic. This experimental observation is consistent with the result of the recent pseudo-potential calculation that there is an energy gap in "isotropic" carbon [2]. The time resolved experiments [1] also show that the phase transformation is completed in time scales as short as ~10 ps. In the work presented here, we directly assess the change of resistivity of a HOPG sample used as a laser activated switch. We confirm the results reported in [1] by observing a large increase in the sample's resistivity under intense picosecond laser illumination. This unique property could allow one to use graphite as an opening switch since it is a semi-metal. Its conductivity in the dark state (=.25 10^5 $(ohm.cm)^{-1}$) is almost as good as that of pure copper. It could then be compared to semiconductor optoelectronic switches, noting that its operation is exactly inverse: it is conductive in the dark and its resistance increases when illuminated above the threshold. The main application of this type of switch is in the pulse power technology where the recent interest for inductive storage systems has created a need for an efficient, repetitive, jitter free opening switch [3]. In [4,5], we proposed to use a semiconductor material as opening switch and demonstrated that it is feasible. In this paper, we demonstrate that graphite is a suitable alternate material for opening switch applications with some advantages. To assess the possibility of using HOPG as a practical device, it is of great importance to measure the speed of the phase transition as well as the speed of its recovery. The technique used in [1] only allows to perform these measurements at the surface of the sample. Here, we directly study the opening speed of the HOPG switch which is equal to the response time for the phase transition and

find the best opening speed to be less than one nanosecond.

To demonstrate the operation of HOPG as opening switch, a circuit configuration of current charged transmission line as described in [4] was used (Fig. 1). In this type of circuit, the energy is stored under magnetic form in a transmission line and a square pulse is generated when the switch opens. The duration of the square pulse (30ns) is determined by the length of the transmission line (3m). The rise and fall time of the square pulse are equal to the switch opening time. A Q-switch mode-locked Nd:YAG, providing 30ps pulses at 1.06μm was used to illuminate the HOPG sample. The waveforms shown in Fig. 2 indicate that the opening switch action was obtained. It was found as in [1] that a high laser fluence is necessary to obtain this result (>140 mJ/cm^2). The opening time was not reproducible from shot to shot; the fastest speed was less than 1 ns (oscilloscope limited). The maximum DC current in the c-plane that the sample can sustain was estimated to be 160 kA/cm^2. The switching efficiency was quite high: 90%, corresponding to a resistance of the sample of 450 ohms after illumination. The lack of reproducibility is attributed to the fact that the laser intensity and mode pattern were fluctuating. One other difficulty was that the thickness of the HOPG sample was not controlled. This is a determining factor since, for the opening action to be optimum, it is necessary that the total sample cross-section illuminated by the laser pulse undergoes the phase transformation. Although it is reported in [1] that the new phase is probably liquid, these first experiments do not allow to accurately identify its nature. A better understanding of the new phase would certainly allow us to better determine the switching parameters. Further research is necessary in this direction.

The subnanosecond opening speed, the fact that the switching efficiency of this material is quite good, and the fact that it can sustain a high current density make it a very promising candidate for opening switch applications. From a more fundamental point of view, it is of particular interest to note that HOPG is, to our knowledge, the only material exhibiting this type of behavior.

Acknowledgements

We are grateful to Professor N. Bloembergen for many stimulating discussions. One of us (CYH) is supported by the US Department of Energy. This work was partially supported by the Air Force Office for Scientific Research.

References

[1] A.M. Malvezzi, N. Bloembergen and C.Y. Huang, Phys. Rev. Lett., 57, 146-149, (1986).
[2] S. Fahy, S.G. Louie and Martin L. Cohen, Private Communication.
[3] K.H. Schoenbach, M. Kristiansen and Gerhard Shoefer, Proc. IEEE, 72, 8, (1984).
[4] E.A. Chauchard, M.J. Rhee and Chi H. Lee, Appl. Phys. Lett., 47, 12, (1985).
[5] E.A. Chauchard, C.C. Kung, M.J. Rhee, Chi H. Lee and V. Diadiuk, Proc. of the Conference on Lasers and Electrooptics, San Francisco, CA (1986).

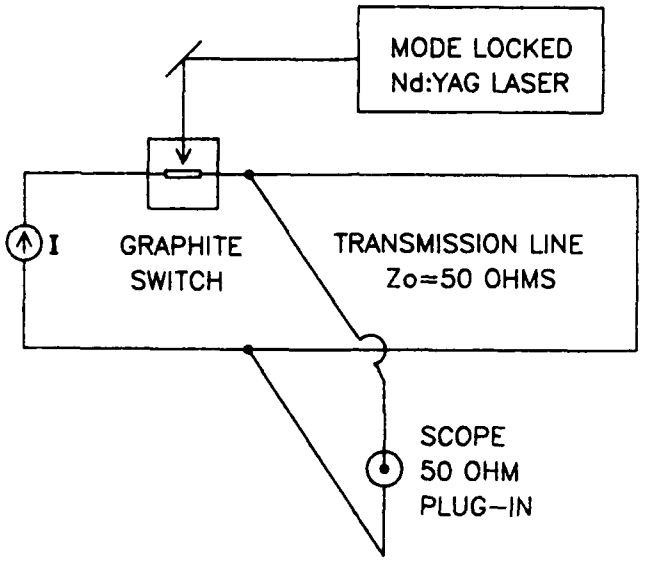

Fig. 1: Experimental set-up for the generation of square pulses using a laser activated switch and a current charged transmission line.

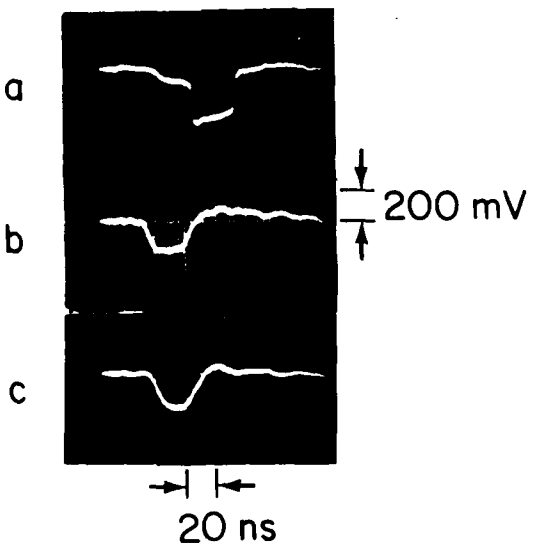

Fig. 2: Three examples of waveforms generated as the graphite switch opens. Each trace is obtained with a different laser pulse but the sample of graphite is the same. The laser pulse energy is: a: 0.15 mJ, b: 0.14 mJ, c: 0.16 mJ.

A Simple Technique to Generate or Gate Microwave Pulses with Picosecond Speeds

W.Margulis - Dept.Appl.Phys. - KTH - Stockholm S10044 Sweden
V.Grivitskas - Semic. Phys. Dept., Vilnius State University, Sauletekio 9, Vilnius 232055 , Lithuania, USSR.
E.Adomaitis, Z.Dobrovolskis, A.Krotkus - Inst. Semic. Phys., Lithuanian Academy of Sciences,Vilnius 232600,Lithuania,USSR.

A number of articles have recently been published (1-4) where microwave signals are switched and controlled by means of a ps photoconductor illuminated by a mode-locked laser pulse. The advantages of such an approach over conventional electronic circuitry include higher speeds, excellent timing and high power capability. Here we describe a simple arrangement which makes it possible to both switch an arbitrary number of cycles from a microwave generator (case 1),as well as to shape microwave pulses from a dc bias source (case 2), with easily adjustable frequency and duration. To that end we use a ps photoconductor with a PEPS (5), which controls the pulse produced.

case 1:
The experiments of gating a number of cycles from an RF source were carried out at a frequency 7 GHz, and the peak voltage of the sinusoidal input was 1.8 V. The results were recorded on a Soviet made oscilloscope type C7-19 with a travelling wave deflector, internal image intens. and a bandwidth 8 GHz. The laser source was a passively m.l. Nd:YAG laser with a rep.rate 12 Hz. An intrinsic Si switch was used, in a conventional microstrip transmission line, with a gap length 200 μm. The single pulses selected, used for the activation of the Si switch had a duration 30 ps and energy 10 μJ. Initially the high resistance of the Si material prevented the transmission of the RF signal, but upon illumination the microwave bias was gated on, with a risetime approximately equal to the pulse duration. Typically a switching efficiency ~60% was observed. The top trace in fig.1 shows the switch-on following illumination.Capacitive coupling across the gap is responsible for the leakage preceeding excitation. In order to control the number of cycles gated, the signal is switched off by introducing a PEPS with short circuited branches between the output of the photoconductive element and the load. In this configuration the PEPS produces a 180° phase shifted reflected electrical signal,cancelling the input after a delay determined by the roundtrip time of the branches, chosen to equal an integral multiple of the RF period. For the bottom trace a 3 cm (280 ps) branch length was chosen. Both 150 and 450 ps lengths were also used,

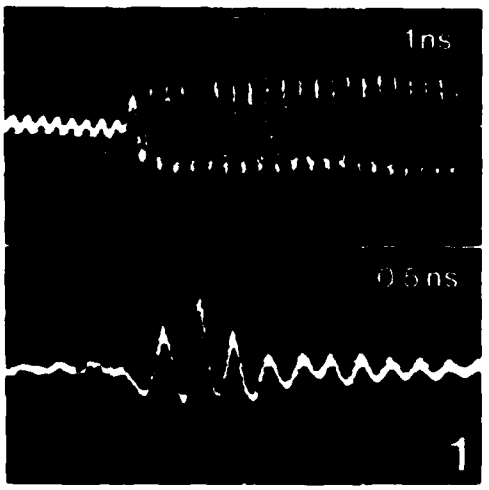

resulting in the switching of a single and of three cycles. Since a continuously adjustable frequency generator was available,for the 1.5, 3.0 and 4.5 cm branch lengths used,the frequencies chosen were 7.06, 7.12 and 7.09 GHz, respect. These optimum values were determined by applying the RF directly to the PEPS,and fine-tuning the frequency for minimum output signal. A particular frequency can also be selected, in which case the branch lenghts must be carefuly adjusted mechanically. For 3 cm branches a lenght accuracy of 0.1 mm is possible (0.3 % at 7 GHz), corresponding in the frequency domain to a precision ~23 MHz. The relatively limited S:N ratio observed in fig.1 is due to a construction problem in the fabrication of the PEPS. This resulted in a mismatch producing ~20% residual leakage following the passage of the pulse. With the design described in (5) square pulses with noise levels <5% have been measured, and therefore the S:N ratio can be greatly improved.

case 2

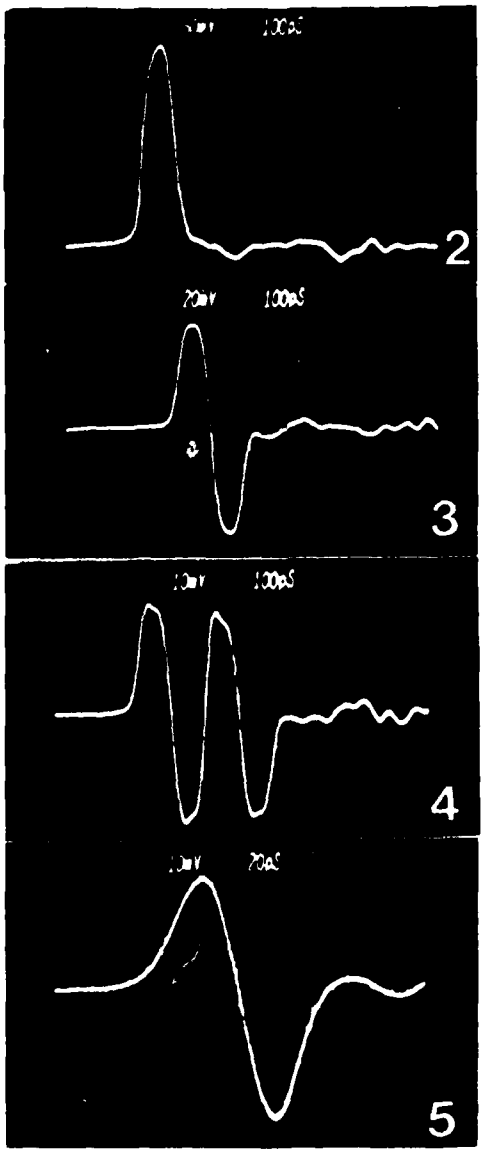

A similar arrangement was used to convert a dc bias into a microwave pulse. This time, upon illumination the photoconductor produced a step-input signal, which was switched off by the PEPS with short-circuited (sc) ends after an adjustable delay. The resulting signal is the first half-cycle of the microwave pulse. A whole cycle was shaped by introducing another PEPS in series with the first one, with equal branch length, also sc at the ends. Preliminary experiments were carried out by producing microwave pulses from a conventional step pulse generator. Fig. 2-4 illustrate the shaping of microwave signals starting from a half-cycle. A single PEPS, which could accomodate three crosses was built, and a single sc cross (75 ps) was used for the record shown in fig.2, two sc crosses (both 75 ps) for the one illustrated in fig.3, and two 75 ps sc and one 150 ps open-circuited crosses were connected for the result displayed in fig 4.Fig.5 shows on a 20 ps/major div. scale a single cycle with period ~76 ps (~13 GHz) shaped with the PEPS, limited in duration by the step generator and scope used for display (Tektronix TDR, S4 sampling head).

The laser pulse used for the record showed in fig.6 was relatively long (120 ps), produced by a

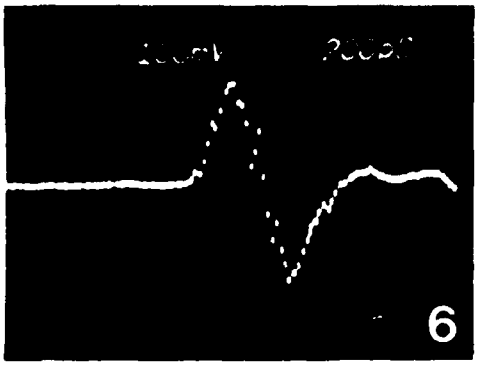

cw mode-locked Q-switched Nd:YAG laser and the photoconductor was an InP switch with Ni-Ge-Au electrodes and a gap ~250 μm. The PEPS branch length was 100 ps. To increase the number of cycles, additional PEPS were used, with open circuited ends. In order to extend this technique into the KV range, a 400 μJ, 200 fs dye laser pulse at 617 nm, with a repetition rate 10 Hz was directed to a 1.5 mm semi-insulating GaAs semiconductor switch, dc biased to 2.5 KV*. A Tek 7834 with a 7A19 amplifier storage scope (risetime 600 ps) was used to record the signals shaped. Figs 7-9 are oscillograms of the pulses produced. The time-scale is 1 ns/small div. Although the spparent switching efficiency is not 100% (when Vout = Vbias/2), when the finite risetime of the oscilloscope is taken into account (6), a peak voltage ~1KV is inferred from fig. 7. Again, shaping the double of the number of cycles only required the additional connection of a single open-circuited cross. To alter the period, various sc branch lengths were selected.

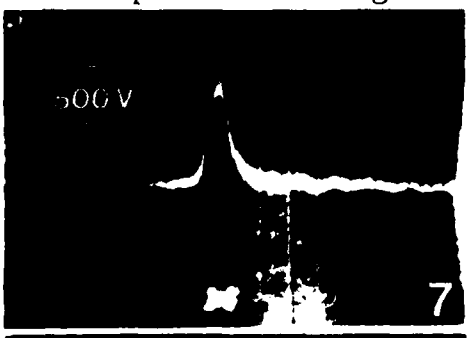

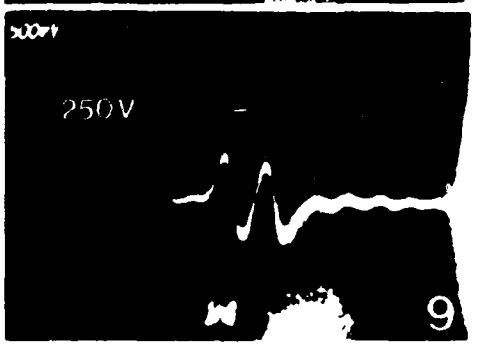

In conclusion we described a simple technique to generate or gate microwave pulses with ps speeds. The same arrangement is used for controlling the number of cycles switched with a microwave generator as a bias source (case 1) and for shaping a microwave pulse from a dc power supply (case 2). A single light pulse and a single photoconductor are used, and a wide range of recombination time (ns-μs) semiconductor materials can be employed. The versatility of the technique (for example the operation required to double the number of cycles of the output pulse takes ~3 seconds to be performed), and its simplicity should make it useful in practical applications.

References:
1-For a good review on optoelectronic microwave switching see W.Platte, IEE proc. 132, Pt.J, 126 (1985) and references therein. See further, 2-C.S.Chang et al, Ultrafast Phen. IV, 423 (1984). 3-A.Moradian, APL 45,494 (1984). 4-P.Paulus et al,IEEE JQE 22, 108 (1986). 5-W.Margulis, R.Persson, Rev. Sci.Ins. 56, 1586 (1985). 6-W.Margulis, S.Laval, APL 40,829 (1982).
* Experiments carried out at the laser group,Imperial College.

A Proposed Quantum Well Injection Transit Time Device (QWITT)

Vijay P. Kesan, Dean P. Neikirk, and Ben G. Streetman
Microelectronics Research Center, Department of Electrical and Computer Engineering
University of Texas at Austin, Austin, Texas 78712

Oscillators using resonant tunneling through a quantum well have been the focus of much research recently [1-4]. Although they are potentially capable of very high frequency operation with low noise, the output power is in the order of tens of microwatts. Transit time devices like the IMPATT (impact ionization avalanche transit time) are capable of operating at 94 GHz and 140 GHz with 0.5 and 0.12 W power output respectively [5,6]. But collision effects in transit time devices seriously degrade the power and efficiency beyond 90 GHz and result in poor noise characteristics. Tunneling in the TUNNETT (tunnel injection and transit time) was proposed as a low noise alternative to the IMPATT, but poor injection phase delay lowers the efficiency of operation [7,8].

We propose here a new transit time device which uses resonant tunneling through a single quantum well to inject carriers into the drift region of the device. This device employs resonant tunneling and hence would not be expected to suffer the conventional degradation of power and efficiency associated with other transit time devices. Large injection phase delays can be obtained in the device, in contrast to the TUNNETT, where the current injection is nearly in phase with the applied voltage. Depending on the power-frequency requirements of a particular application, the device can be biased to produce a $\pi/2$, π or $3\pi/2$ injection phase delay. Further, the presence of a drift region increases the device impedance per unit area, and hence higher output power when compared to quantum well oscillators can be expected. Since this is a quantum well injection transit time effect device, we call it a QWITT.

The physical structure of this device, in keeping with a typical molecular beam epitaxy growth sequence, is shown in Figure 1(a). The device structure consists of a single GaAs quantum well between two AlGaAs barriers, together with a region of undoped GaAs to form the drift region. This structure is then placed between two n^+-GaAs regions to form contacts.

The small-signal time dependent principle of operation of this device can be explained using Figs. 1(c) and 2. The energy band diagram of the device when no d.c. bias is applied is shown in Fig. 1(b). In order to achieve resonant tunneling of electrons at the correct instant of time, for any desired injection phase delay ϕ, the d.c. bias must be adjusted so that the following expression is satisfied:

$$2E_1/e = V\sin\phi + V_i$$

where V is the amplitude of the a.c. voltage, V_i is the effective d.c. voltage drop across the resonant tunneling injection region, and E_1 is the energy level in the well. The impedance of the drift region is much greater than that of the injection region, and hence most of the d.c. bias will drop across the drift region. If an appropriate bias is applied to move the Fermi level in the n^+-GaAs in line with the energy level E_1 in the well (see Fig. 1(c)) and an a.c. signal is superimposed on this d.c. bias, then resonant tunneling of electrons through the well will occur only at a phase delay of π in the a.c. cycle. From the instant π to 2π the electrons traverse through the drift region at their saturation velocity, resulting in a dynamic negative resistance. In this mode of operation, electrons will also be injected into the drift region at the instant 2π, giving rise to a small positive resistance. The d.c. bias can also be altered so that the difference in voltage between $2E_1/e$ and the voltage drop across the injection region V_i is equal to the amplitude of the a.c. signal V causing carriers to be injected at a phase delay of

This work was supported by the Texas Advanced Technology Research Project and the Joint Services Electronics Program under contract # AFOSR F 49620-86-C-0045.

$\pi/2$. This device, when operating with an injection delay of $\pi/2$ or π, has a small positive resistance regime much like the IMPATT or TUNNETT [8].

The QWITT can also be biased to move the Fermi level in the n^+-GaAs above the energy state in the GaAs well, so that current injection takes place at an instant $3\pi/2$ in the negative half of the voltage cycle, as seen in Fig. 2. Current conduction then takes place for only a quarter of the a.c. cycle, but in this mode of operation a pure negative conductance regime is obtained. When current injection through the well is delayed by an angle greater than π, insufficient current conduction and moderate voltage swing could lower the output power. However, by increasing the current density and device impedance per unit area, the output power could be increased. In addition, as current injection into the drift region is delayed, the length of the drift region can be made correspondingly smaller, thus permitting operation at higher millimeter wave frequencies. As the length of the undoped GaAs drift region is reduced, the transit time effect decreases, and one can envisage this device looking more like a resonant tunneling oscillator [2,4,9].

At frequencies greater than 100 GHz several other factors must be considered in the design of the device. For any transit time device the injected carriers may travel through a significant fraction of the transit time region ballistically [10]. This contributes an additional phase delay, which must be accounted for in the determination of the necessary transit time layer thickness for a given frequency of operation. In addition, for the QWITT, the finite amount of time it takes for a resonant state to be established in a quantum well [11,12] will cause a non-negligible time delay. This delay, which might account for a sizable fraction of the a.c. voltage cycle, will also have to be considered in the analysis of the device.

In conclusion, when compared to other transit time devices and quantum well oscillators, the QWITT should have several advantages. Quantum mechanical tunneling in the QWITT is essentially a collision free process that does not degrade the efficiency at high frequency. Large electronic reactances, which cause detuning, thermal breakdown and burnout at high frequencies in IMPATTs, are absent. The drift region need not be as long as in TUNNETTs, and hence there will be less series resistance because of electrons traveling below the saturation velocity. There is also no degradation of efficiency because of a phase delay of less than the optimum 2π as in TUNNETTs [7]. The relative ease of fabrication of this device using molecular beam epitaxy, when compared to other novel quantum well devices for microwave applications, is another attractive feature. Thus, the QWITT should extend the normal frequency limit associated with transit time devices into the submillimeter wave range, without compromising on output power as in quantum well oscillators.

References

1. T. J. Shewchuk, P. C. Chapin, W. Kopp, R. Fisher, and H. Morkoç, Appl. Phys. Lett., **46**, 508-510 (1985).
2. T.C.L.G. Sollner, P.E. Tannenwald, D.D. Peck, and W.D. Goodhue, Appl. Phys. Lett., **45**, 1319-1321 (1984).
3. B. Jogai, K.L. Wang, and K.W. Brown, Appl. Phys. Lett., **48**, 1003-1005 (1986).
4. T.J. Shewchuk, J.M. Gering, P.C. Chapin, P.D. Coleman, W. Kopp, C.K. Peng, and H. Morkoç, Appl. Phys. Lett., **47**, 986-988 (1985).
5. N. B. Kramer and R. J. Johnson, Microwaves & RF, **23**, 5, 243 (1984).
6. H. Essen, J. Esclavy and E. Wennerscheid, Microwave J., **28**, 7, 165 (1985).
7. J. Nishizawa, K. Motoya, and Y. Okuno, IEEE Trans. on Microwave Theory and Tech., **MTT-26**, 1029-1035 (1978).
8. J. Nishizawa, *Infrared and Milllimeter Waves*, Vol. 5, Part I, ed. by K.J. Button, Acad. Press (1982).
9. P.D. Coleman, S. Goedeke, T.J. Shewchuk, P.C. Chapin, J.M. Gering, and H. Morkoç, Appl. Phys. Lett., **48**, 422-424 (1986).
10. K. Hess, IEEE Trans. on Elect. Dev., **ED-28**, 937-940 (1981).
11. B.Ricco and M. Ya. Azbel, Phys. Rev. B, **29**, 1970-1981 (1984).
12. Y. Zohta, J. Appl. Phys., **59**, 962-964 (1986).

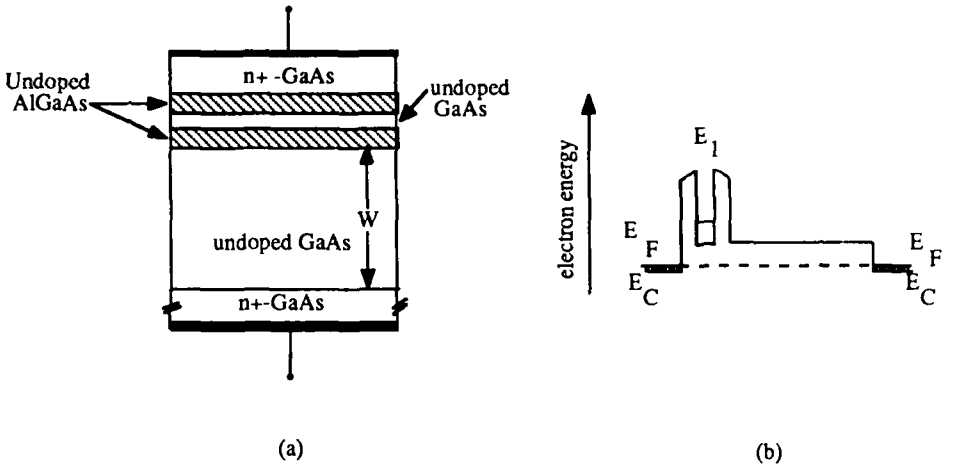

Fig. 1(a). Physical structure of the QWITT. (b) Energy band diagram of the device when no d.c. bias is applied.

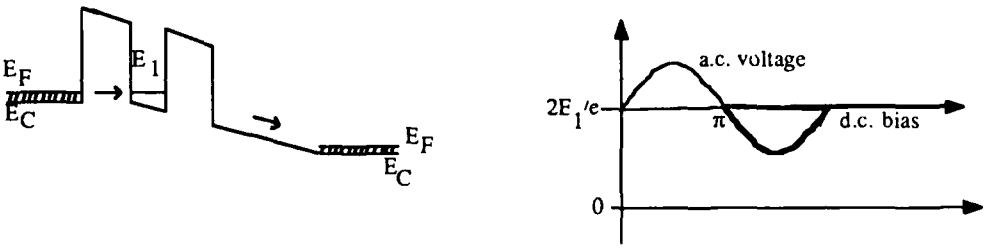

Fig. 1(c). Energy band diagram when the device is biased for the quantum well to be at resonance so that current injection occurs at an instant π (the current conduction cycle through the device is highlighted).

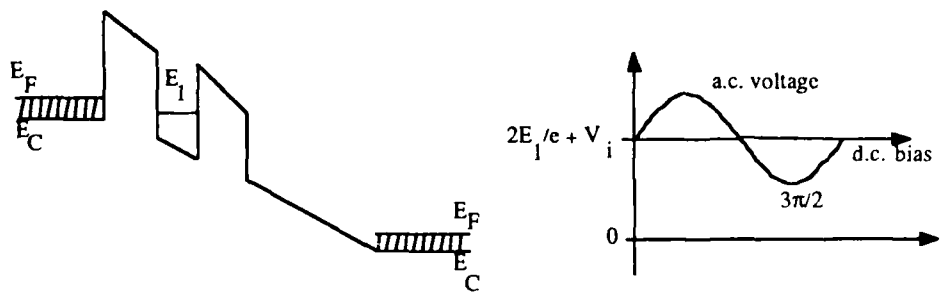

Fig. 2. Energy band diagram when the device is biased for conduction to occur at 3π/2.

Modulation Efficiency Limited High Frequency Performance of the MODFET

M.C. Foisy, J.C. Huang*, P.J. Tasker, L.F. Eastman

School of Electrical Engineering and National Research and Resource Facility for Submicron Structures, Cornell University, Phillips Hall, Ithaca, NY 14850

*Department of Applied Physics, Cornell University

Epilayer design for the MODFET is frequently performed using the depletion approximation [1,2]. The work of authors such as Ponse et. al. and Stern and Das Sarma have provided tools by which electron distributions and capacitances can be calculated without this assumption [3,4]. They demonstrate that for two dimensional electron gas (2DEG) sheet concentrations significantly below the saturation saturation value, free and bound electrons are present in the supply layer. Because these electrons must be modulated with the 2DEG electrons, the gate capacitance is increased while the transconductance is decreased [5]. The unity current gain frequency, f_T, is thus decreased.

In this work we take the above analysis a step further by introducing a figure of merit, the modulation efficiency (ME), which gives an indication of the charge control limited f_T as a function of sheet density, n_s. In this paper, the effect of each epilayer design parameter on the ME is studied via a numerical charge control model which incorporates Fermi-Dirac statistics and Al composition dependent donor energies [6]. It is found that at room temperature, unlike 77K where the depletion approximation is more valid, ME is very sensitive to epilayer design.

We define the modulation efficiency as the ratio of 2DEG capacitance to total capacitance for the 1-D system extending from the gate to the buffer/substrate interface. The classical model used to calculated electron densities was found to give excellent agreement with quantum-mechanical calculations by Vinter [7] as predicted by Yoshida [8]. Agreement with experimentally measured capacitance was also obtained [9]. Although two dimensional effects such as the variation in channel potential and real space transfer are ignored by such an analysis, the ME calculated by this procedure represents a best case result. If the electrons entering the charge control region under the gate (i.e. those electrons at the source end of the gate) cannot be modulated efficiently or are present in the supply layer in excess number, then the situation can only be worsened as the carriers are heated. The correlation between f_T and ME is best illustrated by a using the short channel approximation, neglecting carrier heating, and assuming an electron velocity that is independent of sheet concentration:

$$f_T = \frac{g_m}{2\pi C_g} = \frac{v_{eff}\, dQ_{2DEG}/dV_g}{2\pi\, dQ_{tot}/dV_g} = \frac{v_{eff}}{2\pi}\, ME$$

Obviously, these simplistic assumptions will not hold under all device operating conditions. However, ME will always retain its degrading effect on f_T and the therefore optimization of ME is thus a minimum design objective.

Figure 1 shows the effect of the aluminum mole fraction on ME. Note that the curve representing 77K operation is almost box-like. In the limit of zero temperature (an impossibility due to carrier heating) the depletion approximation is accurate and the ME vs. n_s curve would have an exact box form. ME degradation increases as the difference between donor energy and the GaAs conduction band energy at the interface (ΔE_c-E_d), as measured in thermal volts, is decreased. Since this quantity saturates near 30% Al composition, further improvement in ME

cannot be obtained by varying this parameter. This plot also illustrates the ME consequences of avoiding low temperature operation or reducing Al concentration in an attempt to avoid light sensitivity. Figure 2 shows the effect of spacer layer thickness on ME. Thus it suggests that variations in the designed spacer may be responsible for the wide range of f_T values reported in the literature for submicron gate MODFET's. For example, if the device is biased for a n_s of $6x10^{11}$ cm^{-2}, changing form a 15A spacer to a 45A spacer will reduce ME by more than a factor of 2. The effect of varying other design parameters and the optimization of ME will be discussed in the conference presentation.

We have shown that numerical simulation of the ME of the MODFET can be a powerful tool for understanding the high frequency limitations due to charge control and optimizing the device's epilayer design.

Acknowledgement

We thank S. Plimpton and L. Murray for the use of their graphics package.

References

[1] K. Lee, M. S. Shur, T. J. Drummond, H. Morkoc, "Current-voltage and capacitance-voltage characteristics of modulation-doped field-effect transistors," *IEEE Trans. Electron Devices,* vol. ED-30, pp. 207-212, 1983.

[2] K. Lee, M. S. Shur, T. J. Drummond, H. Morkoc, "Parasitic MESFET in (Al, Ga) As/GaAs modulation doped FET's and MODFET characterization," *IEEE Trans. Electron Devices,* vol. ED-31, pp. 29-35, 1984.

[3] F. Ponse, W. T. Masselink, and H. Morkoc, "Quasi-fermi level bending in MODFET's and its effect on FET transfer characteristics," *IEEE Trans. Electron Devices,* vol. ED-32, pp. 1017-1023, 1985.

[4] F. Stern and S. Das Sarma, "Electron energy levels in GaAs-AlGaAs heterojunction," *Phys. Rev. B,* vol. 30, pp. 840-848, 1984

[5] M. Moloney, F. Ponse, H. Morkoc, "Gate capacitance - voltage characterization of MODFET's: Its effect on transconductance," *IEEE Trans. Electron Devices*, vol. ED-32, pp. 1675-1684, 1985.

[6] N. Chand, T. Henderson, J. Klem, W. T. Masselink, R. Fischer, Y. Chang, and H. Morkoc, "Comprehensive analysis of Si-doped $Al_xGa_{1-x}As$ (x=0 to 1): Theory and experiments," *Phys. Rev. B*, vol. 30, no. 8, pp 4481-4492, 1984.

[7] B. Vinter, "Subbands and charge control in a two-dimensional electron gas field-effect transistor," *Appl. Phys. Lett.*, vol. 44, no. 3, pp. 307-309, 1984.

[8] T. Yoshida, "Classical versus quantum mechanical calculation of the electron distribution at the n-AlGaAs/GaAs heterointerface," *IEEE Trans. Electron Devices*, vol. ED-33, pp. 154-156, 1986.

[9] J. C. Huang, M. C. Foisy, P. J. Tasker, S.R. Seidman, G. W. Wicks and L. F. Eastman, "An $Al_{0.22}Ga_{0.78}As/Al_{0.45}Ga_{0.55}As$/GaAs HEMT: a case for Gate Charge Control," to be submitted for publication.

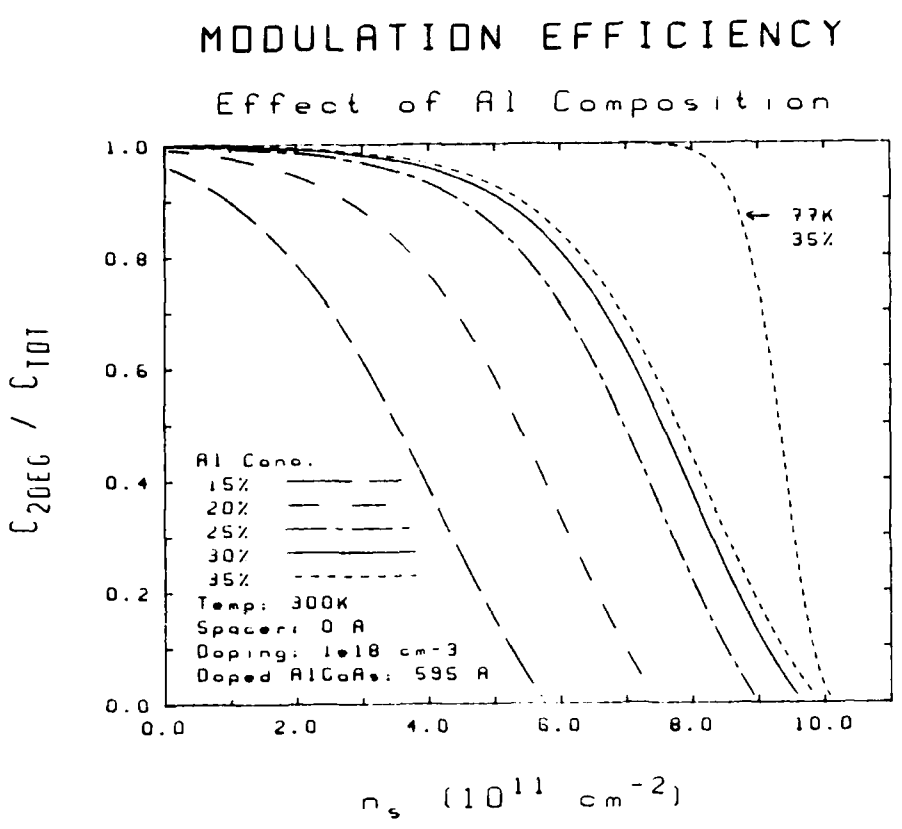

Figure 1

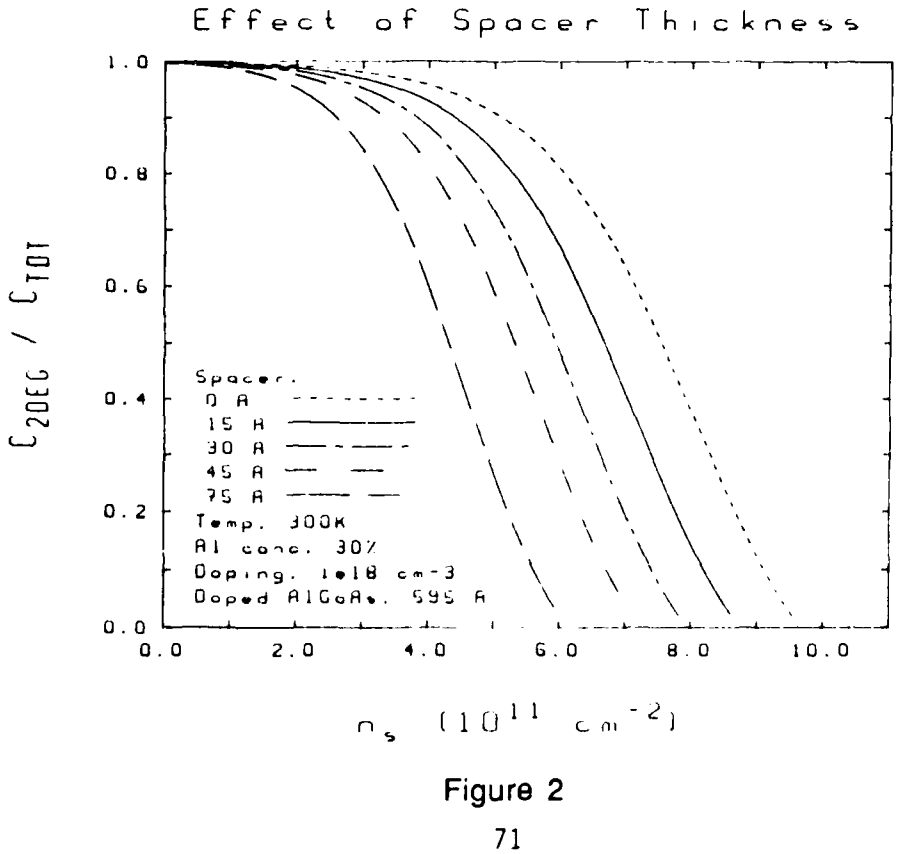

Figure 2

Characteristics of Shielded Microstrip Lines on GaAs-Si at Millimeter-Wave Frequencies

M.I. Aksun and H. Morkoc

University of Illinois at Urbana Champaign
Coordinated Science Laboratory
1101 W. Springfield Avenue
Urbana, IL 61801

The advantages of GaAs on Si technology have stimulated a great deal of interest [1], [2]. Although Si was studied extensively as the substrate material for microwave monolithic integration because of its high thermal conductivity, well established technology, mechanical strength, and availability in larger diameter [3] [5], it lacks millimeter wave three terminal devices which is now afforded with GaAs on Si [6]. Dielectric losses in GaAs on Si, however, must be small in order for this composite technology to be practical. We have thus undertaken a theoretical study of the shielded microstrip lines on GaAs on Si up to 100 GHz for various parameters in Si and GaAs.

In order to show that GaAs layers grown on Si do not affect considerably the insulating quality of high resistivity Si, the dielectric losses in GaAs, Si, and GaAs on Si materials have been investigated and compared. In this study, they are used as substrates for the shielded microstrip structure with 50 Ω characteristic impedance. The results show any loss is dominated by the GaAs layer when high resistivity Si is used.

The characteristics of a shielded microstrip line with double layer substrate were investigated by using the spectral domain analysis [7], [8]. After having found the propagation constant and the field components in each layer, Eq. 1 and Eq. 2 were used to calculate the characteristic impedance and the dielectric loss, respectively [9].

$$Z_0 = \frac{2\mathrm{Re}\int_s \mathbf{E}\times\mathbf{H}^*\cdot\hat{a}_z ds}{I_i^2} \tag{1}$$

$$\alpha_d = \frac{\omega\epsilon\tan\delta\int_{s_{diel}} |\mathbf{E}|^2 ds}{2\mathrm{Re}\int_s \mathbf{E}\times\mathbf{H}^*\cdot\hat{a}_z ds} \tag{2}$$

This dielectric loss calculation assumes that the loss tangents of the dielectric materials being used are sufficiently small. Data were obtained for different thicknesses and resistivities of GaAs over layers, and typical results are shown in Fig. 1 and Fig. 2. From the figures, one can conclude that a) the resistivity of the substrate material will not be degraded considerably if the resistivity of GaAs overlay material is less than that of Si substrate provided that the thickness of the overlay material is relatively small. b) the equivalent resistivity of the entire structure can be higher than that of the Si substrate depending upon the GaAs overlayer thickness when the high resistivity GaAs overlay material is used.

In conclusion, we have investigated the dielectric loss in GaAs on Si material as substrate for microstrip line and we have found that GaAs overlay material modifies the resistivity of the entire structure depending upon its thickness and resistivity relative to those of Si material. As far as the dielectric loss is concerned, by using high resistivity GaAs overlayer on Si, the dielectric loss can be reduced. So it may be concluded that this combination offers exciting possibilities for monolithic microwave and millimeter-wave integration.

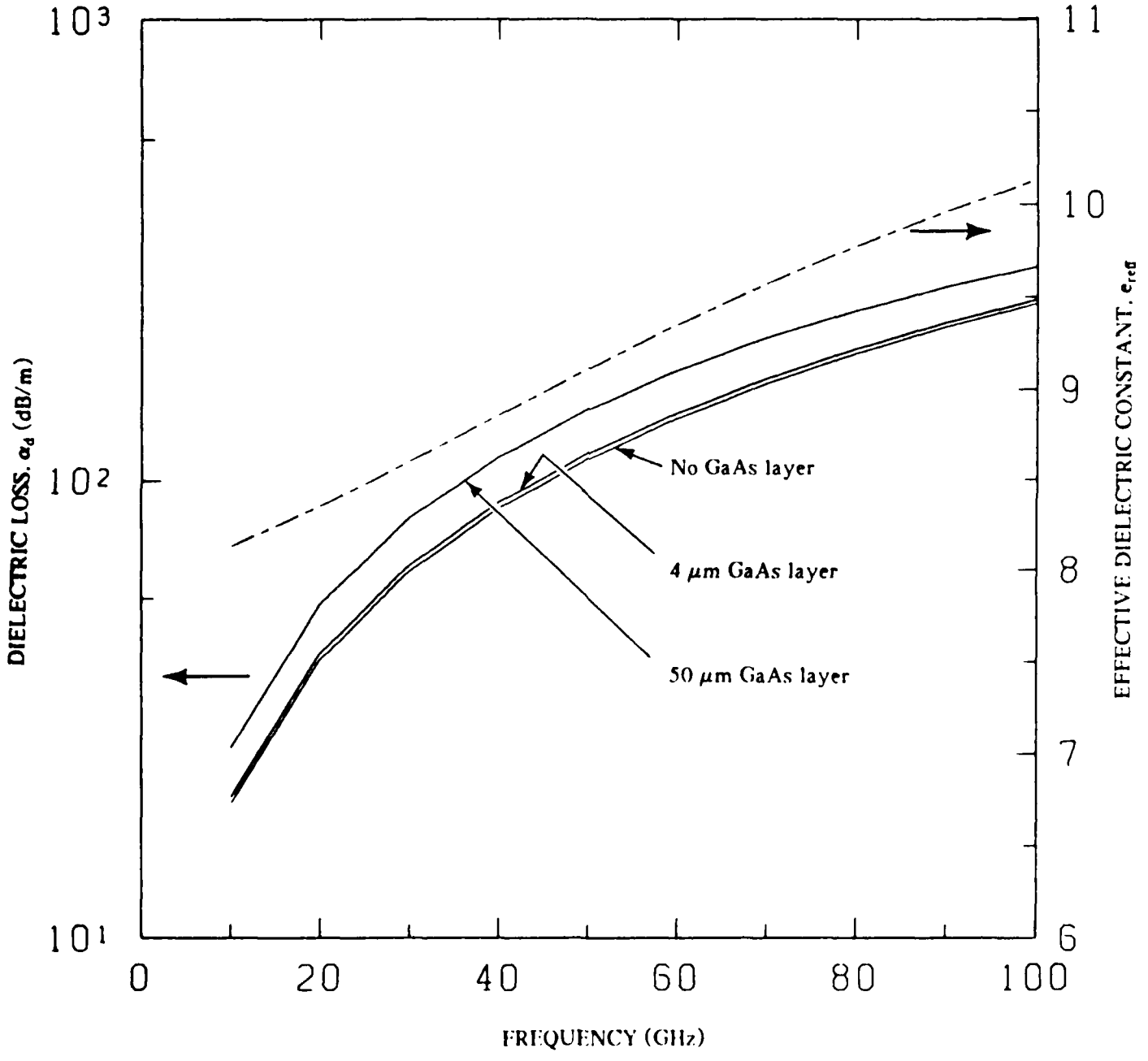

Fig. 1. Dielectric loss and effective dielectric constant versus frequency for $\rho_{Si} = 2000\,\Omega$-cm, $\rho_{GaAs} = 1000\,\Omega$-cm.

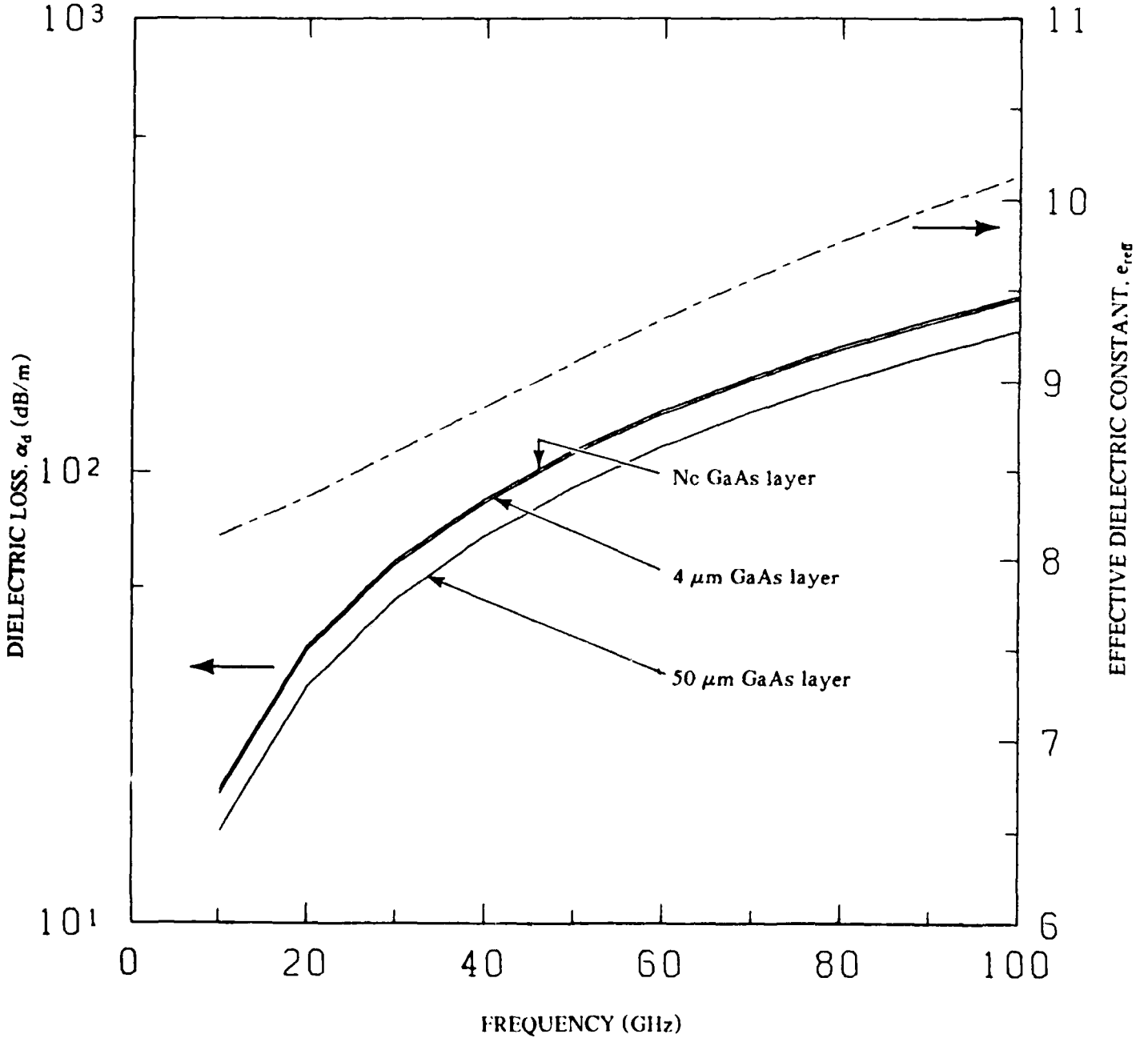

Fig. 2. Dielectric loss and effective dielectric constant versus frequency for $\rho_{Si} = 2000\,\Omega$-cm, $\rho_{GaAs} = 4000\,\Omega$-cm.

References

[1] G.M. Metze, H.K. Choi, and B.-Y. Tsaur, "Metal Semiconductor Field Effect Transistors Fabricated in GaAs Layers Grown Directly on Si Substrates by Molecular Beam Epitaxy," *Appl. Phys. Lett.*, vol. 45, pp. 1107-1109, 1984.

[2] H. Morkoc, N. Otsuka, and H. Zabel, "New Structures Formed by Molecular Beam Epitaxy: The Case of GaAs on Si," *Science*, in print.

[3] A. Rosen, M. Caulton, P. Stabile, A.M. Bombar, W.M. Janton, C.P. Wu, J.F. Corboy, and C.W. Magee, "Silicon as a Millimeter-Wave Monolithically Integrated Substrate - A New Look," *RCA Review*, vol. 42, pp. 633-660, 1981.

[4] H. Sobol and M. Caulton, "The Technology of Microwave Integrated Circuits," *Advances in Microwaves*, vol. 8, pp. 11-66, 1974.

[5] K.M. Strohm, J. Buechler, P. Russer, and E. Kasper, "Silicon High Resistivity Substrate Millimeter-Wave Technology," IEEE 1986 Microwave and Millimeter-Wave Monolithic Circuits Symposium, June 4-5, 1986.

[6] R. Fischer, N. Chand, W. Kopp, C.K. Peng, H. Morkoc, K.R. Gleason, and D. Scheitlin, "A dc and Microwave Comparison of GaAs MESFET's on GaAs and Si Substrates," *IEEE Trans. Electron Dev.*, vol. ED-33, pp. 206-213, 1986.

[7] T. Itoh and R. Mittra, "A Technique for Computing Dispersion Characteristics of Shielded Microstrip Lines," *IEEE Trans. Microwave Theory and Techniques*, vol. MTT-22, pp. 896-898, 1974.

[8] J.B. Davies and D.M.-Syahkal, "Spectral Domain Solution of Arbitrary Coplanar Transmission Line with Multilayer Substrate," *IEEE Trans. Microwave Theory and Techniques*, vol. MTT-25, pp. 143-146, 1977.

[9] D.M.-Syahkal and J.B. Davies, "Accurate Solution of Microstrip and Coplanar Structures for Dispersion and for Dielectric and Conductor Losses," *IEEE Trans. Microwave Theory and Techniques*, vol. MTT-27, pp. 694-699, 1979.

Nonequilibrium Phonons and Disorder in $Al_xGa_{1-x}As$

J.A. Kash, J.C. Tsang, and S.S. Jha*

IBM Thomas J. Watson Research Center
Yorktown Heights, New York 10598

Despite alloy disorder, picosecond Raman measurements show significant nonequilibrium phonon effects in $Al_xGa_{1-x}As$. The virtual crystal approximation is demonstrated to apply. Implications for heterojunction devices are considered.

In polar semiconductors like GaAs, the Fröhlich interaction between hot carriers and LO phonons is the dominant mechanism for carrier cooling[1]. Because of the long wavelength character of the coupling, LO phonons of small wavevector are preferentially generated, resulting in a hot LO phonon distribution strongly peaked at small wavevectors. As a result, a large excess phonon population can build up in these small wavevector modes, leading to the so-called "hot phonon" effects[2] which may play an important role in carrier cooling in high mobility devices.

The generation and decay of nonequilibrium phonons is well understood in GaAs. However, heterojunction devices consisting of both binary semiconductors like GaAs and ternary alloys like $Al_xGa_{1-x}As$ are of considerable technological interest. The random substitution of aluminum and gallium on the crystal lattice can lead to important alloy disorder effects in the phonon spectrum[3,4]. First, instead of a single LO phonon mode, there are now two modes. One is near the GaAs LO phonon frequency (the "GaAs-like" mode), while the other is near the AlAs LO frequency (the "AlAs-like" mode). Compared to the binary materials, the cw Raman spectrum of both LO phonon lines in the alloy are broader and asymmetric. This observation has been interpreted as an uncertainty in wavevector for the LO phonon caused by alloy disorder. The concept of a phonon correlation length L_c has been introduced, which is the inverse of the wavevector uncertainty. L_c is typically 5 - 10 nm. The volume in k-space of the wavevector uncertainty in $Al_xGa_{1-x}As$ therefore exceeds (by several orders of magnitude) the volume which is populated by nonequilibrium phonons in GaAs. One might expect that the uncertainty would increase the k-space populated by nonequilibrium phonons, thus decreasing the peak mode occupancy $\Delta n(k)$ of any given phonon mode. Alternatively, the wavevector uncertainty might correspond to an inelastic scattering mechanism which greatly shortens the lifetime τ_{LO} of the LO phonons. Either of these effects would greatly reduce the role played by hot phonons in carrier cooling, and thus would have important implications in devices containing semiconductor alloys. A related question is the relative strength of the Fröhlich interaction for the two LO modes in

$Al_xGa_{1-x}As$. If there is substantial interaction between carriers and the AlAs-like mode, the nonequilibrium population of GaAs-like LO phonons would be reduced, again reducing the importance of hot phonon effects.

To investigate these questions, we have studied nonequilibrium phonon production in $Al_xGa_{1-x}As$ by picosecond pump-probe Raman scattering[5,6]. We first compare nonequilibrium phonon production in GaAs to the GaAs-like LO phonon mode in $Al_xGa_{1-x}As$. Surprisingly, as shown in Fig. 1, both $\Delta n(k)$ and τ_{LO} are basically the same in $Al_xGa_{1-x}As$ as in GaAs. We typically find $\Delta n(k) \simeq 0.05$, while the room temperature phonon lifetime remains at about 3.5 psec. Figure 2 compares the relative efficiency of nonequilibrium phonon production for the AlAs-like mode compared to the GaAs-like mode. From such curves, we are able to deduce that the lifetime of the AlAs-like mode is still about 3.5 psec, even though the phonon linewidth has increased by a factor of two. We also find that less than 20% of the nonequilibrium phonons are AlAs-like in $Al_{0.24}Ga_{0.76}As$. For smaller values of x, still fewer AlAs-like phonons are produced.

These results suggest that nonequilibrium phonon dynamics in $Al_xGa_{1-x}As$ are not substantially different than in GaAs. That is, the virtual crystal approximation is valid. To understand why the wavevector broadening observed in cw Raman scattering has little effect on the hot phonon population, we have theoretically examined the Fröhlich coupling for the case of a semiconductor alloy. We calculate the Fröhlich matrix elements for the GaAs-like and AlAs-like modes, and find that the coupling for the AlAs-like mode is small for small x. Furthermore, if the concept of the correlation length is carefully introduced properly, one can account for both the observed broadening in cw Raman scattering and the substantial hot phonon effects observed in our transient measurements.

References

* Permanent address: Tata Institute of Fundamental Research, Bombay, India.

1. E.M. Conwell and M.O. Vassel, IEEE Trans. Electron. Devices 13, 22 (1966).
2. See, for example, P. Kocevar, Physica 134B, 155 (1985).
3. Bernard Jusserand and Jacques Sapriel, Phys. Rev. B24, 7194 (1981).
4. P. Parayanthal and Fred H. Pollak, Phys. Rev. Lett.52, 1822 (1984).
5. D. von der Linde, J. Kuhl, and H. Klingenburg, Phys. Rev. Lett. 44, 1505 (1980).
6. J.A. Kash, J.C. Tsang, and J.M. Hvam, Phys. Rev. Lett. 54, 2151 (1985).

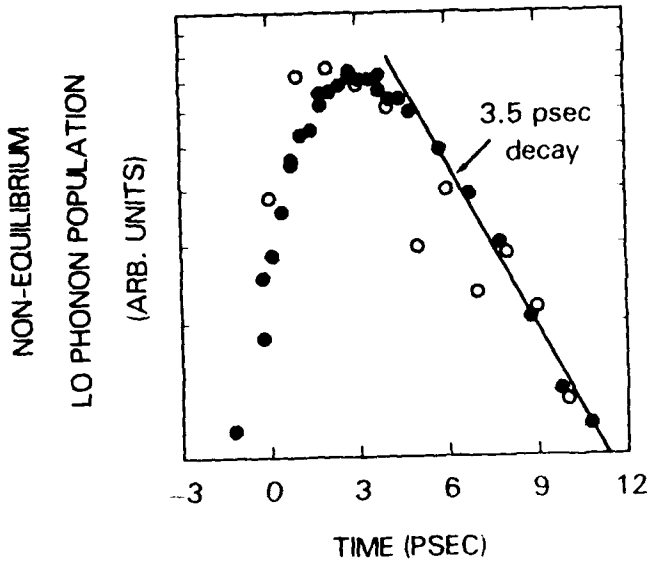

Figure 1. Room temperature nonequilibrium phonon kinetics for LO phonons in GaAs (filled circles), and the GaAs-like LO phonon in $Al_{0.24}Ga_{0.76}As$ (open circles). Laser wavelength is 580nm for GaAs, 567nm for $Al_{0.25}Ga_{0.76}As$. Pulse width in both cases is 0.7 psec (autocorrelation FWHM). Risetime differences result from differences in bandgap.

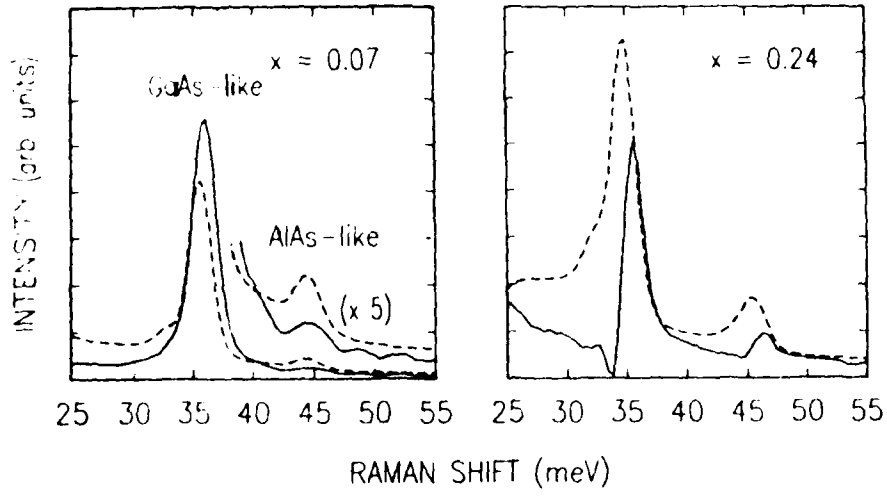

Figure 2. Picosecond Raman scattering from room temperature $Al_xGa_{1-x}As$ excited by 5 psec (autocorrelation FWHM) pulses at 567nm. Dashed curves are spectra from thermal phonons, excited when the probe preceeds the pump by 10 psec. Solid curves are the additional scattering (multiplied by 5) due to nonequilibrium phonons when the probe follows the pump by 2 psec. The slight frequency shift between thermal and nonequilibrium phonons is due to a slight LO phonon-plasmon coupling at our injected carrier concentration of about 10^{17} cm^{-3}.

Investigation of Photoconductive Picosecond Microstripline Switches on Self-Implanted Silicon on Sapphire (SOS)

P. Polak-Dingels and G. Burdge
Laboratory for Physical Sciences, College Park, MD 20740
Chi H. Lee
Department of Electrical Engineering
University of Maryland, College Park, MD 20742
A.C. Seabaugh, R.T. Brundage, M.I. Bell, and J. Albers
National Bureau of Standards, Gaithersburg, MD 20899

Optoelectronic switches, fabricated on amorphous- and implantation-damaged semiconductor thin films, have proven to be among the fastest of the picosecond photoconductors, with switching times less than 50 ps [1]. Ion implantation offers a systematic way to vary the disorder of materials from partially damaged to amorphous. With such materials, the relationship between implantation damage and carrier transport can be explored. Smith and Auston measured the dose dependence of the picosecond photoresponse for oxygen implanted into SOS, reporting an excess carrier lifetime of less than 10 ps [2]. Because oxygen itself may alter the material properties in addition to damaging the crystal, we have studied the photoresponse of Si-implanted SOS. The transport properties as a function of device gap length and bias voltage were measured. Raman scattering and resistivity measurements were made to characterize the material and were compared with the photoconductivity data.

The Monte Carlo code TRIM (TRansport of Ions in Matter) of Biersack and Haggmark, modified by Albers [3] to estimate the damage distribution created by the implant, was used in choosing the implant energy and doses. The critical amorphization dose, i.e., the dose at which the crystal transforms to an amorphous state, is estimated to occur when the energy deposited in the lattice exceeds 6×10^{23} eV/cm^3 [4]. For a 270-keV Si self-implant, the critical amorphization dose in the 0.6-μm Si layer is 1.3×10^{14} cm^{-2}. Implant fluences were chosen to cover the range from above to below this value.

The device design, similar to that introduced by Auston [1], consisted of two photoconductive switches. One switch, connected to the bias voltage, functions as a pulse generator, and the second switch, connected to the lock-in amplifier, acts as a sampling gate. Planar 50-Ω microstriplines, 450 μm wide, were deposited on a 0.6-μm Si layer with a 0.457-mm (18-mil) thick sapphire substrate. The metallization for the striplines was Ti/Au, formed by an oxide-enhanced lift-off process. Gold was then deposited on the back surface of the wafer and the metallization sintered at 300°C for 30 minutes. Three different device sets were fabricated with gap lengths of 2, 5, and 10 μm.

Implantation was performed at room temperature, after the metallization, with the beam current kept below 3 μA to minimize sample heating. The implantation fluences were 10^{13}, 10^{14}, and 10^{15} cm^{-2}, a range predicted to produce material varying from damaged to amorphous. To check for possible contamination by nitrogen or carbon monoxide, which have the same mass as the usual implant species ^{28}Si, one device (10^{13} cm^{-2}) was implanted with ^{29}Si. After implantation, the devices were mounted on brass blocks using K connectors to minimize reflections. Using a network analyzer, we tested the rf performance of the packaged devices up to 20 GHz. The packages were limited by the frequency characteristics of the K connectors to about 20 GHz.

Picosecond photoconductivity measurements were made by the cross-correlation technique developed by Auston [1]. The laser system consisted of a dye laser synchronously pumped by the frequency doubled output of a cw mode-locked Nd:YAG laser. The pulse train had a repetition rate of 100 MHz, a pulse duration of 3 ps, and an average power of 120 mW. The output of the dye laser was split into two beams; one illuminated the sampling gate while the other passed through a variable delay line before illuminating the pulse generator. A stepper motor varied the length of the delay line in steps of 0.4 μm over a total travel distance of 5 cm. The optical pulse train illuminating the pulse generator was chopped at 74 Hz, and the resultant signal from the sampling gate was fed to the lock-in amplifier.

Picosecond cross-correlation measurements show no change in pulse width as the bias voltage is varied. We conclude that the primary influence on the pulse width is the excess carrier lifetime, with no measurable contribution from the transit time. There was no difference between the response of the ^{28}Si- and ^{29}Si-damaged samples; both samples with implant fluences of 10^{13} cm^{-2} have carrier lifetimes of 12 ps. At a higher fluence level of 10^{14} cm^{-2}, the carrier lifetime decreases to 9 ps. Samples damaged with a fluence of 10^{15} cm^{-2} showed no further decrease in carrier lifetime.

Raman scattering measurements were made using the 514.5-nm Ar^+ laser line in a back-scattering geometry. No variation between the spectra was observed at fluence levels of 10^{13} and 10^{14} cm^{-2} for either the ^{28}Si or ^{29}Si implants. However, at 10^{15} cm^{-2}, the optic phonon peak broadened somewhat, with increased scattering in the low frequency wing, indicating the onset of a crystalline-to-amorphous transition.

The resistivity of samples damaged with ^{28}Si at fluences of 10^{12} to 10^{15} cm^{-2} was measured by the van der Pauw method. After implantation at a dose of 10^{12} cm^{-2}, the resistivity increased from a 50 Ω-cm unimplanted value to $10^4\Omega$-cm. The resistivity peaks at a fluence of 10^{14} cm^{-2} and then decreases with increasing fluence. This decrease in resistivity with increasing implant dose is similar to that reported for amorphous Si with an increase in dangling bond density [5]. The resistivity of the ^{29}Si sample is comparable to that of the ^{28}Si sample.

In summary, we have measured picosecond photoconductivity on self-implanted SOS over an implant fluence range of 10^{13} to 10^{15} cm^{-2}. The photoconductive response time decreases only slightly for implant fluences varying over three orders of magnitude. There is no change in the Raman spectrum up to implant fluences of 10^{15} cm^{-2}, where there appears a small amorphous-like component to the optic phonon peak. The highest resistivity occurred at an implant fluence of 10^{14} cm^{-2}. Work is now in progress on samples at a higher fluence level in order to determine the effect of amorphization on the photoconductive response.

References

1. D.H. Auston, "Picosecond Photoconductors: Physical Properties and Applications," in *Picosecond Optoelectronic Devices*, edited by C.H. Lee (Academic Press, 1984).

2. P.R. Smith, D.H. Auston, A.M. Johnson, and W.M. Augustyniak, "Picosecond Photoconductivity in Radiation-Damaged Silicon-on-Sapphire Films," *Appl. Phys. Lett.* **98**, 47(1981).

3. J. Albers, "Monte Carlo Calculations of One- and Two-Dimensional Particle and Damage Distributions for Ion-Implanted Dopants in Silicon," *IEEE Trans. on Electron Devices*, **ED-32**, 1930(1985).

4. J.R. Dennis and E.B. Hale, "Crystalline to Amorphous Transformation in Ion-Implanted Silicon: A Composite Model," *J. Appl. Phys.*, **49** 1119(1978).

5. A.M. Johnson, D.H. Auston, P.R. Smith, J.C. Bean, J.P. Harbison, and D. Kaplan, "Picosecond Photoconductivity in Amorphous Silicon," in *Picosecond Phenomena II*, edited by R. Hochstrasser, W. Kaiser, and C.V. Shank (Springer-Verlag, Berlin, 1980).

"Fast GaAs photoconductive detectors with high sensitivity integrated in coplanar sytems onto GaAs substrates"

H. Schumacher, U. Salz and H. Beneking

Institute of Semiconductor Electronics

Aachen University of Technology

5100 Aachen

F.R.Germany

Hitherto optically activated switches consist of a gap between two metallic contact pads on a semiconductor substrate (fig.1a). To gain a low "On"-resistance a focused laser beam of relatively high intensity has to be applied.

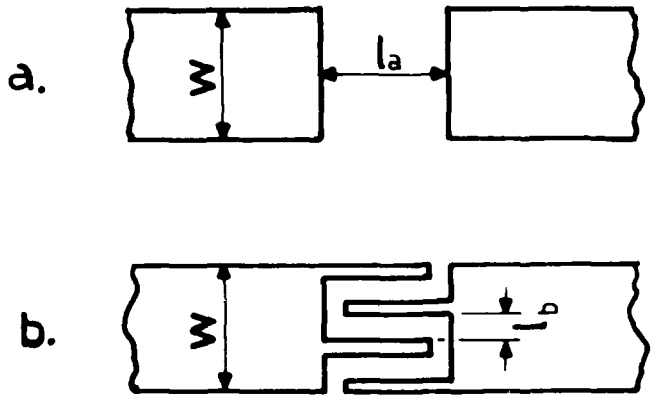

Fig. 1 Detector structures

Aspiring a higher "On"-conductivity without the use of an increased light power leads to the development of an interdigitated structure shown in fig.1,b). That is necessary, because linear conduction characteristics depend on the demand that only the carrier lifetime is determinative concerning the time behaviour. Therefore the length l should not fall below a minimal value.

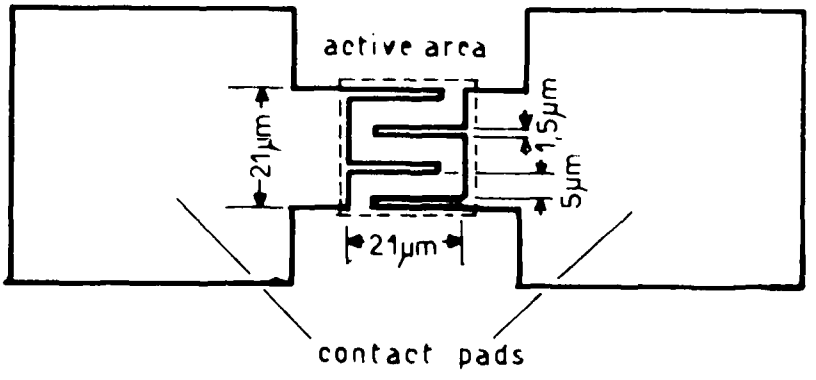

Fig.2: The detector and its dimensions

The calculation of the change in conductivity (ΔG) for the single gap structure (ΔG_a) and the interdigitated structure (ΔG_b) results in:

(1) $\Delta G_a = e(\mu_n+\mu_p) \cdot \frac{(1-R) \cdot E}{l_a^2 \cdot h\nu} \qquad (\sim 1/l^2)$

and

(2) $\Delta G_b = e(\mu_n+\mu_p) \cdot \frac{A_{eff}}{A} \cdot \frac{(1-R) \cdot E}{l_b^2 \cdot h\nu}$

with the reflection coefficient R, lightpulse energy E, photon energy hv, the mobilities $\mu_{n,p}$ and the area of the detector not covered by fingers A_{eff}. Resuming the same irradiated area it can be noticed that the interdigitated structure is advantageous.

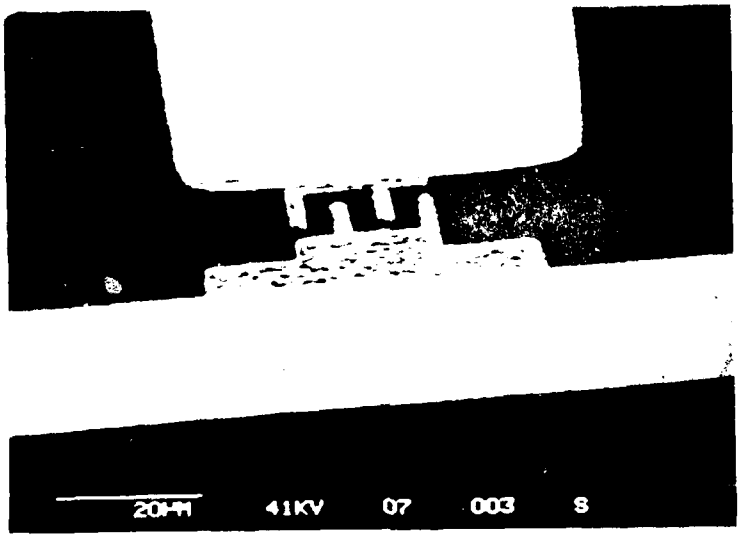

Fig.3 The detector in a coplanar system.

Calculating ΔG_a and ΔG_b under the use of realistic values (E= 100pJ, λ = 615nm, $\mu_n+\mu_p$= 100 cm^2/Vs) leads to the conclusion that ΔG_b has a value 1.5 times higher than ΔG_a. Te small mobilities μ_n and μ_p are caused by the implantation of protons to reduce the carrier lifetime. Up to now a time constant of approximately 5ps has been achieved.
This is important because the parasitic capacitances of the new photoconductive detector are of a low value so that the switching times of both structures remain comparable. The pulse width of the correla-

AD-A187 136 SUMMARIES OF PAPERS PRESENTED AT THE PICOSECOND ELECTRONICS AND OPTOELECT..(U) OPTICAL SOCIETY OF AMERICA WASHINGTON D C J W QUINN 10 OCT 87 2/3

UNCLASSIFIED N00014-87-G-0050 F/G 9/1 NL

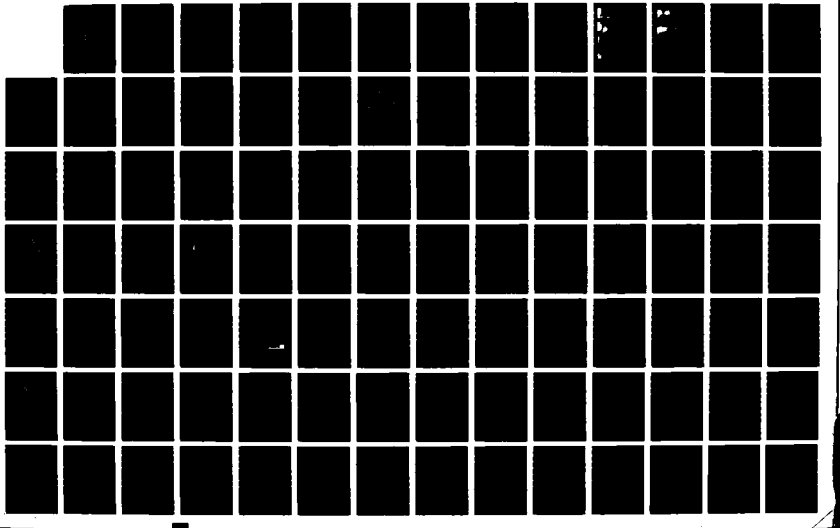

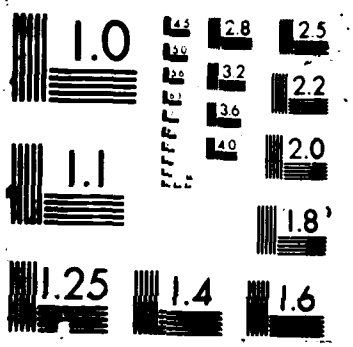
1.0
1.1
1.25
1.4
1.6
1.8
2.0
2.2
2.5
2.8
3.2
3.6
4.0

function shown in fig.4 and measured in an arrangement described in fig.5 is clearly determinated by the carrier lifetime.

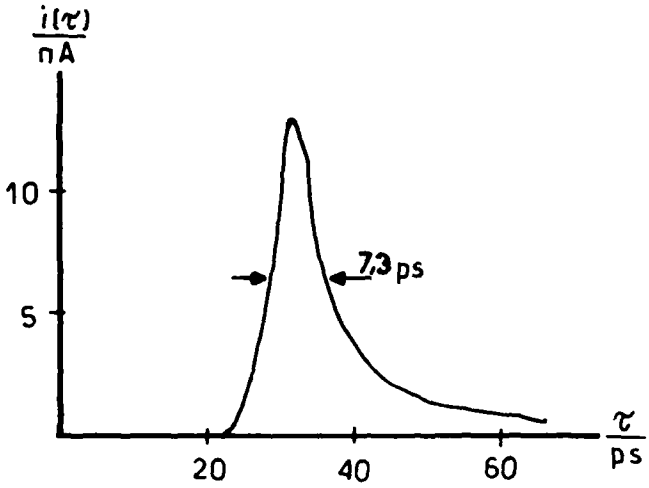

Fig.4: cross-correlation function i(τ)

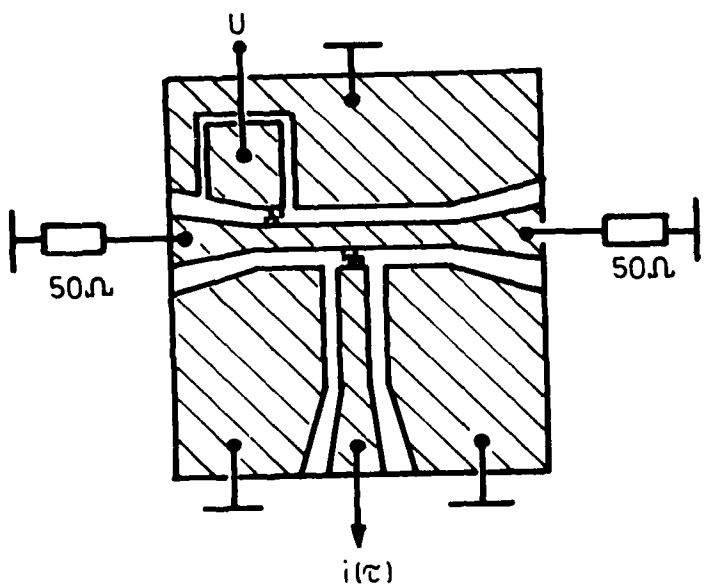

Fig.5: Schematic arrangement for measuring i(τ)

The advantage of the finger structure is obvious: the achievement of a higher sensitivity does not influence the switching time. That is interesting concerning the use of semiconductor lasers instead of dye lasers. Furthermore our aim is to optimize the implantation of the substrate and thereby the temporal behaviour, whereof an account will be given in the paper.

Carrier Lifetime vs. Ion-Implantation Dose in Silicon on Sapphire

F. E. Doany, D. Grischkowsky, and C.-C. Chi

IBM T.J.Watson Research Center, P.O.Box 218, Yorktown Heights, NY 10598

The generation of subpicosecond electrical pulses has recently been demonstrated using fast photoconductive switches driven by short laser pulses [1]. In these measurements electrical pulses on the order of 0.6 ps were obtained by shorting a charged transmission line fabricated on an ion-implanted silicon-on-sapphire (SOS) wafer. The major factors determining the shape and duration of these electrical pulses were the laser pulsewidths, the circuit characteristics of the photoconductive gaps and the transmission line, and the carrier lifetime of the semiconductor [2]. Since laser pulses shorter than 100 fs are routinely obtained from colliding-pulse-modelocked dye lasers, the laser pulsewidth can be made negligible compared to the generated electrical pulse. In addition, the limiting factors on the time response due to the circuit reactance may be eliminated if the capacitance of the generation site is reduced to negligible amounts. Under these conditions the duration of the electrical pulse would be mainly determined by the carrier lifetime in the ion-implanted SOS. However, no systematic measurements of this lifetime are available.

In this paper we present measurements of the carrier lifetimes of a systematic series of SOS samples with increasing amounts of ion implantation. The samples consist of 0.5 μm silicon on sapphire wafers that were implanted with O^+ ions of doses ranging from 1.0 x $10^{12}/cm^2$ to 7.5 x $10^{15}/cm^2$ at 200 keV (and 100 keV in some cases). The carrier lifetimes are measured by time-resolved reflectivity and transmission measurements following excitation with femtosecond optical pulses.

The laser source is a compensated colliding-pulse-modelocked dye laser producing 70 fs pulses at 625 nm (2.0 eV) at a repetition rate of 100 MHz. These pulses are split into two beams to provide the pump and probe pulses. The average power of the pump beam was 2 mW (20 pJ/pulse) and is focused to a diameter of about 10 μm. The probe beam is attenuated to < 0.2 mW and is focused to a diameter of about 5 μm. The polarization of the probe beam is rotated by 90° to suppress interferences between the two beams on the sample surface. The pump is incident on the sample at an angle of 30° relative to the normal while the probe is incident on the opposite side of the normal at an angle of 60°. The pump beam is chopped at 1.0 kHz. Before reaching the sample, the probe beam is additionally split into two beams: one is reflected off the sample onto a photodiode detector and the second, incident directly onto a matched photodiode, is used as a reference. The reflection signal is derived as the difference of these two photocurrents and is detected, using a lock-in amplifier, as a function of time delay between the pump and probe pulses. The sensitivity of our apparatus to changes in the probe beam reflectance is approximately 1 part in 10^6.

Without pumping, the reflectivity at normal incidence of the samples used in this study at 625 nm is relatively constant at a value of 0.2 and increases only slightly at the highest implantation dose. The absorption, however, increases monotonically from 0.3 at a dose

1.0 x $10^{12}/cm^2$ to 0.65 at the highest dose of 7.5 x $10^{15}/cm^2$. For the unimplanted SOS sample the reflectivity and absorption are 0.2 and 0.25 respectively.

Excitation of the silicon with 625 nm optical pulses generates an electron-hole plasma. The associated index change results in a reflectivity/absorption change. Because the pump intensities used in this study are 4 to 5 orders of magnitude below the melting threshold of silicon (ca. 0.1 J/cm^2), lattice heating effects are negligible. Thus, reflectivity and transmission measurements are representative of carrier recombination rates.

The change in reflectivity following photoexcitation of two representative samples is shown in Figure 1. Figure 1a was obtained for SOS sample ion-implanted at a dose of 2.0 x $10^{15}/cm^2$. The smooth curve also shown in Figure 1a is a convolution of our 0.14 ps pump/probe instrument response function with a 0.65 ps exponential decay. Figure 1b shows similar data obtained at a dose of 1.0 x $10^{13}/cm^2$ which is closely simulated by an exponential decay of 4.8 ps.

Femtosecond resolved reflectivity data was obtained for a series of SOS samples with a range of implantation doses covering 4 orders of magnitude and also for unimplanted SOS. In attempting to interpret these data, each curve was fit to a single exponential decay time, which varied from >300ps for the unimplanted SOS wafer down to about 600 fs for the highly implanted samples. These results are summarized in Figure 2. There are two major regions of interest: the variation of the lifetime at low ion-implantation doses, < 3.0 x $10^{13}/cm^2$, and the lack of dependence at the higher doses, > 1.0 x $10^{14}/cm^2$.

At low implant levels, the lifetime decreases linearly with the ion-implantation dose. This is clearly demonstrated by the fit of the low dose data points in Figure 2 to a slope of unity. The linear dependence in this region is consistent with recombination rates proportional to the density of "traps" introduced by the ion-implantation. In this case, the trap density and therefore the carrier lifetime will vary linearly with ion-implantation level.

The variation of lifetime with implantation dosage saturates at a level 3.0 x $10^{14}/cm^2$. Above this dose, the lifetime reaches a limit of 600-700 fs. This lifetime does not vary even as the implantation dose is increased by more than a factor of 20. These lifetimes are clearly resolvable by our experimental resolution as evidenced by the <150 fs risetimes of the data presented in Figure 1. The approximate 600 fs limit is therefore due to the response of the semiconductor itself. Possible interpretations of this lack of dependence on ion-implantation level include saturation of effective trap densities and hot carrier relaxation. Further data, including transmission, power and temperature dependences, will also be presented to clarify the mechanism of the lifetime saturation.

This research was partially supported by the U. S. Office of Naval Research.

1. M.B.Ketchen, D.Grischkowsky, T.C.Chen, C-C.Chi, I.N.Duling, N.J.Halas, J-M.Halbout, J.A.Kash, and G.P.Li, Appl. Phys. Lett. **48**, 24 (1986).

2. D.H.Auston, in *Picosecond Optoelectronic Devices*, edited by C.H.Lee (Academic, London, 1984), pp. 73-116.

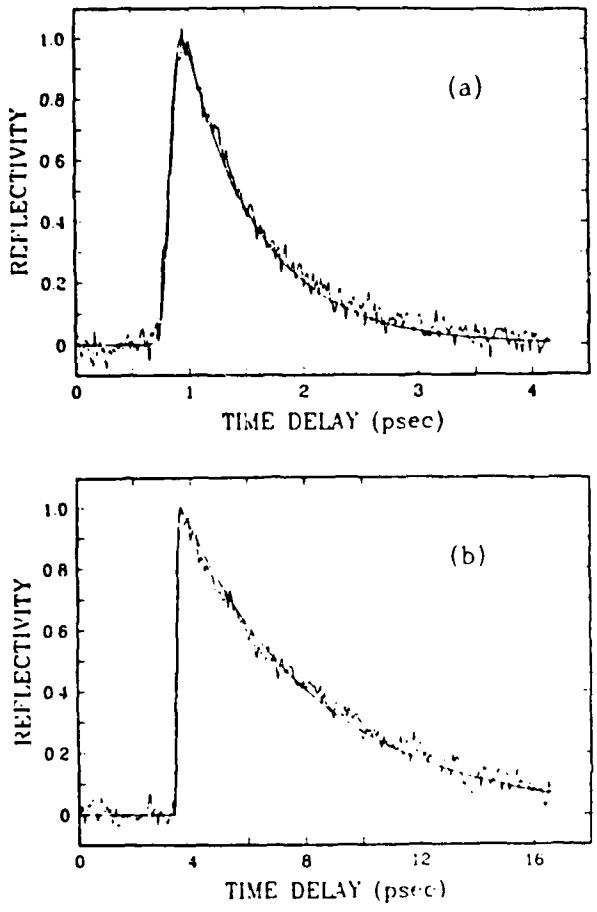

FIGURE 1. Measured change in reflectivity for SOS samples ion-implanted at doses of (a) 2.0 x $10^{15}/cm^2$ and (b) 1.0 x $10^{13}/cm^2$. Smooth curves are fits obtained using a 140 fs instrument response convoluted with (a) 0.65 ps and (b) 4.8 ps exponential decays.

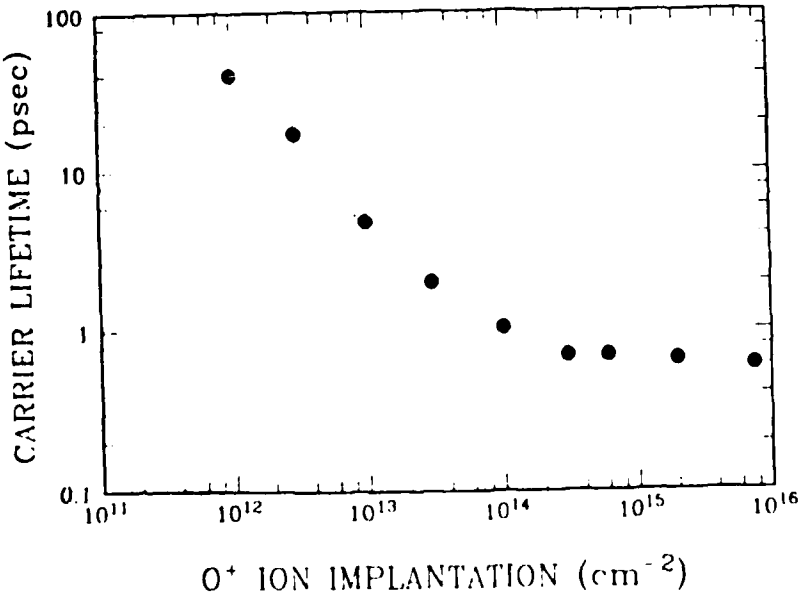

FIGURE 2. Carrier lifetime vs. ion-implantation dose. Lifetimes are derived from individual reflectivity data at each dose.

Picosecond Optoelectronic Switches Using Composite Electronic Materials

E.A. Chauchard and Chi H. Lee
Department of Electrical Engineering
University of Maryland
College Park, MD 20742

V. Diadiuk and G.W. Turner
MIT-Lincoln Laboratory
Lexington, MA 02173-0073

Since the discovery of picosecond photoconductivity, optoelectronic switches made from a variety of materials have been studied [1]. A great number of applications have already been recognized and many new techniques depend on the availability of ultrafast (picosecond) devices. The two switches using composite electronic materials studied in this work are Fe-doped InGaAs grown on InP substrates and GaAs on a silicon-on-sapphire (SOS) substrate. The semi-insulating character of the Fe:InGaAs epilayer makes it very attractive for fabrication of integrated devices such as PIN photodetectors and FETs [2]. This material also exhibits a very high mobility (10000 cm^2/Vs) and a photosensitivity extending up to 1.65 μm. The GaAs on SOS is of interest for the monolithic integration of GaAs and silicon devices where, for example, a GaAs FET could be integrated on a silicon wafer. This process takes advantage of the mature Si technology and the availability of low cost, high quality silicon wafers [3]. There is also interest for SOS as substrate because it provides better isolation and it is transparent. The interface silicon-sapphire exhibits a high density of defects, allowing faster devices to be fabricated. In our experiment, the sapphire substrate was used for mechanical strength. Whatever the material, the fabrication of a switch by deposition of metallic electrodes makes it possible to determine the switch characteristics and possible applications as well as to test the material optical properties.

The study of device speed often reveals several phenomena which can appear as distinct time constants in the observed time waveform. The attribution of each of these different time constants to a particular cause is difficult and often inaccurate. One can classify the phenomena contributing to the speed of the device in two main categories: carrier recombination times (bulk recombination, surface recombination, Auger recombination, etc.) and effects related to the applied electric field (carrier sweep-out). In addition, two other effects can contribute to the observed time waveform: contact fabrication which plays a role because of the formation of a Schottky barrier at the metal-semiconductor interface and optical intensity which can saturate the switch and lead to slower response times.

This paper presents a study of the effect of applied electric field on the speed of the device. We point out the distinction between the true carrier recombination time, which is independent of the field, and the carrier sweep-out effect due to the field-induced movement of the carriers. Measurement of the sweep-out time allows us to calculate the

effective field in the material. Because of the carrier screening of the field [4], the effective field is much smaller than the field expected from the applied voltage.

The light source used in this work was a synchronously pumped CW mode-locked dye laser producing 3 ps pulses at a repetition rate of 100 MHz. The observations were done with a Tektronix sampling scope and/or using a cross-correlation technique for waveform sampling.

For Fe:InGaAs, the time response of three switches of different gap size (3 μm, 10 μm, 20 μm) were studied for an applied voltage varying between 0.2 V and 10 V. Figure 1 is a plot of the observed decay time constants which were found to be slower at lower fields. We interpret this fact as follows. When the applied voltage decreases, the decay time tends towards the true carrier recombination time. At high fields, the sweep-out of the carriers in the field accelerates the decay. The true carrier recombination time could be observed at low field for the 20 μm gap switch and was found to be 4.5 ns. At 10 V bias voltage, the response time of the switch is decreased to 200 ps. Knowing the mobilities of the carriers as a function of the electric field and assuming that the response time corresponds to the time needed by the carriers to cross the gap, we can estimate the effective field seen by the carriers. With 10 V bias in the 3 μm switch, we find this field to be 270 times smaller than the expected field from the applied voltage. The effect of the screening of the field by the carriers is thus very important at this relatively high injection level. A dependence of the waveform on the type of electrodes deposited on the switch was also observed.

The GaAs on SOS switch was designed in a cross-shape with two 4 μm gaps in order to be studied by cross-correlation technique. The cross-correlation result indicates a response time of 19 ps. No dependence on the applied voltage was observed, showing that the device response time can be attributed to carrier recombination time only. As the light intensity illuminating the switch was increased, the device response became slower. This saturation phenomenon has been explained in [5].

In conclusion, the sweep-out effect can be very important in determining the speed of a device if the carrier recombination time is in the hundreds of picoseconds range. By applying sufficient field on a slower device, its response time can be drastically decreased. Other factors such as light level and electrode composition also have to be taken into account. The screening of the field by the carriers can be estimated by the method presented here and was found to decrease the effective field in the switch by a factor of up to 270. The fastest switch studied here was the GaAs on SOS; it exhibits a 19 ps response time.

Acknowledgments

The University of Maryland portion of this work was supported in part by the Laboratory for Physical Sciences and the Air Force Office of Scientific Research.

The Lincoln Laboratory portion of this work was sponsored by the Department of the Air Force.

References

[1] Picosecond Optoelectronic Devices, Chi H. Lee (Ed.), Academic Press (1984).
[2] V. Diadiuk and S.H. Groves, Appl. Phys. Lett., 46, 2, pp. 147-158 (1985).
[3] H.K. Choi, G.W. Turner, T.H. Windhorn, and B.Y. Tsaur, Device Research Conference, June 1986, Amherst, MA.
[4] D.H. Austin, in Picosecond Optoelectronic Devices, Chi H. Lee (Ed.), Academic Press (1984).
[5] Kenneth K. Li, John R. Whinnery and Andrew Dienes, "Picosecond Lasers and Applications," Proc. SPIE 322, pp. 124-130 (1982).

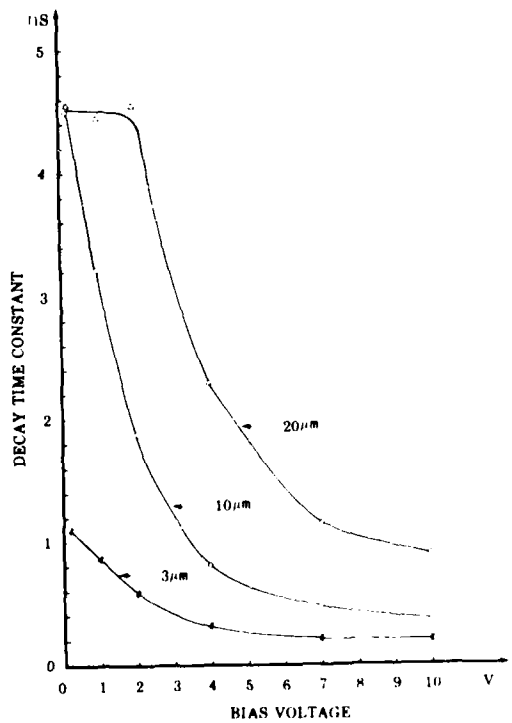

Fig. 1: Decay time constant as a function of applied voltage for three Fe:InGaAs switches of different gap size.

COMPARISON OF SAMPLING OSCILLOSCOPES WITH < 35 PS TRANSITION DURATIONS

James R. Andrews, Ph.D.
Picosecond Pulse Labs, Inc.
P.O. Box 44
Boulder, Colorado 80306
U.S.A.

The purpose of this paper is to compare transient responses of all of the various ultrafast sampling oscilloscopes. This study was limited to the fastest samplers with transition durations (10-90% risetimes) of <35 ps and corresponding bandwidths of >10 GHz. It is very important for users of these instruments to realize that none of them will give the correct answer when measuring picosecond domain signals. The same pulse signal measured with different samplers will result in different pulse waveforms as displayed on the CRT's.

Six samplers from four manufacturers were compared. The manufacturers were: Hewlett-Packard, Colorado Springs, Colorado; Tektronix, Beaverton, Oregon; Picosecond Pulse Labs, Boulder, Colorado and Iwatsu, Tokyo, Japan. The HP samplers were the Models 1430A and 1430C used with both the 140 series (1411A & 1424A plug-ins) and 180 series (1811A plug-in) oscilloscopes. The Tek samplers were the S4 and S6 used with the 7000 series oscilloscopes and the 7S11/7T11 or 7S12 plug-ins. The S4 and S6 could also be used with the older 560 series scopes. The PSPL sampler was a Model S-1430D. PSPL does not manufacture a complete sampling oscilloscope. The S-1430D sampler is designed to be used interchangeably with either the HP 140 or 180 series or Tek 560 or 7000 series sampling oscilloscopes. The Iwatsu sampler was the SH-4B used with their new SAS-8130 digital sampling oscilloscope. It can also be used with their SAS-601B oscilloscope.

Two different pulse generators were used. The first was the fastest tunnel diode we could find. It was an HP1106A powered by a PSPL TD-1105 Bias Supply. It was specified by HP to have a nominal 20 ps transition duraton. We estimate that the particular unit used had a 17 ps transition duration. For the nanosecond domain comparisons a PSPL 6100 Reference Flat Pulse Generator (RFPG) was used. It produces a very flat, clean step from 500 mV to 0 V with a 400 ps transition duration. The 6100 RFPG is based upon an NBS RFPG design.

The collection of photographs in Fig. 1, shows the picosecond domain transient responses of all of these samplers when driven by the same HP1106A tunnel diode. The vertical scale is 50 mV/div. The horizontal scale is 20 ps/div. for the top two rows and 200 ps/div. for the bottom two rows. Fig. 2 shows the nanosecond domain step responses of the samplers when driven by

HP 1430A

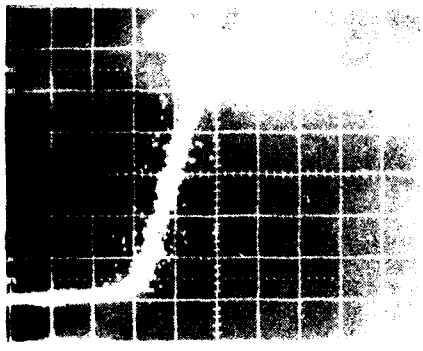

Tek [illegible]

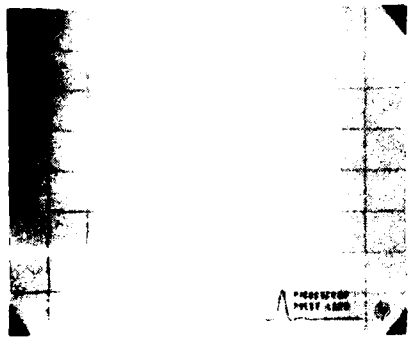

[illegible]

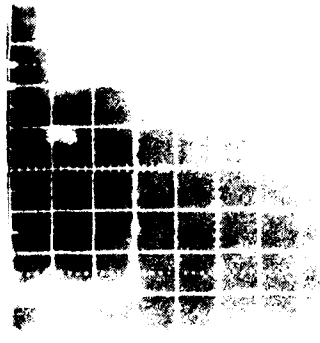

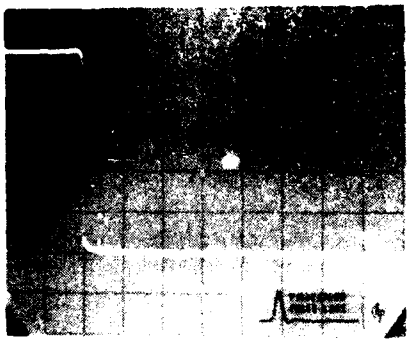

HP 1430A

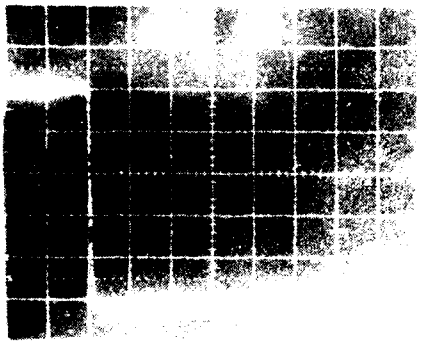

Tek 54

A Technique for Wing Suppressed IR Sampling

John Nees and Steve Williamson
Laboratory for Laser Energetics
University of Rochester
250 East River Road
Rochester, NY 14623
716/275-5101

Short pulses in infrared are useful as *in situ* probes for devices fabricated on electro-optic semiconductors like GaAs.[1] Sources of such pulses are under development with wavelengths extending to 1.6 μm.[2] The most prominent technique currently used to achieve picosecond pulses in the IR is compression of Nd:YAG 1.064 μm in a fiber-grating pair.[3,4] It has been shown that propagation of short (100 ps) pulses through long (2 km) lengths of monomode fiber can lead to picosecond pulses with very low energy outside the central intensity spike. This method of compression makes use of the positive dispersion available in glass fibers at 1.064 μm. In an effort to extend *in situ* electro-optic sampling far below the bandgap of GaAs or to the sample in InP wavelengths longer than 1.35 μm are necessary, but the dispersion in glass fibers also begins to change sign. At color-center wavelengths from 1.4 to 2.3 μm there is no existing technique for such wing suppression.

This paper describes experiments demonstrating the feasibility of using optical frequency doubling as a tool for wing suppression in sampling experiments. The theory is that short compressed pulses at subbandgap energies which have a significant fraction of their energy outside the control spike can be used to sample electro-optic semiconductors provided the energy in the wings is removed before the averaging that occurs in the photodetectors. This can be accomplished by the intensity dependence of second harmonic generation (SHG). Since the conversion efficiency, $\frac{I_{2\omega}}{I_{\omega}}$ is proportional to I_{ω}, the energy in the energy in the picosecond intensity spike is efficiently converted to the second harmonic, while that in the lower intensity wings is left mainly in the fundamental. By detecting the second harmonic, only the information sampled by the shortest part of the compressed pulse is averaged by the detectors. Using differential detection, the linearity of the sampling method can be maintained for small signals.

Using this technique of wing suppresion in a Nd:YAG system with a short (200 m) fiber a sensitivity of 250 mV in GaAs with 135 μW of green from 150 mW of IR in 5 mm KTP is achieved.

Experiments are proceeding to show the actual improvement of temporal resolution and to investigate adaptation to a color-center system.

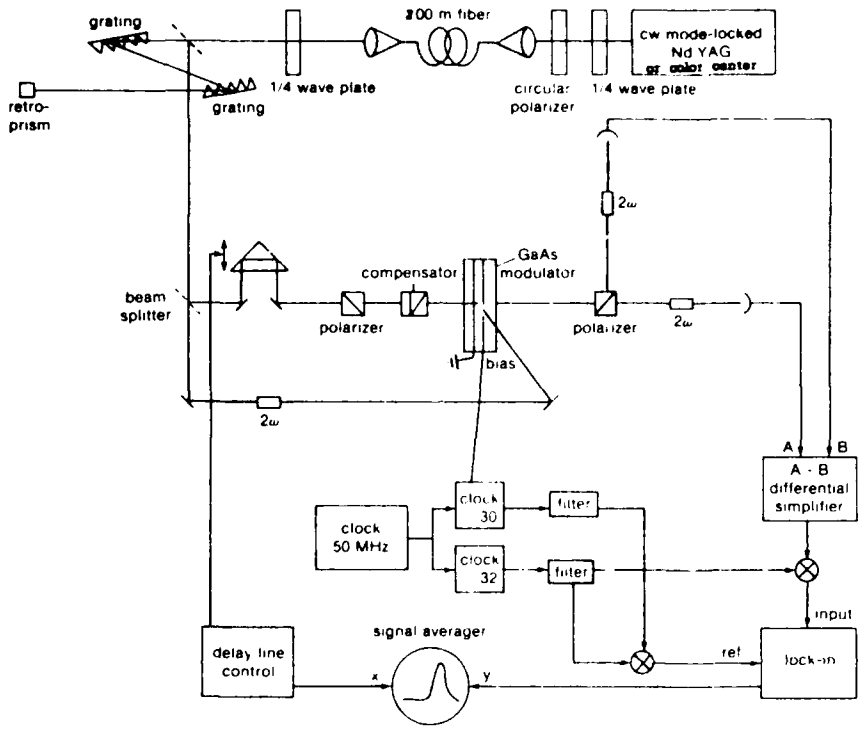

Fig. 1 Schematic of a system for wing suppressed IR sampling.

Acknowledgment

This work was supported by the sponsors of the Laser Fusion Feasibility Project at the Laboratory for Laser Energetics.

References

1. B.H. Kolner and D.M. Bloom, IEEE J. Quant. Elec. QE-22, 79-93 (1986).

2. L.F. Mollenauer and R.H. Stolen, Opt. Lett. 9, 13 (1984).

3. B. Nikolaus and D. Grischkowsky, Appl. Phys. Lett. 42, 1 (1983).

4. B. Nikolaus and D. Grischkowsky, Appl. Phys. Lett. 43, 228 (1983).

WE15-1

HIGH SPEED OPTO-ISOLATOR FOR RADAR APPLICATIONS

J.P. Anthes and P. Garcia, Sandia National Laboratories
P.O. Box 5800 Albuquerque, NM 87185
K.Y. Lau and I. Ury, Ortel Corporation
2015 W. Chestnut St., Alhambra, CA 91803

We have designed, fabricated and tested a high speed opto-isolator utilizing state-of-the-art optoelectronic components operating at frequencies up to 6 GHz. This opto-isolator will be an indispensible component in modern radar systems and is used for preventing frequency-pulling of a low power oscillation due to reflected signals.

The present prototype design incorporated a directly modulated buried heterostructure GaAlAs laser diode[1] coupled to a GaAs photodiode detector using a very short length (1 cm) of optical fiber. The key to the design is to maximize the forward transmission loss (from laser to photodiode) and minimize backward leakage. The former can be maximized by choosing a highly efficient laser and detector, a large NA and large core size fiber and appropriately lensing the tips of the optical fiber, while the latter can be minimized by placing the laser and photodiode and their associating circuitries into two separate compartments of a metallic enclosure. Ideally, the electromagnetic leakage between the two compartments can be made to approach zero if they were placed far apart. But for reasons of size optical reflection effects on laser characteristics as described below, they must be placed as close as possible. A conpromise was made such that the physical separation between the laser and the photodiode is 1 cm, separated by a metallic wall 0.3 mm thick. A 1 cm fiber of NA 1.5, core size 100 μm and O.D. 140 μm guides the laser light into the photodetector. A 250 μm hole in the partition wall allows the fiber to link the components and the hole is sealed by conductive epoxy after the fiber is in place. The completed assembly is shown in Figure 1. The laser diode compartment is equipped with a thermistor and a thermoelectric cooler for temperature stabilization of the laser. The photodiode sensitive area is 60 μm in diameter. Since the fiber core size is 100 μm, a microlens was formed on the tip of the fiber to focus the light onto the detector surface.

The laser diode dc injection current versus photodiode output current is shown in Figure 2. The corresponding photocurrent output signal, when biased at 15 volts, varied between 0.3 - 2.5 mA. The forward dc signal transmission was -19.0 dB. Typical values for quantum efficiency of the laser diode and the photodiode indicated that the overall optical fiber coupling efficiency was ~62%. Also shown is the effect of changing the photodiode dc bias level. Switching action was produced based upon the detector-bias dependance of the photodiode sensitivity. When biased at a forward voltage of higher than 1.16 V, the microwave photocurrent generated by the laser light was switched off.

Shown in Figure 3 are the typical microwave scattering (S-parameter) data when the optical isolator was operated at 0-dBm input modulation power. Forward transmission losses, in the present prototype, were predominantly due to wide bandwidth (resistive) impedance matching circuits and intrinsic quantum efficiencies of the optoelectronic components. These losses can be minimized by impedance matching both the laser and the detector at the frequency band of operation. With the photodiode switched off in the manner described above, the forward transmission drops to within 5 dB of the reverse leakage over the active frequency band.

A sharp feature is evident in Figure 3 near 9.3 GHz. This characteristic frequency is the time required for laser light to travel to the fiber end near the photodiode receiver and then back again to the laser diode. A dielectric antireflection coating on the photodiode surface would reduce the retroreflected

light intensity by ~15 dB and would therefore reduce the effects of optical resonance. Evidence of a harmonic signature, near 5 GHz, was also visible. It is therefore very important that, for operation up to a frequency of x GHz, the length of the fiber in this optoisolator must be
<< C/nx where C is the velocity of light and n is the refractive index of glass. This explains the necessity to bring the components as close together as possible.

Unwanted rf signals can leak through improperly sealed cracks or holes that connect the compartments of the optical isolator. The rf power W radiated into the laser diode compartment through the hole which the fiber passes can be computed using standard electromagnetic analysis. The results illustrate three relevant trends: attenuation for present aperture dimensions was very high (< -80 dB), small changes in aperture dimensions strongly influence microwave transmission, and higher microwave frequencies produce higher reverse transmission. The third point confirms the trend of S_{12} data for increasing frequency shown in Figure 3.

CONCLUSIONS: Overall, the potential for significant device improvements seem likely. Techniques to improve the value of the forward rf transmission power will focus on improved microwave circuits designed to decrease opto-electronic losses. It can be even theoretically configured (in an optimized narrow bandwidth) to exhibit modest rf power gain by carefully matching electrical impedances with signal transformers, biasing the receiver photodiode, and minimizing optical losses at all interfaces. An extended response opto-isolator could conceivably operate in the 20-GHz frequency regime.

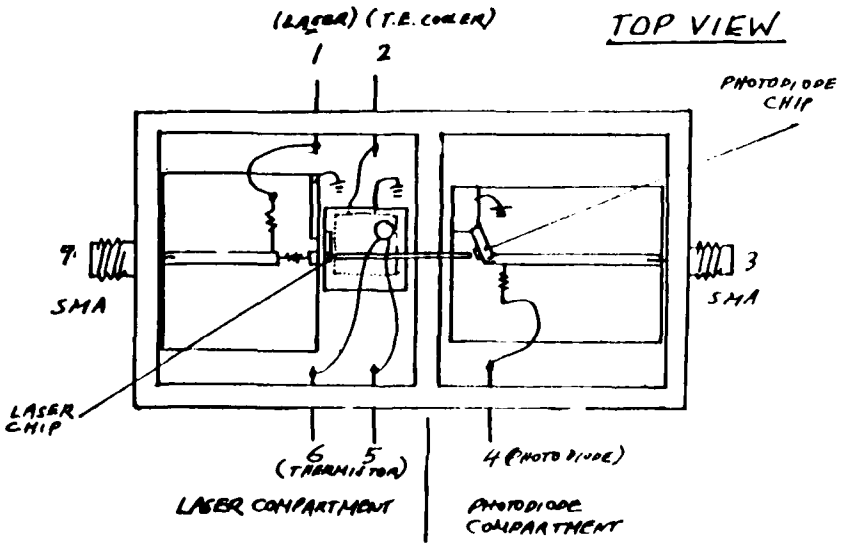

Fig. 1 Schematic top view of the high speed opto-isolator

[1] Kam Y. Lau and Amnon Yariv, IEEE J. Quantum Electron. QE-21, No. 2, 121, 1985

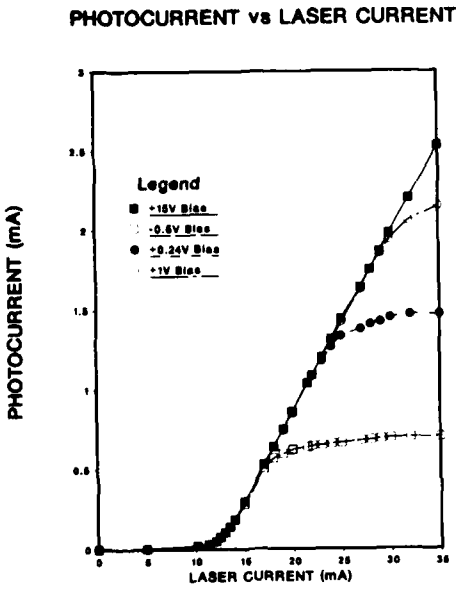

Fig. 2 DC transfer characteristics of the optoisolator at various photodiode bias

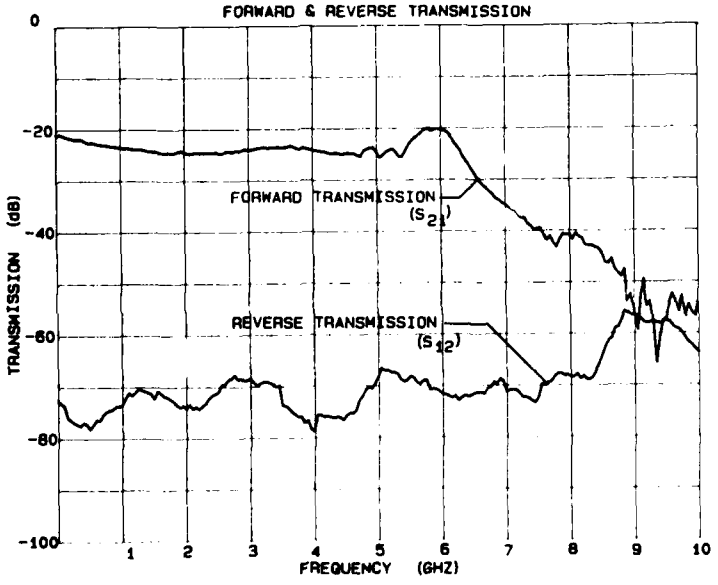

Fig. 3 Microwave forward and backward transfer characteristics

Energy Variations in Optical Pulses from Gain-Switched AlGaAs Diode Lasers

R. T. Hawkins
Tektronix, Inc., P.O. Box 500, Beaverton, OR 97077

J. H. Goll
Tektronix, Inc., P.O. Box 500, Beaverton, OR 97077

*N. A. Anheier**
Tektronix, Inc., P.O. Box 500, Beaverton, OR 97077

One method for producing optical pulses as short as <20 ps FWHM with a diode laser is by gain switching. For such a laser, gain switching is readily achieved by applying an electrical (forward bias) pulse excitation to the diode. The average duration of the resulting optical pulses depend on the detailed shape of the electrical drive pulse and the dynamic response of the laser diode (in its package) to that drive pulse. Streak camera measurements[1-2] have demonstrated that significant temporal substructure is present on the optical pulse, with subpulses of duration below 10 ps. This substructure changes dramatically from pulse to pulse. Previously reported work on gain switching of laser diodes has been almost exclusively confined to minimizing the time-averaged optical pulse duration, spectral width, and time-bandwidth product. An important additional consideration for ultrafast electro-optical sampling applications is the energy contained in the optical pulse, which should ideally be large and constant to minimize both shot noise and averaging time in the optical detection system. Little work has been done heretofore to quantify the variation in energy of diode laser optical pulses. We present here the results of a series of measurements of this energy variance in pulses produced by gain switching commercially available gain guided double heterostructure AlGaAs laser diodes.

The measurement apparatus is shown schematically in Figure 1. The gain-switched laser output was split to allow observation of the temporal structure with a fast photodetector and electronic sampling system while simultaneously measuring pulse energy with a charge-coupled device (CCD). Monitoring the pulse temporal structure was necessary to ensure that only a single relaxation oscillation was generated by the laser under test. The optical pulses were focussed onto the Tektronix four phase, 96 element linear array CCD to maximize the illumination of a single well (to minimize the effects of shot noise). The CCD was always operated well below saturation. Individual CCD waveforms were digitized to 10-bit accuracy (no internal averaging) with a digitizing oscilloscope under computer control. The CCD reset pulse train was used to provide a synchronous trigger for the pulse generator and the oscilloscopes. This triggering scheme minimized the timing jitter in the measurement system. It also ensured that charge generated by one optical pulse could be clocked out of the illuminated region of the CCD before the arrival of the next pulse. The optical pulse is triggered when no charge is being transferred within the CCD. Noise due to CCD dark current was found to be less than the digitization noise of the digitizing oscilloscope. To examine the dependence of variation in laser diode optical pulse energy on variation in drive pulse energy, a system was added, as shown, to digitize the energy of each electrical drive pulse.

* Summer Intern, 1985. Present address: Student, Department of Physics and Astronomy, Western Washington University, Bellingham, WA 98225

Typical optical pulse energy variation is seen in Figure 2(a), which is a multiple exposure of the output wavefonn from the illuminated portion of the CCD for nine separate optical pulse energies. The voltage corresponding to the charge in each well appears as a negative-going square pulse of ~20 μs duration. (Other voltage levels corresponding to CCD charge transfers are not relevant to this discussion and are not seen above the top of the figure.) The sixth well in the figure is the target well for the optical pulses. The camera shutter speed was chosen so that there are ~1000 CCD output waveforms for each exposure. Figure 2(b) shows the high speed photodetector output that corresponds to the energies labeled '1'-'3' in Figure 2(a). Note the progression from a single optical pulse ('1') to two optical pulses ('3') in Figure 2(b). The width of the trace in Figure 2(a) labeled '2', which corresponds to operation at or slightly above threshold for the second relaxation oscillation, is significantly greater than the width of any other trace. This shows a local maximum in the variation of the optical pulse energy. Furthermore, at an optical output energy just below that associated with the initial appearance of the second pulse, a local minimum in the optical energy variation is seen in the width of the trace between those labeled '1' and '2' in Figure 2(a). This energy variation behavior was observed for all the diode lasers tested.

The observed minimum in optical pulse energy variations is well defined. The fast photodetector measurements show that this minimum energy fluctuation point occurs just below the energy at which a second pulse is detectable. Therefore, we define the optical pulse energy at this minimum variation point as the maximum single pulse energy, and refer to its variation as the optical pulse energy variation.

In general, lowest energy variation was found to correlate with minimum pulse duration. Total variation in pulse energy lay in the 2-4% range for all of the lasers tested, with rms energy variation below 1% for pulses with duration < 60 ps FWHM. No correlation was observed between variation in the energy of the electronic drive pulse to the laser and variation in optical pulse energy.

We will discuss the significant increase in the optical pulse energy variation near threshold for a second relaxation oscillation. In addition, we will discuss the implications of this work on the production of gain-switched optical pulses with the lowest possible energy variation.

References

1. R. A. Elliot, H. DeXiu, R. K. DeFreez, J. M. Hunt, and P. G. Rickman, 'Picosecond optical pulse generation by impulse train current modulation of a semiconductor laser', Appl. Phys. Lett. **42**, 1012 (1983).

2. D. Bimberg, K. Ketterer, H. E. Schöll, and H. P. Vollmer, 'Generation of 4 ps light pulses from directly modulated V-groove lasers', Electron. Lett. **15**, 640 (1984).

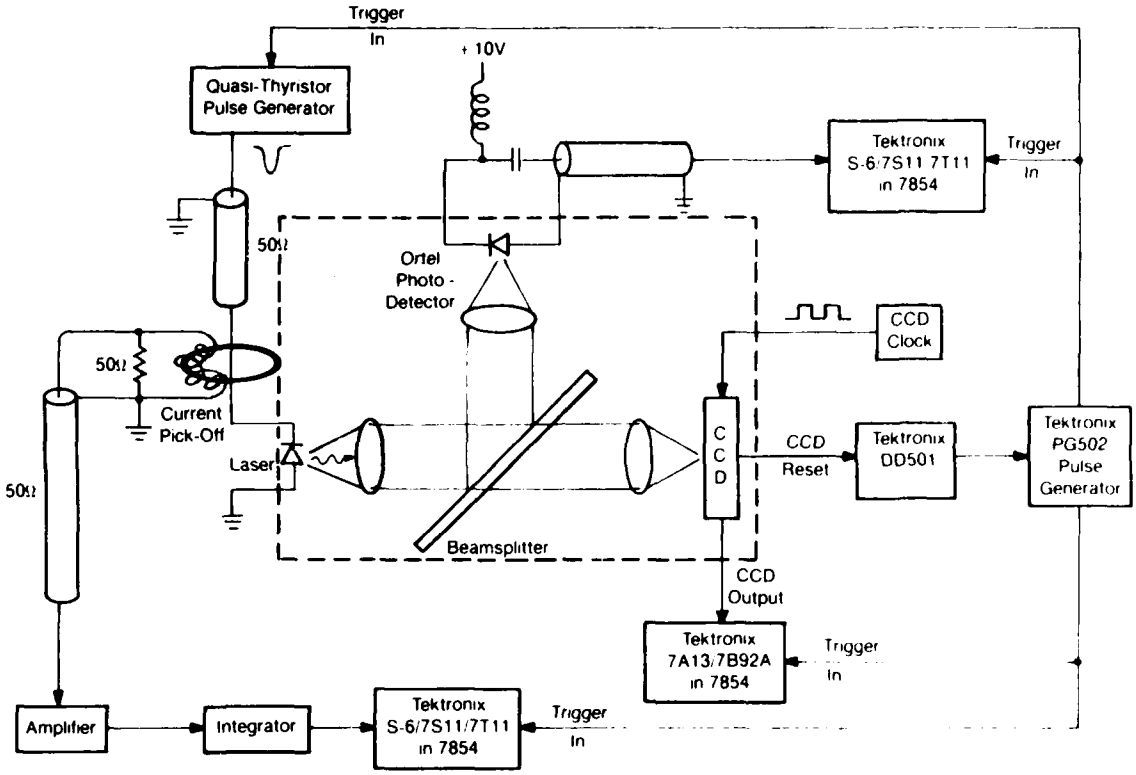

FIG. 1

FIG. 2 (a)

FIG. 2 (b)

THURSDAY, JANUARY 15, 1987

PROSPECTOR/RUBICON ROOM
8:00 A.M.–9:45 A.M.

ThA1–6

LASERS AND DETECTORS

V. Diadiuk, MIT Lincoln Laboratory, *Presider*

Characteristics, Packaging and Physics of Ultra High Speed Diode Lasers and Detectors

J. E. Bowers and C. A. Burrus
AT&T Bell Laboratories
Holmdel, New Jersey 07733

Recently high speed, high power semiconductor lasers with impulse responses of 13 ps, peak powers of tens of milliwatts, and modulation capabilities to 40 GHz have been demonstrated. These small, efficient sources are useful for fiber optic communications, microwave signal transmission for instrument, satellite and military applications, and they can serve as convenient benchtop sources for physics experiments and optical device characterization.

High speed photoconductive detectors and Schottky photodiodes with impulse responses under 5 ps have been demonstrated. More recently, high speed PIN detectors have been made for use at 1.1 to 1.6 μm and 1.8 to 2.5 μm wavelengths, regions important for optical communications using silica fibers and fluoride glass fibers, respectively. InGaAs detectors have an impulse response under 10 ps and are reasonably efficient (35 percent), making them useful in optical communications, microwave signal transmission, and the measurement of very low level (0.1 fJ) repetitive signals with ps time resolution.

Semiconductor lasers can be modulated at rates many orders of magnitude faster than other lasers because the cavity length ($10^{-4} m$) is so short, and the photon lifetime in the cavity is corresponding short ($\sim 1\ ps$). Consequently, the relaxation oscillation frequency

$$f_r = \frac{1}{2\pi\sqrt{\tau_{ph}\tau_{elec}}}$$

can be several tens of GHz for a photon lifetime (τ_{ph}) of 1 ps and an electron lifetime under lasing conditions ($\tau_{elec}^{-1} = g'S$) of 100 ps. This has resulted in modulation at rates to 8 Gb/s and 3 dB bandwidths as high as 31 GHz in cooled lasers.[1] Because of these large modulation bandwidths, mode locking at rates up to 20 GHz has been demonstrated. The pulse widths of active and passive mode locked semiconductor lasers are longer than have been achieved with other lasers. This is not because the gain bandwidth is narrow; in fact it is 500-1000 Å in quaternary lasers. Rather, it is largely due to the strong gain-phase coupling in the active layer waveguide. This phase distortion limits the minimum pulse width.

Quaternary semiconductor lasers with output powers of 200 mW have been demonstrated.[2] This power translates to a stimulated electron lifetime of 60 ps and a calculated relaxation oscillation frequency of 20 GHz, although the actual relaxation oscillation frequency may be less due to gain compression. This effect of gain compression has been inferred from damping of the intensity modulation response and from measurements of transient chirping in lasers. The same value ($\epsilon = 1.8 \times 10^{-23} m^3$ for 1.3 μm InGaAsP for a differential gain dependence on photon density of $g' = g_0(1 - \epsilon s)$) is inferred from both measurements, and recent subpicosecond measurements of carrier dynamics in GaAs have confirmed it.[4,5] However, further measurements are needed, particularly on InGaAsP material. This gain compression results in an ultimate maximum relaxation oscillation frequency, given by[3]

$$f_r = \frac{g_0}{2\pi\sqrt{2(\epsilon + g_0\tau_r)}}$$

For single longitudinal mode GaAs and InGaAsP lasers, this limit is on the order of 20 GHz (maximum 3 dB bandwidth $\sim \sqrt{1+\sqrt{2}} \times 20$ GHz = 30 GHz).

Achieving such bandwidths requires optimization of the laser structure to provide a high photon density with low parasitics, namely a low series resistance and a low parasitic capacitance due to bonding pads and current confinement. Several structures have been demonstrated with a capacitance of 3 pF or less, and these structures will be compared. It is obviously important to package the device with low parasitic connections. Coaxial *K* connector (over moded at 46 GHz) and microwave waveguide packages will be described.

GaAs Schottky diodes[6] and InGaAs p-i-n detectors[7,8] with bandwidths of 100 and 67 GHz, respectively, have been demonstrated. The main limitations to the speed are (1) the transit time across the depleted region, (2) the capacitance of the diode, (3) diffusion of carriers out of absorbing but undepleted regions and (4) charge trapping at heterojunction interfaces. The capacitance can be reduced by making detectors with small area (which, even for the highest speed detectors, is still comparable in size to the output of a single mode fiber). Diffusion current can be reduced by the use of high doping outside the depleted region or larger bandgap cladding layers (to make the undepleted region transparent). Charge trapping can be reduced by grading the heterojunctions. The transit time limitation forces the depleted layer to be thin, which causes a reduced quantum efficiency. The bandwidth efficiency product of detectors in this limit ($\alpha L \ll 1$) is

$$f_{3dB}\eta = 0.44\ \alpha\ v_s$$

where α is the absorption coefficient and v_s is the saturated carrier velocity. This limit is theoretically 40 GHz for InGaAs detectors at 1.3 μm. The measured bandwidth efficiency products for the GaAs Schottky diode and InGaAs pin described above are 5 and 27 GHz.

The bandwidth efficiency limit occurs because the light absorption and current collection directions are parallel. The use of edge absorbing or waveguide detectors, where the light propagation direction and carrier transit direction are perpendicular, allows simultaneous short transit times and long absorption lengths. We will describe such waveguide devices in InGaAsP that have high speed and high efficiency, even at zero bias, since the absorbing layer is fully depleted at zero bias.

The packaging of high speed detectors often limits the response time. Parasitic capacitance is more detrimental to detectors than to semiconnector lasers, because the impedance of a laser is only a few ohms while the effective load seen by the detector is typically 50Ω — and can be even higher in microwave waveguide circuits. We will describe coaxial K-connector mounting, microwave waveguide mounting (*K* and *U* bands) and coplanar waveguide connections

Much of this work was done in collaboration with P. M. Downey, B. R. Hemenway, W. J. Jan, R. S. Tucker and D. P. Wilt.

References

1. J. E. Bowers, Electron. Lett. *21* 1195 (1985).
2. T. Asane and T. Okumara, J. Quantum Electron. *QE-12*, 619 (1985).
3. J. E. Bowers, B. R. Hemenway, A. H. Gnauck, and D. P. Wilt, J. Quantum Electron. *QE-22*, 833 (1986).
4. M. S. Stix, M. P. Keoler, and E. P. Ippen, CLEO, paper THH5, 1986.
5. B. L. Johnson and A. Mooradian, CLEO, paper THH3, 1986.
6. S. Y. Wang and D. M. Bloom, Electron. Lett. *19*, 554 (1983).
7. J. E. Bowers, C. A. Burrus, and F. Mitschke, Electron. Lett. *22*, 633 (1986).
8. R. S. Tucker et al. Electron. Lett. *22*, (1986).

Frequency Chirping in Pulse Modulated Gain and Real Index Guided Single Quantum Well Lasers

A. Larsson and P. Andersson
Department of Electrical Measurements
Chalmers University of Technology
S-412 96 Gothenburg, Sweden

A. Yariv
Department of Applied Physics
California Institute of Technology
Pasadena, CA 91125, USA

Directly modulated semiconductor lasers exhibit a dynamic frequency shift (chirp) which limits the performance of fiber-optical systems using dispersive fibers. This chirp is due to a carrier induced change in the refractive index. Both theoretical [1] and experimental [2] investigations show that the change in refractive index of the guided mode varies linearly with the optical confinement factor. It has also been shown [3] that the time-bandwidth product (TBP), which we use as a measure of the frequency chirp, of a linearly chirped Gaussian pulse is given by

$$TBP = \Delta t \cdot \Delta f = 0.44 \sqrt{1 + \alpha_{eff}^2} \qquad (1)$$

where α_{eff} is the effective linewidth enhancement factor as seen by the propagating mode. Consequently the TBP is directly related to α_{eff}. These considerations suggest that semiconductor lasers having single quantum well (SQW) active layers would exhibit a small frequency chirp since these lasers have a small optical confinement factor and a predicted small α of the active layer [4].

In this paper we present results from an experimental investigation of the frequency chirping in pulse modulated gain and real index guided SQW lasers.

The lasers used are graded index waveguide separate confinement heterostructure single quantum well (GRIN-SCH SQW) GaAs/AlGaAs lasers. The real index guided laser is a ridge waveguide laser fabricated by us from a low threshold current density (300 A/cm^2 for a 500 μm long cavity) MBE-grown wafer with an active layer thickness of 60 Å. The gain guided laser is a commercial GRIN-SCH SQW laser (Thomson CSF, SE-1000) with a narrow stripe defined by shallow proton implantation and an active layer thickness of 100 Å. Both lasers have a 0.4 μm thick waveguide region and similar Al-mole fractions.

The TBP:s are measured using an interferometric technique [5]. The experimental setup is shown in Fig. 1. The modulation consists of short electrical pulses with a repetition frequency of 1 GHz, superimposed on a bias current around threshold. The fringe pattern from the interferometer gives the field autocorrelation function (ACF) of the radiation. From this ACF the frequency power spectrum can be obtained

by Fourier transformation. The pulsewidth is measured using second harmonic generation. Finally, the TBP is obtained by multiplying the power spectrum and the pulsewidth FWHM. As an example, we show in Fig. 2a a measured modulus of the ACF for a pulsed ridge waveguide SQW laser. The corresponding power spectrum, calculated by FFT, is shown in Fig. 2b.

In Fig. 3 we present results from the TBP-measurements for different bias and modulation conditions. Results from measurements on other lasers are also indicated for comparison [6]. Here we notice a significant difference in the chirping behavior between gain and real index guided SQW lasers. We also notice a comparably small chirp in the real index guided SQW laser. The estimated effective α-parameters using eq. (1) for the SQW lasers are 4.2 and 16 for the real index guided and the gain guided laser, respectively. The latter is the highest value yet observed for semiconductor lasers. A notable feature of the gain guided SQW laser is that for high modulation amplitudes, the total chirp exceeds the longitudinal mode spacing. Consequently, the chirp bandwidth can only be assigned a minimum value equal to the mode spacing as indicated in Fig. 3a.

Our results support the theoretically predicted laser structure dependence of α [7]. Here it was suggested that in real index guided lasers the effective α, α_{eff}, is close to the intrinsic α of the active layer, α_a. In gain guided lasers, however, α_{eff} can be substantially larger than α_a. The carrier induced change in the refractive modal index, which determines the complex propagation constant of the optical mode, is therefore larger in gain guided lasers than in real index guided lasers. We conclude that the guiding mechanism is of primary importance for designing lasers with small dynamic frequency shifts. The effect of modifying the active layer, using quantum wells (small intrinsic α), becomes apparent only when real index guiding is present.

REFERENCES

1 J.S. Manning and R. Olshansky, Electron. Lett. 17, 506, 1981.

2 N.K. Dutta, N.A. Olsson, and W.T. Tsang, Appl. Phys. Lett. 45, 836, 1984.

3 T.L. Koch and J.E. Bowers, Electron. Lett. 20, 1038, 1984.

4 Y. Arakawa and A. Yariv, IEEE J. Quantum Electron. QE-21, 1666, 1985.

5 P. Andersson, T. Andersson, S. Lundqvist, and S.T. Eng, J. Lightwave Tech. LT-2, 146, 1984.

6 P. Andersson and T. Andersson, to be published in J. Lightwave Techn. July 1986.

7 K. Furuya, Electron. Lett. 21, 200, 1985.

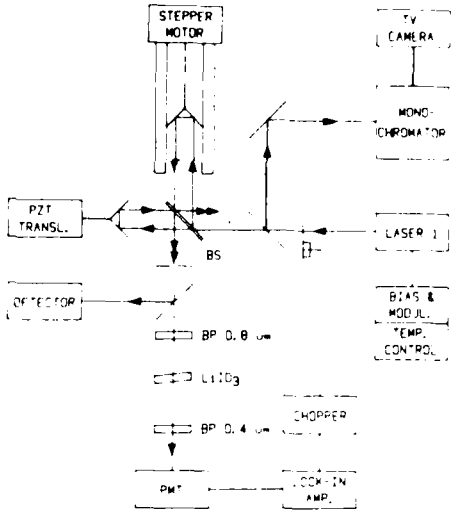

Fig. 1 Experimental setup for temporal coherence measurements

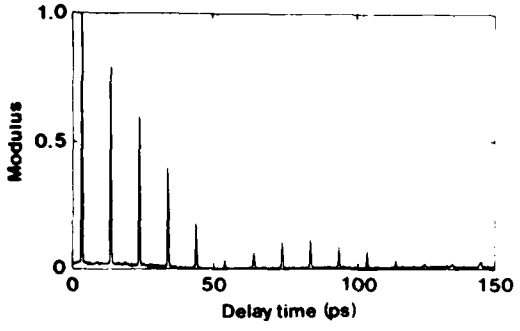

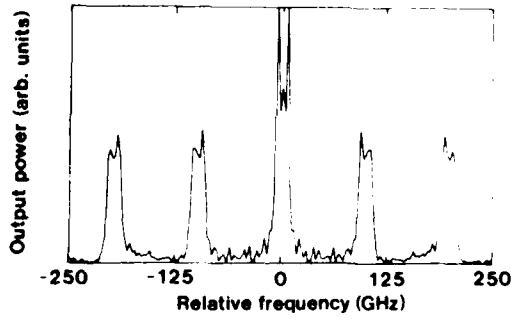

Fig. 2 (a) Measured modulus of the ACF for a pulsed ridge waveguide SQW laser
(b) Power spectrum calculated from Fig. 2a

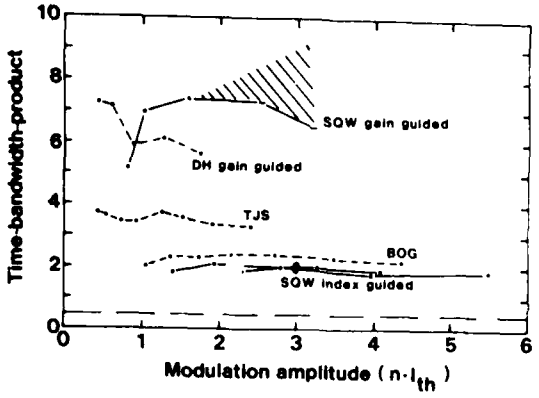

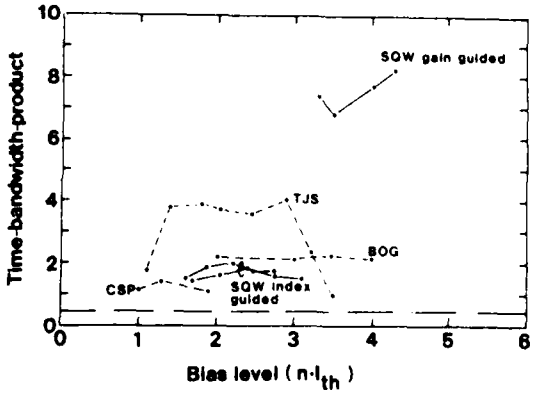

Fig. 3 Results from TBP measurements as a function of (a) modulation amplitude and (b) bias level. The transform limited value of the TBP for a Gaussian pulse (0.44) is also indicated

InP/GaInAs/InP PIN Photodiode with FWHM < 18 ps

S.Y. Wang, K.W. Carey and B.H. Kolner
Hewlett-Packard Laboratories, 1651 Page Mill Road
Palo Alto, Ca. 94304

Introduction:

High speed optical detectors in the 1.3-1.55 μm wavelength range are required for a new generation of microwave-optical instruments to characterize high data rate systems, microwave transmission via lightwave, and other applications requiring true replication of the modulation signal. Front-side illuminated photodiodes have an advantage over back-side illuminated devices in simplicity of packaging. In addition, the transit time of the photocarriers is determined by electrons rather than by holes as for backside illuminated devices fabricated on n-type substrates. The speed of response of the double heterostructure photodiode is wavelength independent since photocarriers can only be generated in the i-layer which is fully depleted. For single heterostructure backside illuminated photodiodes with p-GaInAs, the speed response degrades as the wavelength increases since photocarriers can be generated in the low field p-layer resulting in carrier diffussion . For high speed operation of the device, the i-layer thickness is selected such that the device is transit time limited and is of the order of one absorption length. However one potential obstacle exists that could degrade the speed of a front-side illuminated device, and that is the trapping of holes at the discontinuity in the valance band between the InP and GaInAs. The effect of hole trapping was not evident in the results of Susa et al[1] which utilized a separate absorption and multiplication (SAM) structure for a front-side illuminated avalanche photodiode. This suggests that the quality of interface could play a dominant role in the transit time at heterojunction interfaces.

Structure:

The photodiode is a $P - i - N$ mesa structure whose cross-section is shown in Figure 1. On an N^+ (100) S-doped InP substrate, an undoped GaInAs lattice matched layer 1.5 μm thick and then a Zn doped InP window layer 1.0 μm thick are grown by organometallic vapor phase epitaxy (OMVPE). The photosensitive area is circular in geometry with a diameter of 25 μm in contact with a 25 μm bond pad. The p-contact metallization is Ti-Au on the front surface and the n-contact is NiCr-Ge-Au/Ti-Au on the back surface. SiO_x was used as an antireflection film. The mesa edges were left unpassivated. The operating voltages for our devices were less than 4 volts reverse bias. Dark current density was $< 10^{-5}$ A cm^{-2} at -4 V.

Growth technique:

The epitaxial layers were grown using OMVPE at atmospheric pressure in a horizontal reactor. Trimethylgallium (TMGa) and trimethylindium (TMIn) were the sources for the group III elements, 10% AsH3 in hydrogen was used as the As source and 10% PH3 in hydrogen as the P source. The p-type dopant source was diethylzinc (DEZn) and the carrier gas was hydrogen. The growth rates for GaInAs and InP were 1.5 μm/h and 0.8 μm/h, respectively.. Other details of the growth of atmospheric pressure OMVPE $Ga_{0.47}In_{0.53}As$ can be found in publictions by Carey [2] and Kuo et al[3]. The carrier concentration in P-InP is approximately $1 \cdot 10^{18}$cm^{-3}, and the n-GaInAs was nominally undoped with residual carrier concentrations of $< 4 \cdot 10^{15}$cm^{-3}. Using high resolution transmission electron microscopy the InP(substrate)/GaInAs transition is determined to be about two monolayers (5.8 angstroms) and the transition from GaInAs/InP is found to be about 5 monolayers

(< 15 angstroms)

High-Speed Measurement Technique and Results:
A pulsed diode laser was used to excite the photodiode whose transient response was measured on a sampling oscilloscope.
A 1.3 μm diode laser (Hitachi HLP5400) driven by a step recovery diode at 100 MHz was used as the optical impulse source. The laser pulses were passed through a low pass filter to eliminate internally generated second harmonic radiation and were attenuated to less than 15 microwatts average power before illuminating the photodiode. The photodiode output was connected to a Tektronix S-4 sampling head via a short microwave cable (Gortex) for the time domain analysis. The measured temporal response is shown in Figure 2 where the pulse width at full width half maximum is 29 ps. The impulse response of the S-4 sampling head is 23 ps ; using Gaussian approximation a combined photodiode and laser pulse width of 17.7 ps is calculated. The photodiode response is therefore < 17.7 ps or correspondingly > 18 GHz.

Discussion:
We have developed front-side illuminated double heterostructure P-i-N mesa InP/GaInAs/InP photodiodes with bandwidth in excess of 18 GHz or a FHWM of less than 18 ps at 1.3 μm wavelength. The device has an external quantum efficiency of greater than 85% and a dark current density of $6 \cdot 10^{-6}$ A cm^{-2} at the operating bias of -4 volts. The bandwidth predicted for our device with the given geometries is 20 GHz taking into account only the RC time and transit time which agrees well with our observation. The measured fall time of the photodiode is 31 ps, the slight hump at the trailing edge Figure 2, may be due to ringing in the laser, reflection, carrier diffusion due to dopant redistribution, or hole trapping. This is under further investigation.

References:

[1] N. Susa, H. Nakagome, O. Mikami, H. Ando and H. Kanbe, "New InGaAs/InP Avalanche Photodiode Structure for the 1-1.6 um Wavelength Region", IEEE J. Quantum Electron.,vol. QE-16(8),pp.864-870,1980

[2] K.W. Carey, "Organometallic vapor phase epitaxial growth and characterization of high purity GaInAs on InP", Appl.Phys. Lett., vol.46(1),pp.89-91,1985

[3] C.P. Kuo, J.S. Yuan, R.M. Cohen, J. Dunn and G.B. Stringfellow, "Organometallic vapor phase epitaxial growth of high purity GaInAs using Trimethylindium", ibid,vol.44,pp.550-552,1984

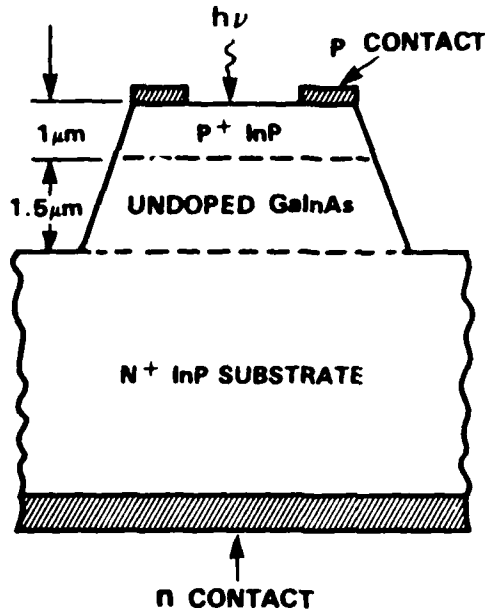

Figure 1:
Layer structure of the InP/GaInAs/InP front-side illuminated photodiode; the absorbing layer GaInAs is 1.5 μm thick, and the window layer P-InP is 1 μm thick. 1000 A SiO_x was used as antireflection. Photosensitive area is 25 μm in diameter in contact with a 25 μm diameter bondpad.

FWHM = 29 ps, 20 ps/DIV, 20 mV/DIV

Figure 2:
Transient time response of the photodiode to 1.3 μm diode laser pulse showing a *full width* at half maximum of 29 ps and a fall time of 31 ps. The impulse response of the sampling head is 23ps. Using a Gaussian approximation a combined photodiode and laser pulse width of 18 ps is calculated.

Picosecond measurements of gain-switching in a semiconductor laser driven by ultrashort electrical pulses

P. M. Downey, J. E. Bowers, R. S. Tucker and J. M. Wiesenfeld
AT&T Bell Laboratories, Holmdel, NJ 07733

We report on the temporal profile of optical pulses emitted by a semiconductor laser when driven by 17 ps electrical pulses. These optical pulses are detected with subpicosecond resolution by optical up-conversion sampling[1,2]. The short duration of our electrical pulses distinguishes this work from previously published reports on gain- switching experiments. The short electrical pulses enable us to operate in a regime where the optical pulse widths are limited only by the laser, even when it is biased at threshold. We have investigated how the risetime, falltime, FWHM, amplitude and delay time of the gain-switched pulses vary with the semiconductor laser's operating conditions (e.g. dc bias current, the width and amplitude of the driving pulse, and temperature).

A schematic of the experimental configuration is shown in Fig. 1. The timing for the experiment is established with a CPM ring dye laser which produces a synchronous pair of beams of 0.3 ps pulses at a wavelength of 0.625 μm and a pulse repetition rate of 120 MHz. One of the CPM beams is used to trigger the photoconductor circuit which drives the semiconductor laser. The second CPM beam, which can be delayed with respect to the first, is mixed with the output of the 1.3 μm InGaAsP laser by sum-frequency generation in a $LiIO_3$ crystal. The temporal profile of the gain-switched pulses is obtained by monitoring the resulting 0.42 μm light intensity vs. the time delay between the CPM beams.

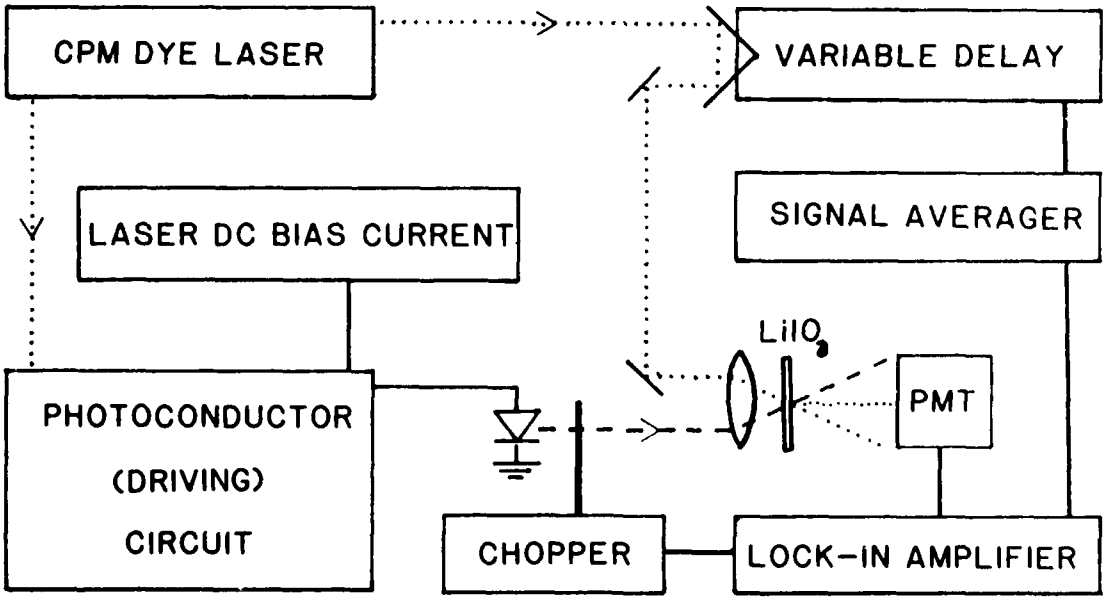

Figure 1. Schematic diagram of the experimental configuration for measuring gain-switched pulses.

The semiconductor laser used was an InGaAsP constricted-mesa laser[3] chosen for its low capacitance (1 pF), low inductance (.2 nH), short cavity length (110 μm) and high resonance frequency (9 GHz at 20 ^{O}C). It is mounted on a cooled copper block containing a Wiltron-K-connector. The driving circuit consists of a dc biased, radiation-damaged InP photoconductor[4] mounted between the center conductors of a Wiltron coaxial cable. A cross-correlation measurement of the output electrical pulse of this circuit sampled by a second picosecond InP photoconductor is shown in Fig. 2, and is characterized by a FWHM of 17 ps. The duration of this circuit's output pulse is limited by the diameter (and hence the bandwidth) of the coaxial cable; the photoconductors respond several times faster when tested with smaller coax. The charge contained in this driving pulse can be deduced from sampling oscilloscope measurements which indicate 3.0 volt pulses with a FWHM of $\approx 50ps$. The waveform of Fig. 2, then, would appear as a 9 volt pulse to a high speed, 50Ω load. A low frequency lead is also connected to the output of the driving circuit, allowing us to independently adjust the amplitudes of the driving pulse and dc bias current through the laser.

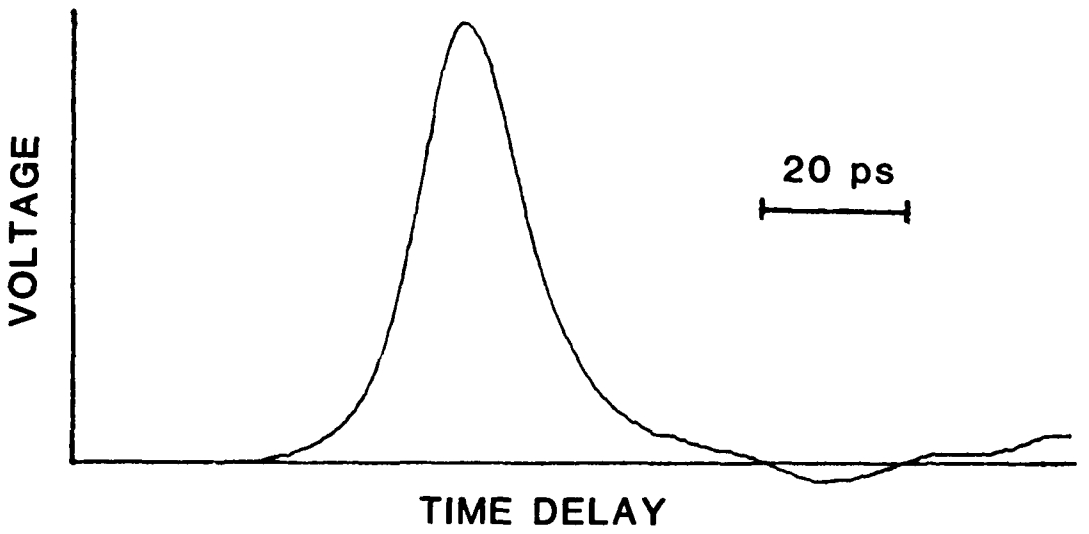

Figure 2. The temporal profile of the electrical pulse used to drive the laser.

A representative set of gain-switched pulse profiles observed for a range of dc bias levels (both above and below threshold) is shown in Fig. 3. Like all the gain-switched pulses which we have observed to date, the profiles are asymmetric, with the 10-90% falltime typically being 1.5-2 times longer than the 10-90% risetime. The injected carrier density is so large near threshold that risetimes as short as 10 ps are realized. For a given drive pulse there is an optimum dc bias level for which the FWHM is minimized; a minimum pulsewidth of 15 ps was observed for the data set of Fig. 3, at a bias current of 28 mA (the laser's cw threshold current). When the laser is biased below this current level the laser pulse amplitude decreases linearly with dc bias, while the pulses broaden and are emitted at progressively longer delay times. As the dc bias is increased above the threshold current we see a transition from this characteristic gain-switching behavior. A few mA above the threshold current the optical pulses become very insensitive to the dc bias level; the pulse amplitude decreases by 10%, the FWHM increases by one ps, and the delay time stays fixed as the bias current is increased from 32 to 35 mA. For all bias currents studied, the gain-switched pulses are limited by the dynamics of the semiconductor laser and are insensitive to the shape of the drive pulse.

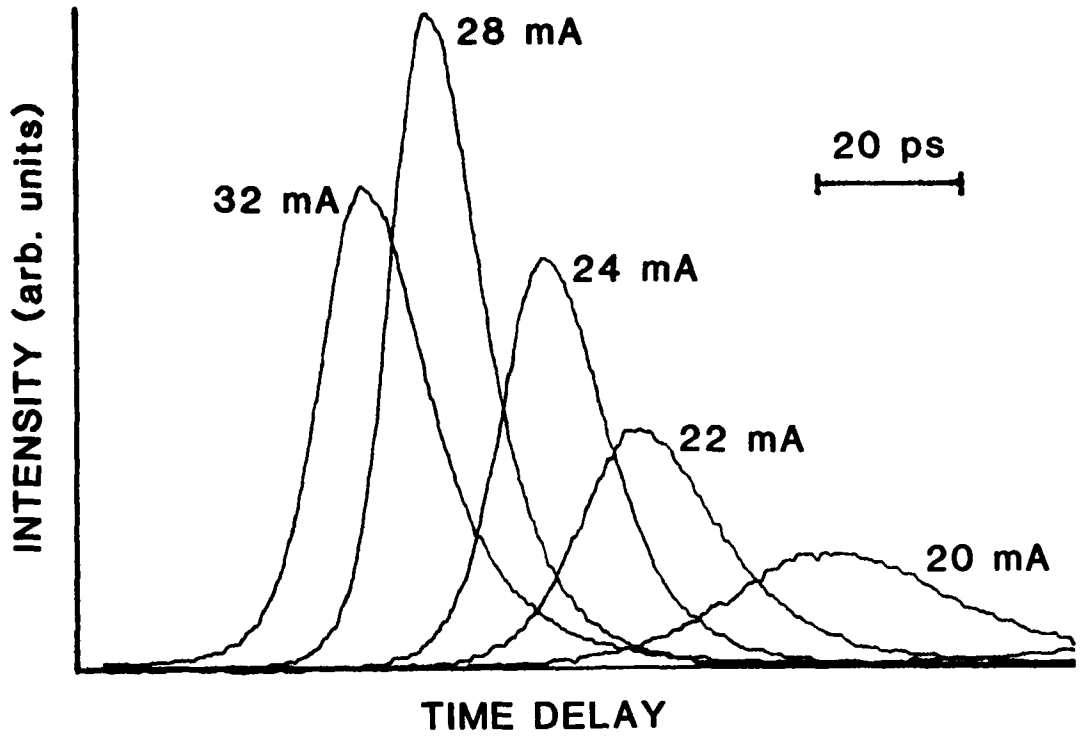

Figure 3. Temporal profiles of the optical pulses from the laser diode operated at 16 °C and driven by 360 mA, 17 ps electrical pulses. The curves are labeled with the dc bias level.

Our drive pulses are sufficiently short that their effect on the laser is approximately a step increment in the injected carrier density N. Depending on the dc bias level, the photon population increases due to spontaneous and/or stimulated emission; this explains the striking dependence of pulse arrival time on bias below threshold. The risetime on the leading edge of the pulse is inversely proportional to the difference between the rate of stimulated emission (which is proportional to N) and the loss rate. During the trailing edge of the optical pulse, however, this difference is smaller and of opposite sign so the falltime is correspondingly slower. This qualitative picture explains the asymmetry of the gain-switched pulses, as well as the dramatic improvement in temporal response (below threshold) with increasing bias current. Above threshold, stimulated emission immediately diminishes the step increment in the injected carrier density so the width of the gain-switched pulse slowly increases and the amplitude decreases with increasing bias current. Computer simulations of the gain-switched laser show general agreement with the experimental data.

REFERENCES

[1] M. A. Duguay and T. C. Damen, "Picosecond Measurement of Spontaneous and Stimulated Emission From Injection Lasers", Appl. Phys. Lett., vol 40, pp. 667-669, 1982.

[2] J. M. Wiesenfeld, R. S. Tucker, P. M. Downey and J. E. Bowers, "Optical Correlation Measurement of Switching Transients in High-Speed Semiconductor Lasers", Electron. Lett., vol. 22, pp. 396-397, 1986.

[3] J. E. Bowers, B. R. Hemenway, A. H. Gnauck, and D. P. Wilt, "High-Speed InGaAsP Constricted-Mesa Lasers", IEEE J. Quantum Electron., vol. QE-22, pp. 833 844, 1986

[4] P. M. Downey and B. Tell, "Picosecond Photoconductivity Studies of Light Ion Bombarded InP", J. Appl. Phys., vol. 56, pp. 2672-2674, 1984.

MESFET Compatible IMSM Detectors

D. L. Rogers

IBM T.J. Watson Research Center
P.O. Box 218
Yorktown Heights, NY 10598

Introduction

One of the challenges in using high speed fiber optic links in computer communications is the recovery of the low level, high speed, electrical signals generated in the photodiode. Not only is high frequency, low noise amplification needed but a very small coupling loop between the detector and amplifier is required to reduce the noise coupled inductively from nearby circuits. Indeed, as the data rate goes up this noise increases as the square of the frequency.

The monolithic integration of the photo-detector with it's companion amplification circuits on the same GaAs chip can greatly reduce these problems creating microscopic coupling loops. The interdigitated Metal-Semiconductor-Metal detector [1] (IMSM) is an attractive candidate for use in such integration due to it's potential compatibility with most GaAs circuit processes and it's potential high performance [2]. Indeed previous workers have demonstrated that high performance detectors of this type can be fabricated on high purity epitaxial buffer layers along with MESFET preamplifiers [3] but only with the use of a relatively low temperature, non-self-aligned MESFET process. On the other hand, detectors fabricated directly on semi-insulating substrates using a high temperature, self-aligned process have suffered from an undesirable low frequency gain [4] that would require subsequent equalization for use in any data transmission system. In this paper we demonstrate the large dark currents and low frequency gain can be greatly reduced using a shallow implant under the active area of the detector.

Theory

A number of mechanisms have been offered to explain the gain observed in the IMSM detector. These are typically based on a photo-induced carrier injection of either electrons at the cathode or holes at the anode . Since at first sight the intrinsic nature of the substrate would appear to preclude a sufficient charging of the substrate to account for the fields needed to induce tunneling, several mechanism have been proposed to account for an accumulation of charge. We have found however that such large fields can be generated simply due to the charging of a low density of traps by the photo-generated carriers without resort to such mechanisms.

We have calcuated the charging of the substrate due to trap charging and have found the charging sufficient to substantually alter the tunneling barrier seen by the electrons and holes. Assuming the photo-generated carriers are trapped at a rate determined by the experimentally observed cross-section for the EL2 trap and assuming that the detrapping time is determined thermal excitation and recombination with other holes and electrons we have calculated the trap charging due to the carriers generated by an incident radiation field. In order to do this calculation the situation in the gap between the fingers of the detector was approximated by the gap between two semi-infinite conducting planes and the potential and Greens function for this simpler geometry were calculated using a conformal mapping. Transforming to the coordinate system defined by these conformal mappings it was possible to reduce the continuity equations to one dimension enabling their solution. Figure 1 shows the induced charge density for an incident radiation flux of 0.005 W/cm^2 , and a trap density of $1x10^{15}cm^{-3}$ which are conditions in which gain has been observed in these detectors. Figure 2 shows the potential calculated using this charge density for several different radiation fluxes along a line parallel to the surface of the semiconductor. Notice

that the tunneling length at 0.1 eV below the top of the barrier is reduced by a factor of 2 thus confirming that the trap charging alone can give rise to a modulation of the tunneling barrier.

The degree of substrate charging and band bending illustrated in these calculations would not be possible in the more conventional type of detector in which the junctions are parallel to the surface. The large amount of tunneling in the IMSM detector is due not only to the large electric fields near the electrode edges but also to the fact tha t the crowding of field lines at these points increases the carrier density and thus the trap charging where it has the most effect on the tunneling barrier.

Although the bulk trap density can be kept quite low by using high purity substrates and epitaxial layers, the carriers still suffer the possibility of being trapped at the surface where, especially in GaAs, there is a large density of surface states. Whether the photo-induced carriers will be trapped there depends of the details of the electric field in the direction perpendicular to the surface. One way to prevent the attraction of the photo-generated carriers to the surface is to create a thin *n* doped layer at the surface of the semiconductor with the doping density and thickness chosen such that the semiconductor remains depleted. As shown in Figure 3, which shows the effect of such a layer on the band structure perpendicular to the surface, the electrons will be repelled from the surface in the doped region. On the other hand although the holes will be attracted to the surface in this region they will be repelled from the surface deeper within the substrate. If the doped layer is kept very thin compared to the absorption depth of the radiation not only the electrons but all but a small fraction of the photo-induced holes will be also repelled from the surface. In what follows we will present results on detectors fabricated in this manner.

Fabrication and Design

The photodetectors described below were fabricated on semi-insulating GaAs substrates using the same process that we use to fabricate enhance/deplete MESFET circuits[5]. The regions under the implanted detectors was first implanted with 100 KeV SiF ions with a dose of $1.3 \times 10^{12} cm^{-3}$ and annealed at 850°C for 20 minutes. The surface was then sputter etch cleaned and approximately 2000 Angstroms of $WSi_{0.11}$ was then deposited and delineated using a subtractive reactive ion etch. Subsequent to these steps the detectors were further subjected to a 800°C anneal for 10 minutes to activate the contact implants used in the IC process. Detectors were fabricated adjacent to each other on the substrate both with and without the implant. The detectors described below have 1 micron finger widths with a 2.25 micron space between fingers. The detectors were square and 100 microns on a side.

Results

The photodiodes were characterized using a probe station equipped with a fiber optic probe. The dark current for the detectors was measured at 7 locations on a 2 inch wafer. The dark currents were 88 na. with a standard deviation of 40 na. for the un-implanted detectors and 11 na. with a standard deviation of 7 na. for the implanted detectors. Figure 4 shows IV curves under illumination for typical implanted and un-implanted detectors. The optical power incident on the detector is 140 microwatts and the horizontal line labeled I_0 in this figure represents the ideal photocurrent coresponding to an internal quantum efficiency of one, taking into account the light masked by the metal fingers and the reflection coeficient at the GaAs-air interface. Clearly the implanted detectors are demonstrate an internal quantum efficiency very close to one and only begin to show low frequency gain at bias voltages above 7 volts. On the other hand the un-implanted detector shows large amounts of gain above about 1.5 volts.

Conclusion

We have shown that a simple trap induced tunneling mechanism can account for the gain observed in IMSM detectors and demonstrated that a shallow implanted region can be used to greatly reduce these effects.

Acknowledgements

The author would like to thank J.H. Magerlein, D.J. Webb, A Callegari, T. Fryxell, H.C. Guthrie, Peter D. Hoh, J.W. Mitchell, A. Pomerene, S. Scontras and G. Spiers for the fabrication of this chip. . . .

T Sugeta, T Urisu, S Sakata and Y Mizushima, "Metal-Semiconductor Metal Photodetector for High-Speed Optoelectronic Circuit", Jap Jour Appl Phys, V19, Suppl 19-1, 1980, p459-464

W Roth,H S.humacher,J Kluge,H Geelen, and H Beneking,"The DSI Diode - A Fast Large-Area Optoelectronic Detector", IEEE Trans Elect Dev v ED-32,n6,1985,p1034

M Makiuchi, H Hamaguchi, T Kumai, M Ito, O Wada, "A Monolithic Four-Channel Photoreceiver Integrated on a GaAs Substrate Using Metal-Semiconductor-Metal Photodiodes and FET's", Elect Dev Lett, v EDL-6, n12, 1985, pp634-635

W S Lee, G R Adams, J Mun, J Smith, "Monolithic GaAs Photoreceiver for High-Speed Signal Processing Applications", Elect Letts, v 22, no 3, 1986, pp147-148

D J Webb, J H Magerlein, A Callegari, J D Feder, T Fryxell, H C Guthrie, Peter D Hoh, J W Mitchell, A J S Pomerene, S Scontras, Guy D Spiers and J H Greiner, "Characterisation of GaAs Self-aligned Refractory-gate Mesfet Integrated Circuits", Jour appl phys, submitted

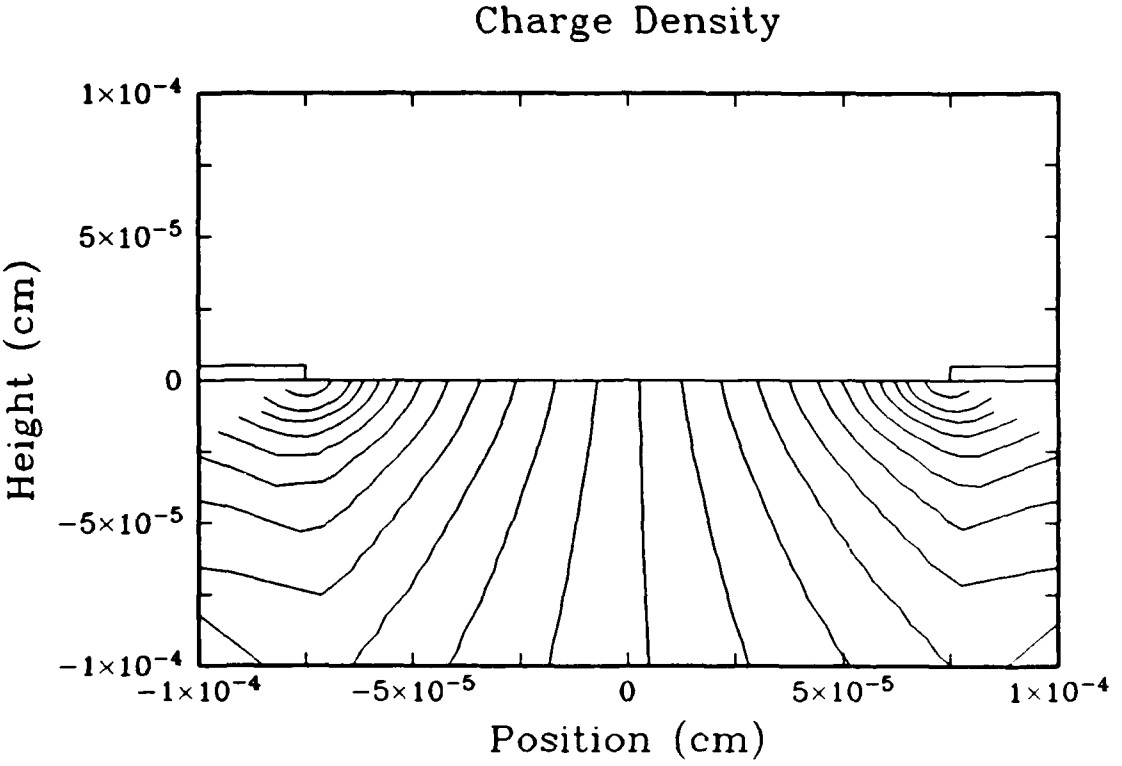
Charge Density
Height (cm)
1×10⁻⁴
5×10⁻⁵
0
−5×10⁻⁵
−1×10⁻⁴
−1×10⁻⁴
−5×10⁻⁵
0
5×10⁻⁵
1×10⁻⁴
Position (cm)

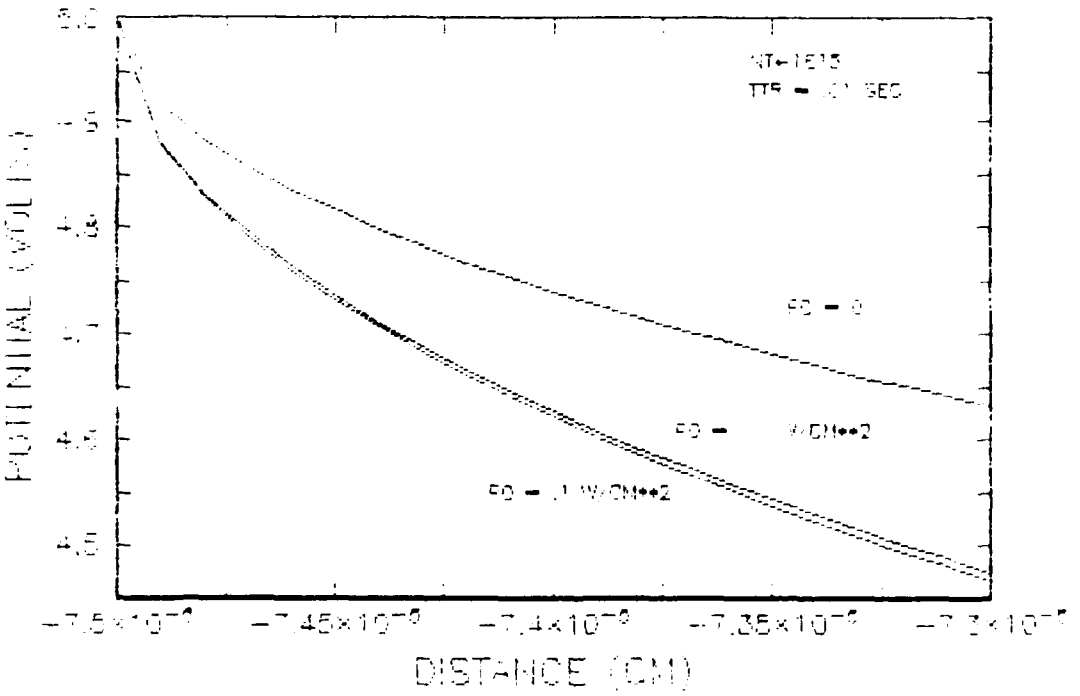
DISTANCE (CM)

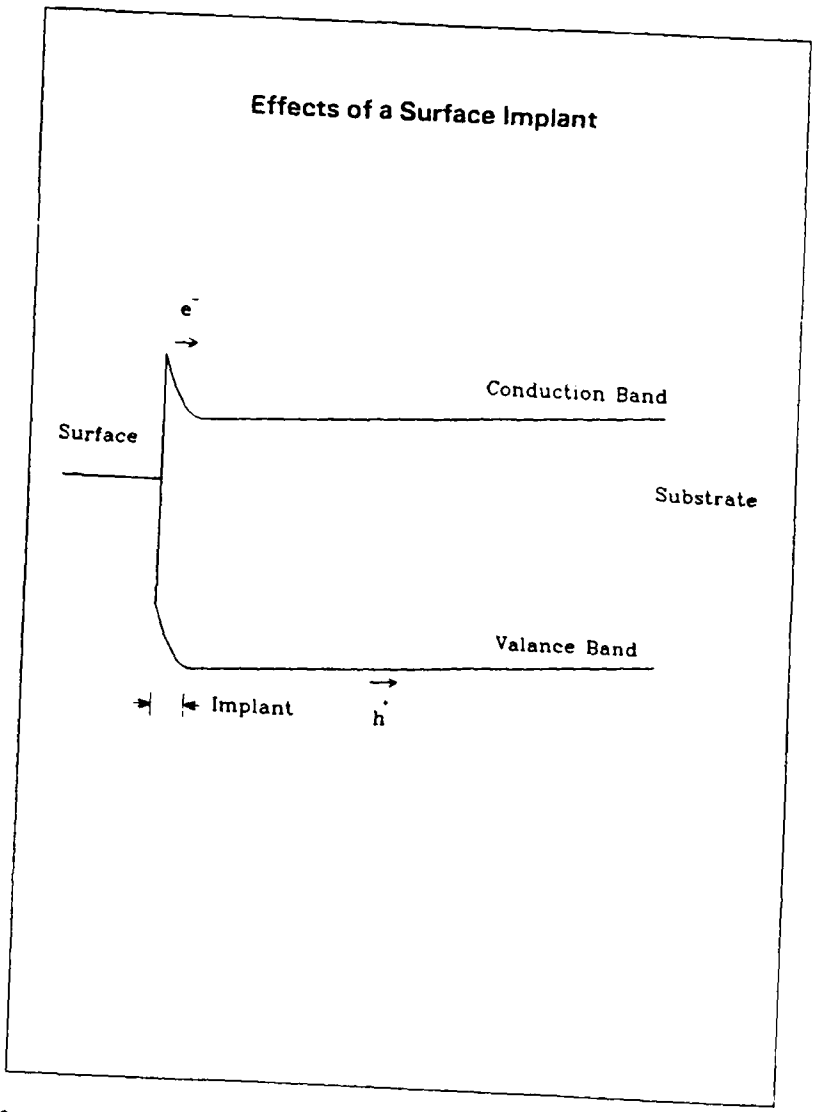
Effects of a Surface Implant
e⁻
Conduction Band
Surface
Substrate
Valance Band
Implant
h⁺

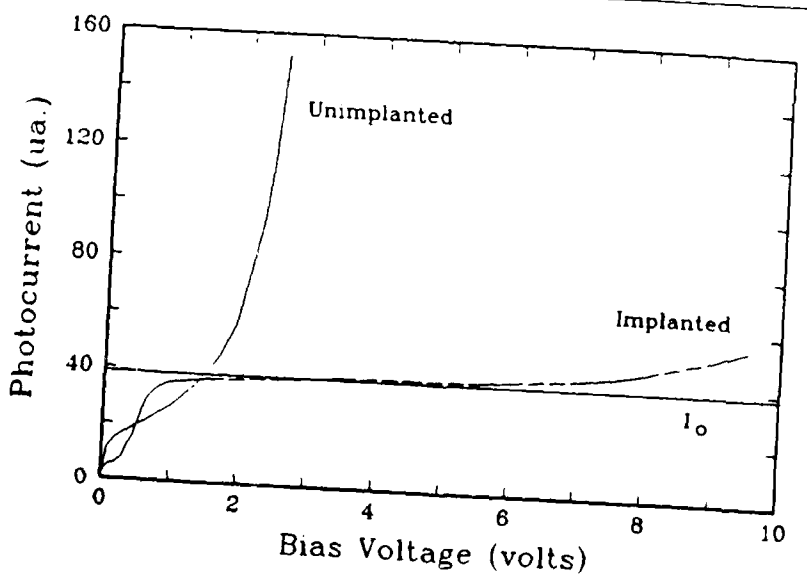
160
120
80
40
0
Photocurrent (ua.)
Unimplanted
Implanted
I_o
0
2
4
6
8
10
Bias Voltage (volts)

PICOSECOND OPTICAL AUTOCORRELATION EXPERIMENTS ON FAST PHOTODETECTORS

T. F. Carruthers and J. F. Weller
Naval Research Laboratory
Washington, D. C. 20375-5000

The nonlinear component of the photoresponse of many optoelectronic devices can be used to determine their response speeds. The technique is of value because measurements are performed upon a single device rather than upon two interconnected devices. Transmission line problems, including bandwidth limitations and spurious signals due to reflections and radiated transients, are therefore avoided, and intrinsic response time measurements are possible on devices that cannot be paired with a high-speed photodetector in a large-bandwidth circuit.

An experiment consists of delaying one beam of picosecond optical pulses a time τ with respect to another and chopping the two beams at different frequencies f_1 and f_2; the beams are focused onto the device being studied, and the nonlinear component of the devices's electrical response at f_1+f_2 is detected. The magnitude of this response varies with the interval τ between the pulses, ranging from a maximum mutual effect for $\tau=0$ to no effect for pulses widely separated in time. In the simplest experimental cases such a measurement yields directly the autocorrelation function of the time response of the device. If the output of a photodetector is assumed to depend on the instantaneous number N(t) of photogenerated carriers, the detected signal $O(\tau)$ at f_1+f_2 has been shown to be

$$O(\tau) \approx \frac{d^2I/dN^2}{(dI/dN)^2} \int_{-\infty}^{\infty} dt\ I_1(t)\ I_2(t+\tau) \qquad (1)$$

to lowest order, where I_1 and I_2 are the signals generated by the two pulse trains. dI/dN and d^2I/dN^2 are coefficients in the Taylor expansion of I(N) and are assumed to contribute no time dependence of their own. A response faster than 2.5 ps has been measured in this manner for a high-speed photodiode [1,2].

Figure 1 compares the two-gap cross correlation and single gap nonlinear autocorrelation responses of a planar photoconductive correlation circuit consisting of gaps in microstrip lines on an ion-bombarded InP substrate; the circuit configurations are sketched in the insets in the figure. The response speeds of about 20 ps measured with the two techniques are essentially equal. The two-gap measurement exhibits a peak at a relative time delay of 70 ps due to the reflection of the initial transient from the end of the microstrip line; the reflected signal is not visible in the single-gap experiment. A slowly varying background is observed with all planar photoconductors and is tentatively attributed to the trapping of charge in the semiconductor.

Similar experiments were performed on a higher speed ion-bombarded InP correlation circuit; the results of a single-gap measurement are presented in Fig. 2. This device has been demonstrated to possess a subpicosecond free carrier lifetime, but its signal in a two-gap cross-correlation measurement is broadened by circuit capacitance and is obscured by reflections of and

electromagnetic radiation from the initial transient[3].

The measured FWHM of 8.0 ps is slower than the known device speed, but the trace is completely free of spurious signals and exhibits an excellent signal-to-noise ratio. The reason for the broadening of the autocorrelation signal is not immediately apparent, since faster responses have been observed in other systems.

The single gap measurements are free from spurious signals simply because the bias across the gap is much greater than any reflected or radiated transient. In the two-gap sampling process the unbiased second gap samples the propagating pulse transient generated by the first gap; the spurious signals can easily be of the same order of magnitude as the initial transient.

Deviations from the simple behavior described by Eq. (1) have been observed in more complicated physical systems. Figure 3 presents the nonlinear response of a nominally 20 GHz GaAs epitaxially grown Schottky-barrier photodiode[4] at a series of incident optical energies W_{opt}; the scale of the vertical axis increases proportionately with W_{opt}. The central peak corresponds to a mutually attenuating effect of the pulses upon one another and is attributed to a lower charge collection efficiency due to decreased fields in the active region of the device. A delayed change in sign, indicating that an optical pulse eventually enhances the device's response to a subsequent pulse, increases strongly with the number of injected carriers. We now attribute this phenomenon to the storage of minority carriers in the diode's epilayer[5] and a consequent time-dependent change in the operating characteristics of the device.

The authors are indebted to P. M. Downey for providing the subpicosecond InP autocorrelator circuit. The GaAs photodiode is on loan to us from Hewlett-Packard Laboratories.

1. T. F. Carruthers and J. F. Weller, Appl. Phys. Lett. 48, 460 (1986).
2. T. F. Carruthers and J. F. Weller, in Ultrafast Phenomena V (Springer-Verlag, New York, 1986), to be published.
3. J. R. Karin, P. M. Downey, and R. J. Martin, IEEE J. Quantum Electron. QE-22, 677 (1986).
4. S. Y. Wang and D. M. Bloom, Electron. Lett. 19, 554 (1983).
5. D. L. Scharfetter, Solid-State Electron. 8, 299 (1965).

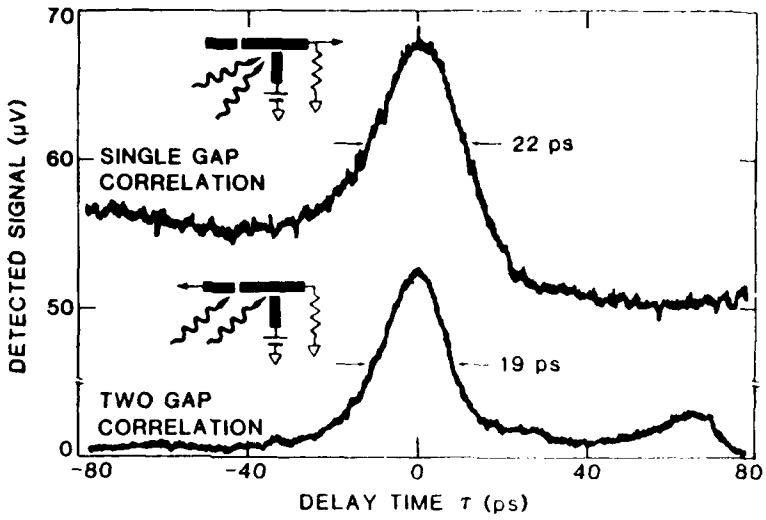

Figure 1. Comparison of two-gap and single gap correlation techniques on an InP correlation circuit.

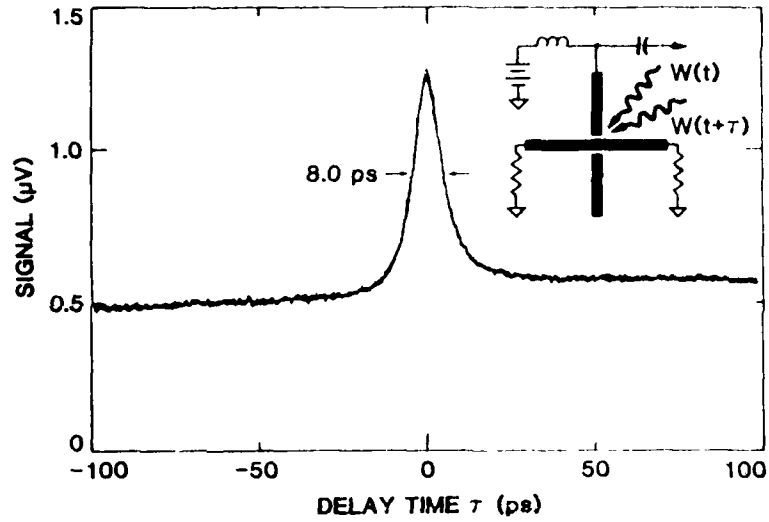

Figure 2. Single gap nonlinear correlation measurement on a subpicosecond InP microstrip photoconductor.

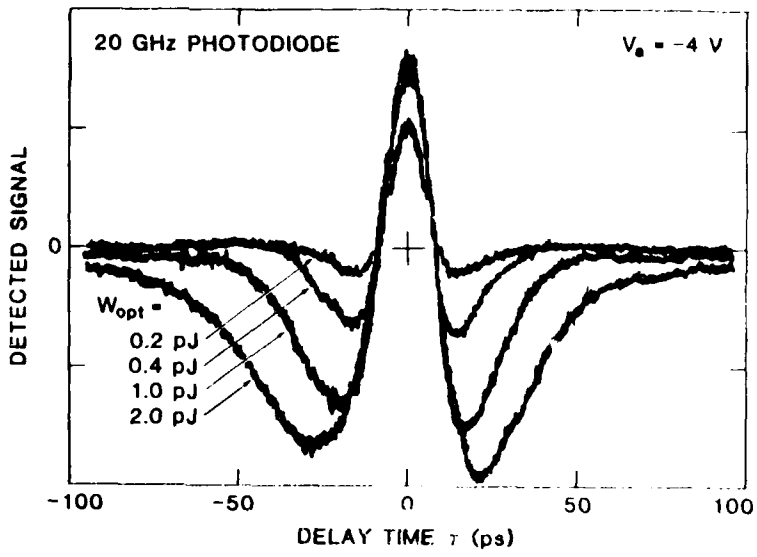

Figure 3. The nonlinear response of a 20 GHz Schottky-barrier GaAs photodiode at several incident optical energies W_{opt}.

THURSDAY, JANUARY 15, 1987

PROSPECTOR/RUBICON ROOM
10:15 A.M.–12:00 M

ThB1–5

TRANSIENT TRANSPORT

J. Frey, Cornell University, *Presider*

Direct Subpicosecond Measurement of Carrier Mobility of Photoexcited Electrons in GaAs

M.C. Nuss and D.H. Auston
AT&T Bell Laboratories, 600 Mountain Avenue, Murray Hill, NJ 07974

The dynamics of hot photoexcited or injected carriers in semiconductors has been studied extensively with picosecond and femtosecond optical pulses[1]. On a subpicosecond time scale, both absorption saturation[2] and photoluminescence techniques[3] were employed to trace the relaxation of the initial nonequilibrium distribution of carriers after their injection. These techniques have in common, that they probe the carrier distribution in the bands, but not the actual time dependent transport properties like mobility or drift velocity. These in turn are the important parameters for high speed devices like hot electron transistors. On the other hand, electron transport in semiconductors has been investigated by microwave conductivity measurements and microwave time-of-flight techniques. However, the time resolution of the existing microwave sources is not high enough to observe transient transport phenomena on a picosecond or even femtosecond time scale.

We have developed a technique using both femtosecond optical and electrical pulses to study the transport parameters of photoinjected carriers in GaAs. The technique can be regarded as an extension of the microwave conductivity method into the subpicosecond time domain, but now, carriers can be injected in synchronism with the electrical probing pulse and hot carrier relaxation and transport phenomena can be studied with subpicosecond time resolution. The measurement technique is non-contacting and does not require electrodes on the sample. Thus, for the first time, we can measure the conductivity of a hot electron gas for the first few picoseconds after carrier injection.

Our technique uses femtosecond electrical pulses generated by optical rectification of femtosecond laser pulses in the electro-optic crystal $LiTaO_3$. These pulses consist of only a single cycle of radiation with a duration of as low as 300 fsec and a spectrum that peaks in the far-infrared range of the electromagnetic spectrum ($\sim$ 1 THz)[4]. A schematic of the experimental setup is depicted in Fig.1. Two femtosecond laser beams ($\lambda = 625$nm) out of a colliding pulse modelocking laser which have been amplified by a copper vapor laser amplifier are focussed to a 10 μm spot size into the 200 μm thick crystal, separated by 20 μm. The first beam is used to create the femtosecond electrical pulse. The electromagnetic transient evolves in form of a Cherenkov shock wave from the propagating ultrashort optical pulse, as indicated in Fig.1 and described in Ref.[4]. The second, much weaker, probe beam serves to measure the propagating electrical pulse via the electro-optic sampling technique. The complete waveform can be mapped out by changing the delay time between generating and probing beams. On one side of the $LiTaO_3$ crystal, an extremely high quality GaAs crystal ($n = 10^{10}$ cm^{-3} residual doping, mobility $\mu = 4200$ cm^2/Vs at 300 K) is optically contacted without cement to the polished crystal face. The electrical pulse, as it travels through the

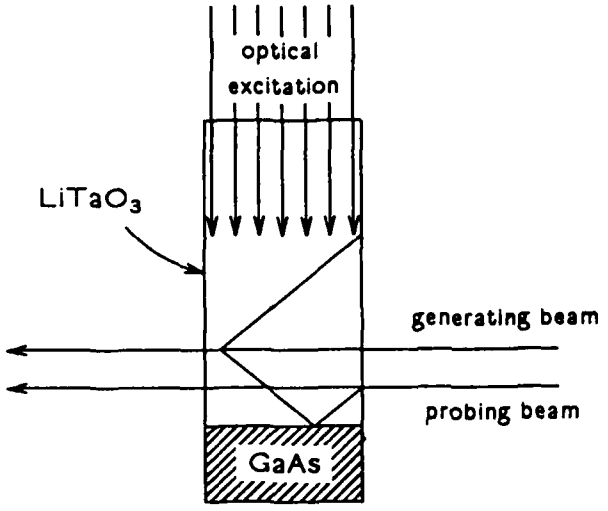

Fig.1. The experimental setup

$LiTaO_3$ crystal, is eventually reflected off the GaAs crystal and crosses the probe beam again after a certain delay time, where it can be detected. From the other side face of the electro-optic crystal, a third femtosecond laser beam ($\sim$ 200 nJ per pulse) illuminates the GaAs crystal, thereby creating carriers with a surface density of $\sim 5\times10^{14}$ cm^{-2} and a excess energy of $\sim$ 500meV in the conduction band. By varying the delay of the optical excitation pulses with respect to the pulses generating the electrical pulses, the reflected electrical pulse can be traced as a function of time after the injection of the hot carriers. The time resolution is presently limited to 1 psec due to the fact, that the optical wave is not synchronized to the wavefront of the electrical pulse. Experiments with a wedged optical wavefront are currently under way and will improve the time resolution significantly.

To derive an expression for the time dependent reflectivity of the optically excited semiconductor plasma, we assume a simple balance equation for the drift velocity v of the electrons:

$$\frac{d}{dt}(m^* v)+\frac{mv}{\tau_m}=eE \qquad \frac{d\epsilon}{dt}=eEv-\frac{\epsilon-\epsilon_0}{\tau_\epsilon} \qquad (1)$$

where τ_m, τ_ϵ are momentum and energy relaxation times, respectively, ϵ is the mean energy of the electron gas, ϵ_0 is the equilibrium energy, e is the electronic charge and E the applied field. Then the boundary conditions at the interface between $LiTaO_3$ and GaAs with a thin layer of injected carriers lead to an analytical expression for the reflected electric field $E_r(t)$ as a function of the incident field $E_i(t)$:

$$E_r(t)=\rho E_i(t)-(1+\rho)\int dt' \frac{n_s e^2}{m^* Y} E_i(t') e^{\gamma(t')-\gamma(t)} \qquad (2)$$

Here, n_s is the sheet carrier density, ρ is the reflectivity given by the Fresnel equations for the insulating GaAs and Y is an inverse impedance dependent on angle of incidence

of the electric pulse and the static dielectric constants of both materials. $\gamma(t)$ is a generalized energydependent momentum relaxation rate of the semiconductor plasma. Eq.2 visualizes how the pulse shape is distorted by the semiconductor plasma. The plasma introduces essentially a convolution with a decaying exponential. Thus for fast relaxation (γ high), the convolution doesn't change the waveform appreciably. However, when the relaxation is slow (low γ), the reflected signal is proportional to the integral of the incident waveform, or 180° out of phase of the incoming wave.

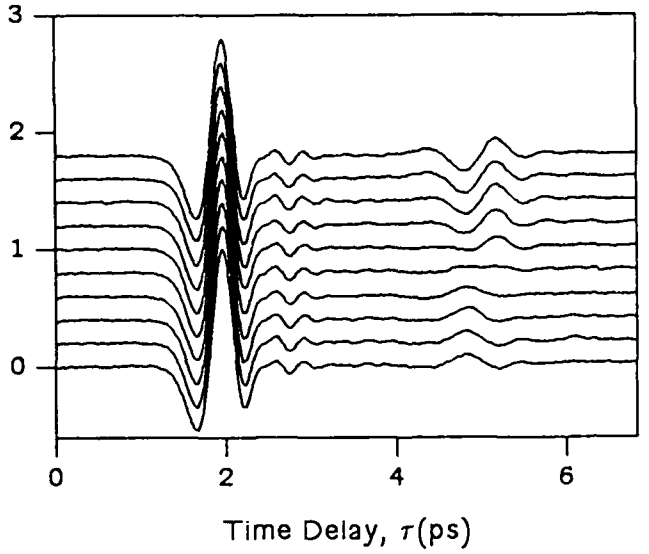

Fig.2. Incident (left) and reflected (right) electrical pulses. The delay time after the injection of the carriers increases by .33 ps from trace to trace from bottom to top.

Fig.2 shows our experimental results. Each trace displays the incident electrical pulse (on the left) and the reflected wave (on the right side) for different delay times after the optical injection of carriers. The time increments in steps of 0.33 psec from trace to trace. The lowest trace is recorded just before carriers are injected into the GaAs. Dramatic amplitude as well as phase changes are observed in the course of time after the carrier injection. The phase changes by 180° as expected when going from a nonconducting state to a state of high mobility. At a fixed delay time, the change of the amplitude of the reflected electrical pulse as a function of the delay of the optical pulse reflects the change of the relaxation rate γ from a high value (low mobility) to a low value (high mobility). We find the rise time for the appearance of the conducting state after the injection of carriers to be $\sim$ 2.2 psec. This time constant can be identified with the energy relaxation time of the hot electron plasma.

Our current experiments are centered on improving the time resolution of the system to less than 200 fsec and to investigate, how long a state of low mobility in the semiconductor persists even after the injection of the carriers. These results should have significance for present and future hot electron devices.

1. for a recent review, see for example C.V.Shank, Science, *233*, 1276 (1986)
2. J.L.Oudar, D.Hulin, A.Migus, A.Antonetti and F.Alexandre, Phys.Rev.Lett. *55*, 2074 (1985)
3. D.Block, J.Shah and A.C.Gossard, Solid State Comm. 59, 527 (1986)
4. D.H.Auston, K.P.Cheung, J.A.Valdmanis and D.A.Kleinman, Phys.Rev.Lett. *53*, 1555 (1984)

Non-Stationary Transport in MODFET's and Heterojuction Devices

K. Hess

Coordinated Science Laboratory and
Department of Electrical and Computer Engineering
University of Illinois
Urbana, Illinois 61801

New horizons have opened up in semiconductor research with the possibility of "band gap engineering" and the combination of signal transport by photons as well as electrons in new forms of ultra thin III-V compound layers.

In this presentation I will report self-consistent simulations of transient transport processes in single layer and single quantum-well modulation doped structures. The availability of vector and parallel computers has given enormous opportunities in recent years for the detailed understanding of these complicated nonlinear transport problems. Detailed Monte Carlo simulations which have been too computer-time consuming in the past can now be accomplished with ease. Also, complex two dimensional physical processes can be transformed into color coded moving pictures. Computation therefore complements conventional theory and experimental research in new ways. This will be demonstrated on the basis of a movie showing the two dimensional dynamics of a high electron mobility single heterolayer structure. As time permits our simulations of picosecond and femtosecond thermalization after optical excitation will also be reported and a comparison of our results with the experiments of Knox et al.[1)] will be given.

1. W. H. Knox, C. Hirlimann, D. A. B. Miller, J. Shah, D. S. Chemla and C. V. Shank; Phys. Rev. Lett. 56 1191 (1986).

Monte Carlo Investigation of Hot Photoexcited Electron Relaxation in GaAs*

M. A. Osman, M. J. Kann, and D. K. Ferry
Center for Solid State Electronics Research,
Arizona State University, Tempe, AZ 85281

P. Lugli
Dipartimento di Fisica e Centro Interuniversitario di Struttura della Materia della Universita, Modena, Italy.

Recently, several authers [1-3] have investigated the dynamics of electron-hole plasma generated by picosecond and sub-picosecond laser pulses in GaAs. In one of these experiments [1] the electron-LO phonon dynamics was directly observed at 77 K by means of a pump-probe Raman scattering experiment using a 600 fs, 588nm laser pulse. They observed an increase in the LO phonon population at 2 ps, which was attributed to the phonons emitted during the cascade of electrons to edge of the band. We have investigated the cooling of carriers excited by a 588nm laser pulse using ensemble Monte Carlo approach. The model takes into account the carrier-carrier and carrier-phonon interactions using a band model which consists of three nonparabolic valleys for the conduction band and two parabolic valance bands. Since the excitation levels used in the above experiment were less or equal to 10^{17} cm^{-3} and the holes were neglected in their theoretical model, we have investigated first a simple model, where only carrier-phonon interactions were active and the presence of the heavy holes was considered, to account for the energy gained by the holes.

The fraction of the photoexcited-electrons in the central valley is shown in Fig. 1 as function of time after application of a 588nm laser pulse which is a delta function in time. From fig. 1, it is obvious that the simple picture of electrons cascading down the central valley by emitting LO optical phonons is not complete. The electrons rather transfer to the upper valleys and cool down in these valleys by emitting phonons through polar-optical and deformation potential interactions. Subsequently, the electrons return to the central valley as indicated by the increase in the population of the electrons in the central valley at later times in Fig. 1. The energy of the electrons in the central valley (curve 1 in Fig. 2) remains above 100 meV up to 3 ps after the excitation and an increase in the average energy occurs at 2 ps due to the return of the electrons to the central valley. The initial rapid drop in the average kinetic energy of the electron ensemble (curve 2 in Fig. 2) is due to the transfer of a large fraction of the electrons to the upper valleys as can be seen in Fig. 1. Curve 3 in Fig. 2 indicates that the cooling of the electron in the L-valley is not negligible. However, in [1] the electron-phonon scattering time was determined to be 165fs, by assuming that each electron emits an average of 12 phonons by the time the optically induced Raman signal reaches its maximum, which occurs when the electrons are within 100 meV of the band edge. This model also

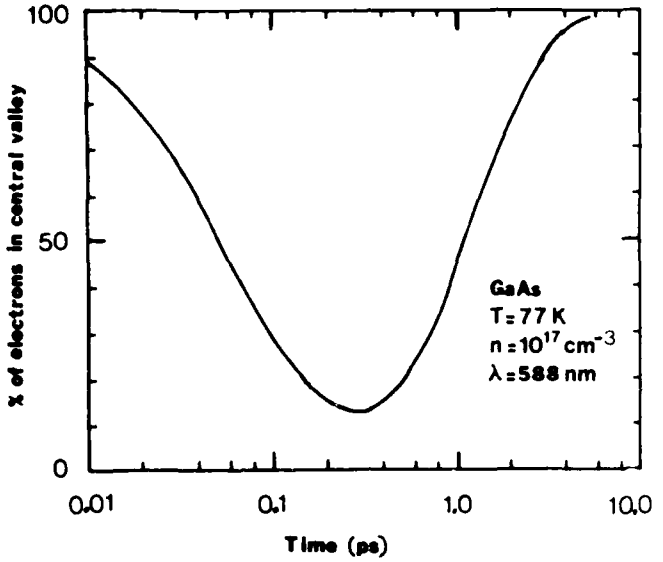

Fig. 1 Fraction of photoexcited electrons in the central valley as function of time after excitation by a 588nm laser pulse.

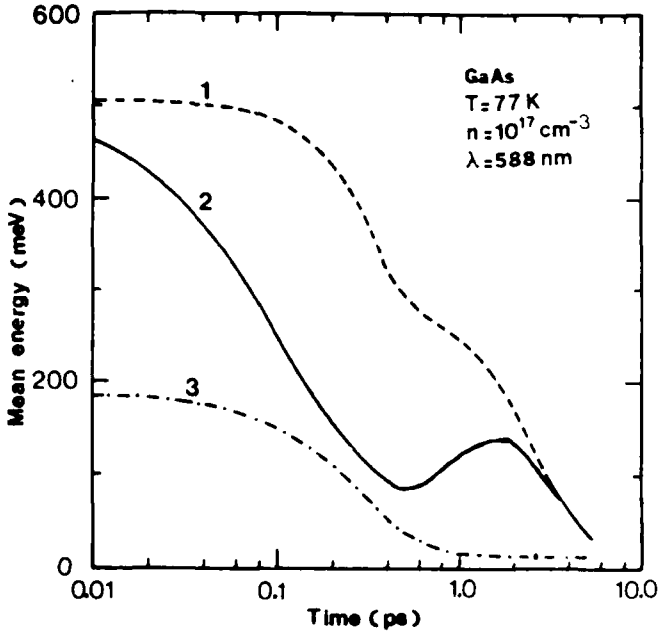

Fig. 2 Mean kinetic energy of the photoexcited electrons in: 1) central valley, 2) central+L-valley, 3) L-valley.

ignores the presence of the upper valleys in GaAs to which electrons are more likely to transfer when their energies exceed .30 eV.

The situation where a very high density of electron-hole plasma is generated is of interest from fundamental physics point-of-view. Under these conditions the roles of electron-electron and electron-hole interactions and hot phonon effect become very important [4,5]. The EMC approach will be used to investigate a range of excitation levels above 10^{17} cm^{-3}. Because the phonon distribution is disturbed under high excitation levels, the time evolution of the LO-phonon distribution is calculated as a function of the wavevector q from the Monte Carlo process. The results indicate a considerable increase of the phonon population over a time scale of a few picoseconds in the absence of electron-hole interaction. The phonon distribution returns back to equilibrium at later times after the excitation pulse through phonon-phonon interaction. We will present the results of the investigation and discuss the roles of electron-hole interaction and the hot phonons on the relaxation of the hot photoexcited electrons.

* Supported by the Office of Naval Research.

References

1. J. A. Kash, J. C. Tsang, and J. M. Hvam, Phys. Rev. Lett. 54, 2151 (1985).

2. J. Shah, A. Pinczuk, A. C. Gossard, and W. Weigmann, Phys. Rev. Lett. 54, 2045 (1985).

3. C. L. Collins and P.Y. Yu, Phys. Rev. B30, 4501 (1984).

4. M. A. Osman, U. Ravaioli, R. Joshi, W. Pötz, and D. K. Ferry, to be puplished in the Proceedings of the 18th International Conference on the Physics of Semiconductors.

5. M. A. Osman, Ph.D. Dissertation, Arizona State University, Tempe (1986).

Longitudinally Localized Optical Carrier Injection for Femtosecond Transport Studies

M.C. Downer, D.H. Reitze, and T.R. Zhang
Physics Department, University of Texas at Austin, Austin, TX 78712

A new generation of microelectronic devices will be based on ballistic and quantum tunneling transport processes, which involve transit times on a femtosecond scale across submicron semiconductor layers. Fundamental experimental studies of these phenomena will require the use of femtosecond optical techniques to inject and probe carriers locally, just as analogous picosecond techniques have been used in studying slower transport processes in thicker layers[1,2]. However, because optical absorption (and therefore carrier injection) depths at near band gap wavelengths (typically ~1μm.) greatly exceed the thickness of the semiconductor layers in which most femtosecond transport phenomena occur (typically .01 to 0.1 μm.), adequate spatial resolution to observe these processes directly has not been achievable. We introduce a new technique for optically injecting carriers of any desired energy within the first few hundred angstroms of the surface of a semiconductor layer with femtosecond time resolution, so that the evolution of femtosecond transport processes can be resolved.

Our technique is based upon internal reflection (see Fig. 1). A light pulse passes through a high index (n) dielectric to the interface with a lower index (n') semiconductor sample at an incident angle Ø greater than the critical angle $\sin^{-1}(n'/n)$. Since the lower index semiconductor is slightly lossy, energy is absorbed from the evanescent wave in the form of photo-excited

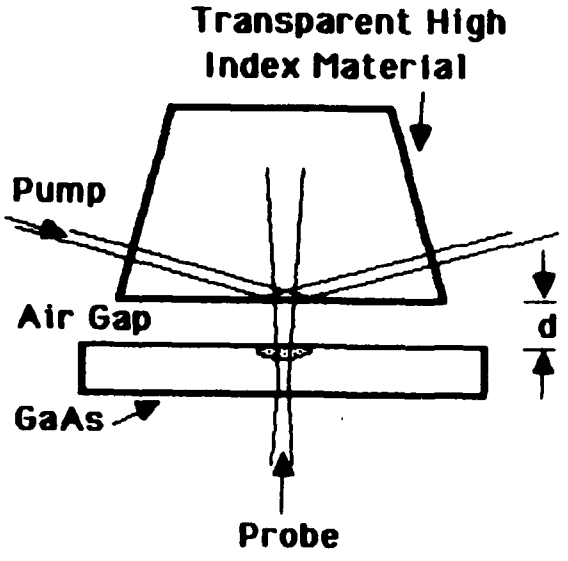

Fig. 1 -- Schematic experimental arrangement for time-resolved transport measurement using internal reflection carrier excitation.

carriers. Note that this absorption occurs within the penetration depth (approximately $\lambda/2\pi n'$) of the evanescent wave, typically only a few hundred angstroms for semiconductor materials

and wavelengths of interest. The extremely small penetration depth of evanescent waves has been used extensively in the past as a tool in cw infrared spectroscopy of thin films and surfaces.[3] Actual contact is not necessary in order to apply the internal reflection method. The presence of a small air, or other low index, gap between the two materials, as shown in Fig. 1, alters neither the critical angle nor the penetration depth of the evanescent wave into the semiconductor, although the *amount* of absorption depends on the size of this gap, as shown in more detail below.

We have calculated absorption depths and absorbances for two practical cases of potential interest in experimental transport studies. These calculations use the thin film optics equations[4] with variable incident angle and complex refractive index. The solid curve in Fig. 2 assumes an excitation wavelength of 0.83 μm. (1.5 eV.), slightly above the room temperature band gap of undoped GaAs. The excitation pulse enters through a prism of trigonal selenium, as shown in Fig. 1, which has a band gap at 1.7 eV., and an extraordinary index higher by approximately 0.1 than GaAs in the 1.5 to 1.7 eV. spectral region[5]. The evanescent wave is therefore absorbed by local electron-hole pair creation. Note that the penetration depth above the critical angle is twenty times smaller than the normal incidence absorption depth. The dashed curve assumes an excitation pulse at 3.0 μm. (0.4 eV.), incident through germanium upon GaAs

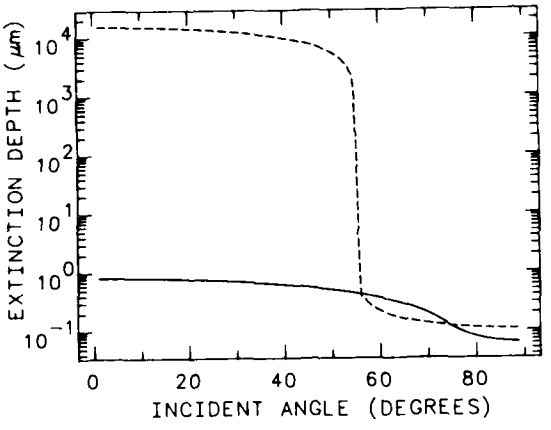

Fig. 2 -- Extinction depth for 0.83 μm. pulses incident through trigonal selenium upon GaAs (solid curve) and for 3.0 μm. pulses incident through Ge upon n-GaAs (dashed curve). Note sharp decreases above critical angles (75° for Se/GaAs, 55° for Ge/n-GaAs).

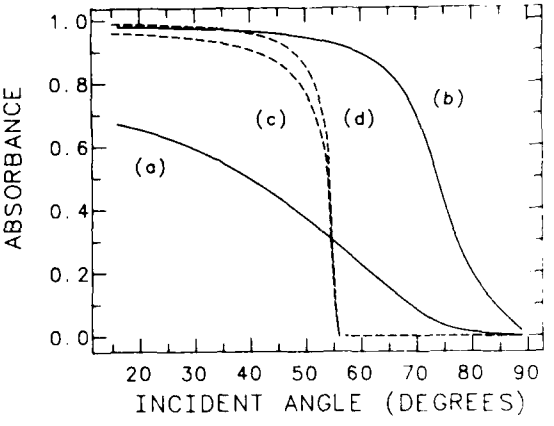

Fig. 3 -- Absorbance of GaAs layer for Se internal reflection element, λ = 0.83 μm., with air gap a) 500 Å and b) 100 Å; and for Ge internal reflection element, λ = 3.0 μm., with air gap c) 500 Å and d) 100 Å (absorbance is ~10^{-4} above critical angle for curves c) and d)).

n-doped to approximately 10^{18} cm^{-3}. Here the absorption mechanism is localized heating of conduction band electrons through free carrier absorption. The evanescent wave absorption is again localized within a few hundred angstroms, smaller by a factor of 10^5 than normal incidence absorption. The absorption depths shown in Fig. 2 are independent of the size of the air gap.

Fig. 3 shows the percent absorption which can be achieved in each of the above cases with an s-polarized incident pulse for 100 Å and 500 Å air gaps. Note that absorbances as high as

30% are achievable even above the critical angle. We have calculated that the phase changes which occur upon internal reflection[6] will broaden 50 fsec. excitation pulses by less than 5% in each of the above cases. Thus carrier injection occurs essentially within the duration of the optical pulse.

In order to conduct meaningful transport measurements, the internal reflection injection technique must be combined with optical probing methods possessing comparable depth resolution. An example is shown in Fig. 1, where a probe beam monitors band edge absorption, an appropriate technique for voltage-biased structures in which the Franz-Keldysh effect is modulated as moving carriers screen the applied electric field[1]. Optical reflectivity[2] provides an appropriate probe in other circumstances.

Experimental demonstration of the internal reflection method is in progress in our laboratory. Dynamics of surface states and absorbates can also be studied with this technique. This work is supported by the Joint Services Electronics Program and the Texas Advanced Technology Research Program.

References

1. C.V. Shank, R.L. Fork, B.I. Greene, F.K. Reinhart, and R.A. Logan, Appl. Phys. Lett. 38, 104 (1981).

2. B.F. Levine, C.G. Bethea, W.T. Tsang, F. Capasso, K.K. Thornber, R.C. Fulton, and D.A.Kleinman, Appl. Phys. Lett. 42, 769 (1983).

3. N.J. Harrick, Internal Reflection Spectroscopy, Wiley, New York, 1967.

4. O. S. Heavens, Optical Properties of Thin Solid Films, Dover, New York,1985.

5. L. Gampel and F.M. Johnson, J. Opt. Soc. Am. 59, 72 (1969); E.D. Palik, ed., Handbook of Optical Constants of Solids, Academic Press, 1985.

6. K.P. Cheung and D.H. Auston, Opt. Lett. 10, 218 (1985).

Femtosecond Nonequilibrium Electronic Heat Transport in Thin Gold Films

S. D. Brorson, J. G. Fujimoto, and E. P. Ippen

Department of Electrical Engineering and Computer Science and
Research Laboratory of Electronics
Massachusetts Institute of Technology, Cambridge, MA 02139

With the advent of femtosecond lasers has come the promise of directly measuring ultrafast electron transport effects in technologically important materials. Using a front pump/back probe[1] measurement of transient reflectivity changes, we have observed ultrafast electronic heat transport through thin films of gold. For film thicknesses of 500 - 2000 Å, we find thermal transport occurs on a time scale of 40 - 200 fs. In this regime, the transport of heat seems to be governed by electronic motion, since lattice heat diffusion times are much slower.

Our experiment is a variation of the usual transient thermomodulation technique. In the transient thermomodulation experiment, an ultrafast laser pulse pumps the surface of a noble metal. The temperature increase caused by the pump pulse smears the occupancy of electronic states near the Fermi level. This causes the reflectivity of the metal to change for frequencies near the d-band to Fermi level optical transition. Thus, monitoring the reflectivity of the sample with a delayed probe pulse gives information about the electron temperature as a function of time. Previous thermomodulation experiments demonstrated that the electrons are out of equilibrium with the lattice for times less than $\sim$ 1 ps. [2-4] The decay of the reflectivity transient was identified with nonequilibrium electron temperature relaxation via the electron-phonon interaction. By pumping the front of the sample and probing reflectivity changes on the back (Fig. 1), we have used this technique to study the propagation of heat through the sample.

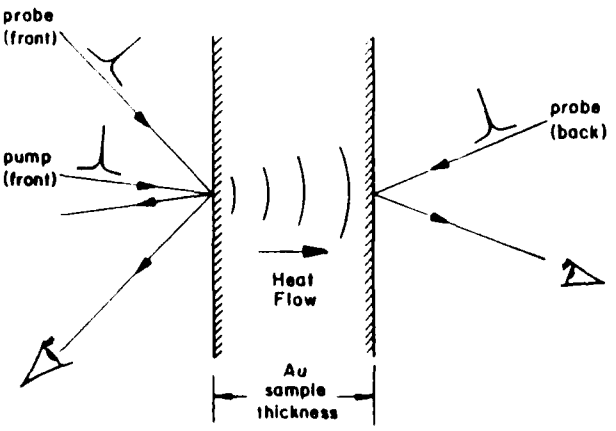

Figure 1. Simplified schematic of the thermomodulation experiment. In the usual case, the sample is pumped and probed on the front surface. By probing the back, we are able to measure the transport of heat across the sample.

The experiments were performed on thin films of Au deposited on sapphire. Gold thicknesses ranged from 500 to 2000 Å. All samples used were thicker than the optical skin depth ($\sim$ 150 Å). The source was a colliding pulse mode-locked (CPM) dye laser employing 4 prisms to control the cavity dispersion (λ_o = 630 nm, $\tau \sim 50fs$ FWHM assuming a $sech^2$ pulse shape). The pump and probe beams were derived from a standard

pump/probe set up. A 0.1 μm resolution stepper stage was employed to vary the delay between the pump and probe pulses. The pump beam was chopped and focused onto the front surface of the sample with a 40× microscope objective, while the probe was similarly focused onto the back of the sample. The reflected probe beam was monitered with a photodiode. The thermomodulation signal was detected with a lock-in amplifier tuned to the chopping frequency of the pump. The zero delay point was determined by reversing the role of pump and probe beams and repeating the experiment.

Figure 2 shows the transient change in reflectance for samples 500, 1000, and 2000 Å thick. The delay between the pump and the arrival of the heat at the back of the sample ranges from 40 to 200 fs, increasing with film thickness. For the thin films used here, the time delay increases approximately linearly with film thickness, giving a propagation velocity of $\sim 10^8$ cm/sec. This is of the same order of magnitude as the Fermi velocity in Au, 1.4×10^8 cm/sec. The delays measured here are much shorter than those expected for simple equilibrium heat diffusion. (In Au in equilibrium, the amount of time necessary for heat to diffuse 1000 Å is on the order of tens of picoseconds.) These results suggest that the electrons are out of equilibrium with the lattice on this time scale, and that the heat is carried by the nonequilibrium electrons.

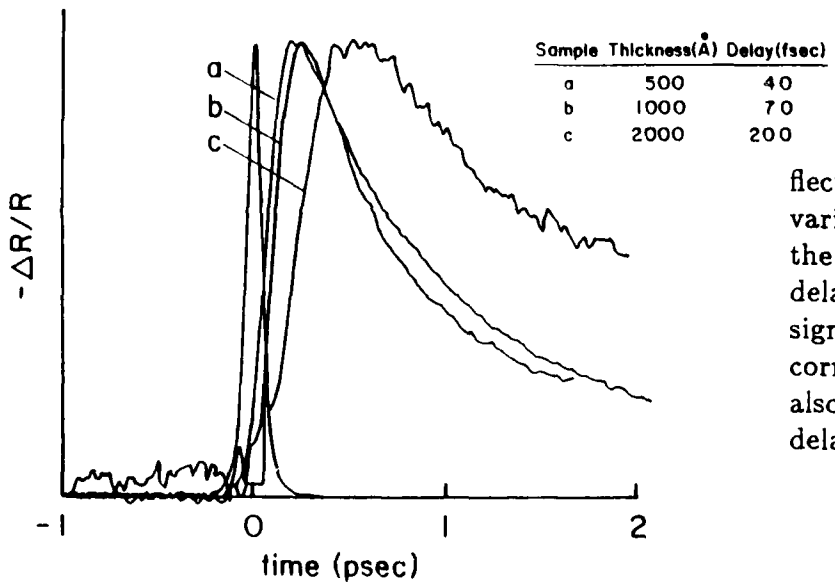

Figure 2. Back surface reflectivity change versus time for various thickness gold films. As the film thickness increases, the delay of the rising edge of the signal also increases. An autocorrelation of the laser pulse is also plotted to indicate the zero delay position.

This picture is corroborated by the results of front pump/front probe measurements on films of varying thickness. Shown in Fig. 3 is thermomodulation data on samples of thickness 500, 800, and 1000 Å. The relaxation time decreases with increasing film thickness. This effect is consistant with transport of heat out of the optically active region on a femtosecond time scale. For film thicknesses comparable to the optical skin depth, the nonequilibrium electrons cannot move out of the optically probed region. In this case, relaxation dominates over transport, and the reflectivity decay time is determined by the relaxation process. For thicker films, both relaxation and nonequilibrium transport occur simutaneously. Hence, the measured reflectivity transient decays more quickly. Since this effect is noticeable even for the thicker films used here (1000 Å), heat transport over this

distance is apparently occurring on a femtosecond time scale.

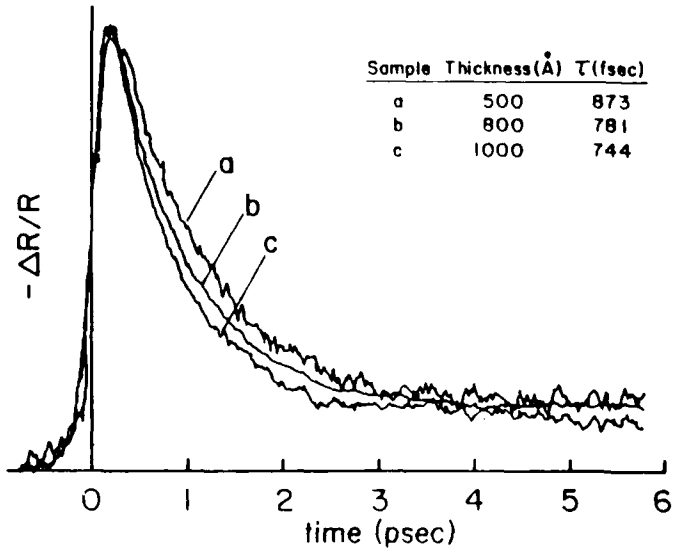

Figure 3. Front surface reflectivity change versus time for various thickness gold films. As the thickness of the film increases, the decay time constant decreases. This can be interpreted as due to the effect of rapid electronic heat transport.

In summary, we have used the transient thermomodulation technique to study the ultrafast transport of heat in thin gold films. Using a front pump/back probe technique, we observed nonequilibrium heat transport occurring on the same time scale as electronic motion. This rapid transport is confirmed by front pump/back probe measurements which show that the reflectivity transient decay time depends on the gold film thickness. Extensions of this technique to other structures may allow for ultrafast probing of transport in materials and devices.

The authors would like to acknowledge helpful discussions with G. L. Eesley, C. A. Paddock, R. W. Schoenlein, and W. Z. Lin. This work was supported in part by the AFOSR Grant 85-0213 and the Joint Services Electronics Program under contract number DAAL03-86-K-0002.

References

1. This technique is similar to that used by Levine, *et al.* to study carrier transport in $Al_xGa_{1-x}As$. B. F. Levine, W. T. Tsang, C. G. Bethea, and F. Capasso, *Appl. Phys. Lett.* **41**, 470 (1982).

2. G. L. Eesley, *Phys. Rev. B* **33**, 2144 (1986), and references therein.

3. H. Elsayed-Ali, M. Pessot, T. Norris, and G. Mourou, in **Ultrafast Phenomena V**, in press.

4. R. W. Schoenlein, W. Z. Lin, J. G. Fujimoto, and G. L. Eesley, **Ultrafast Phenomena V**, in press.

THURSDAY, JANUARY 15, 1987

PROSPECTOR/RUBICON ROOM
7:30 P.M.–9:00 P.M.

ThC1–4

BALLISTIC TRANSPORT AND RESONANT TUNNELING

S. Luryi, AT&T Bell Laboratories, *Presider*

BALLISTIC TRANSPORT AND HOT ELECTRON SPECTROSCOPY IN TUNNELLING HOT ELECTRON TRANSFER AMPLIFIER (THETA)

M. Heiblum

IBM, Thomas J. Watson Research Center

Yorktown Heights, N.Y., 10598

An important aspect of obtaining the fastest electronic devices is minimizing the transit time of charge carriers from input to output. The shortest times can be achieved by having the carriers move at the highest velocity allowed by the band structure of the solid crystal. In present high speed devices collisions redirect and slow down the moving carriers. To avoid this electron scattering, transit regions have to be short enough to make collisions less probable. Such "ballistic transport" of fast carriers (hot carriers) moving at their maximum possible velocity, should in principle allow the fastest device operation.

The family of hot electron devices [1] promises such a fast operation, however, due to the immaturity of the field many stumbling blocks have yet to be surmounted. Among them the most important ones are the relatively low current gain and the small current density exhibited thus far in the devices. The high current density is needed to charge up quickly the parasitic capacitances of the devices so that the ultimate speed of the devices could be approached. Aside from their potential speed hot electron devices serve as unique "mini-laboratories" for studying hot electron transport, for example: the energy distributions of hot electrons generated by different injectors, the ballistic mean free path, the transfer of otherwise ballistic electrons into upper energy valleys, quantum size effects in small structures, and more.

Among the family of hot electron devices, the most notable member is the THETA device [2]. Most THETA devices fabricated so far utilized GaAs-AlGaAs heterostructures and the charge carriers were electrons. In these devices quasi monoenergetic hot electrons are injected via tunnelling through a thin AlGaAs insulating layer (emitter) with the majority traversing ballistically a subsequent thin n-type GaAs layer (base). Those electrons that maintain their energy and direction surmount a barrier created by a thicker AlGaAs insulating layer at the end of the GaAs base. They are eventually collected in a final n-type GaAs electrode (collector). By using an external bias voltage to vary the potential height of the barrier that precedes the collector, one can map the distribution of the arriving hot electrons as a function of their energy [3,4], effectively doing energy spectroscopy.

Such studies led, at the end of 1985 [4] to an unambiguous demonstration of ballistic electron transport through the combined structure of a 300 Å thick GaAs layer doped to 1×10^{18} cm^{-3} and an undoped insulating AlGaAs layer 1000 Å thick. Energy distributions as narrow as 60 meV had been measured for the ballistic electrons. As the width of the doped GaAs layer or its doping level increased, the traversing ballistic fraction decreased, however, the distribution shapes remained invariant. In subsequent studies [5], at least 75 % of the injected electrons had been measured to traverse similar regions of GaAs and AlGaAs ballistically. Coupled modes of plasmons and phonons were proposed to be the responsible mechanism [6,3] for thermalizing the hot electrons, however, a satisfactory theory that is applicable to thin quantized regions is not yet available.

When injection energies exceeded the separation between the L satellite valleys and the Γ central valley (about 0.3 eV in GaAs), a fraction of the ballistic electrons were found to scatter via phonons and impurities into the satellite valleys. This resulted with a randomized motion and a reduced collection efficiency in the devices [7]. Up to 25 % of the electrons were estimated to transfer into the

L valleys in a 300 Å thick base. The effect was verified by an application of hydrostatic pressure on the devices causing a change in the L-Γ energy separation.

As the base width was reduced to less than about 500 Å, quantum size effects began to be noticeable. Quasi two dimensional subbands were then formed in the base, influencing the injected tunnelling current. The resultant transmission coefficient through the device was thus modulated with peaks that indicate the position of the subbands. A self consistent calculation of the potential distribution in the base (satisfying Poisson and Schrödinger equations simultaneously) was needed explain the position of the peaks. Note that at high enough injection energies, when a substantial transfer into the L valleys took place, the modulation peaks vanished due to the reduction in the ballistic (coherent) fraction of the current.

Work is now in progress to optimize the device performance and to check its feasibility as a valiable high speed device.

1. A recent review of the subject is to appear in: M. Heiblum, proceedings of the "High Speed Electronics" (RIFA) conference proceedings, Stockholm, August 1986.
2. M. Heiblum, Solid St. Electron. **24**, 343 (1981); N. Yokoyama et al., Technical Digest of IEDM, San Francisco, 1984, p. 532.; M. Heiblum et al., Appl. Phys. Lett. **47**, 1105 (1985); U. K. Reddy et al., ***ibid*** **48**, 1799 (1986).
3. A. F. J. Levi et al., Phys. Rev. Lett. **55**, 2071 (1985).
4. M. Heiblum et al., ***ibid*** **55**, 2200 (1985).
5. M. Heiblum et al., Appl. Phys. Lett. **49**, 207 (1986).
6. M. A. Hollis et al., Electron Dev. Lett. **EDL-4**, 440 (1983).
7. M. Heiblum et al., Phys. Rev. Lett. **56**, 2854 (1986).

Microwave and Millimeter-Wave Resonant Tunneling Diodes

T. C. L. Gerhard Sollner, Elliott R. Brown and W. D. Goodhue
Lincoln Laboratory, Massachusetts Institute of Technology
Lexington, Massachusetts 02173

Resonant tunneling through double-barrier heterostructures has attracted increasing interest recently, largely because of the fast charge transport[1] it provides. In addition, the negative differential resistance regions which exist in the current-voltage (I-V) curve (peak-to-valley ratios of 3.5:1 at room temperature[2–4] and nearly 10:1 at 77 K have been measured) suggest that high-speed devices based on the peculiarities of the I-V curve should be possible. For example, the negative differential resistance region is capable of providing the gain necessary for high-frequency oscillations[5]. In our laboratory we have been attempting to increase the frequency and power of these oscillators[6], and others have worked toward a better understanding of the equivalent circuit of the device[7] and the underlying processes responsible for the frequency response[8–10]. Three-terminal devices using resonant tunneling in various ways have also been proposed and fabricated[11–13]. In this paper we will describe our most recent results for oscillators as well as some new resonant-tunneling devices that have application in the millimeter and submillimeter-wave spectrum.

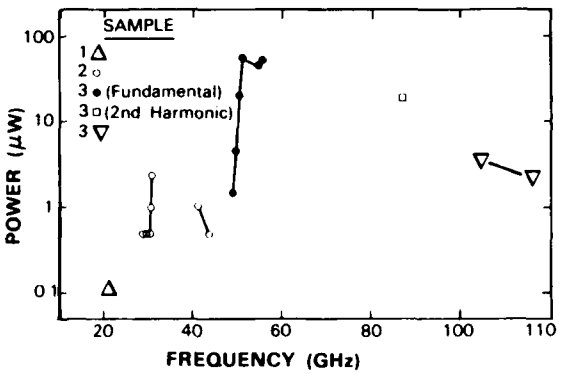

Figure 1. Output power as a function of frequency for recent resonant-tunneling oscillators. The connected dots indicate continuous tunability in a particular waveguide structure. All measurements were made at room temperature.

Our recent room-temperature, millimeter-wave oscillator results are summarized in Fig. 1. The initial experiments at 20 GHz were performed in a coaxial circuit, but the other resonators were made in waveguide. In particular, the oscillations around 30 and 40 GHz were achieved in WR-22 and WR-15 resonators, respectively[14]. A significant improvement in the quality of the devices, especially the use of thin AlAs barriers in place of AlGaAs barriers, resulted in oscillations near 56 GHz in the WR-15 resonator[6]. The oscillations between 104 and 108 GHz were obtained with the same AlAs-barrier material in a WR-6 structure. We believe that this material is capable of oscillations approaching 200 GHz, and that optimized material should be capable of fundamental oscillations as high as perhaps 1 THz. More details on material parameters can be found in Refs. 6 and 15.

Since the resonant-tunneling I-V curve is nonlinear, especially near the negative differential resistance region, the same device can act as both a mixer and an oscillator. Figure 2 shows the difference frequency between two oscillators, one of which is a resonant-tunneling quantum-well oscillator. The oscillator output power of this early device operating at 20 K is rather low; nevertheless, it appears to be an efficient mixer as well as a compact oscillator. The best DC bias point for mixing

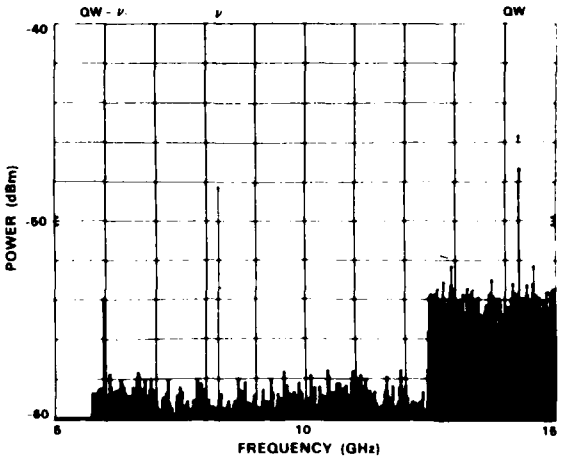

Figure 2. Measured power spectrum of a resonant tunneling oscillator (marked QW) mixing with an injected signal (marked ν) to produce a difference-frequency output (marked QW-ν). This oscillator was cooled to 20 K.

was found to be at either side of the negative differential resistance region, rather than in the center where the oscillator output power is maximized, to take advantage of the larger nonlinearity of the IV curve there.

If a resonant tunneling structure is appropriately pumped at high frequency, a negative resistance can appear with no DC bias applied. The dashed line in Fig. 3 shows a resonant-tunneling I-V curve typical of our early structures at 20 K. Ordinarily, the negative differential resistance regions occur at about ± 0.3 V. If an AC waveform (i.e., the pump) were applied to the terminals with an amplitude of about 0.3 V, the negative differential resistance region would be sampled for some fraction of the pump period, resulting in a negative resistance appearing near $V_{DC} = 0$. The solid curve of Fig. 3 shows the DC I-V curve that results when a sinusoidal pump wave at 1 GHz with an amplitude of about 0.4 V is applied. Note that the negative resistance is larger than that in the unpumped DC curve and that the voltage region it spans is smaller. This occurs because regions of positive differential resistance are also sampled during a pump period.

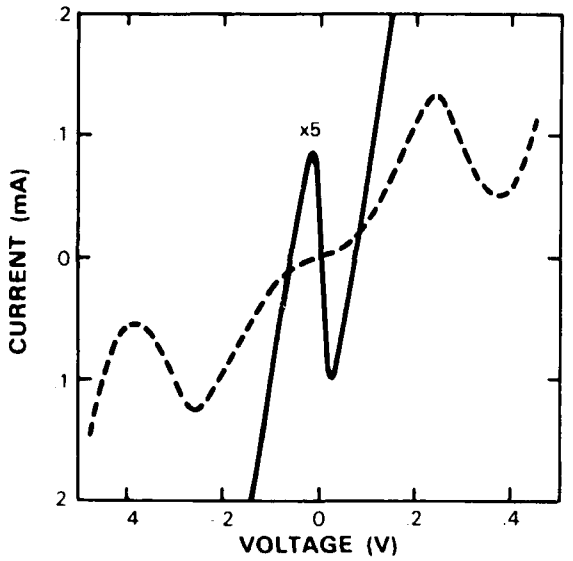

Figure 3. Current-voltage curves for one of our early resonant-tunneling structures operating at 20 K: dashed line is measured DC characteristics; the full line results when a 1 GHz pump with an amplitude of about 0.4 V has been applied. The negative resistance in the region near V = 0 can be varied by changing the amplitude of the pump.

Although such a negative resistance is possibly only useful at frequencies below the pump frequency, there are advantages. The fact that no DC connection need be made to the sample simplifies the problem of stabilizing a two-terminal negative-resistance device, because the low-frequency circuit at which unwanted oscillations could occur is eliminated. Also, the value of negative resistance can be changed simply by varying the pump amplitude, which allows this device to be matched to a given circuit more easily. Finally, this phenomenon is quite generally applicable to any material which has a point symmetric I-V relation with negative differential resistance. It could be useful with materials such as superlattices, which form domains when biased into their regions of negative differential resistance for long times; it may be possible to sweep them into that region for a time short compared to their domain-formation time with a high-frequency pump, so that the negative resistance is retained. There may even be applications involving bulk materials that show negative differential conductivity, such as GaAs.

The undulations of the unpumped I-V curve of Fig. 3 also suggest that there should be large harmonic content to the current waveform, leading to an efficient harmonic multiplier. Figure 4 shows the calculated voltage and current waveforms for this same device when driven by a 50 Ω source with an amplitude of about 0.5 V, and the power spectrum of the current waveform is shown in Fig. 5.

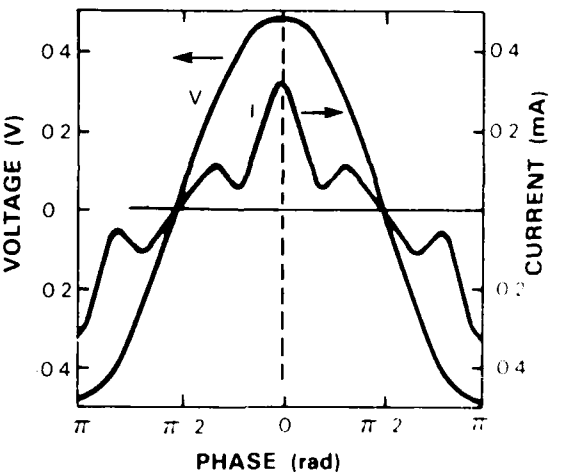

Figure 4. Calculated voltage and current waveforms for the DC I-V curve of Fig. 3 when driven by a pump with a 50 Ω source impedance.

There are several interesting features of this spectrum. One of the most difficult problems in harmonic multiplier design is to terminate reactively all the harmonics lower than the desired output, since these harmonics are usually of larger amplitude than the higher-order ones. In the present case the even harmonics are entirely missing because of the symmetry of the I-V curve, thus reducing by a factor of two the number of harmonics which need to be considered. Also, the largest component after the fundamental is the 5th harmonic, so even if the power in the other harmonics is resistively ter-

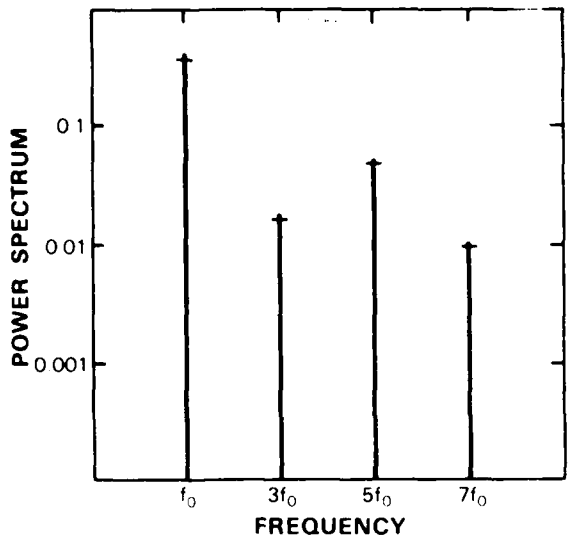

Figure 5. Power spectrum calculated from the current waveform in Fig. 4. The even harmonics are absent because of the symmetry of the I-V curve, while the large 5th harmonic content derives from the occurrence of one negative resistance region.

minated one could expect as high as 10% conversion efficiency to the 5th harmonic. So far we have observed 1% conversion efficiency from 2 to 10 GHz, about the same as current state-of-the-art Schottky diode quintuplers. Optimizing the multiplier structure to provide the proper impedances should raise the efficiency significantly. The probable ultimate limit for the output frequency of a resonant-tunneling quintupler is the same as for the oscillator, on the order of 1 THz.

We have described a few interesting and useful high-speed devices based on resonant tunneling, and there are undoubtedly many more that await discovery. Optical interactions with these devices have not been discussed here, but this is a fruitful area of future research, combining the high temporal resolution of optical pulses with the high speed of resonant tunneling. We expect the general area of resonant tunneling to provide a fertile ground for both solid state physics and active device investigations for some time to come.

We wish to thank G.D. Johnson, K.M. Molvar, and N. Usiak for assistance in fabrication and packaging our devices. We are also indebted to C-L. Chen, P.J. Daniels, and P.E. Tannenwald for helpful discussions, and to C.A. Correa and C.D. Parker for help in making the measurements. This work was supported by the U.S. Army Research Office and by NASA.

REFERENCES

[1] T.C.L.G. Sollner, W.D. Goodhue, P.E. Tannenwald, C.D. Parker, and D.D. Peck, Appl. Phys. Lett. **43**, 588 (1983).

[2] M. Tsuchiya and H. Sakaki, *IEEE Int. Electron Devices Meeting Tech. Digest* (IEEE, New York, 1985), pp. 662-665.

[3] T.J. Shewchuk, P.C. Chapin, P.D. Coleman, W. Kopp, R. Fischer, and H. Morkoc, Appl. Phys. Lett. **46**, 508 (1985).

[4] W.D. Goodhue, T.C.L.G. Sollner, H.Q. Lee, E.R. Brown and B.A. Vojak, Appl. Phys. Lett. **49**, 1086 (1986).

[5] T.C.L.G. Sollner, P.E. Tannenwald, D.D. Peck, and W.D. Goodhue, Appl. Phys. Lett. **45**, 1319 (1984).

[6] E.R. Brown, T.C.L.G. Sollner, W.D. Goodhue, and C.D. Parker, submitted to Appl. Phys. Lett.

[7] P.D. Coleman, S. Goedeke, T.J. Shewchuk, and P.C. Chapin, J.M. Gering, and H. Morkoc, Appl. Phys. Lett. **48**, 422 (1986).

[8] S. Luryi, Appl. Phys. Lett. **47**, 490 (1985).

[9] D.D. Coon and H.C. Liu, Appl. Phys. Lett. **49**, 94 (1986).

[10] W. Frensley, *IEEE Int. Electron Devices Meeting Tech. Digest* (IEEE, New York, 1986), paper 25.5.

[11] T.C.L.G. Sollner, H.Q. Le, C.A. Correa, and W.D. Goodhue, *Proc. IEEE/Cornell Conf. Advanced Concepts in High Speed Semicond. Devices and Circuits* (Inst. Electrical and Electronic Engineers, Inc., New York, 1985), p. 252.

[12] N. Yokoyama, K. Imamura, S. Muto, S. Hiyamizu, and H. Nishii, Jpn. J. Appl. Phys. **24**, L583 (1985).

[13] F. Capasso, S. Sen, A.C. Gossard, A.L. Hutchinson, and J.E. English, IEEE Electron Device Lett. **EDL-7**, 573 (1986).

[14] E.R. Brown, T.C.L.G. Sollner, W.D. Goodhue, B.J. Clifton, and P.E. Tannenwald, *Tech. Digest Device Research Conference* (Amherst, MA, June 23-25, 1986), paper IVB-1.

[15] T.C.L.G. Sollner, E.R. Brown, W.D. Goodhue, and H.Q. Le, submitted, Appl. Phys. Lett. (1986).

Quantum Transport Calculation of Resonant-Tunneling Response Time

William R. Frensley
Texas Instruments Incorporated
P. O. Box 655936, MS 154
Dallas, Texas 75265

A form of quantum transport theory has been developed to model the resonant-tunneling diode and similar devices. The internal state of the device is represented by the Wigner distribution function. The boundary conditions applied to the Wigner function model the open-system nature of the device by coupling it to electron reservoirs. This coupling introduces irreversibility into the model, permitting meaningful calculations of the transient response.

The steady-state I(V) curves derived from this model show the expected negative resistance. Figure 1 shows the I(V) curves derived from the Wigner function calculation and from a more conventional scattering calculation, for the same device structure. The peak-to-valley current ratio obtained from the Wigner function is smaller than that obtained from the scattering calculation and is smaller than the better experimental devices at low temperatures.

The transient response of a resonant-tunneling diode to sudden changes in bias voltage is shown in Figure 2. Transitions across different parts of the I(V) curve require varying times, but are generally of the order of 0.1 ps.

This work was supported in part by the Office of Naval Research and the Army Research Office.

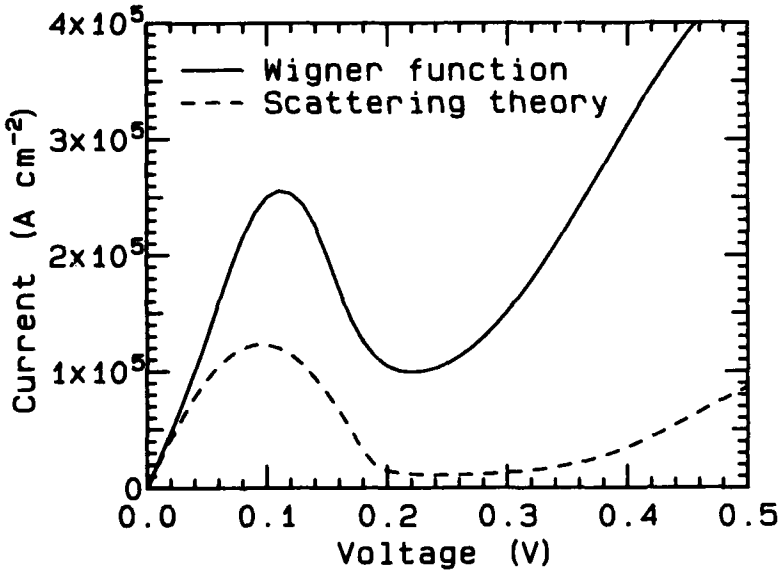

Figure 1. I(V) characteristics derived from the Wigner function calculation and from a conventional scattering theory calculation. The assumed device structure had 2.8 nm barriers of $Al_{0.3}Ga_{0.7}As$ around a 4.5 nm quantum well. The temperature was 300 K.

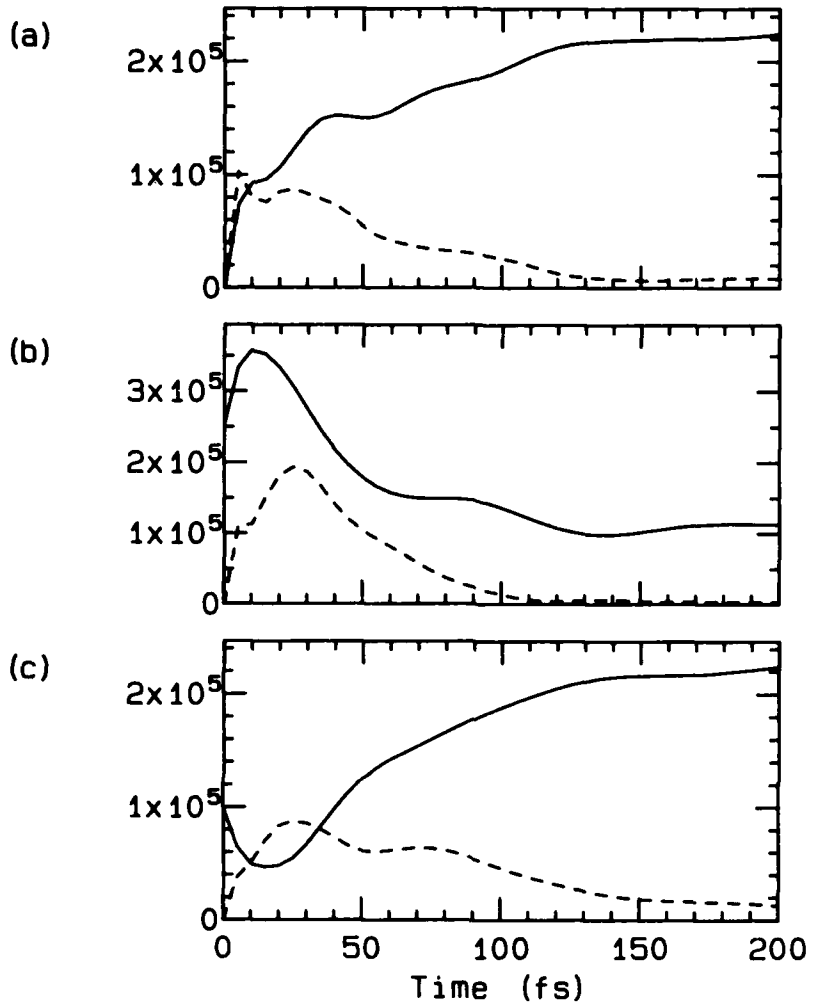

Figure 2. Transient response of the device structure of Figure 1. The solid line shows the current density (in A cm^{-2}) averaged over the structure and the dashed line shows the standard deviation from this average (to provide a measure of the convergence to steady-state). In (a), the voltage was switched from 0 to the peak value at $t=0$. In (b) it was switched from the peak to the valley. In (c) it was switched from the valley to the peak.

Resonant Tunneling Electron Spectroscopy

F. Capasso, S. Sen*, A. Y. Cho and A. L. Hutchinson

AT&T Bell Laboratories
Murray Hill, NJ 07974

In this paper we demonstrate a new electron spectroscopy technique based on resonant tunneling. The key difference compared to conventional hot electron spectroscopy[1] is the use of a resonant tunneling double barrier in the collector of the structure (Fig. 1). The advantage of this new feature is that it allows one to obtain information on the electron momentum distribution $n(p_\perp)$ (or energy distribution $n(E_\perp)$) perpendicular to the layers *directly from the measured resonant tunneling collector current, without requiring the use of derivative techniques*. Figure 1 illustrates the band diagrams of two structures for resonant tunneling electron spectroscopy. The first one (Fig. 1a), realized by us in the present experiment, consists of a reverse biased pn heterojunction and can be used to investigate hot minority carrier transport. Incident light is strongly absorbed in the wide-gap p^+ layer. Photo-generated minority carrier electrons diffuse to an adjacent low-gap layer. Upon entering this region electrons are ballistically accelerated by the abrupt potential step and gain a kinetic energy $\cong \Delta E_c$. Collisions in the low gap layer tend to randomize the injected, nearly mono-energetic distribution, making it "hot". Hot electrons subsequently impinge on the double barrier in the collector. From simple considerations of energy and lateral momentum $p_\perp$ in the tunneling process[2] it can be shown that only those electrons with a perpendicular energy $p_\perp^2/2m_e^*$ equal (within the resonance width) to the energy of the bottom of one of the subbands (i.e., a resonance) of the quantum well, resonantly tunnel through the quantum well and give rise to a current. Thus by varying the applied bias (i.e., changing the energy difference between the resonance of the quantum well and the bottom of the conduction band in the low gap p^+ layer) and measuring the current, one directly probes the electron energy distribution $n(E_\perp)$ or equivalently the momentum distribution $n(p_\perp)$ (Fig. 2). Thermionic currents can be minimized by appropriate choice of the double barrier and low temperature. Identical arguments apply to the unipolar transistor structure of Fig. 1b. The structures were grown by MBE and consist of p^+n heterojunctions. Their band diagram is shown in Fig. 1a at a given reverse bias.

---

* On leave from the Institute of Radio Physics and Electronics. University of Calcutta, Calcutta-700009, India.

The growth starts with a buffer layer followed by an undoped 5000 Å GaAs layer and an AlAs/GaAs/AlAs double barrier, with barrier and well thicknesses 20 Å and 80 Å respectively. The parameters of the double barrier were chosen in such a way that over the applied voltage range (0-10V) the electron energy distribution is probed by only one resonance at a time. In this way at any given bias the current is due to resonant tunneling through a single resonance. For our double barrier the first resonance is at $E_1 = 60$ meV from the well bottom and the second at $E_2 = 260$ meV. A 20 Å undoped GaAs spacer layer separates the double barrier from the p^+ ($= 3x10^{18}cm^{-3}$) GaAs layer. Different thicknesses were used for this region (250 Å , 500 Å , 1000 Å) while keeping everything else the same. The last layer consists of 2 μm thick $Al_{0.3}Ga_{0.7}As$ doped to $p = 3x10^{18}cm^{-3}$. Fig. 3 illustrates the measured photocurrent for a p^+ GaAs layer thickness of 500 Å . Two distinct features are present at 1.2 V and 7 V respectively. One can easily show that the first peak corresponds to electrons with perpendicular energy of a few tens of meV ($\simeq$ 17 meV) that have resonantly tunneled through the first resonance of the quantum well. The second peak, clearly visible only at the lowest temperature, is much broader and corresponds to incident electrons with energy $E_\perp \simeq 122$ meV which have resonantly tunneled through the second resonance of the well. It is therefore clear that the energy distribution of the electrons in the p^+ GaAs layer, following high energy injection (0.233 eV, i.e. the conduction band discontinuity between GaAs and the $Al_{0.37}Ga_{0.7}As$) consists of two parts. One is strongly thermalized, with energies close to the bottom of the conduction band, while the other one is much hotter. Thus the distribution is strongly non-maxwellian similar to what has been found, by conventional electron spectroscopy, in the case of majority carrier electrons in the base of hot electron transistors[1]. Detailed analysis of the data for different p^+ GaAs layer thickness also show that the scattering time for energetic electrons ($\simeq$ 0.2 eV) injected in p^+ ($3x10^{18}cm^{-3}$) GaAs is very short ($\simeq 10^{-14}$ sec). This implies that it will be extremely difficult to implement a ballistic bipolar transistor.

REFERENCES

1. For a review see J. R. Hayes and A. F. J. Levi, IEEE J. Quantum Electron. *QE-22*, 1744 (1986).

2. S. Luryi, Appl. Phys. Lett. *47*, 490 (1983).

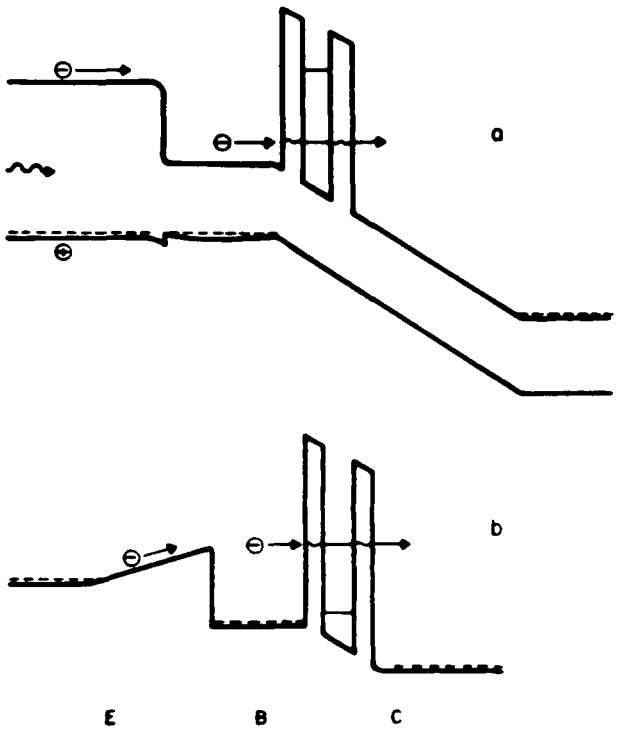

Fig. 1 a. Band diagrams of structure used for resonant tunneling spectroscopy (RTS) of hot minority carrier electrons.

b. Unipolar transistor structure for RTS of hot majority carrier electrons in the base layer.

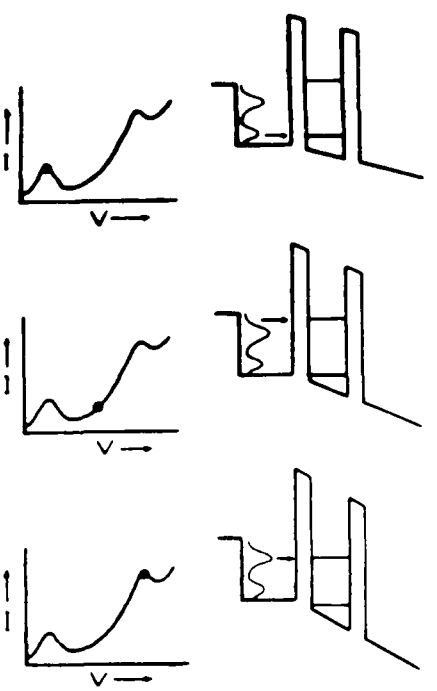

Fig. 2 Schematics of RTS. By measuring the current as a function of reverse bias (left) one directly probes the energy distribution perpendicular to the layers $n(E_\perp)$ (right).

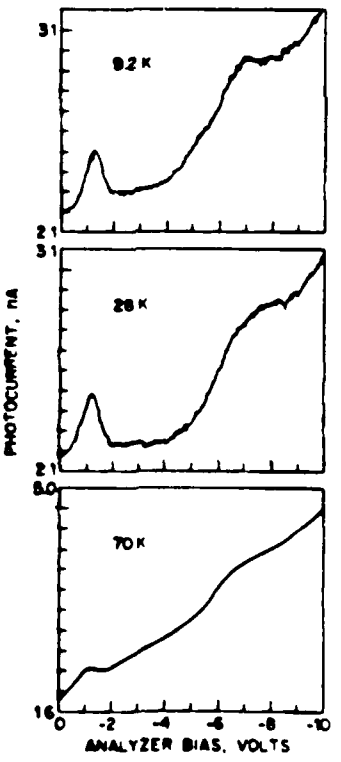

Fig. 3 Photocurrent vs reverse bias voltage of the structure of Fig. 1a with a low gap GaAs p^+ layer of thickness = 500 Å. The wavelength of the incident light is 6328 Å.

NOTES

THURSDAY, JANUARY 15, 1987

PROSPECTOR/RUBICON ROOM
9:00 P.M.

ThD

POSTDEADLINE PAPERS

NOTES

FRIDAY, JANUARY 16, 1987

PROSPECTOR/RUBICON ROOM
8:00 A.M.–9:30 A.M.

FA1–4

QUANTUM-WELL PHYSICS AND DEVICES

C. Weisbuch, Thomson CSF, *Presider*

High-Speed Phenomena in GaAs Multiple-Quantum-Wells

A. Mysyrowicz,* D. Hulin,* A. Migus and A. Antonetti
ENSTA, LOA, Ecole Polytechnique
Palaiseau, France 91120

and

H. M. Gibbs and N. Peyghambarian
Optical Sciences Center, University of Arizona
Tucson, Arizona 85721

and

H. Morkoc
Coordinated Science Laboratory
University of Illinois at Urbana-Champaign
Urbana, Illinois 61801

Type I quantum-well structures are promising candidates as active devices in fast optoelectronics. Because of the forced confinement of electrons and holes in the same layer, pronounced excitonic structures are observed up to room temperature, even in materials with small bulk exciton binding energy. Optically induced changes of such excitonic structures lead to the large and very rapid nonlinearities required in device applications. We describe here some of the underlying physical processes. The discussion is restricted to the case of GaAs quantum wells, with the accent put on those effects affecting the lowest (heavy-hole) exciton resonance on a picosecond or subpicosecond time-scale.

In general, optical injection of electron-hole pairs can lead to a broadening, a shift and a bleaching of the exciton line. Little is known about collision broadening in quantum wells. Some information may be inferred from a recent study in bulk GaAs by Schultheis et al.[1] Large collision efficiencies $\gamma_{xx} \approx 1.6\times10^{-4}cm^3sec^{-1}$ and $\gamma_{xeh} 1.6\times10^{-3}cm^3sec^{-1}$ were found for exciton-exciton and exciton-free carrier scattering, respectively, leading to relaxation times of the order 10^{-12} sec at moderate electron-hole pair densities $n \gtrsim 10^{15}cm^{-3}$. Inhomogeneous broadening from localized excitons complicates the problem in GaAs quantum wells. A dephasing time $T_2 \sim 10^{-11}$ - 10^{-12} has been reported by Hegarty and Sturge,[2] with indication of a rapid decrease of T_2 under increasing excitation intensity.

*Also at Ecole Normale Superieure, Paris, France

A shift of the exciton resonance to higher energy induced by resonant optical pumping has been observed in GaAs quantum wells.[3,4] This new effect depends sensitively upon the well size, being clearly apparent only in wells with thickness of d<100Å .[5] Its origin lies in the hard core repulsive interaction between excitons at short distances, due to the Pauli principle acting on carriers of the same charge. Since the exciton blue shift occurs in the presence of other excitons in a high density regime, it allows one to monitor the dynamics of either electron-hole pairing or dissociation. For example, injection of an initial hot distribution of free carriers in a cold lattice leads to a delayed appearance of the blue shift signaling that the plasma has reached the required conditions for a Mott-like transition. Conversely, injection of an initial excess population of cold excitons in a warm lattice leads to an instantaneous blue shift, which, however, lasts for less than 10^{-12} sec, corresponding to the exciton lifetime limited by thermal dissociation.

Exciton bleaching provides the most dramatic nonlinearity. Two distinct physical processes can be responsible for it. The first is the usual screening of the attractive Coulomb interaction in an electron-hole pair by charged carriers (Debye-screening). This effect follows the injection of free carriers instantaneously with a response time less than 50 fs and is relatively insensitive to the carrier energy distribution.[3,6] The other mechanism is the saturation of the Bloch valence and conduction states available for exciton formation as well as the short range exchange interaction between electrons (holes). In quasi 2-dimensional structures, this second process can become more important than the long-ranged Debye screening if the electron-hole pairs have very low effective temperatures.[7] This leads to unusual effects such as fast transient bleaching of excitons observed by Knox et al.[8] This bleaching always accompanies the blue shift since both effects have their origin in the Pauli exclusion principle.[5,7]

Finally, by irradiating GaAs quantum wells with light falling in the transparency region well below the lowest exciton, it is possible to induce an optical Stark effect.[9,10] This effect is particularly interesting for applications since it follows the input pulse and, therefore leads to ultrafast switch-on and switch-off times. A theoretical treatment has been developed recently which accounts well for the observed behavior.[11]

REFERENCES

1. L. Schultheis, J. Kuhl, A. Honold, and C. W. Tu, *Phys. Rev. Lett.* 57, 1797 (1986).
2. J. Hegarty and M. D. Sturge, *JOSA* **B2**, 1143 (1985)
3. N. Peyghambarian, H. M. Gibbs, Y. L. Jewell, A. Antonetti, A. Migus, D. Hulin, and A. Mysyrowicz, *Phys. Rev. Lett.* **53**, 2433 (1984).
4. Y. Masumoto, S. Tarucha, and H. Okamoto, *J. Phys. Soc. Jap.* **55**, 57 (1984).
5. D. Hulin, A. Mysyrowicz, A. Antonetti, A. Migus, W. T. Masselink, H. Morkoc, H. M. Gibbs, and N. Peyghambarian, *Phys. Rev.* **B33**, 4389 (1986).
6. W. H. Knox, C. Hirlimann, D. A. B. Miller, J. Shah, D. S. Chemla, and C. V. Shank, *Phys. Rev. Lett.* **56**, 1191 (1986).
7. S. Schmitt-Rink, D. S. Chemla, and D. A. B. Miller, *Phys. Rev.* B32, 6601 (1985).
8. W. H. Knox, R. L. Fork, M. C. Downer, D. A. B. Miller, D. S. Chemla, and C. V. Shank, *Phys. Rev. Lett.* **54**, 1306 (1986).
9. A. Mysyrowicz, D. Hulin, A. Antonetti, A. Migus, W. T. Masselink, and H. Morkoc, *Phys. Rev. Lett.* **56**, 2748 (1986).
10. A. von Lehmen, D. S. Chemla, and J. E. Zucker, J. P. Heritage, to appear.
11. S. Schmitt-Rink and D. S. Chemla, to appear.

FA2-1

PICOSECOND CARRIER TRANSPORT IN GaAs QUANTUM WELLS

Jagdeep Shah and R. A. Hopfel*
AT&T Bell Laboratories
Holmdel, N. J. 07733
U. S. A.

We review three recent experiments in which we have used picosecond optical techniques to investigate quantities relevant to high field transport in semiconductors. We will discuss (1) measurement of the drift velocity of minority carriers in GaAs quantum wells by a time-of-flight technique, (2) a simultaneous measurement of the luminescence spectra which allows us to measure the carrier distribution function and investigate the energy exchange rate between electrons and holes and (3) an optical imaging experiment which demonstrates the existence of negative absolute mobility for the minority carrier in modulation-doped quantum wells. The momentum scattering rate between electrons and holes is determined form this experiment.

1. DRIFT VELOCITY BY TIME-OF-FLIGHT TECHNIQUE: Time-of-flight techniques provide a direct means of determining carrier drift velocities in semiconductors [1]. We have determined the drift velocity of minority electrons in p-modulation doped quantum wells as a function of electric field up to 14 kV/cm [2,3]. Minority electrons were injected with a 5 psec pulse from a synchronously pumped, cavity-dumped dye laser operating at 6,200Å. High fields were applied parallel to the layers of the quantum wells with the sample mounted on a microwave stripline to permit fast measurements (system response <50 psec). The photoinjected minority electrons gave essentially a square-topped photocurrent pulse (insert of Fig. 1(a)) from which the electron drift velocity was determined directly. The drift velocity of electrons determined in this manner is plotted in Fig. 1(a). The most interesting feature of the data is that the drift velocity shows a distinct negative differential behavior. Secondly, the low field drift mobility is approximately a factor of five smaller than the typical values for electron mobility in n-modulation doped quantum wells. We attribute the lower value observed to momentum scattering between photoexcited electrons and the majority holes in our sample.

2. ELECTRON-HOLE ENERGY EXCHANGE RATE: In order to understand the observed negative differential mobility, we have made a direct measurement of the electron temperature by measuring the luminescence spectra under the influence of applied electric field. We find [3] that the electron temperature increases with electric field (Fig. 1b) to about 650 K. We have argued that this value is too low for transfer to higher valleys in GaAs and that the observed negative differential mobility arises as a result of real-space transfer to the barrier layers [3]. The hole temperatures, estimated on the basis of the measured I-V curve as well as from the known [4] hole energy loss rates to the lattice [5], are considerably lower than the electron temperatures. In this case, we expect a net flow of energy from electrons to the holes. We plot in Fig. 2 the inverse of the electron temperature as a function of power loss into the lattice (which, in this steady state conditions is equal to the power input from the electric field to the electrons). We compare [5] this with the expected energy loss rate from electrons into the lattice and find that (Fig. 2) the measured energy loss rate is larger than that expected by about a factor of 2. We attribute this difference to energy exchange between electrons and holes. This is supported by a calculation of energy exchange rate between electrons and holes from a simple gas plasma model [5]. While more elaborate calculations more appropriate to the semiconductor case are needed, these measurements provide the first estimate of electron-hole energy exchange rates.

* Present Address: Institut für Experimentalphysik, Universität Innsbruck, A-6020 Innsbruck, Austria

3. NEGATIVE ABSOLUTE MOBILITY OF MINORITY CARRIERS: We describe in this section an unusual manifestation of momentum scattering between electrons and holes in a semiconductor [6]. Minority electrons were photoexcited in a p-modulation doped quantum well sample with a tightly focused (diameter 3 micron) picosecond laser. The sample was mounted in variable temperature cryostat (lowest temperature 15 K). Since luminescence occurs only where the minority electrons are present, the motion of the electrons under the applied electric field can be monitored by measuring where the luminescence originates. We have done this by imaging the sample on a plane and scanning a narrow slit across this plane to measure the image of the time-integrated luminescence. Two typical scans are shown as the insert in Fig. 3. At 15 K the luminescence shifts towards the negative electron; i.e. the minority electrons have a negative absolute mobility at low temperatures! The negative drift decreases with increasing temperature and the drift becomes positive above about 90 K as shown for the 150 K curve in the insert.

The negative drift of electrons is a consequence of the momentum scattering between electrons and holes via Coulomb interaction. The holes in our high mobility samples interact strongly with electrons and drag the electrons with them to the negative electrode. Such an effect was first predicted for the case of In5b by McLean and Paige [7] but has not been observed in any system until now to our knowledge. We have used a relaxation time approximation to the Boltzman equation to analyze this case and found that [6] under certain simplifying assumptions, the electron mobility is given by subtracting the hole mobility from the mobility of electrons due only to electron-hole scattering. The latter quantity can be approximated by mobility due to electron-ionized impurity scattering. In Fig. 3 we have plotted the measured electron mobility as a function of the lattice temperature and compared it with the difference between electron-ionized impurity (for appropriate impurity density) and the measured hole mobility in our sample. We see that the simple theory gives a good agreement with the observations. From these measurements, we deduce a momentum scattering time of approximately 50 fsec for electrons in a hole plasma of areal density $1.5 \times 10^{11} cm^{-2}$ per layer. Recently, we have also observed negative absolute mobility for minority holes in n-modulation doped samples [8] and find that the momentum scattering time for holes in an electron gas is considerably longer.

In summary, time- and spatially resolved luminescence, as well as picosecond photoconductivity, in high electric fields provide excellent tools for studying carrier drift velocities and energy distribution functions in materials and systems relevant for high speed electronics. Using these techniques, we have investigated drift velocities, distribution functions and electron-hole (momentum and energy) scattering rates in GaAs quantum wells.

REFERENCES

[1] L. Reggiani, in "Physics of Nonlinear Transport in Semiconductors", edited by D. K. Ferry, J. R. Barker and C. Jacobani, Plenum Press; pp. 243-254 (1980).

[2] R. A. Hopfel, Jagdeep Shah, A. C. Gossard and W. Wiegmann, Physica 134B, 509 (1985).

[3] R. A. Hopfel, Jagdeep Shah, D. Block and A. C. Gossard, Appl. Phys. Lett. 48, 148 (1986).

[4] Jagdeep Shah, A. Pinczuk, A. C. Gossard, and W. Wiegmann, Phys. Rev. Lett. 54, 2045 (1985).

[5] R. A. Hopfel, Jagdeep Shah and A. C. Gossard, Phys. Rev. Lett. 56, 765 (1986).

[6] R. A. Hopfel, Jagdeep Shah, P. A. Wolff and A. C. Gossard, Phys. Rev. Lett. 56, 2736 (1986).

[7] T. P. McLean, and E. G. S. Paige, J. Phys. Chem. Solids 16, 220 (1960).

[8] R. A. Hopfel, Jagdeep Shah, P. A. Wolff and A. C. Gossard, Appl. Phys. Lett., 49, 572 (1986).

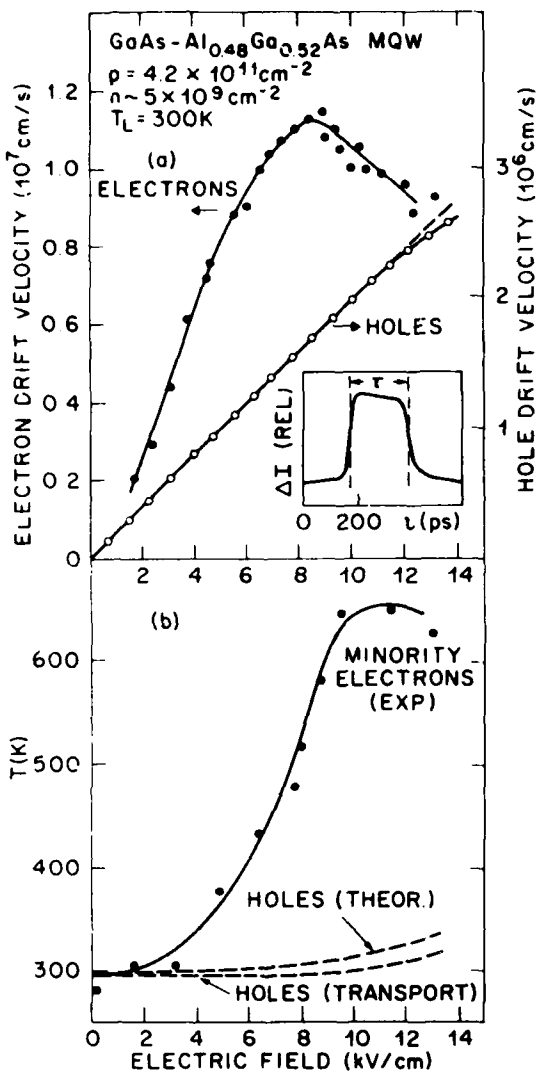

Fig. 1 (a) Electron drift velocity in p-GaAs quantum wells measured by picosecond time-of-flight technique and hole drift velocity from I-V measurements. The inset shows the photocurrent pulse from which drift velocity is determined. (b) Electron temperature as a function of applied electric field deduced from luminescence measurements and hole temperatures as discussed in text.

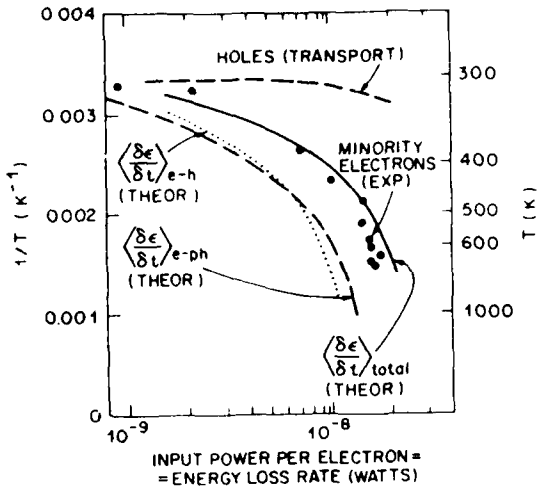

Fig. 2 Inverse of electron temperature vs. electron energy loss rate; circles are experimental and curves are calculated for different scattering mechanisms.

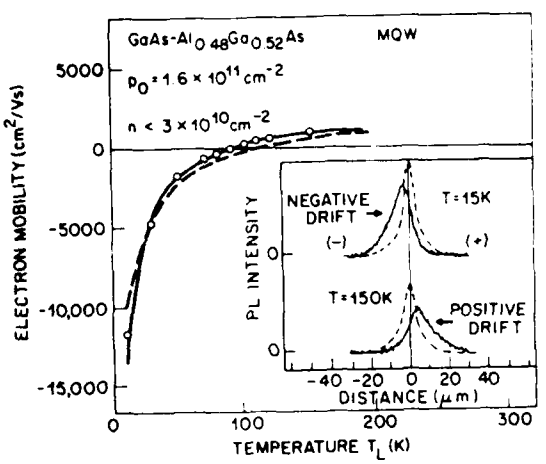

Fig. 3 Minority electron mobility as a function of lattice temperature; the points are experimental and the curve is a comparison with theory. The inset shows the luminescence images, showing negative drift at 15 K and positive drift at 150 K.

Quantum-Confined Stark Effect in InGaAs/InP Quantum Wells Grown by Metal-Organic Chemical Vapor Deposition

I. Bar-Joseph, C. Klingshirn*, D. A. B. Miller, D. S. Chemla,

U. Koren, and B. I. Miller

AT&T Bell Laboratories, Holmdel, N. J.

Multiple quantum well (MQW), composed of alternate very thin layers of two different semiconductors, show unusual optical properties at room temperature. One effect of particular recent interest is the quantum-confined Stark effect (QCSE) [1]. In the QCSE, electric fields applied perpendicular to the MQW layers can shift the optical absorption edge to lower photon energies with the exciton absorption peaks remaining clearly resolved. This electroabsorptive effect has been applied to make small, high-speed optical modulators [2] and optical switching and signal-processing devices [3] in GaAs/GaAlAs MQW.

Perpendicular-field electroabsorption at longer wavelenghts (i.e. $\lambda \sim 1.5\mu m$) has recently been studied in InGaAs and in GaSb MQW. The GaSb wells show relatively clear shifts of the exciton peaks with field[4], but the substrate is opaque at the wavelengths of interest for optical communication. The electroabsorption spectra of InGaAs MQW so far reported [5] only show a large broadening of the peaks with field, and relatively little clearly-resolved shift. Such broadened peaks are of limited interest for applications.

In this paper we report the first observation of the QCSE in InGaAs quantum wells with InP barriers, in material grown by metal-organic chemical vapor deposition (MOCVD). In contrast to previous InGaAs MQW results, the exciton peaks remain well resolved up to very large fields at room temperature.

The sample structure is shown in the insert of Fig. 1. The MQW form the intrinsic region of a p-i-n diode, and consist of 100 periods of alternate InGaAs wells and InP barriers, each 100 Å thick. The sample is processed to form rectangular mesas with gold contacts as shown in the figure. Room temperature absorption spectra at 0V and 30V are shown in Fig. 1. In the absence

of applied voltage one can clearly distinguish the n_z=1 heavy (hh) and light (lh) hole exciton peaks as well as a strong resonance at the n_z=2 transition edge. The 30V spectrum shows the dramatic changes produced by the electric field. The n_z=1 hh-exciton is strongly red-shifted while the n_z=1 lh and n_z=2 transitions present less pronounced shifts. A new feature appears around 0.84 eV. It is located close to the calculated n_z=2 hh to n_z=1 electron "forbidden" transition, which becomes allowed in the presence of the field.

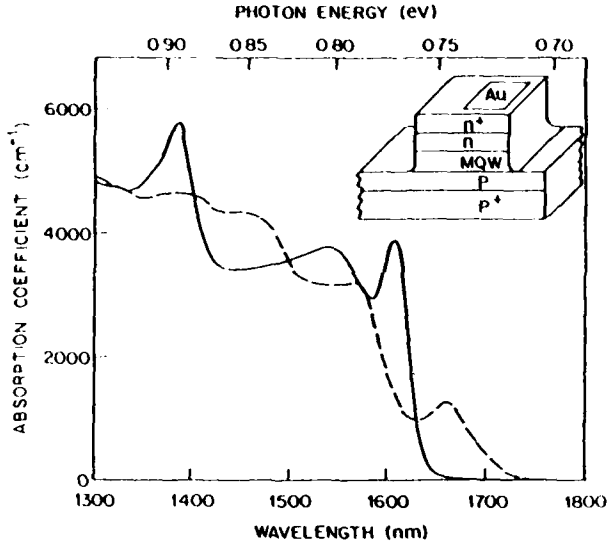

Figure 1: Room temperature absorption spectra at 0V (solid line) and 30V (dashed line). The sample structure is shown in the insert.

In Fig. 2 we present the absorption and photocurrent spectra close to the n_z 1 transitions, for four applied voltages. This is the region of interest for applications to optical modulation. The photocurrent spectra closely follow that of the absorption, although the features are less pronounced. The shift of the n_z=1 hh absorption peak was compared with the theory[1], and very good agreement was found.

The large changes in the absorption spectrum reported here clearly indicate that light modulators made of InGaAs/InP MQW can be constructed. The optical absorption length which can be electrically induced is $\sim 5\mu m$. This length can be further decreased by reducing the barrier width, thus incorporating more active quantum wells in a given thickness.

Alternatively, waveguide modulators with only a few quantum wells may give increased modulation depth and reduce the driving voltage[6]. Self electro-optic effect device operation based on photocurrent feedback is also likely with this material system, as in GaAs MQW[3], offering other optical switching and modulation devices. with this material system. In addition, since the InP substrate is transparent at the wavelengths of interest, these findings are promising for modulators and optical switching devices that will be directly compatible with optical fiber communications.

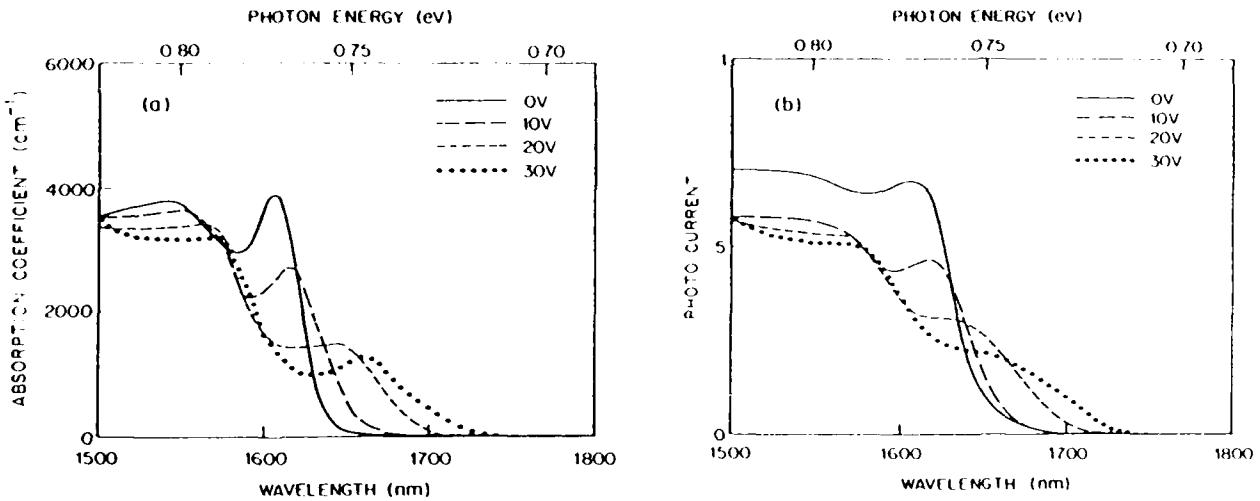

Figure 2:Absorption (a) and photocurrent (b) spectra in the vicinity of the $n_z=1$.

Acknowledgements: We thank J. E. Henry for her help in processing the samples.

*Permanent address: Physikalisches Institute der Universität, D 6000 Frankfurt am Main

[1] D. A. B. Miller, D. S. Chemla, T. C. Damen, A. C. Gossard, W. Wiegmann, T. H. Wood, and C. A. Burrus, Phys. Rev. **32**, 1043 (1985)

[2] T. H. Wood, C. A. Burrus, D. A. B. Miller, D. S. Chemla, T. C. Damen, A. C. Gossard, and W. Wiegmann, Appl. Phys. Lett. **44**, 16 (1984)

[3] D. A. B. Miller, D. S. Chemla, T. C. Damen, T. H. Wood, C. A. Burrus, A. C. Gossard, and W. Wiegmann, IEEE J. Quantum Electron **QE-21**, 1462 (1985).

[4] T. Miyazawa, S. Tarucha,Y. Ohmori, and H. Okamoto, 2nd Int. Conf Modulated Semiconductor Struct., Kyoto, Japan, Sept. 1985.

[5] K. Wakita, Y. Kawamura, Y. Yoshikuni, H. Asahi, and S. Uehara, IEEE J. Quantum Electron. **QE-22**, 1831 (1986)

[6] J.S. Weiner, D. A. B. Miller, D. S. Chemla, T. C. Damen, C. A. Buurus, T. H. Wood, A. C. Gossard and W. Wiegmann, App. Phys. Lett. **47**, 1148 (1985).

Alternatively, waveguide modulators with only a few quantum wells may give increased modulation depth and reduce the driving voltage[6]. Self electro-optic effect device operation based on photocurrent feedback is also likely with this material system, as in GaAs MQW[3], offering other optical switching and modulation devices. with this material system. In addition, since the InP substrate is transparent at the wavelengths of interest, these findings are promising for modulators and optical switching devices that will be directly compatible with optical fiber communications.

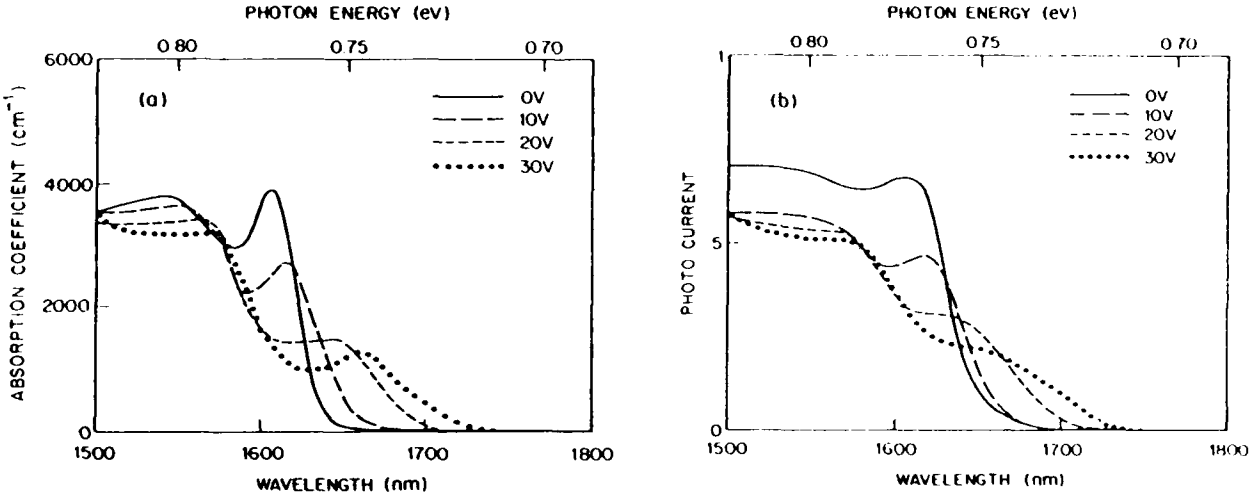

Figure 2:Absorption (a) and photocurrent (b) spectra in the vicinity of the n_z 1.

Acknowledgements: We thank J. E. Henry for her help in processing the samples

*Permanent address: Physikalisches Institute der Universität, D 6000 Frankfurt am Main

[1] D. A. B. Miller, D. S. Chemla, T. C. Damen, A. C. Gossard, W. Wiegmann, T. H. Wood, and C. A. Burrus, Phys. Rev. **32**, 1043 (1985)

[2] T. H. Wood, C. A. Burrus, D. A. B. Miller, D. S. Chemla, T. C. Damen, A. C. Gossard, and W. Wiegmann, Appl. Phys. Lett. **44**, 16 (1984)

[3] D. A. B. Miller, D. S. Chemla, T. C. Damen, T. H. Wood, C. A. Burrus, A. C. Gossard, and W. Wiegmann, IEEE J. Quantum Electron **QE-21**, 1462 (1985)

[4] T. Miyazawa, S. Tarucha,Y. Ohmori, and H. Okamoto, 2nd Int. Conf. Modulated Semiconductor Struct., Kyoto, Japan, Sept. 1985

[5] K. Wakita, Y. Kawamura, Y. Yoshikuni, H. Asahi, and S. Uehara, IEEE J. Quantum Electron **QE-22**, 1831 (1986)

[6] J.S. Weiner, D. A. B. Miller, D. S. Chemla, T. C. Damen, C. A. Burrus, T. H. Wood, A. C. Gossard and W. Wiegmann, App. Phys. Lett. **47**, 1148 (1985)

Dynamics of Below-Gap Photoexcitation in GaAs Quantum Wells

J.E. Zucker[•], A. VonLehmen[+], D.S. Chemla[•], J.P. Heritage[+]

[•] AT&T Bell Laboratories, Holmdel, New Jersey 07733
[+] Bell Communications Research, Red Bank, New Jersey 07701

1. Introduction

We have identified several physical processes by which below-gap photons can modify excitonic absorption in GaAs quantum wells.[1-3] These different phenomena can be distinguished by their temporal response times, which range from tens of nanoseconds to less than one picosecond. Our experiments also show that the relative contributions of these mechanisms to below-gap optical modulation of exciton absorption depend strongly on temperature as well as on the wavelength of the below-gap modulating beam. The size of the modulation indicates that a new class of absorptive and dispersive devices for optical signal processing is possible in which signals propagate in the transparent region of the crystal and experience negligible attenuation. In order to successfully interpret and calculate the magnitude of these exciting new effects, we show that it is necessary to take into account the special properties of two-dimensional excitons in semiconductor quantum wells.

2. Experiment

A differential technique (described elsewhere)[1] is used to monitor the changes in transmission of a weak probe laser induced by a below-gap pump laser. The probe is tuned near the n=1 heavy hole exciton resonance. The pump beam is tuned below the bandedge as far as 60 meV from resonance and ranges in intensity from 10^3 to 10^6 Watts/cm^2. Pump and probe pulsewidths are 6 psec with 6.7 Mhz rep rate and 10 psec cross- correlation. Quantum well samples are mounted on sapphire substrates in a cold finger and cooled to temperatures 70-300K.

3. Free Carrier Bleaching of the Exciton via Phonon-assisted Absorption

We have found that photoexcitation of GaAs quantum wells far below the bandege can produce a marked decrease in exciton absorption which persists for 20-30 nsec. The timescale of this phenomenon is indicative of a free carrier effect. However, in order to produce bleaching of the exciton absorption, carriers are required to be near or at the bandedge.[4] The dynamical process which links absorption of a photon in the transparent region of the crystal to a free carrier at the bandedge is the key step in this type of below-gap modulation.

Our recent measurements are the first to reveal that the process by which carriers are generated at the bandedge is phonon-assisted absorption. The temperature dependence of the effect shows that the magnitude of the change in transmission induced by below-gap photoexcitation is directly proportional to the number of optical phonons present. The participation of optical phonons is even more apparent in the dependence of the bleaching efficiency on pump photon energy, shown in Fig.1. The most prominent feature occurs at 1.513 eV,nearly one longitudinal optic (LO) phonon energy below the exciton resonance. The dashed line represents a calculation of the one-phonon-assisted absorption spectrum which has been modified to include the effects of reduced dimensionality in the quantum well. We find it necessary to take into account both the two-dimensional density of electronic states and the two-dimensional exciton-LO phonon Frohlich interaction. The calculated values for the absorption coefficient contain no adjustable parameters and are in good agreement with the data. The contributions of zero-phonon and two-phonon- assisted

processes to the spectrum, which are not included here, should further improve the agreement between theory and experiment.

4. AC Stark Shift of the Exciton Transition

At low temperature, the value of the absorption coefficient in the bandtail of the quantum well becomes small: in Fig. 1 α is between 0.1 and 10 cm^{-1}. At such low absorption, very few real carriers are created and we find that a new phenomenon appears in the differential transmission spectrum (Fig.2). The increase in probe transmission which is nearly constant for 200 psec after the pump pulse is associated with the free carrier bleaching discussed above. The new feature is the extremely fast increase in probe transmission, which rises and falls within the pump- probe correlation time. As shown in Fig.2, this ultrafast component increasingly dominates the free-carrier bleaching effect as the pump wavelength is detuned from the exciton resonance.

Further contrast between the sub-picosecond and nanosecond effects of below gap photoexcitation are displayed in Fig.3. For a constant pump detuning of 31 meV from the exciton resonance, both fast (fig.3b) and slow (3c) components change in magnitude and sign depending on which part of the exciton absorption feature (3a) is probed. However the lineshapes are completely different. The change in transmission shown in Fig. 3c reflects a broadening and flattening of the absorption peak by free carrier bleaching, symmetric with respect to line center. On the other hand, the asymmetric lineshape shown in Fig. 3b is consistent with a blue shift of the entire exciton absorption line by 0.2 meV. We have interpreted this ultrafast shift in terms of an AC Stark shift of the quantum well exciton transition induced by the optical field of the below-gap laser.

The AC Stark shift is well-known in atoms, where it can be viewed as a dressing of the atomic levels by the pump photons. Although it is possible to carry over the model of the atomic AC Stark shift to the case of excitons in a solid, the calculation requires several ad hoc assumptions in order to arrive at the correct magnitude of the shift. The failure of the "dressed exciton" approach is due to the nature of energy levels in a solid. Each pair of vertical transitions between conduction and valence band can be regarded as a two level system. However these two-level systems all interact and in fact their interaction (via Coulomb forces) is responsible for formation of the exciton. Thus in the presence of a strong external field there exists, in addition to the shift of each level in the field, a change in the interaction between levels. These two effects must be calculated self consistently and both contribute to the shift of the exciton resonance measured by a weak probe beam. Assuming that only 1s excitons participate and in the limit of low intensity, the theory predicts[5] a Stark shift

$$\delta E = \frac{2|\mu_{cv}E_p|^2|U_{1s}(r=0)|^2}{(E_{1s}-\hbar\omega_p)N_s^{PSF}}$$

where E_p is the optical electric field of the pump, μ the dipole moment between conduction and valence band, $\hbar\omega_p$ the pump photon energy, and E_{1s} the exciton transition energy in the absence of E_p. The exciton envelope function U_{1s} and the phase space filling saturation density N_{PSF}[6] are defined in Ref. 4. We have experimentally verified the functional form given above: we find that the shift is proportional to the intensity (E_p^2) and that it varies inversely with the detuning from resonance. Moreover the calculated magnitude of the shift $\delta E = 0.15$ meV is in excellent agreement with the data shown in Fig.3 and is obtained with no adjustable parameters.

[1] A Von Lehmen, J E Zucker, J P Heritage, D S Chemla, A C Gossard, Appl Phys Lett 48 1479 (1986)

[2] A Von Lehmen, J E Zucker, J P Heritage, D S Chemla Proceedings XIV International Quantum Electronics Conference, PD18 1 (1986)

[3] A Von Lehmen, D S Chemla, J E Zucker, J P Heritage, to be published in Optics Letters, October 1986

[4] S Schmitt Rink, D S Chemla and D A B Miller Phys Rev B [illegible] (1985)

[5] S Schmitt Rink and D S Chemla, to be published

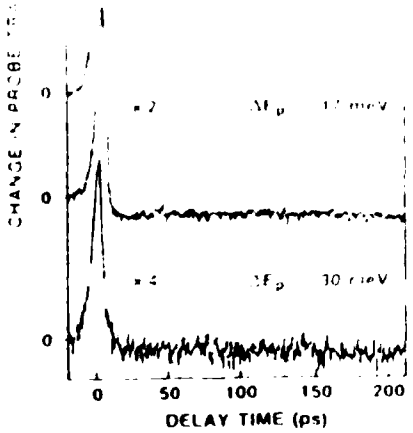

[illegible] change in probe transmission as a function of the time delay between pump and probe. As the detuning is increased the fast component due to the AC Stark shift dominates the slow component associated with free carrier bleaching of the exciton.

Fig. 3 a)Unperturbed transmission showing n=1 heavy (hh) and light (lh) hole excitons. b) and c)Percent change in probe transmission induced by 10^6 Watts/cm^2 pump 31 meV below the n=1 hh transition. (b) zero pump-probe delay; (c) delay = 100 psec.

FRIDAY, JANUARY 16, 1987

PROSPECTOR/RUBICON ROOM
10:00 A.M.–11:45 A.M.

FB1–5

OPTICAL MICROWAVE TECHNIQUES

R. Olshansky, GTE Laboratories, *Presider*

Radar and EW Applications of Multi-Gigahertz Optical Components and Systems

Henry F. Taylor
Department of Electrical Engineering
Texas A & M University
College Station, TX 77843

Recent advances in wideband components for use in optical fiber systems have been very impressive. Laser diodes have shown 3dB modulation bandwidths near 20 GHz at room temperature,[1,2] and external modulators with similar high-frequency performance have been reported.[3] Bandwidths as high as 100 GHz have been achieved in semiconductor photodiodes.[4] Performance of these components at such high frequencies opens a new realm of possibilities for the use of optics in military systems. These include not only signal transmission over optical fibers, but also signal generation, signal processing, and optical control of microwave devices. Coverage spanning the 0 – 18 GHz range, where most radar and electronic warfare (EW) systems operate, is now possible. Some of these techniques can also be applied in the millimeter wave frequency range (> 30 GHz), which is receiving increased emphasis for military applications.

Optical fibers provide an attractive alternative to metallic waveguides for signal transmission in many microwave systems. The fibers are small, flexible, relatively inexpensive, and have enormous information capacity. For example, a single mode fiber with a source wavelength near the dispersion minimum can carry a signal with a 20 GHz bandwidth for distances up to 50 km. The fibers can also be used in signal processing systems for the delay and storage of wideband signals, providing time-bandwidth products in excess of 10^4 vs. 10^3 – 10^4 for conventional acoustic-wave delay lines.[5] A recirculating fiber delay line for a radar moving-target indicator is an example of an application where storage of wideband analog signals for long time periods is needed.[6] The use of integrated optic switches in conjunction with single-mode fiber has been suggested as a way of rapidly rapidly varying the delay time over a wide range of possible values.[7] The tapped delay line signal processor, or transversal filter, can be designed for use as a bandpass or matched filter, or as a waveform generator. Several fiber optic versions of a transversal filter have been demonstrated.[5] To date, however, no suitable method has been devised for providing the large numbers (e.g., hundreds) of taps needed for many applications.

Several optical techniques for the generation of microwave signals have been investigated. One method involves the excitation of a photoconductive stripline gap with picosecond optical pulses.[8,9] A second utilizes illumination of a microwave p-i-n diode in a resonant circuit with the light from a directly modulated semiconductor laser. [10] In that case, a signal at the third harmonic of the laser modulation was obtained at 10.2 GHz. A third technique utilizes injection locking to sidebands of a modulated master laser. Two different slave lasers, or two different longitudinal modes of a single slave laser, are locked

to different sidebands of the master laser. In this manner a signal at 35 GHz with a spectral width of less than 10 Hz was obtained.[11]

The frequency and phase of a microwave oscillator can be controlled by injection locking with a modulated optical carrier. Numerous demonstrations of this have been carried out at frequencies as high as 10 GHz.[10-12,13] For FET oscillators the light can be directly coupled into the gate region of the active device, but for IMPATT oscillators obtaining optical access to the active region generally requires a redesign of the package. One of the attractive features of direct optical locking is that it makes possible the use of fibers to transmit local oscillator signals to remotely located elements in phased-array radars and direction-finding systems without the need for separate optical receivers.

Some other uses of optics in microwave systems should also be mentioned. Bulk acoustooptic spectrum analyzers based on Bragg diffraction of a light beam are capable of processing analog signals with gigahertz bandwidths. Analog-to-digital conversion of wideband signals using the electrooptic effect in an optical waveguide device has been achieved.[14] Phase-shifters for microwave devices can be made by illuminating a photosensitive dielectric waveguide with a CW light beam.[5]

In conclusion, optical techniques are reaching the point of utility in military radar and electronic warfare systems. Transmission, generation, control, and processing of signals in 0 18 GHz and 35 GHz frequency regimes are possible using present technology. Expansion of research in this field appears certain, with emphasis on establishing the systems utility of some of these techniques and extending them to other spectral regions of interest (e.g. 60 and 94 GHz).

References

1. C.B. Su, V. Lanzisera, W. Powazinik, E. Meland, R. Olshansky, and R.B. Lauer, Appl. Phys. Lett. 46, 344 (1985).

2. J.E.Bowers, B.R. Hemenway, D.R.Witt, T.J. Bridges, and E.G. Burkhardt, Electron. Lett. 21, 1090(1985).

3. C.M. Gee, G.D. Thurmond, and H.W. Yen, Appl. Phys. Lett. 43, 998 (1983).

4. B.H. Kolner, D.M. Bloom, and P.S. Cross, Electron. Lett. 19, 574 (1983).

5. K.P. Jackson, S.A. Newton, B. Moslehi, M. Tur, C.C. Cutler, J.W. Goodman, and H.J. Shaw, IEEE Trans. Microwave Theory Tech. MTT-33, 193 (1985).

6. C.T. Chang, D.E. Altmann, D.R. Wehner, and D.J. Albares, IEEE Trans. Circuits and Systems CAS-26, 1132 (1979).

7. H.F. Taylor, in Fiber Optics, ed. by B. Bendow and S.S. Mitra, Plenum, 1979

8. C.H. Lee and V.K. Mathur, IEEE J. Quant. Electron. QE-17, 2098 (1981).

9. P. Paulus, W. Brinker, and D. Jager, IEEE J. Quant. Electron. QE-22, 108 (1986)

10. A.S. Daryoush and P.R. Herczfeld, Electron. Lett. 22, 133 (1986).

11. L. Goldberg, A.M. Yurek, J.F. Weller, and H.F. Taylor, Electron. Lett. 21, 814 (1985).

12. H.W. Yen, Appl. Phys. Lett. 36, 680 (1980).

13. L. Goldberg, C. Rauscher, J.F.Weller, and H.F. Taylor, Electron. Lett. 19, 848 (1983)

14. R.A. Becker, C.E. Woodward, F.J. Leonberger, and R.C. Williamson, Proc. IEEE 72, 802 (1984).

Characteristics and Applications of Waveguide Electro-Optic Devices

C. M. Gee, G. D. Thurmond and H. W. [illegible]

Hughes Research Laboratories, Malibu, CA 90265

High speed guided wave devices are important for [illegible] systems and high speed signal processing applications. These devices are considerably more complex than passive waveguide devices such as couplers and power splitters. [illegible] number of basic device structures and their operating characteristics. [illegible] Table I [illegible] present state of the art performance. [illegible] modulators [illegible] GHz [illegible] switches [illegible] a single [illegible] [illegible]

TABLE I [illegible]

WAVELENGTH	ELECTRODE STRUCTURE	SWITCHING VOLTAGE	SPEED	REFERENCE
$LiNbO_3$				
0.633 μm	[illegible]		110 [illegible]	Ref. 1
0.633 μm	[illegible] TW		12 GHz	Ref. 2
0.83 μm	asym coplanar TW	7V	17 GHz	Ref. 3
0.84 μm	planar TW	2V	13 GHz	Ref. 4
0.85 μm	coplanar TW	4.5V	16 GHz	Ref. 5
1.3 μm	coplanar TW	3.5 V	8 GHz	Ref. 6
1.3 μm	asym coplanar TW	4.5 V	7.2 GHz	Ref. 7
GaAs				
0.851 μm	lumped microstrip	8 V	100 ps	Ref. 8
0.865 μm	lumped microstrip	1.4V	900Mb/s	Ref. 9
0.789 μm	lumped microstrip	4V	3 GHz	Ref. 10

Most of the high speed guided wave modulators are based upon the electro optic effect in $LiNbO_3$. The electo optic effect in GaAs material systems is much weaker and has not been as actively pursued. The $LiNbO_3$ device is fabricated by first photolithographically defining the waveguide pattern in Ti metal on

top of the $LiNbO_3$ substrate. The Ti metal is then diffused into the $LiNbO_3$ to create a guiding channel with a refractive index larger than that of the surrounding substrate and top clad. The dimensions of the guide and the value of the refractive indices determine the number of guiding modes. Single mode waveguides in $LiNbO_3$ are typically designed to be a few microns in dimension. Coplanar stripline electrodes of length L are then deposited over the waveguides by photolithographic techniques. A voltage V applied across the electrodes separated by a gap d would induce an electric field given by

$$E = V/d \quad (2)$$

where n is the optical effective index of the guided mode, r is the electro-optic coefficient for incomplete overlap of the optical and electric fields, and Γ is the relevant electro-optic coefficient determined by the crystal orientation and the polarization of the optical wave.

The operation of the modulator depends upon the electrode configuration. The popular electrode configurations are the traveling-wave (TW) and lumped element designs. In the traveling-wave design, the electrodes form a transmission line which is terminated in a matching transmission line and terminated in a matched load. The device bandwidth is ultimately limited by the velocity mismatch between the microwaves and the optical wave. The 3 dB electrical bandwidth is given by

$$\Delta f = 1.4 / \pi |n - n_m| L ,$$

where n_m is the effective microwave index. For a $LiNbO_3$ air interface, $n = 2.2$ and $n_m = 4.2$, giving a velocity mismatch bandwidth of 6.6 GHz cm. The effective microwave velocity can be increased by introducing lower index dielectric layers around the guiding layer.[11] In this way, the bandwidth is broadened at the expense of higher drive power since only the microwave field in the $LiNbO_3$ guiding region contributes to optical modulation. Besides limitation from velocity mismatch, stripline attenuation and packaging mismatch can reduce the bandwidth. With a lossy transmission line, any impedance mismatch causes resonances and limits the bandwidth.

In the case of a lumped-element modulator, an electrode structure with a capacitance C is driven by a transmission line terminated in its characteristic impedance. The speed of the device is limited by the capacitor charging time:

$$\Delta f = 1/\pi RC.$$

For dimensions identical to those of the traveling-wave structure, the bandwidth of a lumped-element $LiNbO_3$ modulator is 2.3 GHz cm.

Alternative to $LiNbO_3$ devices, GaAs multi-quantum well (MQW) and bulk electroabsorption modulators have recently demonstrated performance up to a few gigahertz (Table 1). The principle of operation is based on the Franz-Keldysh effect in which the absorption edge of semiconductors shifts to longer wavelengths with an applied electric field. Hence, light passing through a piece of GaAs can be modulated by an applied electric field. The modulator structure consist of strip loaded channel waveguides formed by etching ridges in epitaxial layers grown on n^+GaAs.[8-10] An electric field is applied vertically across the guiding layer. The bandwidth of these devices is limited by their capacitance. Higher bandwidth can be achieved with shorter devices.

Due to the advancement of high speed modulators, we have implemented external modulators in microwave fiber optic links. Although direct modulation offers simplicity and low drive power, laser wavelength chirping under high speed modulation might prevent their use in some systems. The use of external modulators relaxes the demand for high frequency lasers and provides the flexibility in selecting a low noise laser.

1. R.C. Alferness, N.P. Economou and L.L. Buhl, Appl. Phys. Lett. 38, 214 (1981).

2. T. Sueta and M. Izutsu, J. Opt. Comm. 3, 52 (1982).

3. C.M. Gee, G.D. Thurmond and H.W. Yen, Appl. Phys. Lett. 43, 998 (1983).

4. P.S. Cross, R.A. Baumgartner and B.H. kolner, Appl. Phys. Lett. 44, 486 (1984).

5. R.A. Becker, Appl. Phys. Lett. 45, 1168 (1984).

6. D.W. Dolfi, App. Opt. 25, 2479 (1986).

7. R.C. Alferness, C.H. Joyner, L.L. Buhl and S.K. Korotky, IEEE J. Quantum Electron. QE 19, 1339 (1983).

8. T.H. Wood, C.A. Burrus, R.S. Tucker, J.S. Weiner, D.A.B. Miller, D.S. Chemla, J.C. Damen, A.C. Gossard, W. Wiegmann, Elec. Lett. 21, 693 (1985).

9. S. Tarucha, H. Iwamura, T. Saku, H. Okamoto, Jap. J. of Appl. Phys. 24, L442 (1985).

10. C.M. Gee, G.D. Thurmond, H.W. Yen and H. Blauvelt, paper ThAA3, Topical Meeting on Integrated and Guided-Wave Optics, Atlanta, Feb 1986.

11. K. Atsuki and E. Yamashita, to be published.

A New Optoelectronic CW Microwave Source

C.J. Clark, E.A. Chauchard, K. Webb, K. Zaki, and C.H. Lee
Department of Electrical Engineering
University of Maryland
College Park, MD 20742

P. Polak-Dingles
Laboratory for Physical Sciences
4928 College Avenue
College Park, MD 20871, U.S.A

H-L.A. Hung and Ho C. Huang
COMSAT Laboratories
Clarksburg, MD 20871

Ultrafast switching utilizing picosecond photoconductors finds many applications, including optoelectronic sampling and characterization of high speed electronic devices [1]. One of the major areas of applications that has not been explored is in microwave and millimeter-wave generation and control. The jitter-free switching characteristic of these devices is very promising since the microwave or millimeter wave signals can be generated in complete time synchronization with the exciting optical pulses. The time synchronization opens the way to unique applications. For example, it becomes possible to use optoelectronic techniques to modulate the CW microwave allowing it to carry information at a very high rate (10 GHz here). Another potentially powerful application is in phased array antennas, where the central issue is to provide the correct phase and amplitude at each element of the array in a manner which allows rapid scanning.

A picosecond photoconductor can respond to optical pulses almost instantaneously, and the photoconductive signal will decay rapidly after the termination of the each optical pulse. As a result, electrical transients with extremely fast rise and fall times, and with no jitter, can be generated. The spectral content of such electrical transients extending from DC to terahertz has already been observed [2]. The rise time of the electrical pulse from the photoconductor is the main factor determining the level of the higher frequency spectral components. Although the contribution of the fall time to the high frequency spectral components is smaller, it is necessary to use photoconductors with carrier lifetimes in the picosecond range. In this paper, we report the first optoelectronic realization of a CW microwave source at 10 GHz. This represents a frequency multiplication of 100 times of the electrical signals. The technique can be extended to higher frequencies and the microwave source (including a diode laser) can be integrated on a single chip.

A biased picosecond photoconductor is illuminated by high repetition rate picosecond laser pulses, producing a train of electrical pulses. A single RF component is selected out of the electrical pulses spectrum and amplified. Hence this technique can produce tunable CW microwave source. The experimental configuration is shown in Fig. 1. A CW mode-locked dye laser generates 3 ps pulses at a repetition rate of 100 MHz. The laser beam is focused on a biased semiconductor switch producing electrical transients with picoseconds rise time. The photoconductive switch consists of a microstrip line with a 100 μm gap deposited on Cr doped GaAs. Its photoconductive lifetime is 200 ps. The spectral components are spaced 100 MHz apart, corresponding to the repetition rate of the generated electrical pulses. The output of the switch is matched to a 50 ohm and fed to a high-Q bandpass 10 GHz filter and a lowpass filter. An X-band three stage GaAs MESFET low noise amplifier designed at COMSAT provides the signal with adequate gain for display on the sampling scope. At the selected frequency, it provides a noise figure of 2.2 dB and a power gain of 30 dB. A power of -18 dBm is obtained with a DC bias on the switch of 15V and a light power of 150 mW at a wavelength of 590 nm. In these experimental conditions, the spectrum extends to 25 GHz.

The 10 GHz signal must satisfy general stability requirements so that it may be used in the applications mentioned above. It is thus of great interest to measure its total rms time jitter which was done by applying the technique described in [3]. The spectral component at 10 GHz measured after the amplifier by a HP8566B spectrum analyzer exhibits a continuous noise pedestal as well as discrete sidebands at multiple frequencies of 100 Hz. The total system time jitter including discrete noise and continuous noise from the laser was found to be quite small: 3.53 ps. The sidebands could be detected at the output of the RF source driving the laser mode-locker and could be attenuated by using a more suitable driver. The continuous noise was mostly attributed to the laser fluctuations and could be greatly improved by stabilizing the laser [4].

Our results can be compared with the two following works. In [5], the generation of CW 3 GHz microwave is reported. The authors have used a mode-locked Krypton-ion laser and an avalanche photodiode or an optoelectronic switch. No measurement of microwave power or source noise is given. In [6], a technique of FM sidebands injection locking of laser diodes has been used to generate a CW 35 GHz microwave. This technique requires a careful temperature stabilization of the lasers.

In conclusion, we have demonstrated a new method of generating microwave signals in the multigigahertz range by picosecond optoelectronic technique. The source phase noise is 3.53 ps, primarily due to noise in the lasers. The microwave signal generated is in time synchronization with the laser allowing further optoelectronic processing. Higher power can be obtained by driving arrays of such devices and/or using higher gain amplifiers. The source could be made tunable over the 100 MHz separated frequency components provided that one uses a tunable bandpass filter. Although 10 GHz generation is reported here, the extension of the method to generate microwave in the 100 GHz range is in principle straightforward since femtosecond laser and photoconductors with picosecond carrier lifetime are currently available.

Acknowledgements

The authors would like to thank Dr. Geoffrey Burdge and Dave Rush for technical discussions and measurement assistance. This work was supported in part by the Laboratory for Physical Sciences and the Air Force Office of Scientific Research.

References

[1] For a review, the reader is referred to the book Picosecond Optoelectronic Devices, Chi H. Lee, Ed., Academic Press (1984).

[2] D.H. Auston, K.P. Cheung, J.A. Valdmanis, and P.R. Smith, in Picosecond Electronics and Optoelectronics, G.A. Mourou, [illegible], and Chi H. Lee (Eds.), Springer Series in Electrophysics, [illegible], (1985).

[3] V.F. Kroupa (Ed.), Frequency Stability: Fundamentals and Measurement, IEEE Press, New York (1983).

[4] M.J. Rodwel, K.J. Weingarten, D.M. Bloom, T. Baer, and B.H. [illegible], submitted to Optics Letters (May 1986).

[5] A. Mooradian, Appl. Phys. Letter, 45, 5, pp. 494-496 (1984).

[6] L. Goldberg, A.M. Yurek, H.F. Taylor, and J.F. Weller, Electr. [illegible], 21-18, pp. 814-815 (1985).

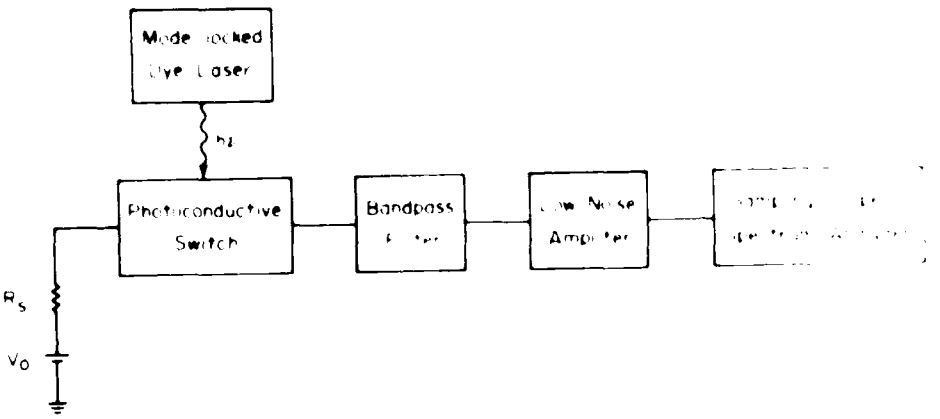

Figure 1. Experimental set-up for the generation of CW microwave signals.

Optical Modulation above 20 GHz using a Waveguide Electrooptic Switch

S.K. Korotky, G. Eisenstein, R.S. [illegible]
J.J. Veselka, and J.G. [illegible]

AT&T Bell Laboratories
Crawfords Corner Road
Holmdel, NJ [illegible]
[illegible]

Optical modulators operating from below 1 GHz [illegible] are of interest for many applications including wideband [illegible] subcarrier modulation. External laser modulators [illegible] optical transmitter for high modulation [illegible] maintaining excellent spectral purity [illegible] fiber communication. Electrooptic modulators [illegible] obtain modulate [illegible] optical waveguides with [illegible] approximately 16 GHz have been demonstrated [illegible] extension of these results to higher frequencies has been [illegible] design requirements and a lack of sufficiently high speed detection systems.

Here we describe a $Ti:LiNbO_3$ foreshortened electrode directional coupler modulator [2] operating at drive frequencies in excess of 20 GHz and an experiment to detect the optical modulation in the time domain using the self sampling method [3]. The $Ti:LiNbO_3$ modulator was designed for 1.5 μm wavelength and consists of a 1 cm optical waveguide directional coupler of single coupling length and a 2.8 mm traveling wave electrode located midway along the length of the coupler. Such a structure has a switching characteristic and frequency response similar to a Mach-Zehnder interferometric intensity modulator. The expected small signal 3 dB electrical bandwidth of the modulator, taking into account optical-electrical walkoff (velocity mismatch) [4] and electrode transmission loss, is approximately 22 GHz.

The modulator electrode consists of a 35 Ω asymmetric coplanar transmission line with a strip width of 15 μm and gap of 5 μm in the active portion of the device and over an additional passive length of 7.5 mm. Connections to 50 Ω coaxial cable at the input and output ends of the microscopic electrode were made using 2.5 mm coplanar tapers and Wiltron K-connectors. The measured switching voltage, V_π, of the modulator is 26 V. The electrical characteristics of the entire structure were measured from 45 MHz to 22 GHz using an HP-8510 vector network analyzer and to 40 GHz using a Wiltron 5669 scalar network analyzer. We display the total electrical transmission loss as a function of frequency in Figure 1. There is little structure in the RF transmission and group delay below 22 GHz indicating fundamental mode operation and negligible dispersion into the 20 GHz range.

The *electrooptic* frequency response of the modulator between 2 and 20 GHz was evaluated using a cw injection laser, a very high speed InGaAs photodiode, and the HP-8510 network analyzer. For this transfer function measurement, two HP-8349 2-20 GHz amplifiers were used to provide a drive power of ~20 dBm to the modulator and a gain of ~15 dB following the detector. The network analyzer compared the transmitted and received electrical power as a function of frequency to determine the relative small signal frequency response. We show the measured electrooptic modulator response in Figure 2. The rolloff

observed from 2 to 20 GHz is just slightly greater than 1 dB, indicating the usable bandwidth extends to higher frequencies. However, it is clear from the figure that the signal to noise ratio of the setup is degrading as a function of frequency, thereby precluding measurements above 20 GHz.

Because of the lack of suitable broadband amplifiers above 20 GHz, it was necessary to employ an alternate approach to evaluate the device above this frequency. The method used here is an adaptation of a previously demonstrated optical sampling technique for characterizing electrooptic modulators.[3] We illustrate the experimental arrangement in Figure 3. The cw laser light source of the previous measurement is replaced by a pulsed laser. In the initial experiments described here, we used a gain-switched semiconductor laser to produce the optical sampling pulses. The laser was driven from a microwave synthesizer to generate 33 ps optical pulses at a repetition rate of 2 GHz. A slow detector was used to measure the average optical power arriving at the output of the crossover waveguide of the coupler. The modulator was driven at the n'th harmonic of 2 GHz ($n \sim 1$-13) with a power of +7 dBm using a second synthesizer phase-locked to the first. In this manner, the average optical power level at the detector contains a component that is proportional to the modulator response at a point of the RF cycle determined by the relative phase of the modulator drive signal and the optical sampling pulses.

The time-domain response of the modulator is mapped out by measuring the optical power as a function of the relative phase of the laser and modulator drives. For convenience, this relative phase is changed by slightly offsetting the frequency of the modulator drive signal with respect to a harmonic of 2 GHz.[5] In Figure 4 we display the detected waveform for a modulation frequency of 26 GHz with an offset frequency of 16 kHz. Using this measurement technique, the frequency response can be mapped out by driving the modulator at different harmonics of the laser pulse rate and also by varying the laser pulse repetition rate itself. The measurement is limited only by the laser pulse width and the frequency range of the synthesizer. Preliminary measurements indicate that the modulation efficiency falls off by 1 dB from 20 to 26 GHz.

In conclusion, we have demonstrated 26 GHz optical modulation using a $Ti:LiNbO_3$ waveguide switch. The device was evaluated in a self-sampling arrangement which should permit testing of devices to approximately 40 GHz with only minor modifications.

Acknowledgement

We are grateful to C.A. Burrus for providing the fast InGaAs photodiode.

References

[1] R.A. Becker, Appl. Phys. Lett. **45**, 1168 (1984) and
C.M. Gee, G.D. Thurmond, and H.W. Yen, Appl. Phys. Lett **43**, 998 (1983).

[2] S.K. Korotky, IEEE J. Quantum Electron. **QE-22**, 953 (1986).

[3] R.C. Alferness, N.P. Economou, and L.L. Buhl, Appl. Phys. Lett. **37**, [illegible]

[4] I.P. Kaminow and J. Liu, Proc. IEEE **54**, 1374 (1963).

[5] M.J.W. Rodwell, K.J. Weingarten, J.L. Freeman, and D.M. [illegible]
499 (1986).

AD-A187 136 SUMMARIES OF PAPERS PRESENTED AT THE PICOSECOND ELECTRONICS AND OPTOELECT..(U) OPTICAL SOCIETY OF AMERICA WASHINGTON D C J W QUINN 10 OCT 87 3/3

UNCLASSIFIED N00014-87-G-0050 F/G 9/1 NL

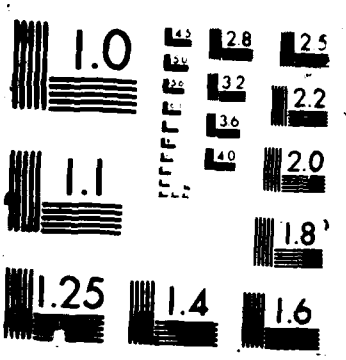
1.0
1.1
1.25
1.4
1.6
1.8
2.0
2.2
2.5
2.8
3.2
3.6
4.0

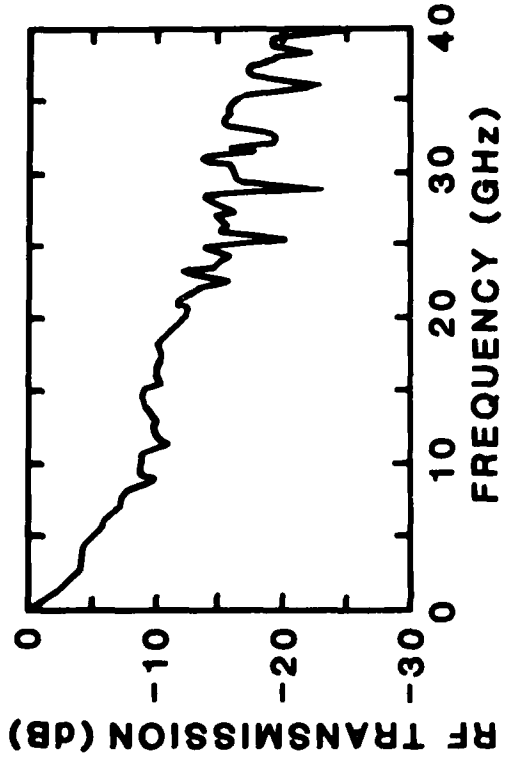

Fig. 1: RF transmission characteristic of traveling-wave electrode. The total electrode length is longer than 1 cm.

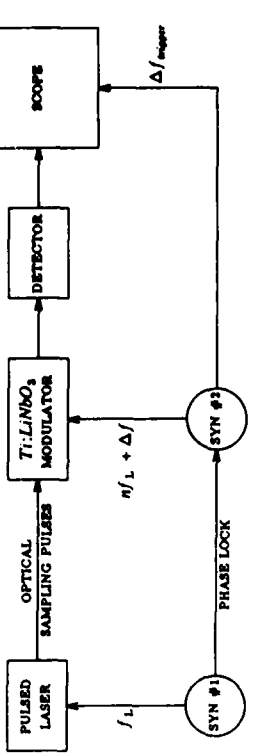

Fig. 3: Arrangement for self-sampling evaluation of modulator

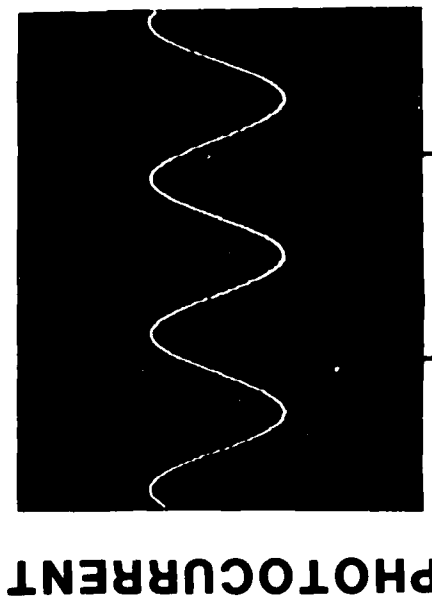

Fig. 4: Oscillograph of 26 GHz optical signal detected using self-sampling method.

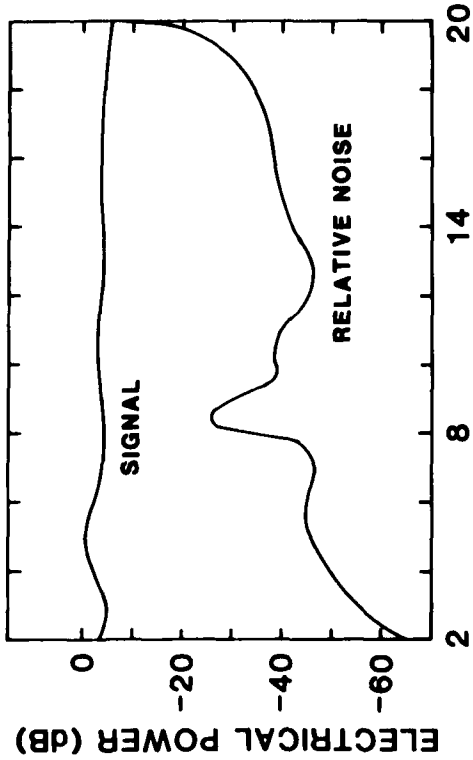

Fig. 2: Electrooptic frequency response of modulator

Picosecond Response of an Optically Controlled Millimeter Wave Phase Shifter

C.-K. C. Tzuang, D. Miller, T.-H.Wang, T. Itoh, and D. P. Neikirk,
Department of Electrical and Computer Engineering
and
P. Williams and M. Downer
Department of Physics
University of Texas at Austin
Austin, TX 78712

This work was supported by the Texas Advanced Technology Research Program and by the US Air Force under grant number AFOSR 86 0036.

Introduction

The introduction of electro-optic sampling techniques now allows the study of very high speed pulse propagation on planar transmission lines. In the frequency domain, recent work on microstrip and coplanar waveguides (CPW) on semiconductor substrates has shown the existence of slow-wave phenomena [1][2]. Since these phenomena are frequency dependent, strong dispersive effects on picosecond pulses would be expected. For a lossless substrate, a spectral domain technique has been used to calculate pulse dispersion for a coplanar waveguide (CPW) and coplanar strips [3], and for a particular geometry and lossy layer both mode matching and finite element techniques have been used to predict pulse behavior in microstrip and CPW [4]. In a typical structure exhibiting strong slow wave effects there are three distinct layers in the substrate: first, a thin, lossless spacer layer immediately below the CPW; second, a somewhat thicker lossy (i.e. doped) layer; and third, a very thick lossless layer. The slow-wave phenomenon (and corresponding variation in effective dielectric constant) occurs as a result of the different interactions of the electric and magnetic fields of the propagating wave with the lossy layer below the CPW. The complex effective dielectric constant of the guide is a function of the conductivity of the lossy layer, the separation of the CPW from this layer, the transmission line dimensions, and the frequency. For frequency domain applications, we have recently proposed a new method to control the slow wave factor in these structures by replacing the doped lossy layer with an (CW) optically generating electron-hole plasma layer in the semiconductor substrate [5]. The device could then serve as a phase-shifter, controlled by varying the optical excitation level, and thus the conductivity of the lossy layer. In this paper we discuss the the effects of the lossy layer on picosecond pulse dispersion.

Device Structure and Model

In this device we would generate the lossy layer within the substrate and confine the induced electron-hole plasma through the use of a multilayer AlGaAs/GaAs structure. A cross section of the device is shown in Figure 1. The wide band gap AlGaAs layer immediately below the CPW is undoped, and serves as the lossless spacer layer. The second layer, made of narrower band gap, unintentionally doped GaAs, is optically excited by continuous wave illumination entering from above (through the gaps between the CPW conductors).The excess carriers generated then cause the formation of the lossy layer. By choosing light of an energy that is below gap for the AlGaAs but well above gap for the GaAs (about 600-700nm for the Al mole fraction shown) the plasma is formed only in the GaAs layer. The band gap discontinuity between the AlGaAs and GaAs presents a barrier to carrier diffusion out of the GaAs layer, so another buffer layer of AlGaAs is used below the GaAs to confine the excess carriers. Based on carrier diffusion calculations, the optically induced electron-hole plasma density in the GaAs layer should be fairly uniform. The interactions between millimeter-waves and such electron-hole plasmas has been studied extensively in dielectric (high resistivity semiconductor) slab waveguides [6], and we follow a similar model. The frequency dependent complex conductivity of the lossy layer is calculated based on a Drude-Lorentz model and an assumed carrier density. This information, along with all guide dimensions, is then used with a mode matching technique to calculate the ac fields in the CPW as a function of frequency. In conjunction with a Fourier transform technique, the frequency domain results can finally be used to predict picosecond pulse behavior.

Results

Figures 2 and 3 show the results for a gaussian input pulse with a full-width-half-maximum of 20psec for two different carrier concentrations in the lossy layer. For the lower density, $1x10^{15}cm^{-3}$, the pulse is very rapidly attenuated, and broadens dramatically after propagating only a few millimeters. In contrast, for the higher density case, $1x10^{17}cm^{-3}$, the pulse does not attenuate as quickly, and only broadens slowly as the pulse propagates. Although this seems somewhat counter-intuitive, due to the presence of the lossy layer, the characteristics of this type of transmission line cannot be obtained by use of quasi-static (i.e. dc) concepts. This lossy layer also presents theoretical and numerical complications in the analysis, so these results should be viewed as illustrative, rather than as quantitatively correct predictions. However, it is clear that the presence of lossy layers in the substrate supporting a planar transmission line must be considered when studying the behavior of picosecond pulses.

Conclusions

In this paper we have calculated the effects of a lossy layer on the propagation characteristics of picosecond pulses on coplanar waveguides. Dramatic changes in pulse dispersion and attenuation are seen as the conductivity of the layer is varied. Experimental verification of these results is being pursued. By using the optically controlled structure discussed here it should be possible to measure pulse dispersion as a function of lossy layer conductivity with the same device. Such studies must be performed if high speed pulse waveforms are to be understood for transmission lines constructed on semiconductor substrates.

References

[1] D. Jager, IEEE Trans. Microwave Theory Tech., vol. **MTT-24**, pp.566-573, Sept. 1976. [2] Y. Fukuoka, T. Itoh, IEEE Trans. Microwave Theory Tech., vol. **MTT-31**, pp.567-573, July 1983.

[3] G. Hasnain, A. Dienes, and J.R. Whinnery, IEEE Trans. Microwave Theory Tech., vol. **MTT-34**, pp.738-741, June 1986.

[4] C.-K. Tzuang, and T. Itoh, IEEE MIC Conf., June 25-26, 1985.

[5] P. Cheung, D. Fun, D. Miller, C.K. Tzuang, D.P. Neikirk, and T. Itoh, Tenth International Conference on Infrared and Millimeter Waves, Lake Buena Vista, Florida, Dec. 9-13, 1986.

[6] C. H. Lee, P. S. Mak, and A. P. DeFonzo, IEEE J. Quantum Electron., vol. **QE-16**, pp.277-288, Mar. 1980.

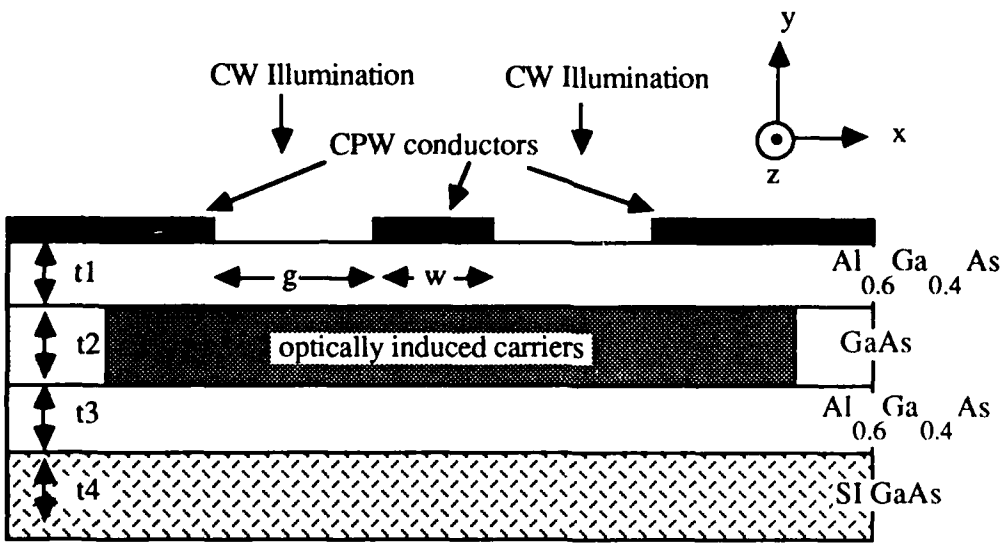

Figure 1: Cross section used to model pulse propagation (in the z direction) on a coplanar waveguide phase shifter; t1 = 0.1μm; t2 = 3.2μm; t3 =3.4μm; t4 = 250μm; d = 12μm; g = 7μm; w = 10μm.

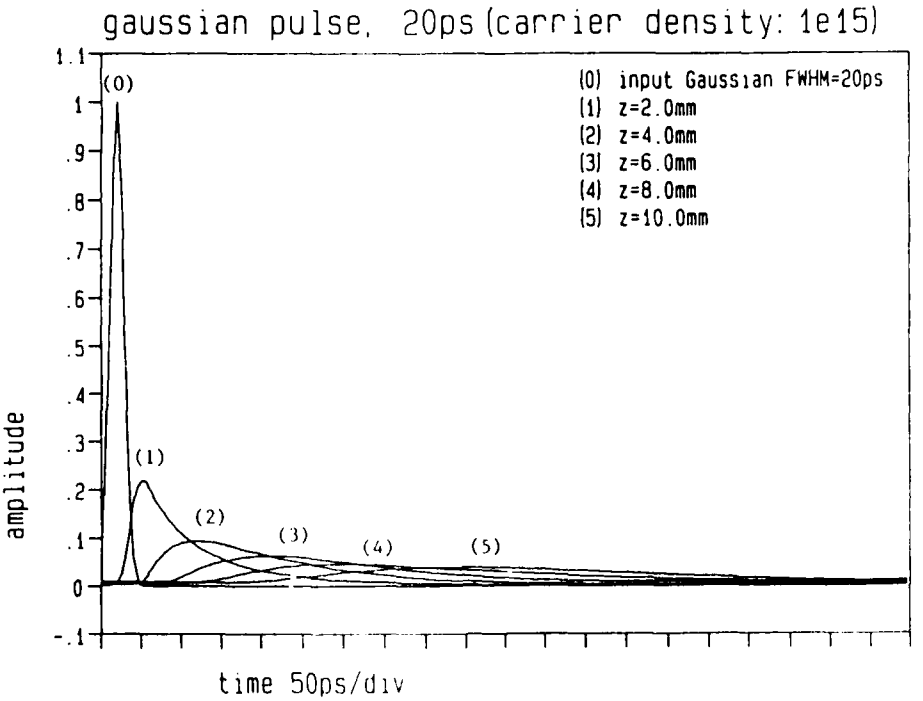

Figure 2: Pulse evolution with electron concentration in layer 2 of Fig. 1 at 10^{15} cm^{-3}.

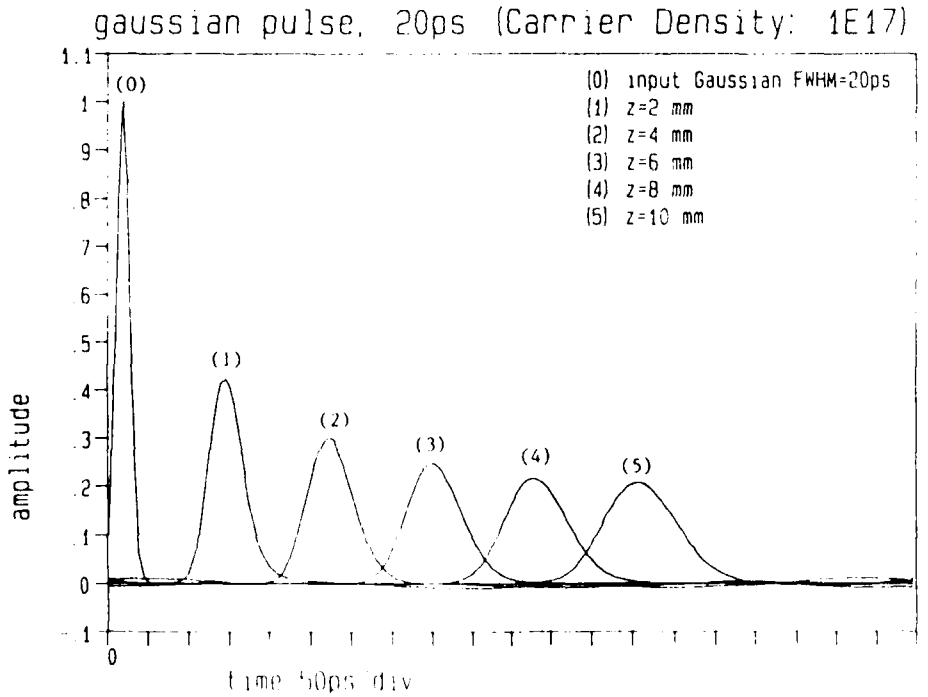

Figure 3: Layer 2 with $10^{17}cm^{-3}$ concentration.

FRIDAY, JANUARY 16, 1987

PROSPECTOR/RUBICON ROOM
1:30 P.M.–2:45 P.M.

FC1–4

HIGH-SPEED AND MICROWAVE DEVICES: 2

G. Burdge, Laboratory for Physical Sciences, *Presider*

Electron Device Probing in the Femtosecond Time Scale

Gerard A. Mourou
Laboratory for Laser Energetics
University of Rochester
250 East River Road
Rochester, NY 14623
716/275-5101

The advent of ultrashort pulses used in conjunction with the electro-optic effect has made possible the temporal analysis of electrical phenomena on the picosecond time scale. On this time scale nonequilibrium transport such as velocity overshoot and ballistic effects as well as resonant quantum mechanical tunneling can take place. These effects will govern the operation of the next generation of electronic three-terminal devices. Using ultrafast techniques such as electro-optic samping it is possible to directly monitor these effects.

Velocity overshoot occurs when the momentum relaxation time is smaller than the energy relaxation time. The electron velocity can significantly exceed the carrier equilibrium velocity. To directly visualize this effect, the photocurrent produced in an intrinsic GaAs biased by a 1 to 10 kV/cm DC field is electro-optically sampled when carriers are suddenly produced by a 100 fs optical pulse (Fig. 1). This study has been performed at different excitation wavelengths so the effect of initial carrier velocity could be examined.

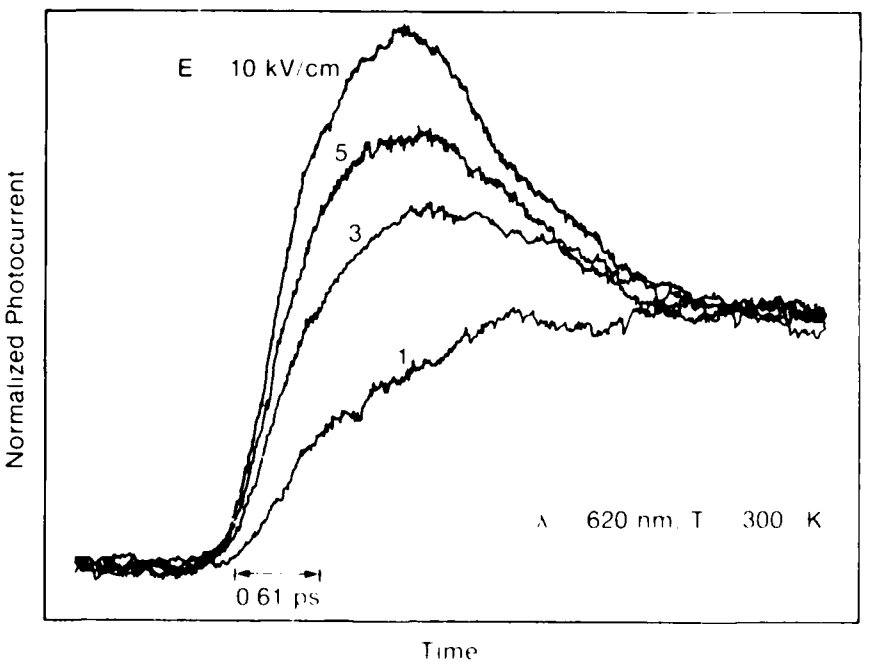

Fig. 1 The photocurrent induced in intrinsic GaAs by a 100 fs pulse is shown as a function of time for different electric field strengths. The photocurrent exhibits a strong enhancement indicating the presence of velocity overshoot.

Transistors with gate lengths shorter than the distance between collisions should exhibit ballistic transport. An example of such a device could be the Permeable Base Transistor where switching time as short as 3.2 ps (Fig. 2) has been measured. When unfolded with the instrumental response these switching times could be indicative of ballistic effects.

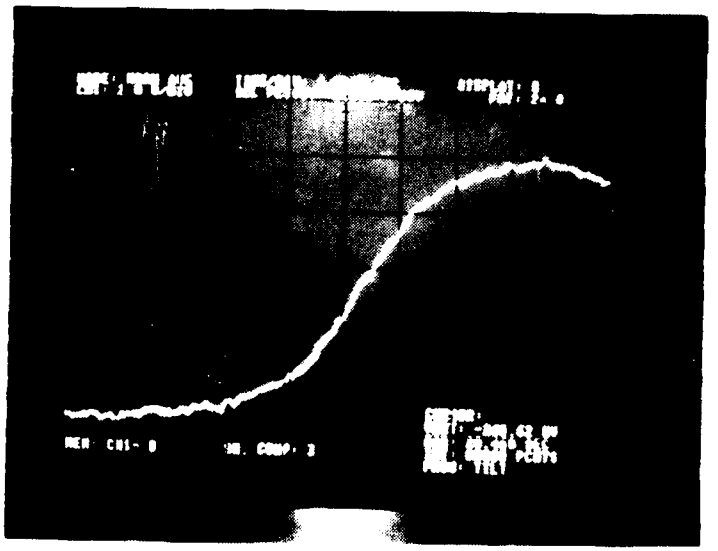

Fig. 2 Switching response of the Permeable Base Transistor when a step function is applied to the transistor gate.

Transport in future devices may rely on quantum mechanical tunneling with possible response in the range of 100 fs. We have time-resolved the response of a resonant tunneling diode when biased by a fast-step function in order to differentiate the contribution of capacitive coupling and true resonant tunneling.

In summary, we will present some of the latest optical measurements on hot electron transport with emphasis on velocity overshoot, ballistic motion, and resonant tunneling transport.

This work was supported by the sponsors of the Laser Fusion Feasibility Project at the Laboratory for Laser Energetics.

ELECTRICAL PULSE COMPRESSION BY TRAVELING-WAVE PHOTOCONDUCTIVITY

D. H. Auston, M. C. Nuss and P. R. Smith

AT&T Bell Laboratories
600 Mountain Avenue, Room 1C-424
Murray Hill, New Jersey 07974
(201) 582-3188

SUMMARY

A substantial amount of work has been devoted to the development of nonlinear optical techniques for compressing ultrashort optical pulses to even shorter durations. To our knowledge, the possibility of developing analogous techniques for compressing picosecond and subpicosecond electrical pulses has not yet been considered. Although loaded nonlinear transmission lines have been used to propagate electrical soliton and shock-type waves, these techniques have not yet been adapted to the picosecond time range.

In this paper, we describe a novel technique for compressing picosecond electrical pulses by reflecting them from a "moving mirror" produced by traveling-wave photoconductivity. As illustrated in figure 1, the moving mirror is produced by illuminating a co-planar strip transmission line by an optical pulse which has a tilted wave-front so that the resulting photoconductance has a traveling wave character. If the conductance is very large it has the appearance of a moving short circuit. An electrical pulse propagating along the line in the direction opposite to the moving conductance will be reflected from it. An analysis of the reflected wave shows that it will be substantially compressed if the velocity of the moving conductance approaches the electrical wave velocity.

The compression mechanism can be regarded as a relativistic Doppler effect whereby each frequency component of the incident pulse is substantially up-shifted by the moving mirror to produce a shorter reflected pulse. A full description of the pulse compression can be obtained by a transformation of the transmission line equations to the moving reference frame of the traveling-wave conductance. This can be done by a Lorentz transformation. The transformed equations have essentially the same form in the moving frame as in the rest frame except now the conductance is stationary and the reflection can be readily determined. Voltage and current are mixed but the electrical wave velocity and the characteristic impedance are invariant. A transformation back to the rest frame then gives the desired result for the compressed pulse.

We first consider the case of the ideal moving mirror represented by an infinite conductance having a steep leading edge moving with a velocity, v. The reflection coefficient in the moving frame is -1. The reflected pulse can be determined exactly in this case and is given by the explicit expression:

$$V_r(t) = -\eta V_i(\eta t)\,, \qquad (1)$$

where $V_i(t)$ is the incident voltage pulse and the compression ratio, η, is

$$\eta = \frac{1-\beta}{1+\beta} \qquad (2)$$

where β is the velocity of the moving conductance relative to the electrical propagation velocity. For example, if $\beta = 0.9$, a compression ratio, η of 19 should be possible. An interesting feature of the compression mechanism is that it is charge conserving, and not energy conserving. The peak amplitude of the reflected pulse is increased by the compression ratio so that the area of the reflected and incident pulses are the same. The peak power is proportional to η^2 and the total energy in the reflected pulse is increased by the compression ratio. The moving mirror imparts energy to the pulse in the reflection process.

In practice, the moving conductance has a finite value and can strongly influence the reflection process. The reflection coefficient will be frequency dependent having values close to -1 for low frequencies only and decreasing for higher frequencies. Frequency dependent phase shifts also occur. To estimate these effects we have solved for the reflected waves from a moving conductance which has a sharp leading edge and a steady state value of G. The reflected waves can be written in the general form

$$V_r(t) = \eta \frac{2}{\pi} \int_{-\infty}^{+\infty} d\omega e^{-i\omega t\sqrt{\eta}}\, \rho(\omega) \int_{-\infty}^{+\infty} V_i(\sqrt{\eta}\, t') e^{i\omega t'}\, dt' , \tag{3}$$

where $\rho(\omega)$ is the frequency dependent reflection coefficient in the moving frame. A closed form expression for $\rho(\omega)$ has been derived which can be used for estimating the effects of the finite conductance. As an example, figure 2 shows the reflected waveforms from a moving conductance having different velocities relative to the electrical wave velocity. The reflected waveforms are shown for relative velocities, β equal to 0.5,0.7,0.8,0.9, and 0.95. In all cases, the incident waveform was a square pulse of unit amplitude and unit time duration. As can been seen from figure 2, the compression can be appreciable, reaching a value of approximately 36 for the case where β=0.95. The conductance was assumed to have a value equal to $10G_o$, where the parameter G_o is defined as

$$G_o = \frac{2}{Z_o v_e \tau_p} , \tag{4}$$

where Z_o is the characteristic impedance, v_e is the electrical wave velocity, and τ_p is the incident pulse duration. The conductance, G, must be much greater than G_o to obtain the full effects of the compression. If not, the pulse amplitude is diminished and the duration broadened.

The experimental conditions necessary to observe this type of pulse compression are well within existing capabilities. We estimate that optical pulse energies of only 100nJ are required to compress electrical pulses on a coplanar microstrip transmission line having linewidths and spacings of approximately 10μm. The velocity matching required to obtain large compression ratios should be possible to achieve with the use of a diffraction grating to produce a tilted wavefront. Experiments are currently in progress to evaluate these concepts.

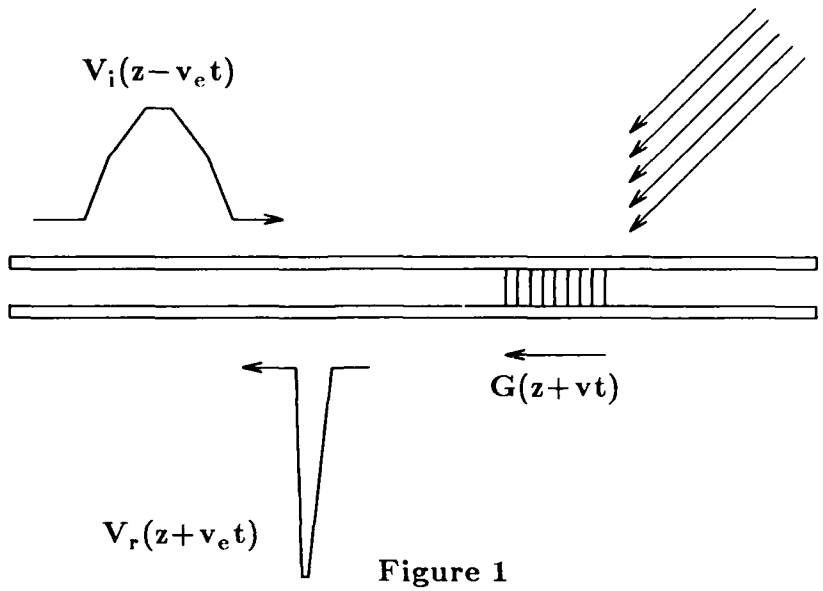

Figure 1

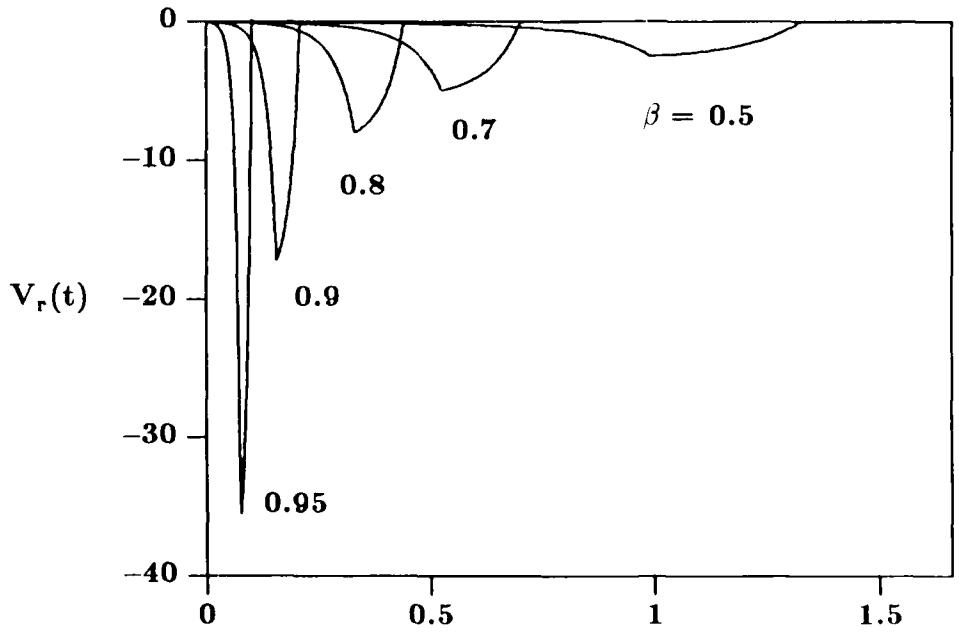

TIME (arbitrary units)

Figure 2

Picosecond Optoelectronic Study of a Thin Film Transmission Line Structure

G. Arjavalingam, J-M. Halbout, G.V. Kopcsay, and M.B. Ketchen.

IBM T.J. Watson Research Center,
Yorktown Heights, NY 10598

In several laboratories high-speed logic circuits which are capable of generating electrical pulses with risetimes in the order of ten picosecond have been demonstrated [1] . Consequently it is now important to be able to transmit these pulses without significant distortion and to be able to characterize the transmission line structures used for this purpose with picosecond time resolution. In addition to the delay and distortion of the pulses as they propagate between generating and receiving points, knowledge of the noise coupled onto adjacent lines is of critical importance to the workings of computers and communication systems. Here we present measurements of high-speed pulse propagation and coupling on an experimental thin film transmission line structure. Photoconductive switches are used for generating and sampling the ultrashort electrical pulses used in this study [2].

A schematic of the experimental layout is shown in figure 1. The thin film structure shown consists of 8μm wide copper microstrip transmission lines separated from a uniform ground plane by a 6.5μm thick layer of polyimide. Center to center spacing of the lines is 25μm . Photoconductive switches fabricated on polysilicon and which have been described elsewhere [3] were connected electrically to both ends of each of two adjacent lines using wirebonds. The switches are known to produce 2ps wide electrical pulses when triggered by 1.5ps wide optical pulses. It has been shown previously that there is no significant degradation of the ultrashort electrical pulses when they propagate through wirebonds of 25μm diameter and 250μm length [4] , and this was further confirmed for the 1 mm long bonds used here. Miniature capacitors were attached across the far ends of the lines of all four switching devices to provide known impedances and facilitate modelling.

The laser source used to drive the photoconductive switches is a Nd:YAG laser, acousto-optically mode-locked at 100MHz repetition rate. Its 73 ps pulses are compressed by passage through 40 meters of single mode optical fiber followed by a double-pass optical delay line composed of a pair of grazing incidence gratings. The compressed pulses are frequency doubled in a 0.5cm thick KTP crystal to yield pulses of autocorrelation width 2ps and average power 350 mW. The pulses launched on the structure that is investigated are produced at point a (figure 1) in a sliding contact configuration [2] and characterized at point b with a side gap detector. A representative pulse is shown in figure 2a. The pulse transmitted by the 3.75 cm long microstrip line is coupled onto the second semiconductor structure and sampled at point c. The near and far end coupled noise are measured at points d and e respectively.

A set of input and transmitted pulses measured at points b and c in figure 1 are shown in figure 2a and 2b respectively. The various features of the input pulse correspond to different aspects of the configuration of the semiconductor switch and the wire bonds connecting the switch to the structure under investigation. For instance the negative feature p in figure 2a is due to the pulse generated at point a in figure 1 reflecting back from the interface between the wirebonds (high impedance) and the transmission line structure (low impedance). The propagation of the input pulse along 3.75 cm of the thin film transmission line was modelled using a microstrip dispersion model [5] . From this the contributions of the different characteristics of the transmission line to the distortion of the pulses are inferred. It is interesting to note that the geometrical dispersion due to the mixed dielectric (insulator and air) and the dispersion due to resistive losses in the conductor have a relatively greater effect on the pulse distortion than the losses in the substrate. In addition the frequency dependent complex propagation constant of the transmission line is calculated. The near and far-end coupled noise (sometimes referred to as cross talk) have a more complicated relationship to the pulse travelling along the active line, and were modelled using a transient circuit analysis program (ASTAP) [6]. Results of these models will also be presented.

The authors wish to acknowledge the Yorktown Silicon Facility for making the photoconductive switches and V.Ranieri for expert technical assistance.

REFERENCES

1. See for example R.A. Murphy, in Picosecond Electronics and Optoelectronics, ed. G.A. Mourou, D.M. Bloom, and C.H. Lee, (Springer Verlag) Berlin, 1985, and references therein.

2. D.H. Auston, in Picosecond Optoeletronic Devices, ed. by C.H. Lee, (Academic Press), London, 1984.

3. M.B. Ketchen, D. Grischkowsky, T.C. Chen, C-C. Chi, I.N. Duling III, J-M. Halbout, J.A. Kash and G.P. Li, Appl. Phys. Lett. 48, 751, (1986); see also D.R. Dykar, T.Y. Hsiang, and G.A. Mourou, in Picosecond Electronics and Optoelectronics, ed. by G.A. Mourou, D.M. Bloom, and C.H. Lee (Springer Verlag), Berlin, 1985.

4. P.G. May, G.P. Li, J-M. Halbout, M.B. Ketchen, C C. Chi, M. Scheuermann, I.N. Duling III, D. Grischkowsky and M. Smyth, in Proceedings of the Topical Meeting on Ultrafast Phenomena V, Optical Society of America, June 1896, Snowmass, Colorado.

5. G. Hasnain, G. Arjavalingam, A. Dienes and J.R. Whinnery, SPIE Proceedings, 439 159, (1983).

6. W.T. Weeks, A.J. Jimenez, G.W. Mahoney, D. Mehta, H. Qassenzadeh and T.R. Scott, IEEE Transactions on Circuit Theory, CT-20 628, (1973)

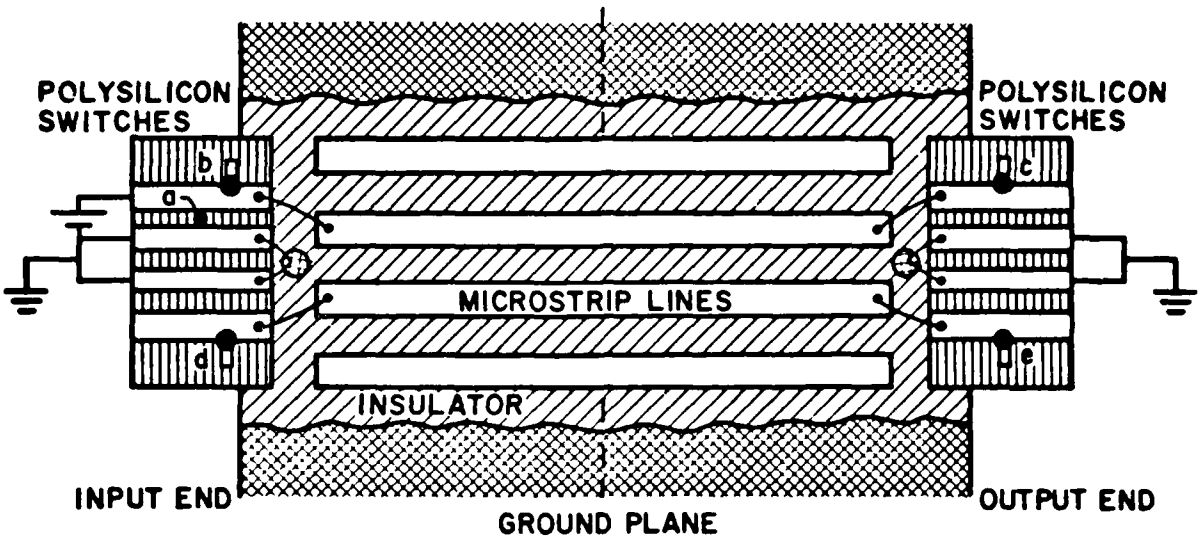

Figure 1. Experimental Layout:. The polysilicon switches are connected to the the transmission line structure usings wirebonds. The total length of the lines is 3.75 cm. The figure is not to scale.

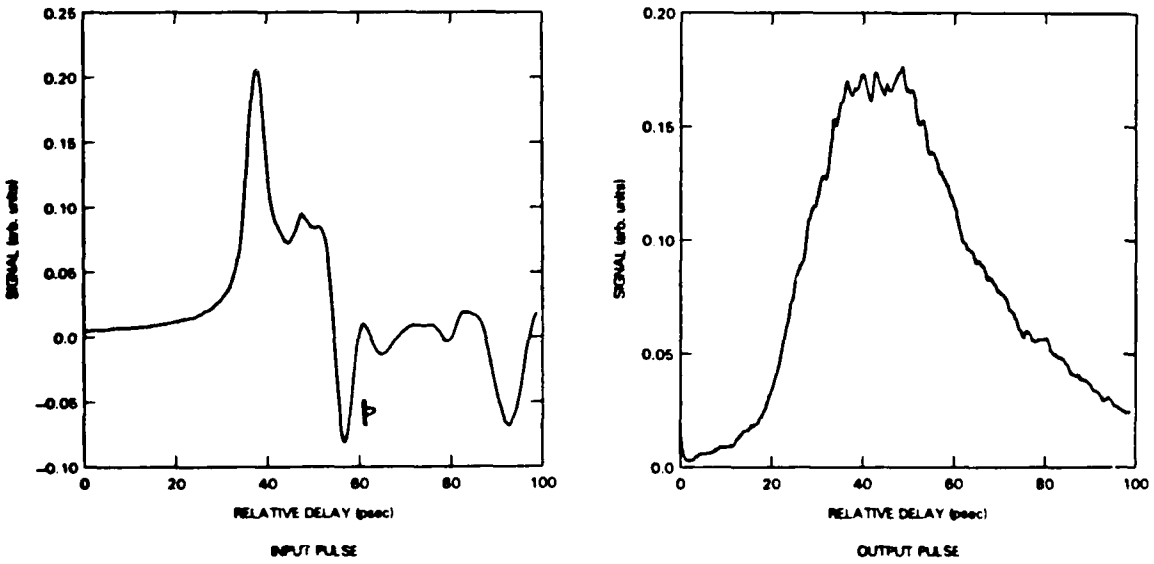

Figure 2. Input and output pulses measured at points b and c in figure 1. The negative feature p is due to the pulse generated at point a in figure 1 reflecting back from the interface between the wirebonds and the low impedance transmission line.

Silicon Pulse Sharpening Diodes - Switching Kilovolts in 10's of Picoseconds+

M. D. Pocha, J. D. Wiedwald, C. G. Dease, and M. M. Contreras *

Lawrence Livermore National Laboratory
P.O. Box 5504, L-156
Livermore, California, 94550
(415) 422-8664

Silicon pulse sharpening diodes were first described by Grekhov et al. [1] in the USSR. Grekhov's work described generation of several kilovolt pulses with rise times in the order of 200 ps. We have been studying these diodes for applications requiring fast, high voltage, low jitter, electrically triggered pulses. The fastest rise times we have observed to date are approximately 70 ps for 1-2 KV pulses. Theoretical calculations using a numerical simulation of the operation of theses devices indicates that rise times shorter than 30 ps should be achieved with optimally designed structures.

Figure 1 shows the basic concept of pulse sharpening using these diodes. A silicon diode with reverse breakdown of greater than 1000 volts is connected in series with an electrically triggered slow pulse generator and a load. The slow pulse generator produces a pulse rising in 1-3 ns (trace A in Fig.1), which substantially exceeds the breakdown voltage of the diode. The current through the diode follows trace B in Fig.1. Initially a small amount of displacement current flows due to the capacitance of the diode. Once the diode's breakdown voltage is exceeded, avalanche second breakdown occurs and the current through the diode increases rapidly. Fig. 2 shows one of the fastest rise times we have generated to date. By using passive circuit elements, the capacitive pre-cursor can be greatly diminished. Pulse forming networks have also been used to generate short duration, flat-topped pulses.

We have used a general one dimensional numerical analysis to model the diode's behavior and attempt to determine the physical mechanisms involved. The numerical model includes a solution of Poisson's equation and the transport equations including a generation term using the standard avalanche integral formulation [2]. Our computer code allows display of plots of the internal values for free carrier densities, current density, electric field, etc. at any time step during the calculation. This simulation has proved to be very useful in visualizing how these parameters are changing as the diode switches into second breakdown and has led to a qualitative understanding of the operation of these devices in this unusual mode. We are making measurements and refinements to the theoretical calculations that will give us good quantitative agreement between theory and experiment.

Qualitatively, it appears that due to the high electric field, avalanche generation floods the interior of the device with an electron-hole plasma. This causes the electric field to collapse resulting in a large current flow in the external circuit. This electron-hole plasma first forms at one end of the depletion layer (where the electric field is the highest) and propagates to the other end as the electric field collapses. Fig. 3 is a plot of the calculated electric field in the depletion layer for several different times showing the propagation of the plasma wave. Our theoretical calculation shows that the rise time of the current pulse is coincident with this propagation of the plasma wave across the depletion layer. Therefore, we conclude that the rise time is determined by the velocity of this wave across the depletion layer.

It is not clear at this time what determines the velocity of this plasma wave. We are

+ This work performed under the auspices of the U.S. Department of Energy by Lawrence Livermore National Laboratory under contract No. W-7405-Eng-48.

performing a number of calculations to separate out the effects of various parameters such as the current density, doping concentrations, and physical width of the depletion layer on this plasma velocity to get a better understanding of the key contributions to the plasma wave velocity. Fig. 4 shows an example of calculated current and voltage waveforms. Since current densities are very high, we feel that an accurate model will require two dimensional calculation. We are therefore in the process of extending our model to two dimensions.

* M. M. Contreras is now at the Dept. of Elect. and Comp. Engin., University of New Mexico, Albuquerque, NM., 87131

References:

[1] I. V. Grekhov et al., "High Power Subnanosecond Switch," Electronics Letters, 17, 7, pp. 422-423, 11 June, 1981.

[2] W. J. Orvis, J. H. Yee, "Semiconductor Device Modeling With BURN42; A One-Dimensional Code for Modeling Solid State Devices," Lawrence Livermore National Laboratory, UCID 20602, Aug. 1985, available from National Technical Information Service, U.S. Department of Commerce, 5285 Port Royal Road, Springfield, Va., 22161.

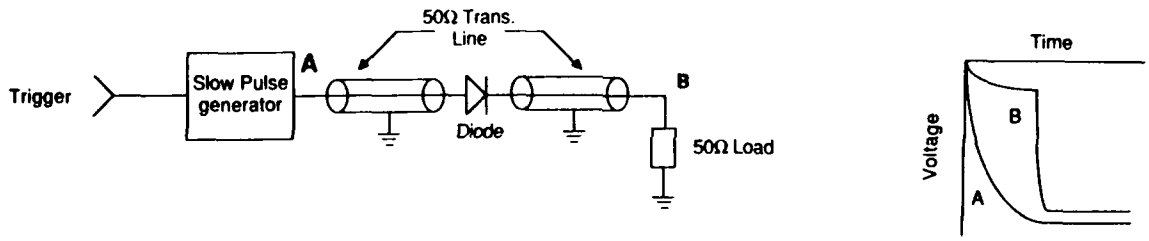

Figure 1. Schematic diagram of pulse sharpening diode circuit and typical voltage waveforms at points A and B in the circuit.

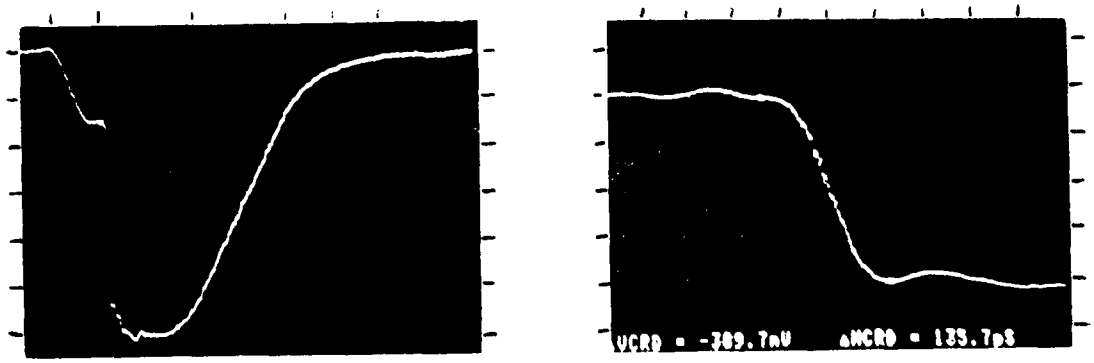

Figure 2. Fastest rise (fall) time waveform generated (63 ps - fast transition). Left picture - 500 V/div vert, 1 ns/div horiz; Right picture - 500 V/div vert, 50 ps/div horiz.

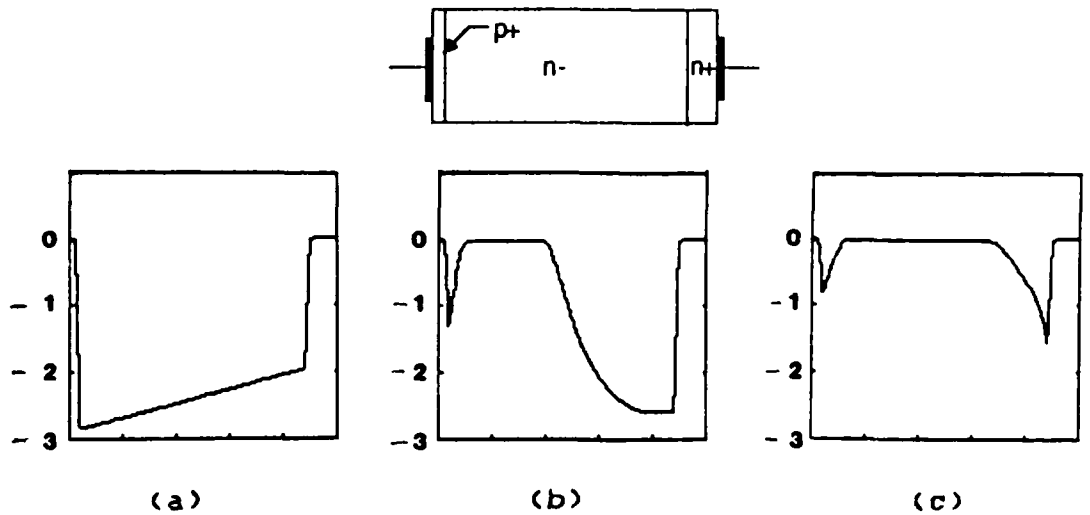

Figure 3. Calculated electric field at three different times during the breakdown process. a) 0.7 ns, b) 0.85 ns, and c) 1.0 ns after trigger (see Fig. 4 for corresponding current and voltage pulses). Scales: V/cm x10^5 vert, relative distance across diode horiz.

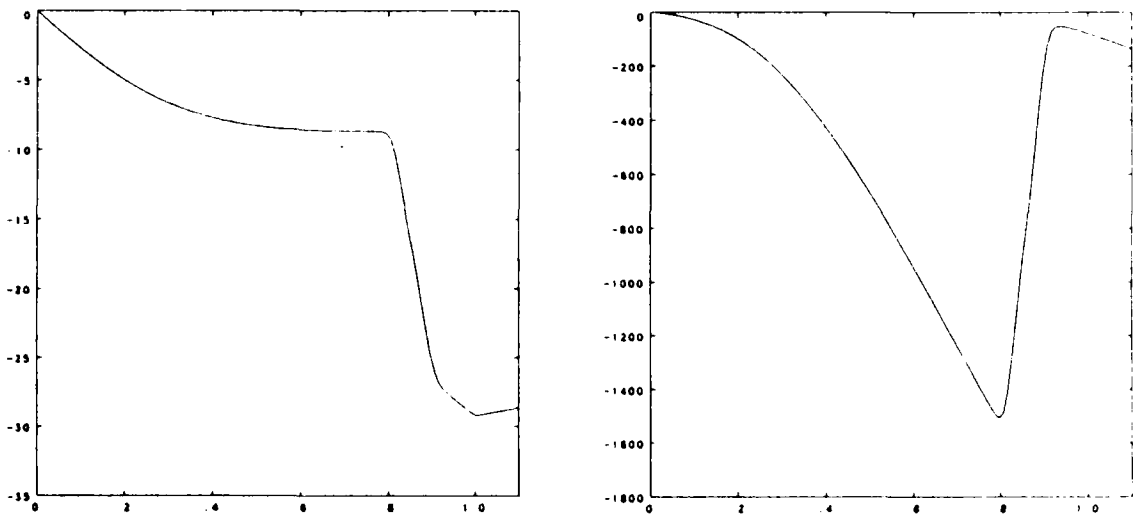

Figure 4. Calculation of current through diode (left) and voltage across diode (right) corresponding to Fig. 3. Scales: Amps or Volts vert, nsec horiz.

FRIDAY, JANUARY 16, 1987

PROSPECTOR/RUBICON ROOM
2:45 P.M.

CLOSING REMARKS

Federico Capasso, AT&T Bell Laboratories
and
Hadis Morkoc, University of Illinois at Urbana
Meeting Program Cochairs

KEY TO AUTHORS AND PAPERS

KEY TO AUTHORS AND PAPERS — *Continued*

END

DATE

FILMED

FEB.

1988